THE INSTITUTE OF PAPER CHEMISTRY, APPLETON, WISCONSIN

PULPING PROCESSES

PROJECT ADVISORY COMMITTEE MEETING
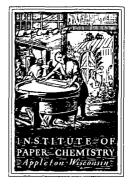
October 21-22, 1985

The Institute of Paper Chemistry

Appleton, WI   54912

NOTICE & DISCLAIMER

October 4, 1985

TO: Members of the Pulping Processes Project Advisory Committee

The next meeting of the Project Advisory Committee for the Pulping Processes
area will be held in Appleton on October 21 and 22, 1985. The meeting will
convene at 8:00 o'clock Monday morning, October 21, in the Seminar Room of the
Continuing Education Center at The Institute of Paper Chemistry. Accommodations
are available for Committee Members at the Continuing Education Center. You
may also stay at the CEC while you are attending other PAC meetings. Enclosed
is a pink "Security Card" which has instructions for entering the CEC building
in the event you find it locked when you arrive. If you have not yet let us
know your plans, including lodging, please do so immediately.

The information enclosed with this letter is for your review prior to the
upcoming meeting. The enclosures include:

    (1) A list of current Committee Members;

    (2) the Agenda for the October meeting;

    (3) a list of current M.S. and Ph.D. student work currently
         in progress at the IPC;

    (4) the status reports for the individual funded projects; and

    (5) a report to the D.O.E. containing details of recent D.O.E.-
         funded work on fiber structure by R. H. Atalla (note that a
         brief summary of this report is included in the status
         report on Project 3521).

In addition, at the PAC meeting you will receive a formal report covering
D.O.E.-funded activity in the recovery area. Edited portions of this report
are included in the recovery section of the Status Report.

The Monday morning and afternoon sessions will cover individual funded projects. The evening session will be in a somewhat lighter vein and include discussions on alternative pulping methodology plus student research in the general pulping processes area. Please note that the fall sessions for PAC meetings are open to the general membership. Hence you can expect other company representatives besides yourself to be present at this meeting.

The Tuesday session will begin at 8:00 a.m. and end at noon. It will be held in Room K108-109 of the Krannert Building. This session is for Committee business and is not open to the general membership. Please note that Tuesday breakfast (7:00 a.m.) and lunch (noon) will be available at CEC.

I look forward to seeing you in Appleton. If you have any questions, please give me a call.

Sincerely,

Earl W. Malcolm
Director
Chemical Sciences Division

EWM/gmk
Enclosures

PULPING PROCESSES PROJECT ADVISORY COMMITTEE

Mr. Allen Rosen (Chairman) -- 6/87
Section Leader - Products Section
Union Camp Corporation
Technology Center
P. O. Box 3301
Princeton, NJ 08540-0148
(609) 896-1200

Mr. Dean W. DeCrease -- 6/88
Group Leader, Pulping Research
Hammermill Paper Company
1540 East Lake Road
P. O. Box 10050
Erie, PA 16533
(814) 456-8811

Dr. Donald C. Johnson -- 6/88
Research Advisor
Weyerhaeuser Company
WTC 2B42
Tacoma, WA 98477
(206) 924-6531

Dr. Thomas C. Kisla -- 6/88
Supervisor of Process Engineers
Stone Container Corporation
P. O. Box 4000
Florence, SC 29502
(803) 662-0313

Dr. Glen C. Smith -- 6/86
Technical Manager-Pulping/Bleaching
Central Research Laboratories
The Mead Corporation
8th & Hickory Streets
Chillicothe, OH 45601
(614) 772-3513

Dr. Roger W. Strauss -- 6/86
Director, Technical & Environmental
  Services
Bowater Incorporated
Pulp & Paper Group
P. O. Box 1028
Greenville, SC 29602
(803) 271-7733

Mr. Jiri Tichy -- 6/88
Principal Engineer
Mill Research Group
Container Corporation
450 East North Avenue
Carol Stream, IL 60188-2195
(312) 260-3530

Dr. Benjamin F. Ward -- 6/88
Research Director
Charleston Research
Westvaco Corporation
P. O. Box 5207
North Charleston, SC 29406
(803) 745-3505

Dr. John R. Wood -- 6/86
Manager of Chemical Pulping
Champion International Corporation
P. O. Box 87
Cantonment, FL 32533
(904) 968-2121

10/85

A G E N D A

PULPING PROCESSES PAC MEETING

THE INSTITUTE OF PAPER CHEMISTRY
APPLETON, WISCONSIN

OCTOBER 21-22, 1985

MONDAY, OCTOBER 21, 1985
CONTINUING EDUCATION CENTER SEMINAR ROOM

Time		
8:00	CONVENE	A. Rosen
8:05	RESEARCH OVERVIEW	E. Malcolm
8:20	PROJECT PRESENTATIONS	
	Improved Processes for Bleached Pulp (Project 3474)	T. McDonough N. Thompson
	Fine Structure of Wood Pulp Fibers (Project 3288)	R. Atalla U. Agarwal
10:20	BREAK	
	Fundamentals of Selectivity in Pulping and Bleaching (Project 3475)	D. Dimmel L. Schroeder
	Development and Application of Analytical Techniques (Project 3477)	D. Easty
12:00	LUNCH	
12:50	PROJECT PRESENTATIONS (CONTINUED)	
	KRAFT CHEMICAL RECOVERY	
	Fundamental Processes in Alkali Recovery Furnaces (Project 3473-1)	T. Grace J. Cameron D. Clay R. Kapheim
	Incremental Capacity in Recovery Boilers (Project 3558)	
	Smelt-Water Explosions (Project 3456-2)	

3:00 BREAK

HIGH-YIELD PULPS -

    Fundamentals of Brightness Stability   W. Lonsky
    (Project 3524)

    Separation of Strong, Intact Fibers   T. McDonough
    (Project 3566)   S. Aziz

5:30 SOCIAL HOUR

7:00 EVENING DISCUSSIONS

    ALTERNATIVE PULPING METHODS

        Biochemical Applications   J. Maxham

        Solvent Sequences   S. Aziz

    STUDENT RESEARCH   Staff/Students

8:30 END OF MONDAY SESSION

TUESDAY MORNING, OCTOBER 22, 1985

7:00 BREAKFAST (CEC)

8:00 COMMITTEE MEETING (K108-K109)
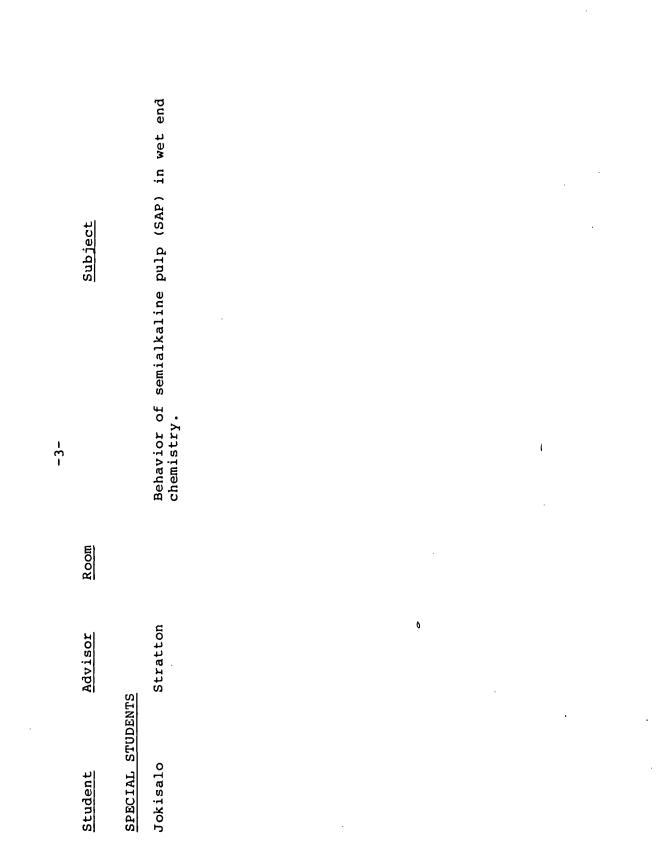
12:00 LUNCH (CEC) END OF TUESDAY SESSION

NEXT MEETING: MARCH 31-APRIL 1, 1986

A291

INDEPENDENT STUDY

Student	Advisor	Room	Subject
Breining	Malcolm		Kraft - sulfite - anthraquinone pulping of southern yellow pine.
Buehler	Grace		Reductive gasification of kraft black liquor in a cocurent porous bed reactor.
Burns, Barbara	McDonough	Pulp Lab	Laboratory fluidization of medium consistency pulp.
Burns, James	Grace		Identification of recovery furnace incremental capacity limits.
Cartwright	Clay		Fluidized bed drying of black liquor.
Charles	Waterhouse		The effect of supercalendering on the strength properties of paper.
Coenen	Cameron	SR8	A kinetic study of catalytic reduction of sodium sulfate with carbon monoxide.
Crane, D.	Parker, P.		Computer simulation of a filtration saveall.
Crane, K.	Clay		Modeling the combustion of a spherical black liquor particle.
Duckart	Thompson	100	Purification of kenaf xylan.
Fisker	Lonsky		Supercritical ammonia pulping.
Fox	Lonsky		A kinetic study of the photo-bleaching reaction.
Goerg	Cameron		Gasification of kraft char with carbon dioxide.
Goulet	Stratton		The adsorption characteristics of cationic poly-acrylamide on cellulose fibers and fines.
Harper	Parker, P.	K115	A MAPPS model of a brown stock washer.

Student	Advisor	Room	Subject
Harris	Sprague		Characterization of corrugator bonding system.
Jones	Sprague		An evaluation of new corrugating adhesives.
Kapik	Johnson, M.		Phenolic components of the primary cell wall and their possible role in the regulation of growth.
Knauf	Doshi		Scientific measurement of paper porosity.
Peterman	Yeske		An investigation of the mechanism of thiosulfate corrosion of carbon steel in kraft white liquor.
Rogers, J.	Malcolm		Computer control of a laboratory batch digester.
Ross	Dugal		An investigation of the source of permeate flux limitation in kraft black liquor ultrafiltration.
Sajdak	Yeske		The effect of thiosulfate on stainless steel pitting.
Sime	McDonough	68	The design and construction of a flow-through reactor.
Standley	Stratton		Measurement of pulp fiber surface area by polymer adsorption.
Sumnicht	Grace		Recovery furnace model: smelt bed through liquor guns.
Unertl	Dugal		An investigation of the z-direction distribution of alkaline size.
Waterman	Baum		The measurement of smoothness using a stylus type instrument.
Westervelt	Baum	1232	The effects of nonuniform drying restraints on the three dimensional mechanical properties in the cross direction of paper.
Wimer	Doshi		Evaluation of sticky contaminants in recycled fiber.

-3-

Student	Advisor	Room	Subject
SPECIAL STUDENTS			
Jokisalo	Stratton		Behavior of semialkaline pulp (SAP) in wet end chemistry.

June 17, 1985

THESES IN PROGRESS

Student	Passed to Candidacy	Thesis Approval	Subject	Committee	Room
Forbes (Not in residence summer 1980)	7/23/80	1/14/81	Ultrasonic characterization of layered composite systems	Baum, chr. Ahrens Habeger	K214
Gentile (Not in residence from August, 1984 on)	9/9/80	12/2/80	The effect of cellulose physical structure on its alkaline degradation	Schroeder, chr. Atalla Thompson	
Fang (Not in residence from July, 1983 on)	9/25/80	12/9/80	An investigation of the drying mechanism in the press drying process.	Ahrens, chr. Chang Wahren	
Pankonin	3/24/81	3/31/81	Viscoelastic relaxation properties of cellulosic materials using ultrasonic techniques.	Habeger, chr. Atalla Baum	K27
Brigham	6/11/81	8/31/81	The role of particle size and polymer molecular weight on the adsorption and flocculation of pulp fines with a cationic polyelectrolyte.	Stratton, chr. Chang Dugal	220
Devlin, C. (Not in residence summer 1981)	6/11/81	4/23/82	An investigation of the drying mechanism of paper at high temperatures and mechanical pressures.	Ahrens, chr. P. Parker Sprague	CR#31

Student	Passed to Candidacy	Thesis Approval	Subject	Committee	Room
Apfeld	12/22/81	3/12/82	The design, preparation, and use of heterogeneous lignin models	Dimmel, chr. Schroeder McDonough	K232
Burazin	12/22/81	12/16/81	Development of a kinetic model of behavior of single chips during kraft pulping	McDonough, chr Halcomb Malcolm	67
Bovee	6/11/82	8/9/82	The synthesis and evaluation of a heterogeneous cellulose model	Schroeder, chr. Dimmel Lonsky	K213
Pounder (Not in residence summer 1982)	6/11/82	11/12/82	The mathematical modelling of high intensity drying.	Chang, adv.in residence Ahrens, chr. Wahren (ex officio)	K118
Furman	9/13/82	10/19/82	The contribution of charge-transfer complexes to the color of kraft lignin	Lonsky, chr. Dimmel Atalla	K203
Wiley	9/13/82	10/14/82	A Raman investigation of cellulose in the cell walls of selected plant species.	Atalla, chr. Litvay Thompson Agarwal	K113
Smith, D.	12/14/82	2/25/83	Studies on the condensation reactions of lignin	Dimmel, chr. Schroeder Thompson	K222
Henderson	6/10/83	3/16/83	Alkaline degradation of 1,5-anhydromannobiitol	Schroeder, chr. Dimmel Thompson	K231
Burton	9/2/83	10/12/83	An investigation of dynamic densification under impulse drying conditions.	Sprague, chr. Wahren Chang	241

Student	Passed to Candidacy	Thesis Approval	Subject	Committee	Room
Geddes (Not in residence Sept. 1983)	9/2/83	1/10/84 & Oct.	Alkaline degradation of amylose: a kinetic model	Schroeder) co-chr. Halcomb) chr. Johnson	K209
Heazel (Not in residence summer 1984)	11/29/83	2/14/84	The influence of sulfonation on sulfite CMP properties.	McDonough, chr. Whitsitt Litvay [adjunct member]	K216
Miller, P.	1/4/84	3/13/84	Swelling of kraft black liquors: an understanding of the associated phenomena during pyrolysis.	Clay, chr. Grace Lonsky	So. Res. Bldg. #1
Nealey	1/4/84	2/24/84	Isolation and characterization of xyloglucan from suspension cultured loblolly pine cell medium.	Thompson, chr. Easty Johnson	34
Biasca	1/4/84	2/24/84	Oriented fiber refining: application of individual modes of mechanical action to single pulp fibers.	Baum, chr. Habeger McDonough Michael Jackson (Weyerhaeuser) [adjunct member]	71
Earnshaw	3/20/84	4/19/84	An investigation into the functions of glutathione and ascorbic acid in growth and development of wild carrot suspension cultures and plants.	Johnson, chr. Litvay Schroeder	111
Lebo	6/8/84	6/29/84	The rates and quantum yields of the photoyellowing and photobleaching processes.	Lonsky, chr. McDonough	203
Pugliese	6/8/84	11/7/84	Kinetics of chlorination.	McDonough, chr. Cameron P. Parker	K211

Student	Passed to Candidacy	Thesis Approval	Subject	Committee	Room
Byers	9/4/84	10/4/84	An autoradiographic study of the hemicellulose distribution in the cell walls of Pinus Resinosa tracheids.	Thompson, chr. / Johnson / Litvay	209
Reed	9/4/84	12/11/84	The role of sulfur species in pulping reactions.	Dimmel, chr. / Malcolm / Schroeder	K232
Molinarolo, S. (Not in residence Sept. Dec. 1984)	9/4/84	3/14/85 thru 1984	Sorption of xyloglucan onto cellulose fibers.	Thompson, chr. / Stratton / Johnson	
Molinarolo, W. (Not in residence Sept. Dec. 1984)	9/4/84	3/14/85 thru 1984	High temperature degradation of phenyl-β-D-glucopyranoside.	Schroeder, chr. / Dimmel / Thompson	
McCarthy (Not in residence Sept. Dec. 1984)	9/4/84	3/14/85 thru 1984	An investigation of the mechanism of alkaline sizing with alkenyl succinic anhydride.	Stratton, chr. / Easty / Dugal	K121
Robinson	11/27/84	2/19/85	Characterization of black liquor droplet drying.	Clay, chr. / Grace	69
Proxmire, P.	11/27/84	2/19/85	The influence of aluminum salts on the retention of titanium dioxide when using cationic polyelectrolyte as a retention aid.	Stratton, chr. / Dugal / Easty	K121
Berger, Brian	3/28/85	3/14/85	The effects of refining and yield on the z-direction elastic properties of paper.	Baum, chr. / Habeger / Waterhouse	66
Aiken	6/7/85	6/6/85	The use of a char pile reactor to study char bed processes.	Cameron, chr. / Grace / Parker, P.	So. Res. Lab.

STATUS REPORT

TO THE

PULPING PROCESSES

PROJECT ADVISORY COMMITTEE

OCTOBER 21-22, 1985

THE INSTITUTE OF PAPER CHEMISTRY

APPLETON, WI 54912

TABLE OF CONTENTS

THE INSTITUTE OF PAPER CHEMISTRY

Appleton, Wisconsin

Status Report

to the

PULPING PROCESSES

PROJECT ADVISORY COMMITTEE

Project 3473-1

FUNDAMENTAL PROCESSES IN ALKALI RECOVERY FURNACES

Char Burning

Fume Generation

Black Liquor Burning

August 15, 1985

PROJECT SUMMARY FORM

DATE: August 6, 1985

PROJECT NO. 3473-1: FUNDAMENTAL PROCESSES IN ALKALI RECOVERY FURNACES

PROJECT LEADERS: T. M. Grace, J. H. Cameron, and D. T. Clay

IPC GOAL:

Increase the capacity potential of existing systems.

OBJECTIVE:

A quantitative description of all key processes in the burning of alkaline pro-
cess black liquor, encompassing reaction paths and rate equations for drying,
pyrolysis, gaseous combustion, char oxidation, sulfide production, and fume for-
mation. The final goal is a comprehensive theory of black liquor combustion.

CURRENT FISCAL BUDGET: $220,000

SUMMARY OF RESULTS SINCE LAST REPORT:

The summary technical report on the char burning work has been issued. This
comprehensive report provides the quantitative verification of the sulfate-
sulfide cycle theory of char burning, and discusses the implications for recovery
boiler operation. A separate report specifically dealing with operational
implications is currently being reviewed and should issue shortly. Papers
dealing with char burning and fume formation were presented at the 1985
International Chemical Recovery Conference in New Orleans.

Some progress was made on understanding the causes of fume formation. Previous
work had shown that intense fuming occurred when sodium sulfide was oxidized to
sodium sulfate in a sodium carbonate melt. This phenomenon, which we called
oxidative fuming, was unexpected and difficult to interpret in terms of existing
concepts of fume formation. Initially we suspected a volatile sodium-oxygen
intermediate. Later studies suggested an alternate explanation: elimination of
gas-side mass transfer resistance to sodium volatilization by reaction of oxygen
and sodium vapor very close to the gas-melt interface. We have not yet reached
a definitive conclusion as to the cause of oxidative fuming. However, it is
becoming increasingly clear that the gas-side mass transfer resistance phenomenon
is a real phenomenon, and does exist to some extent in a recovery boiler.

The phenomenological study of black liquor burning behavior is well underway.
Twenty-five mill liquors have been obtained and the planned set of tests have
been run on these liquors. Analysis of the data is not yet complete, and there
is a need to repeat some of the tests. More detailed information is provided in
the attached report.

Work on sulfur release during pyrolysis of black liquor was carried out by a
Finnish summer student, Goran Nyman, as part of the DOE project. The results of
this work are summarized in the attached report.

The Phase I Central Unit of the DOE Continuous Flow Reactor has been placed in operation. A brief status report on the DOE project is included in the attached material.

There is a good deal of related student work which contributes heavily to this project. Within the current reporting period

P. Miller completed the phenomenological portion of his Ph.D thesis on swelling of black liquor during pyrolysis. Key variables governing swelling have been defined. He is presently looking at liquor composition effects.

M. Robinson initiated a Ph.D. thesis on the drying of black liquor drops.

G. Aiken initiated a Ph.D. thesis on pile burning of black liquor char.

J. Wozniak completed an M.S. project which resulted in an experimental system for measuring the density, viscosity, and surface tension of molten salt mixtures.

B. Moreland completed an M.S. project on the effects of moisture content on the combustibility of high solids black liquor.

D. Hennesy completed an M.S. project which showed that sulfate reduction by hydrogen gas is quite complex.

J. Cantrell is working on an M.S. thesis on sulfur release during burning of black liquor.

In addition, five new M.S. projects were initiated:

K. Goerg - gasification of kraft char with CO_2

T. Coenen - effect of catalysts in sulfate reduction with CO

K. Crane - modeling the combustion of a spherical black liquor particle

D. Sumnicht - recovery furnace model-smelt bed through liquor guns

J. Burns - global aspects of intensified combustion in the bed region

PLANNED ACTIVITY THROUGH FISCAL 1986:

Work on fundamentals of fume formation will continue. This work should reach a definitive conclusion on the cause of oxidative fuming and a quantitative understanding of the variables that control it.

The phenomenological study of burning behavior will continue. The data base will be broadened by including more mill liquors. We especially want to include liquors that burn remarkably well or very poorly.

We will initiate a study of the fundamentals of sulfur release and recapture in black liquor burning. This information is important in furnace performance and

will be essential to interpreting the data obtained on the DOE Continuous Flow Reactor (Project 3473-6).

We will extend our capability to measure physical properties of smelt and char and begin measurements on key eutectic mixtures.

During this period the Phase I DOE reactor will become fully operational. We will obtain extensive data on the in-flight processes of drying, pyrolysis, gasification, and gaseous combustion under continuous flow conditions. Design of the Phase II reactor for continuous char combustion will be undertaken.

As many as four more Ph.D. theses will be initiated. The exact problems to be worked on are still to be defined.

FUTURE ACTIVITY:

Simulation of present and new black liquor combustion concepts on the DOE Continuous Flow Reactor.

Develop a new mathematical model (or computer code) for a recovery boiler, incorporating information gained in these studies.

Write a book on the theory of black liquor combustion and its application to recovery boiler operation.

Work with individual companies, trade associations, and manufacturers in applying results for improved recovery boiler operation.

Status Report

FUNDAMENTAL PROCESSES IN ALKALI RECOVERY FURNACES

CHAR BURNING

The most effective summary of the char burning work is the paper "Role of the Sulfate/Sulfide Cycle in Char Burning - Experimental Results and Implications" presented at the 1985 International Chemical Recovery Conference in New Orleans. That paper is attached and constitutes the main part of this report.

A comprehensive technical Progress Report on char burning has been issued. Extra copies are available and may be obtained by request. A second Progress Report dealing specifically with implications for operation is in preparation. A draft is currently being reviewed by a number of operating people to get specific feedback on some of the more speculative aspects of the report. The finished report will be available at the October PAC meeting.

ROLE OF THE SULFATE/SULFIDE CYCLE IN CHAR BURNING -
EXPERIMENTAL RESULTS AND IMPLICATIONS

T. M. Grace, J. H. Cameron, and D. T. Clay
The Institute of Paper Chemistry
Appleton, Wisconsin 54912

ABSTRACT

Kraft char burns via a sulfate/sulfide cycle. The
char carbon reacts with sulfate to form sulfide and
gaseous CO_2 and CO. The sulfide, in turn, reacts
with oxygen in combustion air to reform sulfate.
The result of this cycle is an exothermic process
in which the char carbon is burnt off and the
sulfur compounds are reduced to sulfide. We devel-
oped quantitative, predictive equations for char
burning which agreed well with experimental
measurements of char particle burns.

This work indicates that a substantial fraction
of the total burning load should take place on the
surface of the char bed. Reduction is an inherent
part of the char burning process, and is not
jeopardized by combustion air impinging on the bed.
Measured kraft char burning rates were much higher
than those corresponding to typical boiler design
hearth loadings, suggesting a large potential for
increased bed burning rates. There are two keys to
increased bed burning:

1. Providing an adequate supply of combus-
    tion air to the whole bed surface,
    matching the stoichiometric requirement
    of the fuel landing on the bed
2. Maintaining high temperatures in the
    bed surface zone

If these two requirements are met, all chemical
functions in the lower furnace will take care of
themselves.

CHAR BURNING

Burning of a black liquor drop in air occurs in
three distinct stages: drying, volatiles burning,
and char burning ($\underline{1}$). These are described in Fig.
1. Char burning is the last stage in the burning
process and occurs as a heterogeneous reaction be-
tween the char particle and the oxygen in the com-
bustion air. There is no visible flame, but rather
an intense glow at the reacting surface. The
residual carbon burns away and the inorganic salts
are reduced and smelted out. Char burning does not
tend to begin until volatiles production ceases,
permitting oxygen to reach the char particle.

Black liquor drop burning times are strongly
influenced by the size of the liquor drop and the
nature of the air-drop contact. For drops of the
size range normally encountered in the furnace
burning in air, burn times are about 5-10 s. Dry-
ing and char burning stages tend to be the slowest
($\underline{1}$).

Char Characteristics

Char is the residual solid product from black
liquor pyrolysis. It is a black, porous, friable

material containing essentially all of the sodium
and about one-half the carbon in the incoming black
liquor. For most purposes, char can be considered
to consist of three inorganic salts, sodium car-
bonate, sodium sulfide and sodium sulfate, along
with carbon and bound hydrogen. Because the black
liquor fired into the recovery furnace contains a
large amount of recirculated sodium sulfate from
the precipitator and dust hoppers, the sulfate con-
tent of the char will be high. A representative
composition for kraft char before char burning
reactions occur is

		Moles / Mole Na_2	Wt.%
Sodium sulfide	Na_2S	1/6	9.0
Sodium sulfate	Na_2SO_4	1/6	16.4
Sodium carbonate	Na_2CO_3	2/3	49.0
Carbon	C	3	24.9
Bound hydrogen	H	1	0.7

Drying

Water in black liquor is evaporated
Major heat sink - keeps temperatures down
Rate governed by heat transfer
Little volume expansion occurs
Normally a relatively slow process

Volatiles Burning

Two processes - pyrolysis and gaseous
    combustion
Pyrolysis yields combustible gases and
    residual char
Gases burn when contacted by air
Visible flame surrounds drop
Considerable volume expansion occurs
    (swelling)
Source of sulfur gases, H_2S and SO_2
Rate governed by temperature
Normally a relatively fast process

Char Burning

Burning occurs on particle - no flame
Residual carbon is burned out
Inorganics melt
Sulfur compounds are reduced to sulfide
Source of volatile inorganics (fuming)
Rate governed by temperature and air supp..
Normally a relatively slow process

Fig. 1 Black liquor burning stages.

From a chemical standpoint, carbon is the domi-
nant species in the char. Carbon is the excess
reactant. There is more than enough carbon present

to reduce all of the sulfate to sulfide. Converse-ly, there is not enough oxygen present in the sulfate to burn off the carbon. Most of the oxygen needed to burn off the carbon in the char must come from combustion air. Hydrogen is a minor species and can be ignored for most purposes.

The most significant parameter governing the stoichiometric air requirement for char is the relative proportion of carbon monoxide (CO) and carbon dioxide (CO_2) in the product gas. About twice as much air is needed if the char carbon is burned to CO_2 rather than CO. The char burning air requirement is about 25 to 45% of the air required for burning all of the black liquor, depending on the CO/CO_2 split. Very limited data on the gas composition just above the bed in a recovery fur-nace gives $CO/CO_2 = 1/2$. This would correspond to a char air requirement of about 40% of the theoret-ical air required by the liquor solids.

Char burning is an exothermic (heat releasing) reaction. The heating value of char in a bomb calorimeter is about 4500 Btu/lb char. The effec-tive heating value of char in the furnace will be significantly lower than this because of the net reduction of sulfate that occurs and because some CO will be formed. Heating values under various conditions for the representative kraft char are

Bomb calorimeter
  (fully oxidized products):   4380 Btu/lb

Smelt fully reduced, all CO_2:   3430 Btu/lb

Smelt fully reduced, all CO: 910 Btu/lb

Bed Burning

The definition of char used in this paper puts it in a process context. Char is the residual solids after black liquor pyrolysis. It is not the material landing on the char bed. Char formation is an inherent step in the burning of black liquor. When the black liquor solids pyrolyze and the pyrolysis gases burn, char is formed. This can occur as droplets rise or fall in the furnace, on the wall, or in the char bed. Char burning takes place after char is formed and oxygen (from air) has an opportunity to reach the char. This can occur (and mostly occurs) on the char bed, but can occur in flight, on the walls, etc.

Char burning and burning in the char bed of the recovery furnace are not identical. Char burning (a process) is the last stage in the black liquor burning process. Where it takes place in the fur-nace is dependent on operating conditions. Some char burning always occurs on the bed but it may also occur as the particle falls to the bed or as it is swept upward with the combustion gases. Bed burning, on the other hand, includes all of the processes occurring in and on the bed in the fur-nace. These include char burning, but may also involve volatile burning and even drying. In an individual small liquor particle the processes tend to occur sequentially. Within the furnace, large numbers of particles are involved at various stages in the burning process. This tends to blur the distinctions between the process steps.

Prediction of the composition and heating value of the partially burnt liquor landing on the bed is beyond the scope of present knowledge. This has its biggest impact on char bed material and energy balance calculations. It appears to be a reason-able first approximation to identify bed burning with char burning. All of the conclusions derived from understanding char burning are directly appli-cable to interpreting bed behavior.
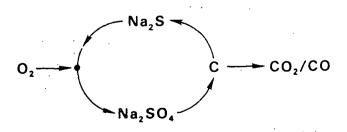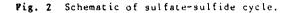
SULFATE/SULFIDE CYCLE

Kraft char burns via a sulfate/sulfide cycle. The carbon in the char reacts with sulfate, reducing it to sulfide and forming CO_2 and CO. The sulfide in turn reacts with oxygen from the combustion air, reforming sulfate and completing the cycle. The sulfate/sulfide cycle acts to carry oxygen to the carbon which is burnt off. The importance of the sulfate/sulfide cycle is that it permits simultan-eous sulfate reduction and carbon burnup in the presence of an oxygen-containing atmosphere as long as the rate limiting step during char burning is oxygen mass transfer to the burning char.

Description

The concept of the sulfate-sulfide cycle is illus-trated in Fig. 2. Oxygen comes in from the com-bustion air and reacts with sulfide (Na_2S). This oxidizes sulfide to sulfate (Na_2SO_4). The sulfate carries the oxygen over to the carbon where it reacts to form CO_2 and CO. The sulfate, in turn, is reduced back to sulfide, completing the cycle. The cycle can operate at any level of sulfur or average reduction state in the system. The opera-ting sulfur reduction state (reduction efficiency) during char burning is determined by the relative rates of sulfide oxidation and sulfate reduction. If the rate limiting step is the oxidation of sulfide by air (e.g., an oxygen mass transfer limit), the carbon will tend to react with sulfate as fast as it is formed and keep the concentra-tion of sulfate low (high reduction efficiency). Conversely, if the rate limiting step is the reac-tion between sulfate and carbon, the sulfide will be oxidized as fast as it is formed and the sulfide concentration would be very low (low-reduction efficiency). It is evident that simultaneous carbon burning and sulfate reduc-tion can occur if the rate limiting step is the oxidation.

Sulfate - Sulfide Cycle

Fig. 2 Schematic of sulfate-sulfide cycle.

Significance

The significance of the sulfate-sulfide cycle is that it permits two apparently contradictory processes, carbon burnup and sulfate reduction, to take place simultaneously in the furnace. It is entirely possible to burn off char carbon in an oxygen containing atmosphere while still achieving very high degrees of sulfur reduction. The only necessary condition for this to occur is for the rate of the carbon-sulfate reaction to exceed the rate of oxygen supply. The carbon-sulfate reaction rate increases exponentially with increasing temperature. The high temperatures required to insure a sufficiently high carbon-sulfate reaction rate tend be self generated because char burning (even with net overall reduction) is an exothermic process. It is not necessary to maintain a gaseous reducing zone (oxygen deficient atmospheres) in the lower furnace in order to get good reduction. In fact, starving the lower furnace for air is counterproductive because it results in low bed temperatures and lower rates of reduction.

QUANTITATIVE ANALYSIS OF CHAR BURNING

The sulfate/sulfide cycle can be treated quantitatively. The following assumptions are made:

1. The only significant chemical species in char are C, Na_2S, Na_2SO_4, and Na_2CO_3.

2. Fume formation and sulfur gasification are neglected.

3. The only gaseous species of interest are O_2, CO_2, and CO.

The second assumption is useful because it makes Na_2CO_3 and total alkali a constant and also makes the sum of Na_2S and Na_2SO_4 constant. This is a good first approximation for treating char carbon burnup and sulfate reduction. Even though fuming is significant in a recovery furnace, its effect on carbon burnup and reduction is minor. Sulfur gasification occurs before char is formed.

The composition of the char is then completely specified by three variables:

$[C]$ = moles char carbon/mole Na_2 (alkali)

r = reduction efficiency = $Na_2S/(Na_2S + Na_2SO_4)$ (in moles)

s = moles S/mole Na_2

Note that s is constant by assumption, and only two variables, $[C]$ and r, are functions of time.

The following reactions are considered to take place:

1. The only reaction between char species and O_2 is

$$Na_2S + 2O_2 = Na_2SO_4$$

Let R_O = rate of above oxidation in moles O_2/mole Na_2, time

then $1/2\ R_O$ = rate of Na_2SO_4 production by this reaction

$1/2\ R_O$ = rate of Na_2S depletion by this reaction.

2. Char carbon is oxidized by sulfate according to the reaction

$$C + \frac{(2-f)}{4} Na_2SO_4 = \frac{(2-f)}{4} Na_2S + f\ CO + (1-f)\ CO_2$$

where f is the mole fraction of CO in the product gas.

Let R_C = rate of $C-Na_2SO_4$ reaction in moles C/mole Na_2, time

then fR_C = rate of CO production by $C-Na_2SO_4$

$(1-f)R_C$ = rate of CO_2 production by $C-Na_2SO_4$

$\frac{(2-f)}{4} R_C$ = rate of Na_2SO_4 depletion by $C-Na_2SO_4$

$\frac{(2-f)}{4} R_C$ = rate of Na_2S production by $C-Na_2SO_4$

Material balances (in moles) can be written per unit mole of alkali in the form:

rate of production -
rate of consumption =
rate of accumulation.

Only two material balances are needed, given the assumptions that are made. Balance for carbon and sulfide totally describe the system (Na_2CO_3 doesn't change and Na_2SO_4 is known if Na_2S is known).

Carbon balance:

Rate of production = 0

Rate of consumption = R_C

Rate of accumulation = $\frac{d}{dt}[C]$

$$R_C = \frac{-d[C]}{dt} \tag{1}$$

Sulfide balance:

Rate of production = $\frac{(2-f)}{4} R_C$

Rate of consumption = $1/2\ R_O$

Rate of accumulation = $\frac{d[Na_2S]}{dt} = s\frac{dr}{dt}$

$$\frac{(2-f)}{4} R_C - \frac{R_O}{2} = s\frac{dr}{dt} \tag{2}$$

3

3

Carbon-Sulfate Rate

The rate of reaction between sulfate and three different types of carbon (pulverized graphite, kraft char and soda char) was found to be represented by Eq. (3). This was determined in a laboratory pool reactor described in Ref. (2) and (3).

$$\frac{d[SO_4]}{dt} = -k_1' \left\{ \frac{[SO_4]}{k_2 + [SO_4]} \right\} [C] \, e^{+ \, k_3 \left(\frac{\Delta T}{1 + \Delta T / T_R} \right)} \quad (3)$$

where $[SO_4]$ = sulfate concentration
$\qquad [C]$ = carbon concentration
k_1', k_2, k_3 = rate constants in Eq. (3)
$\qquad T_R$ = reference temperature = 1200°K
$\qquad \Delta T$ = temperature difference = T - 1200°K

Best fit values for the parameters in Eq. (3) are given in Table 1.

Table 1   Rate parameters for carbon-sulfate reactions.

(T_R = 1200°K, ΔT in °C)

	k_1', s^{-1}	k_2, mole/L	k_3, °C^{-1}
Kraft char	6.3×10^{-3}	0.022	0.0102
Pulverized graphite	4.8×10^{-4}	0.026	0.0154
Soda char	1.7×10^{-2}	0.041	0.0139

The effect of carbon concentration, sulfate concentration and temperature on the reaction rate is illustrated in Fig. 3. A key feature of the carbon-sulfate rate behavior is that the rate is independent of sulfate concentration for all reduction efficiencies up to 95%. Sulfate concentration does not have a major effect on the reaction rate until reduction efficiencies exceed 99%.
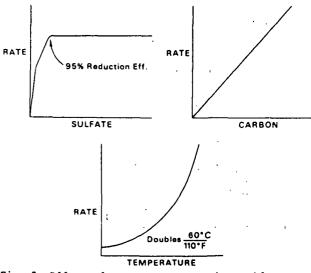

Fig. 3   Effect of parameters on carbon-sulfate rate.

Sulfide Oxidation Rates

Sulfide oxidation in molten carbonate is an inherently fast reaction. In experiments in which air was bubbled thru molten carbonate containing sulfide, the oxygen was consumed as fast as it was supplied until very low sulfide concentrations were reached. The break occurs at about 0.1 mole/liter which corresponds to a reduction efficiency of 2% in a typical smelt.

These results indicate that sulfide oxidation would be oxygen mass transfer controlled under almost any circumstances. Control would shift to inherent chemical kinetics only when the sulfide is essentially depleted.

If the oxygen supply is mass transfer limited we might have

$$R_O = k_{O_2} A \, P_{O_2} \quad (4)$$

where k_{O_2} = oxygen mass transfer coefficient, moles O_2/area time atm
$\qquad A$ = contact area between oxygen supply and char, area/mole Na_2
$\qquad P_{O_2}$ = oxygen partial pressure, atm

Predicted Behavior

A predictive set of equations for burning kraft char can be developed using the rate constants in Table 1 and assuming f = 0 (no CO produced)

$$\frac{-d[C]}{dt} = 1.26 \times 10^{-2}$$

$$\left\{ \frac{(1-r) \, s}{0.0011 + (1-r)s} \right\} [C] e^{+0.0102 \Delta T / (1 + \Delta T / T_R)} \quad (5)$$

and $\qquad \frac{dr}{dt} = -\frac{1}{2s} \frac{d[C]}{dt} - \frac{R_O}{2s} \quad (6)$

subject to the restriction that $0 \leq r \leq 1$.

In deriving Eq. (5) and (6), use was made of the fact that $[SO_4]$ in moles/mole Na_2 = s (1-r), and $k_2 = 0.022$ mole/L = $\frac{0.022 \text{ mole/L}}{20 \text{ mole } Na_2/L}$ = 0.0011 mole/mole Na_2.

A generalized solution can be written for Eq. (5) defining $k''(T) = 1.26 \times 10^{-2} \, e^{+0.0102 \, \Delta T / (1 + \Delta T / T_R)}$ and $f(r) = \frac{(1-r)s}{0.0011 + (1-r)s}$.

The solution is

$$[C] = [C]_o e^{-\int_0^t k''(T) f(r) dt'} \quad (7)$$

where $[C]_o$ is the initial carbon concentration.

Equation (6) can be solved directly by integration.

$$r - r_0 = \int_0^t \left(\frac{dr}{dt}\right) dt' = -\frac{1}{2s} \int_0^t \frac{d[C]}{dt'} dt' - \frac{1}{2s} \int_0^t R_0 dt'$$

where r_0 = initial reduction.

Thus for a constant value of R_0,

$$r = r_0 + \frac{1}{2s}\{[C]_0 - [C]\} - \frac{R_0}{2s} t \qquad (8)$$

It is most convenient to have temperature constant. In this case $k''(T)$ is a constant and comes out of the integral in Eq. (7). Then Eq. (7) states that the carbon will decay along an exponential curve, except for the effect of $f(r)$. The function, $f(r)$, has a value close to one until r begins to approach one, at which point $f(r)$ begins to drop rapidly. Marked deviations from exponential decay occur at very high reductions. Equation (8) is a simple, linear algebraic equation which is an oxygen balance over the duration of the burn.

Equations (7) and (8) can be solved numerically. The resultant curves show how the carbon content [C] and the state of reduction vary with time as char burns. These are very useful in demonstrating the essential features of the char burning process.

Figure 4 shows two cases at a temperature of 1700°F. The values of the parameters are:

$[C]_0 = 3$ moles/mole Na_2

$r_0 = 0.5$

$s = 1/3$ mole S/mole Na_2

$T = 1200°K = 1700°F$

$R_0 = 0.01$ and 0.05 mole O_2/mole Na_2, s.

These two values of R_0 span the range between oxygen limited burning and unlimited oxygen access.

The case with $R_0 = 0.01$ is one where the burning rate is limited by the rate of oxygen supply. There are three distinct periods in the burning curve. In the initial period the sulfate initially present in the char is reduced and the reduction rises quite rapidly to very high values (99+%). During this period the carbon content falls rapidly along an exponential curve. The second period begins when the limit on reduction efficiency is reached. Reduction remains very close to 100% during this period, and the carbon burnup rate slows down to match the rate of oxygen supply. The third period begins when the carbon content has dropped to the point that the carbon burnup rate cannot match the oxygen supply rate. At this point sulfide reoxidation to sulfate begins and the reduction efficiency drops with increasing rapidity. During this period the carbon burnup rate reverts to an exponential decay. The time scale of the process is on the order of 5 minutes (300 s).

Fig. 4   Calculated burning curves at 1700°F.

The case with $R_0 = 0.05$ is one of excess oxygen supply. Oxygen is supplied at a faster rate than carbon can consume it, even at the initial carbon concentration. The sulfide is rapidly oxidized to sulfate until no sulfide remains. The carbon follows an exponential decay through the entire burning process.

Figure 5 shows two cases at a temperature of 2420°F ($\Delta T = 300°C$). Values of the parameters $[C]_0$, r_0, and s are the same as in the previous two cases (at 1700°F). Because of the much faster burnup rates possible at 2420°F, much higher oxygen transfer rates can be sustained. Two oxygen transfer rates, 0.15 and 0.30 mole/mole Na_2,s are shown.

The most obvious difference in behavior at the higher temperature is the much shorter time scale of the event (about 20 s). Both cases shown have the characteristic of an initial period of rapid reduction, an oxygen supply controlled carbon burnup period at very high reduction efficiency, and a period in which simultaneous sulfide reoxidation and carbon burnup occurs. This third period sets in faster, and with more carbon remaining, when the oxygen supply rate is higher.

These expressions apply to a char particle (a finite amount of char burning as a discrete entity) as well. One additional parameter is needed to define the char composition as burning proceeds. This is N = total moles of Na_2 in the particle (assumed constant).

Fig. 5 Calculated burning curves at 2420°F.

Fig. 6 Calculated mass vs. time burning curves at 2420°F.

The mass of a char particle, M, during burning is directly related to the four parameters, N, [C], r, and s by

$$M = 106(1-s)N + 142 Ns(1-r) + 78 Nsr + 12 N[C] \quad (9)$$
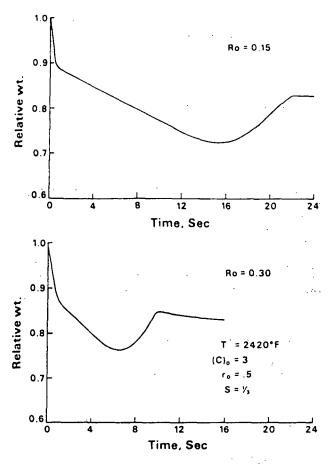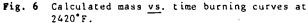
or

$$M = N\{106 + 36s - 64 sr + 12 [C]\} \quad (10)$$

Equation (10) can be used to develop mass vs. time curves for the two cases at 2420°F shown in Fig. 5. The value of N is chosen so that M = 1 at the initial conditions ([C] = 3 and r = 0.5). The mass-time curves are shown in Fig. 6. These curves show four distinct zones.

1. An initial rapid drop as the sulfate originally present in the char is reduced.

2. A constant rate of drop-off as carbon is burned off under oxygen limited conditions (at a fixed, very high state of reduction).

3. A period of weight gain as sulfide is reoxidized to sulfate.

4. A final falling rate period of exponential decay as the final carbon is burnt out in a fully oxidized melt.

It is assumed that both the oxygen supply rate and the temperature remain constant throughout the burn. Neither of these are likely to occur over the entire burning process.

If R_0 is governed by oxygen mass transfer rate, the factors that control it are mainly external to the burning char particle. If we represent R_0 by Eq. (4), R_0 depends on a mass transfer coefficient (which will be a function of gas flow, gas properties, and system geometry), oxygen partial pressure, and the contact area per unit mole of Na_2. The only particle features that would influence R_0 are its external geometry.

Char burning rates are very sensitive to temperature, and thus the actual burning curves would be affected significantly by temperature changes occurring during burning. Because there are significant heat of reaction effects associated with char burning, such temperature changes would be expected. The carbon-sulfide reaction by itself is endothermic, while sulfide oxidation and carbon burnup (at a fixed reduction state) are exothermic.

Heat of reaction effects would tend to straighten out the mass burning curves (as shown in Fig. 6) to some extent. The initial rapid drop is due to net reduction occurring. Since this is endothermic, temperatures would tend to be lowered, thus

decreasing rates in this period. The oxygen-limited burning rate period would occur under exothermic conditions but at a constant rate, so that a stable temperature level should be reached in that period. In the period where sulfide reoxidation is occurring, the reaction is highly exothermic. This will tend to increase temperature, which will increase the rate of carbon-sulfate reactions. This will increase the carbon depletion rate and lower the net rate at which reduction falls off.

EXPERIMENTAL VERIFICATION

The experiments on the burning of single particles of char were carried out on a specially designed apparatus referred to herein as the single particle reactor (SPR). This reactor is designed to provide a direct measurement of mass changes as a char particle reacts. The particle is suspended from a sensitive microbalance and is continuously exposed to a convective gas stream of controlled temperature and composition. The composition of the gases leaving the reaction zone can be monitored. A viewport allows visual observation and photography of the burning particle. A coiled wire and pan help to support the burning particle and retain the smelt.

The particle is suspended from the microbalance in the area of the viewport. Typical particles contain about 0.1-0.2 g of black liquor solids or char and are about 1/4 inch in diameter. Swollen char particles have dimensions on the order of 1/2 to 1 inch. Preheated gas (N_2, air, etc.) passes through a flow straightener and then downward over the reacting particle. Gas flowing in this direction helps keep fume and other combustion products out of the microbalance. A bypass arrangement and dampers are used to stabilize gas flow and temperature before the gas is passed over the particle. Available instrumentation on the off-gas allows measurement of CO, CO_2, O_2, $H_2O_{(v)}$ and Na fume as a function of time.

Burning Rate Curves

The prime measurement of burning rate in the char particle experiments was the particle weight as a function of time. A large number of experimental burns were carried out. A typical result for kraft char burning in air (21% O_2) is shown in Fig. 7. There is a period of a reasonably linear decline in weight followed by a weight gain at the end. These correspond to the periods of oxygen-limited burning followed by sulfide reoxidation discussed previously. The slow rate at the beginning is due to ignition lag and the time to establish high temperature conditions. For kraft char burning in air, burn times were normally 10 to 20 seconds. The major gas product was CO_2 with little CO. The total amount of air passing the particle in the course of a burn was well in excess of that needed for complete burning of the particle.

A typical weight vs. time curve for kraft char burning in 10% O_2 (90% N_2) is shown in Fig. 8. The general shape of the curve is similar to that for kraft char burning in air. However, the constant rate period is much longer in the 10% O_2 case. Total burn times ranged from 25 to 30 seconds. Again there is a weight gain at the end due to

sulfide reoxidation. The behavior in this case is also in close agreement with prediction. Oxygen limited burning rates would be expected to be proportional to the oxygen concentration.

Fig. 7 Kraft char particle burning in air.

Fig. 8 Kraft char particle burning in 10% O_2.

A typical weight vs. time curve for burning a soda char particle in air is shown in Fig. 9. The times for all weight changes for soda char are about the same as for kraft char, 10 to 20 seconds. However, this is a bit misleading, because some residual carbon remained at the end of the burn. A partial lattice of carbon would not burn out. This is probably due to a coupling between low rates, low heat production, and temperature. In contrast to the kraft char, no weight gain was observed at the end of the burnout with soda char. This confirms that the weight gain at the end of char burns is due to sulfide oxidation.

Addition of Na_2SO_4 to the soda char (15% based on the initial black liquor solids) resulted in a weight gain at the end of the burn and eliminated the residual carbon matrix at the end of the burn. In other words, addition of sulfate to the soda char before the burn caused the system to behave like a kraft char.

Fig. 9 Soda char particle burning in air.

Interpretation

All of these results on the SPR are consistent with
the predictions of the theory of the sulfate-
sulfide cycle and with the fundamental work on
reduction and oxidation.

The linearity of the weight vs. time curves and
the similar "total burn times" between kraft char
and soda char are what would be expected for an O_2
mass transfer controlled process. The variables
influencing the mass transfer rate lie mainly out-
side the particles and hence are not changed as
burning proceeds. Visual evidence also confirms a
mass transfer controlled burn. The reaction ini-
tiates at the leading edge of the particle where
the air impacts the particle and burning then pro-
ceeds down along the particle as the top portion
burns away. Burning remains most intense at the
top of the particle.

The weight gain at the end shows that sulfur is
present in a reduced state as burning proceeds.
This is in accordance with predictions from the
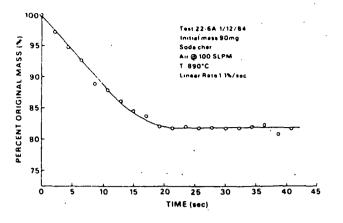analysis of the sulfate/sulfide cycle. The sulfur
remains in a reduced state until the carbon becomes
depleted and then the reduced sulfur oxidizes. The
weight gain at the end of the oxidations of kraft
char and soda char with sulfate, (and the absence
of a weight gain with soda char) can only be
interpreted as being due to the reoxidation of
sulfide.

The concentration of O_2 in the convective gas
stream flowing past the particle had a pronounced
effect on kraft char burning. The burning rate was
reduced at lower O_2 concentrations. For 10% O_2
(90% N_2), the time for complete burnout ranged from
25 to 30 seconds. When burning was carried out
with only 2% O_2, the rate was very slow and burn
times exceeded 60 seconds. For a mass transfer
controlled process, one would expect the burning
rate to tend to be related to the O_2 concentration
and that seems to be what is observed in these
experiments.

IMPLICATIONS ON OPERATION

The results of this work can be used to provide
an overall view of how black liquor burns in a

recovery furnace. The two most significant fin-
dings in this respect are

1. Kraft char burns via a sulfate-
    sulfide cycle. This permits
    reduction to occur simultaneously
    with carbon burnup, even though
    sizable quantities of oxygen reach
    the char.

2. Char burning is an exothermic
    reaction. Heat release on the
    burning char bed can provide the
    heat needed to maintain the bed
    temperatures required by the tem-
    perature sensitive reaction rates.

It is not necessary to maintain an oxygen defi-
cient atmosphere above the char bed in order to
achieve satisfactory reduction efficiencies. Ade-
quate reduction can be obtained as long as bed tem-
peratures are high enough and there is an excess of
carbon in the bed. The chemically active region of
the bed is that portion where the char has access
to oxygen from the combustion air. Char reactions
in the absence of oxygen tend to be self limiting,
since they are endothermic and the reaction rates
decrease rapidly as temperature decreases.

In our view a substantial fraction (up to 50%)
of the total combustion should occur on the bed,
(along with a demand for a corresponding amount of
the total air to be supplied to the bed). The
capability to burn large amounts of combustible on
the bed permits operations with very coarse sprays
(which minimizes entrainment). All that is
required to achieve this is an adequate supply of
combustion air to the bed and sufficiently high bed
temperatures.

The advantage of our view is that it provides a
rationale for maximizing combustion on the bed.
Air must be supplied directly to the bed in propor-
tion to the distribution of combustible over the
bed. Temperature is the other key variable.
Increased burning rates are obtainable by increas-
ing bed temperature. Since the temperature is
self-generated by the combustion exotherm, the
effective heating value of the material reaching
the bed is very important. Complete dryness of the
material landing on the bed would be very impor-
tant. So would the extent of pyrolysis and prior
char burning.

Burning Rates

Typically, design firing rates in a recovery fur-
nace correspond to about 2 to 2.5 lb dry solids per
sq ft of floor area per minute. Our work indicates
that a four-inch thick reaction zone at 1700°F (or
a two-inch thick zone at 1800°F) is capable of
handling the entire char burning load at design
firing rates. This suggests there is ample oppor-
tunity to increase bed burning rates.

There are two basic requirements for increasing
the burning rate on the char bed:

1. The required amount of air to
    satisfy the stoichiometric needs
    of the bed material must be

8   8

supplied under conditions that
sufficiently high mass transfer
rates are attained.

2. The reacting zone on the bed surface
   must be kept at a sufficiently high
   temperature. Air-bed contact must
   be maintained over the entire bed
   surface in proportion to the amount
   of fuel landing on any particular
   area of the bed. Bed temperatures
   are increased by increasing the
   fuel value of the material landing
   on the bed, increasing burning
   rates, and by keeping all heat
   sinks (e.g., wet liquor) away from
   the bed.

Reduction

High reduction efficiencies should be relatively
easy to obtain. Reduction rates depend on the tem-
perature and carbon content of the char. Reduction
is a relatively rapid reaction. Given enough car-
bon, reduction can be completed with a residence
time of a few minutes at 1700°F and within a few
seconds at 2100 to 2200°F. Reduction rates can
always be increased by increasing temperature. If
low reduction efficiencies are caused by low reduc-
tion rates, the cure is to increase the bed surface
temperature. This can be achieved most readily by
increasing the air supply to the bed to increase
the bed burning rates.

Low reduction efficiencies in the furnace can
also be caused by sulfide reoxidation before the
smelt runs out of the furnace. The bed plays a
protective role here, by providing a path for
molten reduced smelt to move out of the active sur-
face layer and away from the combustion air. A
properly sized and shaped char bed can shield the
smelt from the primary air. Anytime combustion air
comes in direct contact with molten smelt, some
reduction efficiency is being lost.

The smelt discharge temperature is not an
effective measure of proper temperature levels for
reduction. Reoxidation of smelt is exothermic and
will raise the temperature of the smelt. Thus a
process that causes a loss in reduction efficiency
can also increase the smelt discharge temperature.
(A small amount of reoxidation close to the spouts
may sometimes be beneficial in raising smelt tem-
perature and improving flow out the spouts). The
critical temperature for effective reduction is the
bed surface temperature.

Bed Temperature

The most important parameter for optimizing the
processes occurring in the lower furnace is bed
temperature. More specifically, it is the tem-
perature in the thin, air-accessible, surface layer
of the bed. Higher temperatures increase the
potential burning rate and provide for better
reduction efficiencies. Higher burning rates on
the bed increase the tolerance for handling coarse
sprays which should lead to less entrainment. The
only apparent detrimental effect of excessive bed

temperature is increased fume production. This may
not be a severe limit.

Bed temperature is determined by heat balance
considerations involving coupling between the
burning rate, the heat of reaction and radiation to
and from the bed. Radiation to the waterwalls will
tend to cool the bed surface, especially along the
sides of the bed. Hotter bed surface temperatures
could be sustained if the same burning rate were
achieved on the part of the bed near the center of
the furnace.

Air/Fuel Distribution

If the bed surface temperature is kept hot enough
(we believe it should be at least 2000°F) the
chemical recovery functions in the furnace tend to
take care of themselves. No other special actions
need to be taken to achieve acceptable reduction,
sulfur scavenging and low residual carbon in smelt.
The main additional requirement is to introduce the
black liquor in such a way that all of the sodium
salts end up on the hearth (minimum entrainment).

With the chemical functions thus self-estab-
lished the combustion process can be treated in
essentially the same manner as it is for any other
fuel. Each element of black liquor fuel has a
requirement for a certain amount of air. The
essence of good combustion control is to introduce
the fuel (black liquor) and air into the furnace in
such a manner that the air reaching a given loca-
tion is proportional to the stoichiometric demand
of the fuel at that location. This implies that
the black liquor spray system and the air supply
system should be coupled. The distribution of air
to the bed must match the distribution of char
landing on the bed. If most of the char is landing
close to the walls, most of the air is needed near
the walls. If the char is spread uniformly over
the bed surface, the combustion air to the lower
furnace should also be distributed evenly over the
bed. Changes in liquor spray patterns without a
parallel adjustment in air distribution will always
result in less than optimum performance.

REFERENCES

1. Solin, P., Hupa, M., and Hyoty, P. Combustion
   behavior of black liquor droplets. Presented
   at 1985 International Chemical Recovery Confer-
   ence, New Orleans, LA, May, 1985.

2. Cameron, J. H., and Grace, T. M. Sulfate
   reduction with carbon is strongly influenced by
   bed surface temperature. Tappi, 65(7): 84-7
   (July, 1982).

3. Cameron, J. H., and Grace, T. M. Kinetic
   study of sulfate reduction with carbon. I&EC
   Fundamentals, 22(4): 486-94(1983).

Status Report

FUNDAMENTAL PROCESSES IN ALKALI RECOVERY FURNACES

FUME GENERATION

The most effective summary of the current status of our understanding of fume formation is the paper "Oxidative Fuming - The Phenomenon and Possible Interpretations" presented at the 1985 International Chemical Recovery Conference in New Orleans. That paper is attached and constitutes the main report on fume generation.

Since the paper was written additional data have been obtained which clearly show that "oxidative fuming" is strongly dependent on gas-side variables. This tends to support the view that "oxidative fuming" is a manifestation of vapor-phase oxidation enhanced fuming during sulfide oxidation. The role of oxygen is to react with sodium vapor very close to the melt interface and create a sink which increases sodium diffusion rates. The role of sulfide is to serve as a sufficient reducing agent in the melt to provide a reasonable sodium vapor pressure. There is now no doubt that this phenomenon is present during "oxidative fuming." What remains to be established is whether or not it is the only mechanism and to develop a quantitative treatment that can be translated to the furnace.

Formal Progress Reports on fume generation are in progress and should be issued by the end of the calendar year.

OXIDATIVE FUMING - THE PHENOMENON AND POSSIBLE INTERPRETATIONS

J. H. Cameron, D. T. Clay, and T. M. Grace
The Institute of Paper Chemistry
Appleton, Wisconsin 54912

ABSTRACT

Sodium based fumes, originating from volatilization
of sodium compounds in the furnace, play a signifi-
cant role in the recovery boiler. They are the
source of the dust load to the precipitator and
economizer, serve as collectors for oxidized sulfur
gases, and influence and may contribute to the
fouling of heat transfer surfaces and plugging.
"Oxidative Fuming" is a name given to the process
of forming copious quantities of sodium carbonate
fume when sodium sulfide is oxidized to sodium
sulfate in a sodium carbonate melt. The fuming
process is clearly connected with oxidation, since
it ceases abruptly when all of the sulfide is oxi-
dized. This phenomenon was unexpected and very
difficult to interpret in terms of existing con-
cepts of fume formation by elemental sodium for-
mation and volatilization at high-temperature
reducing conditions, or sodium hydroxide volati-
lization. We will review the experimental data on
this phenomenon and the variables that influence
it. Quantitative rate equations for oxidative
fuming will also be presented. Two possible
interpretations of the phenomenon will be
discussed. These are formation of a volatile
sodium-oxygen intermediate during sulfide oxidation
and elimination of gas-side mass transfer
resistance to sodium volatilization by reaction of
oxygen and sodium vapor close to the gas-melt
interface.

INTRODUCTION

Reduced sodium salts are produced during combustion
of black liquor within a char bed. The main reac-
tion is reduction of Na_2SO_4 by carbon, yielding
primarily Na_2S and CO_2. The molten salts (smelt)
consist mainly of Na_2S and Na_2CO_3 in approximately
a 1 to 3 molar ratio (1).

Sodium salt fume is another significant com-
bustion product. Temperatures and volatilities of
the sodium species are such that vaporization can
occur under the right conditions. Such conditions
could exist in the char bed or in intensely burning
small liquor particles in flight from the nozzle to
the bed. Submicron fume particles of Na_2CO_3 and
Na_2SO_4 are present in the upper regions of the
furnace (2,3).

Sodium salt fumes affect the design and opera-
tion of recovery boilers. Fumes coat tube surfaces
throughout the convective gas passages, signifi-
cantly increasing the amount of surface area
required for a given steam load. A minimum of 3%
of the steaming output from a recovery boiler is
used to blow fume deposits from the tubes (4). The
fumes are eventually captured by an electrostatic
precipitator. The collected fume is mixed with
black liquor and recycled to the furnace. This
increases the inorganic content and reduces the

fuel value of fired black liquor. Lastly, the
reduction of heat transfer rates via fume deposits
significantly decreases the black liquor solids
capacity of a given recovery boiler. In recovery
boiler limited mills, this decreases the potential
pulp capacity.

A beneficial effect of fume is the capture of
sulfur gases released during the combustion pro-
cesses. Sodium salt vapors react with SO_2 and O_2
to form Na_2SO_4. Sodium sulfate is then removed
from the gas stream and recycled back to the fur-
nace. Any attempt to decrease fuming rates should
not result in higher SO_2 levels (2).

The generally accepted reactions which produce
fuming are (5,6)

$$Na_2CO_3 + 2C \longrightarrow 2Na_{(v)} + 3CO \qquad (1)$$

$$Na_2CO_3 + H_2O \longrightarrow 2 NaOH_{(v)} + CO_2 \qquad (2)$$

The first reaction requires very strong reduc-
tion conditions. The second does not involve
either oxidation or reduction.

A recently published study (3) reports field
test results which give insight into charac-
teristics of recovery boiler fume. The main fin-
dings were

- The coarse particulate fraction (2-20 mm
  and black) only constitutes 3-5% of the
  total dust load. This fraction disap-
  pears when liquor firing stops.

- The fine particulate fraction (submicro-
  scopic and white) is a fine, white dust
  which persists even after liquor firing
  stops.

- The fines fraction continues to enrich
  in Na_2SO_4 as the furnace height
  increases. At the tertiary air level
  it is 64% Na_2SO_4, while at the furnace
  outlet it is 96% Na_2SO_4. No free NaOH
  was found.

- The Na_2SO_4 level in the fines fraction
  decreased as the bed temperature
  increased.

- Total particulate loading after the
  economizer was a directly proportional
  function of the bed temperature at the
  primary air level.

- The suggested way to reduce high par-
  ticulate levels is to prevent high
  local temperatures and high intensity
  burning in the char bed.

This experimental study identifies additional
fuming systems. The most intense fuming observed
is under oxidizing conditions when Na_2S is oxidized
to Na_2SO_4 in a Na_2CO_3 melt. Commercial smelt also
had the highest fuming intensity under these con-
ditions. This result conflicts with the view that
reactions (1) and (2) are the main fume generating
reactions.

1   1

The results of this study are contained in the following two sections of this report. In Section I, the experimental conditions which produce fume are described. A fume generation hypothesis based on the formation of oxide intermediates is described. Section II of this paper presents the results of a quantitative study on fume generation during sulfide oxidation. A second hypothesis based on oxidation enhanced mass transfer from the melt to the gas phase is also described.

SECTION I

Observations

Preliminary experiments identified conditions which produced high intensity visible fume. Fuming during sulfide oxidation produced the greatest fume intensity.

Figure 1 shows the experimental system for these qualitative tests. An electrically heated, fused alumina crucible contained the melt. The nominal smelt charge was 2650 grams. Melt temperatures ranged from 820°C to 980°C. The purge and/or reactive gases entered the melt either above or below the melt surface at 5 to 6 sLpm. Black-and-white photographs of the fume against a black background documented the fume intensity.

Fig. 1 Experimental system for initial fuming observation.

Fig. 2 Range of fume intensities observed. Ranking numbers are the Fume Intensity Rating (FIR).

The range of fume intensities observed is displayed in Fig. 2. The numbers 0 to 7 represent a ranking system for fume intensity. Intensities less than 4 were produced in melts purged with N_2. Air purging below the melt surface produced ratings between 5 and 7 when Na_2S (nominally 1 mole) was present in a Na_2CO_3 melt.

Similar testing was done under a wide range of melt, purge gas, and temperature conditions. Both synthetic and commercial kraft smelts were used. No significant difference in fuming performance existed between the synthetic and commercial melts. The significant findings of these studies are listed in Table 1.

The physical characteristics of the fume varied with conditions of testing. Figure 3 shows a scanning electron micrograph (SEM) of fume produced during oxidation of Na_2S in a Na_2CO_3 melt. Figure 4 shows SEM photographs of fume generated under nonoxidizing conditions. The oxidative fumes are small, white spheres 0.25 to 1.0 μm in diameter. The nonoxidation fumes, however, have widely different shapes. By comparison, Fig. 5 shows SEM photographs of two fume samples from operating recovery boilers. This clearly shows that both

types of laboratory generated fume can be found in commercial units.

Table 1 Fume intensity rating (FIR) variation observed during initial qualitative tests.

OXIDATION[a]	FIR
• Na_2S in Na_2CO_3 melt	7
• Commercial kraft smelt	7
• Na_2S with C in Na_2CO_3 melt	5
• Na_2S with $H_2O(v)$ in air in Na_2CO_3 melt	5
• Na_2S with CO_2 in air in Na_2CO_3 melt	3
• Na_2S in Na_2CO_3 melt at 860-890°C	3-4
• Commercial kraft smelt at 860°C	1-2
• Na_2S in Na_2CO_3 melt (air across surface)	1-2
REDUCTION[b]	
• C in Na_2CO_3 melt	3-4
• Na_2SO_4 with C in Na_2CO_3 melt	2
• Commercial kraft smelt	1-2
• NaOH in Na_2CO_3 melt purged with 10% CO	2
• C with NaOH in Na_2CO_3 melt	1
• Na_2SO_4, NaOH, and C in Na_2CO_3 melt	0

[a]Temperatures are between 900-980°C with air purge below melt surface unless otherwise listed.
[b]N_2 purge below melt at 900-980°C unless otherwise listed.

Fig. 3 Scanning electron micrographs of fume produced during oxidation of Na_2S in a Na_2CO_3 melt.

Fuming can occur from molten sodium salts under both oxidizing and reducing conditions. The fuming reaction path, however, is different for these two conditions.

Reductive fuming at 1200°C via Reaction (1) was an early commercial process for sodium production

(6). Reaction (1) may occur under reducing conditions at local high temperatures in the char bed. The reaction is endothermic and, as expected, experimentally showed lower fuming intensities at lower temperatures.

a

b

Fig. 4 Scanning electron micrographs of fume produced under nonoxidizing conditions:
a. Na_2S in a Na_2CO_3 melt purged with N_2.
b. Na_2CO_3 melt purged with 10% CO and 90% N_2.

The corresponding reaction with CO is presumed to be

$$Na_2CO_3 + CO \longrightarrow 2Na(v) + 2 CO_2 \qquad (3)$$

The observed reduced fume intensity with CO compared to carbon is consistent with a lower free energy for Reaction (1).

The main oxidative fuming reactions occur when Na_2S is oxidized by air in Na_2CO_3 melts. Essentially all the oxygen is depleted from the incoming

stream. Fuming ceases when inlet air stops or the sulfide is completely oxidized.

a

b

Fig. 5 Scanning electron micrographs of fume collected in an operating kraft recovery boiler:
a. Superheater region.
b. Economizer region.

The overall oxidation reaction

$$Na_2S + 2O_2 \longrightarrow Na_2SO_4 \qquad (4)$$

does not explain fume formation. The vapor pressures of both Na_2CO_3 and Na_2SO_4 are too low at 900°C to generate significant fuming. The vapor pressure of Na_2CO_3 at 900°C is 0.45 Pa (8) and that of Na_2SO_4 is 3.3×10^{-3} Pa (9). Neither compound visibly fumed when purged with N_2 even at 980°C.

The presence of sodium oxides in carbonate melts has been reported by Andersen (10). These oxides are, in decreasing order of concentration in the liquid phase, Na_2O, Na_2O_2, and NaO_2. Also, NaO, a volatile and highly reactive oxide, is present and may be the initial fuming species. All of these oxides may contribute to the fume forming process.

Postulated overall reactions might be:

$$2CO_3^= + 3O_2(g) \rightleftharpoons 2CO_2 + 4O_2^- \qquad (5)$$

$$4O_2^- + S^= \rightleftharpoons SO_4^= + 4O^- \qquad (6)$$

$$4Na^+ + 4O^- \rightleftharpoons 4NaO(g) \qquad (7)$$

This is undoubtedly not the oxidation path for all Na_2S. These reactions are believed to be side reactions of the main Na_2S oxidation to Na_2SO_4.

There are several experimental observations that support the intermediate oxide hypothesis. First, when SO_2 was added above the melt during Na_2S oxidation, there was no O_2, yet all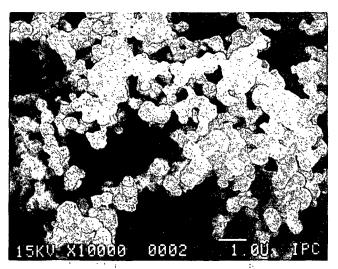 the fume was Na_2SO_4. If either Na, Na_2, or Na_2O had been the initial species, a significant level of Na_2SO_3 would have been expected. These facts suggest the following reaction:

$$2NaO + SO_2 \longrightarrow Na_2SO_4 \qquad (8)$$

Second, the addition of C, H_2O, or NaOH reduced fume intensity. Increased Na_2SO_4 was noted in the fume in the first two cases. These reactants could have upset the balance between either the supply of O_2^- or $S^=$ necessary for NaO formation. Since sulfur was released, and no O_2 was present above the melt, and Na_2SO_4 was the product, a reaction such as (8) is suspected.

Finally, the fume composition was greater than 95% Na_2CO_3 for most experiments with both synthetic and commercial smelts. The balance was Na_2SO_4. At lower temperature (< 880°C) the percentage of Na_2SO_4 increased rapidly as SO_2 partial pressure exceeded CO_2 partial pressure. This shows that at high temperatures where fuming predominated, Na_2CO_3 disproportionates, making Na_2O available for oxide formation. Experimentally, CO_2 added to the air used for oxidation did supress fuming.

SECTION II

This section contains a quantitative study of the effects of the experimental variables on fume generation during sulfide oxidation. These variables include melt temperature, oxidation rate, nitrogen purge rate, and melt-gas contact configuration. Also described is the mechanism responsible for fuming during the oxidation of molten metals. An understanding of oxidation-induced fuming in molten metals may provide insights into the mechanism responsible for fuming during the oxidation of sulfide in alkali carbonate melts.

Experimental Apparatus

The fume generation experiments were conducted using an induction furnace. In a typical fume generation experiment, 80 g of melt containing 0.77 mole Na_2CO_3 and 0.03 mole Na_2S were oxidized using an air/nitrogen purge.

Two configurations of introducing the purge into the reactor were employed during this study. These configurations consisted of either introducing the purge directly into the melt or introducing the purge above the melt. Figure 6 illustrates the experimental system with the purge introduced below the melt surface. With the purge introduced into the melt, the oxygen content of the purge was totally consumed by sulfide oxidation. Introducing the purge above the melt allowed the effect of a residue oxygen partial pressure on the rate of fume generation to be studied.
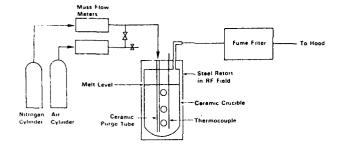

Fig. 6 Experimental system.

The fume generation rate was determined by filtering and weighing the fume particles generated. To ensure that all the fume was collected by the filter, the gas passing through the filter was tested for sodium using a flame photometer.

Purge Introduced Below the Melt Surface

In this section the effects of sulfide concentration, sulfate concentration, temperature, purge oxygen content, and purge rate on fume generation with the purge introduced into the melt are described.

Typical experimental results obtained with the purge introduced below the melt surface. Typical fume generation data obtained during sulfide oxidation are illustrated in Table 2.

Table 2 Typical experimental fume generation results with purge introduced below the melt surface.

Run 38
Initial Melt Composition   Purge = 1 L/min at 2.1% O_2
Na_2CO_3 = 0.77 mole   Temperature = 1255.6°K (1800°F)
Na_2S = 0.03 mole

Time, s	Calculated Composition Na_2SO_4, mole/L	Na_2S, mole/L	Fume Generation Rate, g/min	Fume Concentration $\frac{\text{Moles } Na_2CO_3}{\text{Mole } N_2}$
755	0.136	0.549	0.0099	0.00214
1280	0.231	0.455	0.0104	0.00224
1760	0.318	0.368	0.0106	0.00288
2240	0.405	0.281	0.0104	0.00224
2721	0.492	0.195	0.0099	0.00214
3114	0.563	0.124	0.0088	0.00190
3639	0.656	0.029	0.0005	0.00011

As illustrated in this table, the fume generation rate remains at a constant level until the sulfide is nearly totally oxidized. Once the sulfide is oxidized, the fume generation rate rapidly decreases. Although a significant change in the levels of sulfide and sulfate occurs during the sulfide oxidation, no change in the fume generation rate is observed. The addition of various

initial levels of sulfide and sulfate also had no effect on the rate of fume generation during sulfide oxidation. Therefore, the fume generation rate is independent of the sulfide and sulfate concentration.

Effect of oxygen partial pressure on the rate of fume generation. To determine the effect of oxygen in the purge to the reactor on the rate of fume generation, the oxygen level in the purge was varied. By monitoring the oxygen level in the off-gas from the reactor, it was found that essentially all the oxygen supplied to the melt is consumed by sulfide oxidation. Therefore, to maintain a constant off-gas flow rate from the melt, the nitrogen level in the purge to the reactor was held constant and the oxygen level was adjusted. The gas flow rate to the melt then varied, but the gas flow rate from the melt remained constant. The results of a series of experiments with varying purge gas oxygen levels are shown in Table 3.

Table 3 Effect of oxygen in purge on rate of fume generation.

Temperature = 1200°K (1700°F)

Run	N_2, L/min	O_2, L/min	Fume Generation Rate, g/min
45	1.02	0.0105	0.00892
46	1.02	0.021	0.0105
47	1.02	0.042	0.0121
48	1.01	0.063	0.0145
49	1.02	0.084	0.0146

As illustrated in this table, the increase of oxygen in the purge to the reactor tends to increase the rate of fume generation. However, the fume dependence on the oxygen purge rate appears to be slight. Although the initial level of oxygen increased by a factor of eight, the fume rate less than doubled.

Temperature effect. To determine the form of temperature dependence for fume generation, a number of gravimetric fume generation rate measurements were made at various temperatures. These measurements were made during a series of seven experiments with melt temperatures ranging from 1200 to 1311°K (1700 to 1900°F). To generate the fume, a Na_2CO_3-Na_2S melt was oxidized using a 90% N_2-10% O_2 gas mixture.

To determine if the fume generation rate followed an Arrhenius type temperature dependence, the ln of the fume generation rate was plotted vs. 1/T°K, Fig. 7. As seen in this figure, the fume generation rate has an exponential temperature dependence.

Effect of nitrogen purge rate on fume generation. To determine the effect of the volumetric purge rate on the fume generation rate, the nitrogen flow rate was varied while the oxygen flow rate was held constant. Since all the oxygen in the purge was consumed by sulfide oxidation, the rate of oxidation during each experiment was constant and only the volumetric flow rate of the purge gas was varied. The results of these experiments using the gravimetric method of following fume generation are illustrated in Table 4.

5   5

Fig. 7 Effect of temperature on fume generation.

Table 4 Effect of purge rate on fume generation.

Initial Melt Conditions: Na_2CO_3 = 0.77 mole
Na_2S = 0.03 mole
Temperature = 1200°K
(1700°F)

Run	N_2, L/min	Air, L/min	Total N_2, L/min	Fume Generation Rate ± Std. Dev., g/min
50	0.4	0.1	0.48	0.00680 ± 0.00032
51	0.6	0.1	0.68	0.00850 ± 0.00076
52	0.8	0.1	0.88	0.01004 ± 0.00042
38	0.9	0.1	0.98	0.01024 ± 0.00032
53	1.06	0.1	1.14	0.01204 ± 0.00042
54	1.23	0.1	1.31	0.01474 ± 0.00198

As seen in Table 4, the fume generation rate is highly dependent on the volumetric purge rate.

Sodium hydroxide effect. One of the generally accepted mechanisms which produce fume is the formation and vaporization of NaOH. To determine if NaOH is a major source of fume, NaOH pellets were added to Na_2CO_3-Na_2S melts and the fuming rates were measured under N_2 and N_2-O_2 purges. Table 5 contains the fume generation rates from melts containing different levels of NaOH. Also shown in this table is the fume generation rate during sulfide oxidation with no NaOH present.

Table 5 Effect of NaOH on fume generation.

Temperature = 1228°K (1750°F)

Run No.	Initial Melt Composition			Purge		Fume Generation, g/min
	Na_2CO_3 mole	Na_2S mole	NaOH mole	O_2, L/min	N_2, L/min	
190	0.77	0	0.012	0	1.0	No fume measured
191	0.77	0	0.031	0	1.0	0.00006
192	0.77	0.03	0.010	0	1.0	0.0007
193	0.77	0.03	0.10	0	1.0	0.0007
194[a]	0.77	0.03	0.0	0.021	1.0	0.013
195	0.77	0.03	0.03	0.021	1.0	0.0048
196	0.77	0.03	0.06	0.021	1.0	0.0015

[a]Standard, no NaOH.

As illustrated in this table, the addition of NaOH does not result in a large amount of fume. The rate of fume generation from the two melts containing NaOH under a N_2 purge was an order of magnitude less than those obtained during the oxidation of the sulfide containing melts. At the levels of sulfide used in these experiments, the addition of NaOH suppressed the fume generation rate during sulfide oxidation.

Rate expression describing fume generation. During sulfide oxidation with the purge introduced below the melt surface a large quantity of Na_2CO_3 fume is generated. During this study the fume generation rate was found to be dependent on the nitrogen and oxygen flow rates to the reactor and on the melt temperature. The sulfate and sulfide concentrations of the melt had little effect on the fume generation rate. Therefore, the fume generation rate was described using the following rate expression.

Rate of fume generation, g/min =

$$K(N_2 \text{ Flow Rate, L/min})^M$$

$$(O_2 \text{ Flow Rate, L/min})^N e^{-\Delta E/RT} \quad (10)$$

Here K is a constant whose dimensions depend on the values of M and N;
M and N are powers to which the N_2 and O_2 flow rates are raised; and
ΔE is the activation energy.

The values of these parameters were determined using a nonlinear regression analysis program (10) and the data from 24 separate experiments. These experiments included a large range of oxygen and nitrogen flow rates and temperatures. Table 6 illustrates the values of the parameters in Eq. (10).

Equation (10) accurately describes the fume generation during sulfide oxidation over a wide range of experimental conditions. One of the more significant findings illustrated by this equation is the high dependence of the fume generation rate on the nitrogen flow rate relative to the dependence on the oxygen flow rate. The rate of fume generation is almost directly proportional to the nitrogen purge rate into the melt, but only proportional to the oxygen purge rate to the 0.27 power.

6

Table 6 Rate expression describing fume generation from a carbonate melt.

Rate of Fume Generation, g/min =

$$K(N_2, L/min)^M (O_2, L/min)^N e^{-\Delta E/RT}$$

Parameter, Value	Linear Estimate of Std. Dev.
K = 161	26
M = 0.907	0.096
N = 0.274	0.024
ΔE = 20,540 cal/mole	1,360 cal/mole

Purging Above the Melt

In this section fume generation experiments during sulfide oxidation with the purge gas introduced above the melt are described. This configuration allows the effects of mode of oxygen introduction and residue oxygen partial pressure on fume generation to be determined.

These experiments were conducted using the smaller radio frequency heated reactor. The oxygen-nitrogen purge was introduced into the steel retort approximately 6 centimeters above the surface of the melt. The fume generation rate was followed by the gravimetric method. In addition to measuring the weight of fume generated, the oxygen content of the off-gas was also measured. This allowed the rate of sulfide oxidation to be calculated.

Typical fume generation rates with a nitrogen-air purge located above the melt. Typical fume generation rates during sulfide oxidation with the purge located above the melt are illustrated in Fig. 8 and 9. Figure 8 illustrates the fume generation rates for low levels of oxygen in the purge. At these rates of oxidation, there is not much change in the melt composition, and the rate of fume generation remains essentially constant. In Fig. 9, the rates of fume generation for higher levels of oxygen in the purge are illustrated. At these rates of oxidation, the rate of fume generation decreases as the sulfide content of the melt is oxidized to sulfate.

The major findings illustrated by these figures are

1. The oxidation of a sulfide in a sulfide-carbonate melt with the oxygen introduced above the melt resulted in a decrease in the fume generation rates; only in extremely low levels of oxygen did the fume generation rate increase. This is in distinct contrast to sulfide oxidation with the purge introduced below the melt surface, which resulted in a large level of fume.

2. As the sulfide is oxidized, the oxidation rate and fume generation rate decrease. This contrasts to the constant oxidation rate and fume generation rate observed with the nitrogen-air purge introduced below the melt surface.

3. The fume generation rate was considerably less with the purge introduced above the melt than

with the purge introduced below the surface of the melt. Table 7 compares the fuming rate for sulfide oxidation with the purge introduced above the melt to the rate for the purge introduced below the surface of the melt. Since the fume generation decreases during sulfide oxidation when the purge is introduced above the melt, the initial rate of fume generation is shown for this configuration.

Fig. 8 Effect of O_2 concentration above melt on fume generation.

Fume Generation During Molten Metal Oxidation

During the oxidation of many molten metals, large amounts of metal oxide fumes are generated (11,12, 13). Since there are several similarities between these fuming systems and fuming during sulfide oxidation in a carbonate melt, a review of fuming during oxidation of molten metals is included here.

Metals in which the fuming of metal oxides during oxidation has been studied include Cu, Co, Mn, Ni, Fe and Cr (11). During oxidation an increase of several orders of magnitude is observed in the vaporization rate of these metals.

Another system in which an increase in fuming rate results from oxidation is the decarbonization of iron (13). Here, as the carbon content of the iron is oxidized, a large quantity of iron oxide fume is generated.

The increase in fuming during oxidation is attributed to the reaction of the metal vapor with

oxygen to form a condensed metal oxide fume. This may be considered to be a counterflux transport process. Here, oxygen diffuses toward the molten metal surface, and metal vapor diffuses away from the surface. At some distance from the surface, the metal vapor and oxygen react to form a metal oxide condensed phase, Fig. 10.

Fig. 9 Effect of O_2 concentration above melt on fume generation.

Table 7 Effect of oxidation on fume generation.

	Initial Conditions		
	Na_2CO_3 = 0.77 mole		
	Na_2S = 0.03 mole		
	Temperature = 1228°K (1750°F)		

Purge Introduced Below Melt		Purge Introduced Above Melt	
Oxidation Rate, moles O_2 consumed/min x 10^4	Fume Rate, g/min	Oxidation Rate, moles O_2 consumed/min x 10^4	Fume Rate, g/min
9.38	0.0106	0.84	0.00146
9.46	0.0134	3.88	0.00100
		7.80	0.00115
		12.00	0.00079
		17.70	0.00044

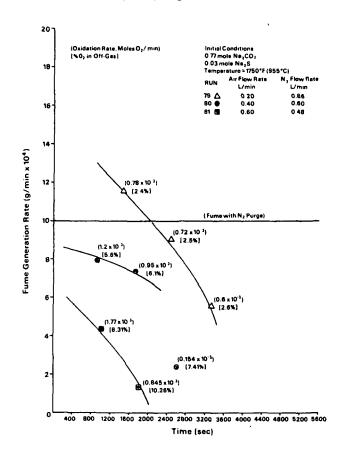In these systems, the rate of the metal vaporization is dependent on the rate of diffusion of the metal vapor away from the metal surface. For a molten metal with inert gas-oxygen mixture blowing across the surface, the rate of diffusion of the metal vapor is described by Eq. (11).

$$ J_m = \frac{D_m}{\delta RT} (p_m^* - p_m) \quad \text{moles/cm}^2\text{-s} \qquad (11) $$

Here, J_m is the molar flux of the metal vapor;
    D_m is the diffusivity of the metal vapor;
    δ is the distance from the metal surface where the metal oxide is being formed;
    R is the gas constant;
    T is the absolute temperature;
    p_m^* is the vapor pressure of the metal at the surface; and
    p_m is the partial pressure at δ where the metal oxide is being formed.

Oxidation Enhanced Metal Vaporization

Fig. 10 Gas phase oxidation enhanced vaporization.

Since $p_m \ll p_m^*$, Eq. (11) can be rewritten as

$$ J_m = \frac{D_m}{\delta RT} p_m^* \qquad (12) $$

A similar expression can be written for the flux of oxygen toward the metal surface. Oxygen diffuses from a distance above the melt, Δ, where the oxygen partial pressure is constant through an aerodynamic boundary layer to the area of the oxygen-metal vapor reaction, distance δ from the melt. The molar flux of oxygen toward the metal surface is then described by Eq. (13).

$$ J_{O_2} = \frac{-D_{O_2}}{(\Delta - \delta)RT} (P_{O_2} - P_{O_2}'), \quad \text{moles/cm}^2\text{-s} \qquad (13) $$

Here J_{O_2} is the molar flux of oxygen;
    D_{O_2} is the diffusivity of oxygen;
    P_{O_2} is the partial pressure of oxygen at distance Δ; and
    P_{O_2}' is the partial pressure of oxygen at distance δ from the partial melt surface.

Since $P_{O_2} \gg P_{O_2}'$, and $\Delta \gg \delta$, Eq. (13) can be written as:

$$ J_{O_2} = \frac{-D_{O_2} P_{O_2}}{\Delta RT} \qquad (14) $$

At distance δ, the metal vapor is reacting with oxygen to form the metal oxide. If one mole of metal reacts with one mole of oxygen, then $J_m = -J_{O_2}$. The flux of metal vapor from the metal surface is then described by Eq. (15).

$$J_m = \frac{D_{O_2}\, P_{O_2}}{\Delta\, RT} \qquad (15)$$

For an inert gas-oxygen mixture blowing across the melt, Eq. (15) predicts that the vaporization of metal should be directly proportional to the oxygen partial pressure in the gas phase at Δ.

The maximum rate of the metal vaporization with this mechanism is the equivalent to the rate of vaporization in a vacuum. At the maximum fuming rate, the metal oxide fume is forming at the metal surface. If the oxygen partial pressure is increased beyond this value, the flux of oxygen toward the metal surface is greater than the vaporization rate of the metal. Oxidation then occurs within the molten metal, forming a metal oxide film. This metal oxide film results in a significant decrease in the vaporization of the metal.

The dependence of fume generation on oxygen partial pressure for a typical molten metal is illustrated in Fig. 11. Here, an inert gas-oxygen mixture is passed over the melt and the rate of metal oxide fume generation is measured. As illustrated in this figure, the fume generation rate is initially proportional to the oxygen partial pressure in the gas phase. However, as the oxygen partial pressure is further increased, the fume generation rate abruptly falls to zero at a certain oxygen partial pressure. This sudden decrease in fuming results from oxidation of the metal within the melt, forming a layer of metal oxide at the metal surface. This metal oxide film effectively prevents metal evaporation.

Fig. 11   Effect of oxygen partial pressure on metal vaporization.

Vapor Phase Oxidation Enhanced Fuming During Sulfide Oxidation

One explanation for the fuming behavior observed during sulfide oxidation is that the mechanism responsible for fume generation during sulfide oxidation in a carbonate-sulfide melt is similar to that for fume generation during oxidation of the molten metals. With this mechanism, the Na_2CO_3 fume from sulfide oxidation in a Na_2CO_3-Na_2S melt results from the reaction of Na vapor with O_2 above the melt to form Na_2O, Eq. (16). The Na_2O then reacts with CO_2 to form Na_2CO_3, Eq. (17).

$$2\ Na(v) + 1/2\ O_2 \longrightarrow Na_2O(s) \qquad (16)$$

$$Na_2O(s) + CO_2 \longrightarrow Na_2CO_3(s) \qquad (17)$$

The formation of Na_2O decreases the partial pressure of Na above the melt. Since the driving force for Na vaporization from the melt is the difference between the vapor pressure of Na at the surface of the melt and the partial pressure of Na in the gas phase, this reduction of the partial pressure of Na increases the driving force for Na evolution and hence the fuming rate. In this mechanism, fuming occurs principally at low oxygen partial pressure. At high oxygen partial pressure, oxidation of Na occurs in the melt instead of in the gas phase, resulting in little fume generation.

DISCUSSION

Two hypotheses were proposed to explain fuming. At this time neither has been conclusively proven or discarded. The first is based on the presence of oxide intermediates, both in the melt and the gas phase. The second hypothesis is based on mass transfer between a gas bubble and the melt surface. Experimental work is currently in progress to define the role of these two mechanisms in fume generation.

CONCLUSIONS

(1) These results demonstrate that there are several modes of fuming in melt systems similar to those in a recovery furnace. The most important source of fume may be the oxidation of sulfide.

(2) In comparison to the level of fume generated during sulfide oxidation, the vaporization of NaOH is a minor source of fume.

(3) There are at least two possible explanations for fume generation during sulfide oxidation. The actual mechanism for fume generation during sulfide oxidation may be one of these mechanisms, an entirely new mechanism, or a combination of these mechanisms.

LITERATURE CITED

1. MacDonald, R. G., Pulp and Paper Manufacture. The Pulping of Wood, 2nd edition, Volume I, McGraw-Hill, New York (1969).

2. Reeve, D. W., et. al., _Tappi_, **64**(5): 109
    (1981).

3. Rizhinshvili, G. V., and Kaplun, L. V.,
    Bumazh. Prom. (Moscow), **1**: 26(1983); Available
    Inst. Paper Chem. Translation No. T-2260.

4. Spanbauer, J., _Southern Pulp Paper_, Nov.,
    1982:14.

5. Warnqvist, B., _Svensk Papperstid._ (Stockholm),
    76(12): 463(1973).

6. Lovering, D. G. _Molten Salt Technology_,
    Plenum Press, New York (1982).

7. Andresen, R. E., _J. Electrochem. Soc._, **126**(2):
    328(1979).

8. Fryxell, R. E., Trythall, C. A., and Perkins,
    R. J. Corrosion-NACE 29 (11): 423(1973).

9. Andersen, B. K., _Acta Chem. Scand._
    (Copenhagen), A31: 242(1977).

10. Dye, J. L., and Nicely, V. A., _J. Chem. Education_, **48**: 443(1971).

11. Turkdogan, E. T., Grieveson, P., and Darken,
    L. S., _J. Phys. Chem._, **67**: 1647(1963).

12. Turkdogan, E. T., _Physical Chemistry of High
    Temperature Technology_. Academic Press, New
    York, 1980.

13. Turkdogan, E. T., Grieveson, P., and Darken,
    L. S., Proc. Natl. Open Hearth Steel Con.,
    470(1962).

Status Report

FUNDAMENTAL PROCESSES IN ALKALI RECOVERY FURNACES

Black Liquor Burning

INTRODUCTION

NEED

The energy and chemical value of kraft black liquor needs to be efficiently and safely recovered. At the same time, the total black liquor processed should meet or exceed its production rate from pulping. Satisfying these needs becomes the three major objectives of the chemical recovery boiler.

The high capital intensity of chemical recovery boilers often results in mill production being limited by the recovery boiler, i.e., the recovery boiler is the pulp mill production bottleneck. Under these circumstances a compromise in objectives must be made. At the present time, compromises such as the one above must be made with only limited supporting data on the burning characteristics of black liquor. The present task will document a wide range of black liquor burning phenomena, with the hope of providing a consistent data base to aid in making such decisions.

OBJECTIVE

The objective of this task is to characterize black liquor burning. The burning phenomena will be observed and documented. A battery of analytical and process related tests will be used and/or developed for this purpose. Finally, mill liquors covering a wide range of test variables plus a few synthetic liquors will be included in this study.

BACKGROUND

The burning characteristics of black liquor at a particular mill can significantly vary. The ratio of hardwood to softwood or the ratio of semi-chemical liquor to kraft liquor are two variables that reportedly influence burning. The most extensive burning characteristic study to date has been by Hupa (1985). Hupa divides combustion into four stages: drying, combustion of volatiles, char burning, and inorganic reactions. He has shown that the required time for the first three stages varies significantly with initial droplet diameter, furnace temperature, and liquor type. The char burning stage was the critical one for distinguishing "good" and "bad" burning liquors. Hupa found that increased liquor swelling during formation of volatiles tended to decrease char burning time, i.e., more "good" burning. Levels of Na_2SO_4, tall oil, and pH were all shown to influence swelling.

Miller (1985) at IPC has reported the influence of both physical and chemical variables on black liquor swelling. The most significant variables affecting swelling were initial liquor solids content, temperature, the ratio of kraft lignin to hydroxy acids, and the extractives content. These variables in some way influence the rheology of pyrolyzing liquor solids so that, as pyrolysis gases escape, chars with different swollen volumes remain. This continuing student thesis work will be reported in more detail at the PAC meeting.

WORK TO DATE

The IPC funded research task on black liquor burning began in the Spring of 1984. Initial results of reaction times to reach maximum swollen volume and final smelt bead coalescence for a single liquor were reported at the

1984 Fall PAC meeting. Three test conditions and four measurement methods were
outlined to study the burning characteristics. A key finding in this preliminary
work was that droplets less than 8-10 mg (~ 2.4 mm in diameter) proceeded in
sequence through the four stages of combustion. This confirmed the work of
Hupa (1985). However the first three sequences were not at all clearly separated
for particles greater than this size. This latter finding is in sharp contrast
to Hupa's work, which for all sizes reported sequential steps. The basic dif-
ference may be in the gas velocity past the particle. The IPC tests had air
velocities of 2.8 m/s (9 ft/sec), while Hupa's work used stagnant air. Furnace
conditions probably include both regimes as well as combinations of them.

Test results for 14 different mill liquors were presented at the 1985
Spring PAC meeting. The number of desired tests per liquor had expanded to 10
by this time. The preliminary results of the work at this point were:

a. The swollen volume of the liquor solids during pyrolysis
   correlated best with original liquor residual active alkali.

b. Two liquors behaved significantly differently in all tests
   than others.

c. Sulfur dioxide released during pyrolysis correlated with
   the swollen volume and the residual active alkali.

d. The swollen volume was not significantly related to the
   heating value, sulfated ash or the percent volatilized.

Although these results were based on a small sampling which contained
significant scatter, the test methods and range of liquor test results appeared
reasonable. During the last six months the total number of liquors tested
increased to 26. Twenty nine (29) liquor samples have been received. Some

additional test measurements were also added. The test methods and results are reported in the remaining sections of the report.

<div align="center">APPROACH</div>

LIQUOR SAMPLES

Black liquor grab samples were collected at individual mills by operating or technical mill personnel. The guidelines given to the mills by IPC were:

a. The pulp mill and recovery system should be in a relatively stable operating condition.

b. The collection point should be either after the concentrator for a low odor design or before the cascade/cyclone evaporator in a direct contact design. In either case it should be before salt cake recycle addition.

c. One quart of liquor per sample should be submitted.

d. A completed questionnaire was to be returned with each sample. This listed general pulp mill conditions and a qualitative assessment of how well the liquor burns.

There were some cases where not all of the guidelines were met. Several mills sent more than one liquor sample. Many times in these cases the samples represented different ratios of hardwood liquor to softwood liquor. When the samples arrived at IPC they were placed in a 12°C (54°F) cold room where they remained until needed for testing.

ANALYSES

Liquor analyses were divided into three groups. These are listed below.

Process measures

    a. High heating value
    b. Sulfated ash
    c. Residual active alkali

Composition measures

    a. NaOH
    b. Na_2S
    c. Na_2CO_3
    d. Na_2SO_4
    e. Solids content

Elemental analyses

a.	Na	e.	C
b.	K	f.	H
c.	S	g	O
d.	Cl		

With the exception of the elemental analysis for C, H, and O, all measurements are made by IPC Analytical. The C, H, and O measurements were done only on selected samples. These were determined by Huffman Laboratories, Wheatridge, Colorado. Test procedures and results of screening are listed in Appendix I.

COMBUSTION TESTS

Combustion tests were performed on liquor aliquots which were between 62-76% solids content. A summary for the solids method used is given in Appendix I. The combustion tests performed with the liquors were developed at IPC. These are listed below.

    a. Pyrolysis specific swollen volume
    b. Pyrolysis average rate
    c. Pyrolysis specific reaction time
    d. Combustion average rate
    e. Reaction time from ignition to maximum specific
       swollen volume

      f.   Reaction time from ignition to smelt bead coalescence
      g.   Gas concentration maximum under pyrolysis and
           combustion conditions.

Appendix II contains a description of each one of these tests. All questionnaire and test data will be stored in an INSYTE data base for easy access, analysis, and expansion.

COMBUSTION TEST EQUIPMENT

The IPC single particle reactor (SPR) was used for most of the combustion tests. Figure 1 is a cross section of the SPR.

SINGLE PARTICLE REACTOR

Microbalance

Alumina Tube

Gas In ← From Heater

Flow Straightener

Gas Bypass ←

Sample

lower unit (moveable)

Optical Trench ⊥ to Diagram

Gas Out to Analyzers

Insulation

Note: All gas passages are 50mm x 50mm

Figure 1. Gravimetric-convective single particle reactor (SPR).

The reactor convectively heats the particles in a hot gas stream. The maximum gas temperature in the particle zone is 900°C (1650°F). Dampering and a pneumatically positioned lower reactor zone enables rapid heating of the particle to the gas temperature. Heat flux measurements during water evaporation show fluxes up to 30,000 Btu/h-ft^2. These fluxes are comparable to those measured on wall tubes in a recovery furnace. Infrared pyrometer measurement of the burning particle showed a temperature of 1150°C (2100°F). Periodically the holding wire for the liquor also burns through. Its melting point is 1340°C (2450°F). These temperatures are comparable or slightly higher than those in a recovery furnace. Phenomena occurring in the recovery furnace should be observable in the SPR.

The SPR is equipped with a microbalance for real time mass tracking. A 51 x 51-mm (2 x 2-inch) optical trench allows photographic documentation of the burns. Gas analysis equipment is available for CO, CO_2, SO_2, O_2, H_2O, and Na fume measurements.

A second radiant heater is used for maximum SO_2 emitted during pyrolysis. The radiant particle furnace is shown in Fig. 2. Its primary use has been in sulfur release studies reported under Project 3473-6 and in a student M.S. thesis project by James Cantrell. Gas temperature in the radiant furnace can exceed 1090°C (2000°F). The entire gas flow is sent to the SO_2 analyzer. Gas sweep velocities are approximately 0.01 m/s @ 500°C (0.04 ft/s @ 932°F) at nominal rates of 300 standard mL/min (0.011 scfm).

RADIANT SINGLE PARTICLE REACTOR

Gas Outlet

Removable
Reactor Cover

Mullite Reactor
Tube 21½ in. x 1⅝ in. ID.
Heated Length 13 in.

sample
support
rod

8 in.

13½ in.

sample

3½ in.

Electric Heater

Ceramic Packing

Type K Thermocouple

Gas Inlet

Figure 2.   Radiant single particle reactor.

RESULTS

LIQUOR SAMPLES

Thirty liquor samples have been obtained for study. Twenty-nine (29) are mill samples and one is a synthetic liquor. The range of collected liquor sources is shown in Table 1. As more samples become available they will be added to the data base.

Table 1. Black liquor source characterization.

Number: 29 mills
                1 synthetic

Mill locations: 17

Country: U.S. (all regions), Canada, Brazil

Wood supply: softwood, hardwood, mixture

Type of liquor: kraft (26), NSSC (1), soda (2)

Digester kappa No.: hardwood 9-42
                          softwood 21-80

Oxidized: yes and no

Burning assessment: good to poor

The synthetic liquor was produced by Paul Miller for his thesis work.
The cooking conditions are listed in Table 2.

Table 2. Synthetic liquor cooking conditions.

Sulfidity – 25%	Time to temperature – 90 min
Effective alkali – 16%	Time at temperature – 94 min
Liquor to wood – 4/1	Cooking temperature – 173°C (343°F)
% Solids–wood – 94%	H-factor – 2000

Yield	45.7%
Kappa No.	25.7
B. L. Solids	16.5%

The 29 liquors showed a wide range of results in the analytical
analyses and combustion tests. Table 3 shows the variable ranges for liquors
collected from kraft mills. The soda, NSSC, and synthetic liquors are not
included in this tabulation. The NA means that these variable measurements are
not complete and that the ranges are "not available" yet.

Table 3. Black liquor survey measured variable range.
          (Kraft mill only.)

Process measures

       a. High heating value   5080-6840 Btu/lb
       b. Sulfated ash   NA
       c. Residual active alkali   0-13 % ODS as Na_2O

Composition measures (% ODS)

       a. NaOH   0-14.5
       b. Na_2S 0-6.0
       c. Na_2CO_3 5.1-12.5
       d. Na_2SO_4 0.95-9.5

Elemental analyses (% ODS)

       a. Na   16.8-21.0   e. C   34.0-40.9
       b. K   1.0-3.0   f. H   3.2-4.0
       c. S   3.5-6.8   g. O   29.7-35.6
       d. Cl   0.21-5.5

     Note: C, H, O only on 9 samples

Combustion tests

       a. Pyrolysis specific swollen volume   7.2-172 cc/g-S
       b. Pyrolysis average rate $0.015-0.029 \text{ sec}^{-1}$
       c. Pyrolysis specific reaction time   0.66-1.4 sec/mg-s
       d. Combustion average rate   NA
       e. Rxn time from ignition maximum volume 1.6-3.4 sec
       f. Rxn time from ignition to coalescence 3.0-5.2 sec
       g. Gas concentration maxima   NA

       The results presented below should be taken as preliminary. As will be

evident later, our knowledge is not yet sufficient to fully identify all possible

measurement errors. Further work will be done to improve the data in this regard.

ANALYSES AND TESTS

       Statistical analysis of all the data produced no obvious single

variable that consistently influenced the combustion test parameters. One

qualifier to this statement is the effect of both heating value and sulfated ash. An insufficient number of these values were available for inclusion at the time of analysis. They should be included by the time of the PAC meeting.

The variables that had the best correlation with the combustion test parameters are listed in Table 4 along with the associated correlation coefficient, r^2.

Table 4. Variables best correlated with combustion test parameters. (Only variables with $r^2 > 0.50$ are listed.)

Combustion Parameters	Variables	r^2
Time from ignition to max volume	Time IG-SB	+0.83
	Na_2CO_3	+0.74
	Solids	-0.58
Time from ignition to smelt bead	Time IG-MV	+0.83
	Time MV-SB	+0.64
	Kappa No.	+0.60
	Hardwood amt.	-0.59
Swollen volume	Na_2SO_4	-0.69
	Time MV-SB	+0.61
	Kappa No.	-0.61
	Pyrolysis time	-0.53
Pyrolysis rate	Solids	-0.52
Pyrolysis time	Swollen volume	-0.53
Time from max volume to smelt bead	Kappa No.	+0.73
	Time IG-SB	+0.64
	Swollen volume	+0.61
	Hardwood amt.	-0.54

It is interesting to note that very few of the composition or elemental analysis measures related consistently to anything in this overall look. There are, however, important additions to this overall initial screening. These are presented below as we discuss the individual data graphs.

Swollen Volume. The specific swollen volume was reported previously to be positively influenced by the liquor residual active alkali. Additional survey results confirm this behavior. However, they also show that this is by no means the only significant variable. The residual active alkali results were separated into its two components, Na_2S and $NaOH$. The $NaOH$ content was the component that caused the variation. The remaining discussion will focus on the influence of $NaOH$.

Figure 3 shows an apparent wide scatter in the data. The top + data point (No. 14) and the left-most * data point (No. 1) were previously suggested as different in some way from other liquors. The second highest + data point (No. 15), obtained since the original, is also different. Liquors 14 and 15 have Cl/S ratios of 1.2 and 0.74, respectively, while the remaining kraft mill liquors have Cl/S which average 0.11 ± 0.04 (1 standard deviation) with one exception. Liquor 16 is the exception with a Cl/S of 0.58. Its swollen volume (+ Cl @ 100 cc/g S) appears to fall in the normal population. The other apparent different liquor is No. 1, which is a eucalyptus liquor. A later second eucalyptus sample No. 22 (* @ 92 cc/g S) fell within the majority of the other liquors. Liquor 18 (# right-most at 50 cc/g S) is vastly different than the others. At worst there is an analytical error. This will be checked. At best it suggests that there may be a maximum in the swollen volume vs. NaOH relationship. Note that the three all hardwood data points (#) show this trend. It is encouraging to note that Paul Miller's thesis work has also found a maximum in swollen volume with pH.

The other variable which significantly influenced pyrolysis swollen volume was the percent Na_2SO_4. Figure 4 shows that the swollen volume decreases

as Na_2SO_4 increases. Note again the outliers on the right side (No. 14, 15, and 18). Miller and Hupa both have reported the detrimental effect of inorganics on swelling. Their work suggests a simple dilution effect. The survey results suggest a stronger influence below 5%. The influence of both Na_2CO_3 and the sum of Na_2CO_3 and Na_2SO_4 was checked on swollen volume. There was no significant correlation with Na_2CO_3, and a weaker one with the sum.

BLSURVEY

Figure 3. Pyrolysis specific swollen volume vs. NaOH in initial black liquor solids.

BLSURVEY

Figure 4. Pyrolysis specific swollem volume $\underline{vs}$. Na$_2$SO$_4$ in initial black liquor solids.

Total Burn Time. The time from ignition to the final smelt bead coalescence (total burn time) had a variable dependence on the maximum swollen volume produced in pyrolysis. This dependency is shown in Fig. 5. The parameters that appear to influence this plot are the amount of NaOH and the Cl/S ratio. At low NaOH, lower swollen volumes are obtained. The two left-most data (0, No. 6 and 7) have sharply longer burn times than liquors with SV above 40 cc/g S. Below 40 cc/g S total burn time decreases as the swollen volume increases. Above 40 cc/g S the total burn time in general increases with swollen volume. There is an exorbitant amount of scatter in these data, but we think the trend is correct. Further work will be done to explain and will hopefully reduce the scatter. The high Cl/S liquors (No. 14 and 15) are again outliers.

Their shorter time for a given swollen volume may be because ignition occurs more rapidly. Kubes has shown that char ignition temperatures are lowered with a chloride increase in mill liquors up to 3% Cl. Since the third chloride liquor (No. 16) behavior does not show this trend even though it has 3.5% Cl, this data point is suspect.

Figure 5. Total burn time (ignition to smelt bead coalescence) vs. pyrolysis specific swollen volume.

Pyrolysis Time. The time from ignition to maximum swollen volume during combustion (pyrolysis time) was significantly related to the Na_2CO_3 content of the liquor. Figure 6 shows that the pyrolysis time increased as Na_2CO_3 increased for mill liquors. The one outlier on this plot (No. 26 + @ 1.9 sec) is the synthetic liquor. There was no significant difference between wood species data or between the liquor oxidation status. Na_2SO_4 or the sum of $Na_2SO_4 + Na_2CO_3$ was not a significant influence.

BLSURVEY

Figure 6.   Pyrolysis time (ignition to maximum volume during combustion)
vs. Na$_2$CO$_3$ in initial black liquor solids.

Char Buring Time.   The time from maximum swollen volume to final smelt

bead coalescence depended significantly on Na$_2$SO$_4$.   Figure 7 shows this depen-

dence.   The other influencing parameters were wood species and Cl/S ratio.   All

the data suggest that char burning time decreases with the added Na$_2$SO$_4$.   The

influence of the Cl/S ratio was to reduce the time at a given ratio.   Liquors

16, 15, and 14 had successively higher Cl/S ratios and also lower char burn

times.   The overall trend to lower times at higher Na$_2$SO$_4$ levels is consistent

with the kinetic findings of Grace (1985).   His work showed that higher initial

sulfate levels did produce higher sulfate reduction rates and hence higher char

burning rates.   Finally, the last trend was that softwood liquors (+) had longer

char burn times than hardwood (#) liquors.

Figure 8. Pyrolysis time at 500°C (932°F) vs. pyrolysis specific swollen volume.

Figure 7. Char burning time (maximum volume to smelt bead coalescence) vs. Na₂SO₄ in initial black liquor solids.

Other Trends. The pyrolysis time in nitrogen in general was shortest for liquors which produced the largest swollen volume. Figure 8 shows the trend with a significant amount of data scatter.

The specific rate of solids mass loss during the nitrogen pyrolysis depended most heavily on the initial droplet solids content. This is shown in Fig. 9. No significant trend of other parameters was noted. Since liquors were burned over this solids range, some of the scatter in the earlier plots may be from solids variation. This is additional information that is consistent with the findings of Moreland (1985) that varying solids do influence combustion even though the water has left the sample prior to combustion.

Figure 9. Pyrolysis rate at 500°C (932°F) vs. the tested black liquor solids content.

Tests on the remaining combustion parameters are incomplete. More should be available at the time of the PAC meeting.

DISCUSSION

The presented results provide a starting point for understanding the phenomena of black liquor burning. The survey has generated a wide range of liquor composition. The existing and developed tests have provided some insights on why liquors have wide differences in burning behavior. The results to date, however, do not fully explain all the differences. There are still many discrepancies within narrow data sets.

Black liquor burning of the survey samples, despite wide differences in specific burning parameters, does proceed in the four stages outlined by Hupa. The drying, combustion of volatiles, char burning, and inorganic reactions can, however, be very different between liquors. Our work to date suggests that the levels of NaOH, Na_2SO_4, Na_2CO_3, NaCl, and initial solids content can influence various aspects of the burning phenomena. No one single variable controls the burning phenomena. There are undoubtedly other significant parameters which have not yet been identified. To date we do not yet have a single test that alone will characterize black liquor burning.

The potential to explain more of the burning phenomena exists. The present results together with cooperative student research will suggest the direction of the next work phase. This will be expanded upon at the October PAC meeting.

REFERENCES

Grace, T. M.; Cameron, J. H.; Clay, D. T. Role of the sulfate/sulfide cycle in char burning - experimental results and implications. Proceedings of the 1985 International Recovery Conference, New Orleans, 3:371(April, 1985).

Hupa, M.; Solin, P.; Hyöty, P. Combustion behavior of black liquor droplets.
    Proceedings of the 1985 International Recovery Conference, New Orleans,
    3:371(April, 1985).

Miller, P. T. Ph.D. Thesis Project Reports, IPC, 1984 and 1985.

Moreland, B. A.; Clay, D. T. The influence of water on black liquor combustion.
    To be presented at the 1985 TAPPI Pulping Conference, November, 1985.

THE INSTITUTE OF PAPER CHEMISTRY

David T. Clay
Research Associate
Recovery Group
Chemical Sciences Division

Ronald J. Kapheim
Research Associate
Recovery Group
Chemical Sciences Division

APPENDIX I

TEST PROCEDURES

Process measures

     a. High heating value - essentially TAPPI Test Method T 684 pm-84.

     b. Sulfated ash - TAPPI Test Method T 625 ts-64.

     c. Residual active alkali - TAPPI Test Method T 625 ts-64.

Composition measures

     a. NaOH - calculated difference between residual active alkali and Na_2S.

     b. Na_2S - NCASI Technical Bulletin No. 68.

     c. Na_2CO_3 - Ion chromatography exclusion.

     d. Na_2SO_4 - TAPPI Test Method T 699 pm-83.

     e. Solids - Surface area extended via ignited sand. Dried at 105°C (221°F) in a forced air convection oven for at least 6 hours, preferably overnight.

Elemental analyses

     a. Na - perchloric acid digestion followed by flame emission.

     b. K - same as Na.

     c. S - Schoniger flask oxidation followed by TAPPI Test Method T 699 pm-83.

     d. Cl - TAPPI Test Method T 699 pm-83.

     e. C - Measured by Huffmann Laboratories, Wheatridge, Colorado.

     f. H - Same as C.

     g. O - Same as C. Merz modification.

SCREENING OF RESULTS

Process Measures

     Tests done in at least duplicate. Values for HHV with standard deviation of 100 or less were accepted. Sulfated ash not available yet. Residual

active alkali values with standard deviation of $< \pm 0.2$ for liquors 1-15.

Single determination for liquors 16-29.

Composition Measures

NaOH was the same as active alkali. Na_2S for the most part was single

determination; selected samples were done in duplicate or triplicate. Na_2CO_3

and Na_2SO_4 were single point determinations.

Elemental Analyses

Na and K were single dilutions and at least duplicate aspirations into

FE detector. S and Cl were single determinations. C, H, O were single deter-

minations.

APPENDIX II

COMBUSTION TESTS

Pyrolysis Specific Swollen Volume

A black liquor droplet at room temperature and nominally 40 mg in total

mass is suspended on a wire within a wire spiral. The solids have been measured.

The sample is hung from the Cahn microbalance in the convective SPR (Fig. 1).

The reactor is sealed, then 500°C (932°F) N_2 flows over the droplet. Photographs

are taken as the droplet swells. The particle maximum volume is determined from

the largest area measurement of the photographs. The calculated swollen volume

is that of a sphere with the same measured frontal area. Dividing this volume

by the original mass of the droplet solids yields the specific swollen volume.

Pyrolysis Average Rate

During the pyrolysis described above the microbalance records the

droplet mass loss. The mass loss is approximately linear. The slope of the

mass loss vs. time plot divided by the mass of the initial solids is the pyrolysis average rate. The wire spiral around the droplet maintains a relatively constant drag despite a changing particle size.

Pyrolysis Specific Reaction Time

This is the time, extracted from the mass loss vs. time curve, when the slope has been linearized.

Combustion Average Rate

The same procedure described above is done, except in air, with nominally an 8 mg droplet and at 800°C (1472°F). The slope of the mass loss vs. time curve, near the end of the burn, is linearized. This is during the char burning. The slope divided by the mass of the initial solids is the combustion average rate.

Reaction Time from Ignition to Maximum Volume

During the combustion tests described above black/white films (@ 64 fps) were taken of the droplet burns. The time from ignition to the maximum volume was obtained by measuring film length. This was converted to time.

Reaction Time from Ignition to Coalescence

This is similar to the previous time. It is the time from the maximum volume until the char mass collapses into a tight smelt bead. The first appearance of the smelt bead is the measurement point. This continues to glow for some time until the inorganics are fully oxidized. The difference between this time and the time to maximum volume is the char burning time.

Gas Concentration Maxima

These results are not fully analyzed. The procedure is still under development. We anticipate measuring at least the gases SO_2, CO, and CO_2.

THE INSTITUTE OF PAPER CHEMISTRY

Appleton, Wisconsin

Status Report

to the

PULPING PROCESSES

PROJECT ADVISORY COMMITTEE

Project 3473-6

FUNDAMENTAL STUDIES OF BLACK LIQUOR COMBUSTION

(DOE FUNDED PROJECT)

August 26, 1985

PROJECT SUMMARY FORM

DATE: August 26, 1985

PROJECT NO. 3473-6:   FUNDAMENTAL STUDIES OF BLACK LIQUOR COMBUSTION
                      (DOE FUNDED PROJECT)

PROJECT LEADER: D. T. Clay

IPC GOAL:

Develop fundamental data on black liquor combustion which can be used to enhance
energy efficiency and productivity of recovery boilers.

OBJECTIVES:

The three main objectives are

a) To develop laboratory scale flow reactor systems which will enable the study
    of both state-of-the-art and advanced recovery systems

b) To study gas phase and char bed mechanistic processes under realistic and
    controlled environments with advanced optical and spectroscopic techniques

c) To develop a data base which will bridge the gap between ongoing fundamental
    research and commercial application of the resultant findings, culminating
    in increased thermal efficiency, productivity, and capital effectiveness

CURRENT FISCAL BUDGET (Dec. 1, 1984 through Dec. 31, 1985:

$904,000(Contract with DOE, OIP) ($340,000 of this will be a subcontract to the
National Bureau of Standards, NBS)

SUMMARY OF RESULTS SINCE LAST REPORT:

This is the first written reporting of the project to PAC. Significant project
background is included in the Introduction section. The first Progress Report
to DOE will be issued in October 1985. The attached report includes both high-
lights from this report and more recent test work.

Operating versions of two reactor systems, one at IPC and one at NBS, are in
place. Test data are being obtained from both. Continuous droplet formation
and injection at low flow rates into hot gas environments have been accomplished.
Initial droplet residence times, sulfur loss, and fixed and lost carbon were
measured and related to test variables during char formation tests.

Pyrolysis chars and gases were generated in two single particle reactors. The
equilibrium mass, carbon loss, and sulfur loss as a function of temperature were
determined. The identity and quantity of pyrolysis gases as a function of
solids, particle size, and moisture content were determined.

The flow reactor tests indicate that some modifications are needed. Particles can
either fall through the reactor partially pyrolyzed, or, if pyrolyzed, expand and
stick to the wall. Flow and temperature changes are being considered.

The single particle test results, supported by char chemistry measurements from the flow reactor, show that during pyrolysis reduced sulfur gases can be readily released at low temperatures. At higher temperatures the released reduced sulfur is substantially less, while the hydrocarbon gases are the major component of the pyrolysis gases. The specific gases released suggest key changes in the particle chemistry.

PLANNED ACTIVITY THROUGH FISCAL 1986:

The Phase 1 reactors at both IPC and NBS will be completed. Char formation and characterization will be done. Photographic documentation of the initial in-flight processes will be made. Variables influencing droplet size and repetition rate from the injector will be studied.

FUTURE ACTIVITY:

Initial design of the char bed module.

Complete characterization of the in-flight processes (Phase 1).

Status Report

FUNDAMENTAL STUDIES OF BLACK LIQUOR COMBUSTION

INTRODUCTION

The efficient recovery of chemicals and high level energy from black liquor contributes heavily toward the dominance of the kraft pulping process. Kraft chemical recovery boilers used to burn black liquor have been commercially available for approximately 50 years. Potential still exists for significant improvements in energy recovery and black liquor throughput. This project addresses both areas.

The identified industry-wide potential energy benefits amount to over 2 x 10^{13} Btu/year, an approximate value of $100,000,000/year at $5/$10^{6}$ Btu. Since the energy benefits are achieved through process condition changes, these same changes can potentially increase black liquor solids throughput. For recovery boiler bottlenecked mills, pulp production should increase as solids throughput increases. This is especially significant, since the high capital intensity of recovery boilers often results in mill production being limited by recovery boiler solids throughput. An industry wide production increase of 1% corresponds to an approximate value of $100,000,000/year. This project, in close cooperation with other complementary IPC projects, seeks to provide process understanding that will assist in achieving both energy and productivity benefits.

Project 3473-6 is fully funded by the Department of Energy, Office of Industrial Programs. The Institute of Paper Chemistry, Chemical Recovery Group, has prime contract responsibility to DOE. The National Bureau of Standards, Combustion Metrology Group, has a subcontract with IPC for a significant portion of the project work.

The project's three objectives focus on advancing kraft recovery boiler technology. First, develop test systems to study both state-of-the-art and advanced recovery processes. Second, apply advanced optical and spectroscopic techniques to study the burning processes. Third, develop a data base of process fundamentals which will bridge and enhance prior research findings and their commercial application.

The recovery processes of interest include all those that occur within a recovery boiler. Drying, pyrolysis, gasification, oxidation, reduction, and fuming will be studied with conditions similar to the recovery boiler. The two distinctive conditions are: first, reacting particles in flight from the liquor spray to the char bed at the bottom of the furnace; second, reacting particles on or within a char bed. These two conditions form the basis for the first two phases of the project. The last two phases focus on fume formation and the simultaneous study of all process steps.

The four phases are specifically:

Phase 1. In-flight chemical and thermal processes

Phase 2. Char bed processes

Phase 3. Inorganic fume formation processes

Phase 4. Recovery furnace simulation

Phase 1 lasts nominally two years, since the initial part involves reactor design and construction. This report covers the first 22 months of Phase 1 (through July, 1985). The remaining phases each extend nominally one year, resulting in a total contract length of five years. Figure 1 summarizes the 5-year plan.

FUNDAMENTAL STUDIES OF

BLACK LIQUOR COMBUSTION

PROJECT SCHEDULE

YEARS FROM PROJECT START

	Start	1	2	3	4	5	
Phase I.	In Flight Processes						
Phase II.	Char Bed Processes						
Phase III.	Inorganic Fume Formation						
Phase IV.	Recovery Simulation						

Figure 1. Five year project schedule. Project began September, 1983.

At the writing of this report the initial modules of the Phase 1 reactor systems are operational at both IPC and NBS. Both units have successfully injected droplets via the NBS-developed droplet generator into their respective reactor modules at high temperature. NBS is developing data to characterize droplet formation from its injector. IPC is evaluating the droplet trajectory, temperature and velocity profiles, and char characterization (chemical and physical) under pyrolysis conditions. This report will discuss the developed equipment and the above mentioned tests. The first Progress Report to DOE (January, 1985) contains more details in each of the areas with the exception of the tests. The tests are covered in depth in this report.

APPROACH

MILESTONES

Each of the four phases has specific project milestones. Table 1 lists the current milestones. The first four in Phase 1 are complete. Milestones 5 and 8 are where the present work focuses.

The first four plus 6 and 7 involve extensive equipment design, construction and startup. The remaining ones cover tests to understand the in-flight processes. The equipment, process flows, and initial tests will be outlined below.

Table 1. Project milestones - Phase 1.

Milestone	Target Completion by End of Year.Quarter
In-Flight Chemical Processes	
1. Reactor preengineering	84.1
2. Preliminary combustion experiments	84.3
3. Phase 1 reactor detailed engineering	84.4
4. IPC reactor central units and NBS reactor first modules installed	85.2
5. Reactor temperature/flow/droplet characterization	85.3
6. Phase 1 reactors completely installed	85.4
7. Phase 1 reactors fully operational	86.1
8. Process and diagnostic tests, liquid feed	86.2
9. Process and diagnostic tests, solid feed	86.3
10. Phase 1 report	86.4
Phase 2 - Char Bed Processes	
1. Design of char chamber	85.4
2. Installation of char chamber	86.3
3. Char oxidation and reduction tests (IPC)	87.3
4. Above-bed diagnostics (NBS)	87.3
5. Phase 2 report	87.4
Phase 3 - Inorganic Fume Formation Processes	
1. Design of fume equipment	87.1
2. Installation of fume equipment	87.2
3. Gas phase reaction tests (NBS)	87.4
4. Fume formation tests (IPC)	87.4
5. Phase 3 report	88.1
Phase 4 - Recovery Furnace Simulation	
1. Process variables interaction tests	88.1
2. Control strategy tests	88.2
3. Next generation tests	88.3
4. Final report (draft)	88.3

EQUIPMENT

Two continuous laboratory reactor systems, one at The Institute of Paper Chemistry (IPC) and one at the National Bureau of Standards (NBS), will be the equipment used to study the burning processes. This equipment will be supplemented with existing bench reactors (single particle, molten salt, etc.) at IPC as needed. NBS will complement its reactor system with existing advanced diagnostic instrumentation. Although the basic scaling parameters (gas flow, reactor length and diameter, and temperature) are similar, important differences exist (gas heating system, black liquor flow rates, and optical access), which reflect each system's objective.

The IPC system will be used for overall process studies and complete furnace simulation. The burning processes to be tested under continuous flow conditions include drying, pyrolysis, gasification, reduction, oxidation, and fuming. These will be tested both individually and together. The design flow rate [nominally 10 lb/h (4.5 kg/h)] of black liquor solids coupled with the equipment design is sufficient to produce conditions similar to those found in recovery furnaces. The nominal gas flow rate is 12 scfm (0.34 Std. m^3/min).

The NBS system will be the test bed for instrumentation, development, and diagnostic tests. These studies will include flowing single particle and gas phase intermediate work. The NBS studies will also validate reaction mechanisms. Both conventional and advanced diagnostic instrumentation will be used at NBS. The advanced instrumentation includes fiber optic thermometry (black body or specific gas species spectra), laser induced fluorescence temperature sensing, gas absorption measurements for intermediate species concentration, laser

extinction/scattering for particle size and density, and Laser Doppler Velocimetry for particle velocities. The equivalent NBS black liquor solids flow will be less than 1 lb/h (0.5 kg/h). The gas flow will be the same as for the IPC system.

Figures 2 and 3 show the components of the IPC and NBS systems, respectively. Table 2 describes the function of the modules. The units now under testing are the Central Units (CU) at IPC and the Initial Reactor Modules (IRM) at NBS. Upgrading of both units to their respective Phase 1 reactor systems will be completed by the end of this year. The Phase 1 system costs and preliminary engineering were developed by Xytel Corporation, Mt. Prospect, IL. The IPC CU was constructed and installed by Xytel. The major equipment to complete the Phase 1 system flue gas treatment package will be purchased on a turnkey contract from MEI Systems, Appleton, WI. Other items will be handled by IPC. The NBS reactor construction will be handled mainly by NBS personnel, with some outside contractors (Xytel being one) supplying the basic components.

Schematics of the reactors are shown in Fig. 4-7. Figure 4 illustrates the IPC complete reactor system in downflow gas mode. Figure 5 is the IPC CU with upflow gas. Figure 6 is the NBS complete reactor system in downflow mode. Figure 7 is the NBS IRM with upflow gas.

(a)
Central Units

(b)
Phase 1
Reactor System

(c)
Complete Reactor System

Module Key

A   Solids delivery (hi cap)
B   Liquor delivery (hi cap)
C   Air delivery (elect. htr)
D   In-flight reactor
E₁   Phase 1 char collection
E₂   Phase 2 char chamber
F   Fume chamber
G   Incinerator
H   Gas treatment
I   Alkali system
J   Control panel
K   I/O interface
L   Computer
M   Analytical equipment
N   Safety
O   Integration

NOTE: Lower case letters indicate partial completion
       of module with same capital letter.

Figure 2.   IPC flow reactor system block diagram.

(a)
Initial Reactor Modules

(b)
Phase 1 Reactor System

(c)
Complete Reactor System

Module Key

A   Solids delivery (low cap)
B   Liquor delivery (low cap)
C   Air delivery (gas htr)
D   In-flight reactor
E₁   Phase 1 char collection
E₂   Phase 2 char chamber
G   Incinerator
J   Control panel
K   I/O interface
L   Computer
M   Analytical equipment
N   Safety
O   Integration

NOTE: Lower case letters indicate partial completion
       of module with same capital letter.

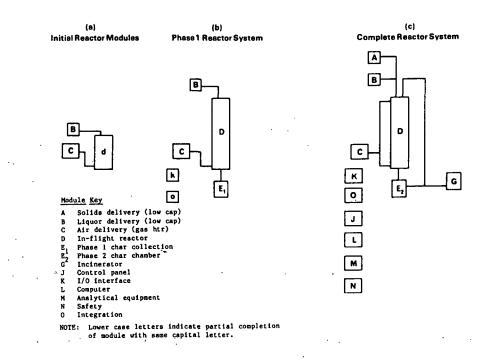Figure 3.   NBS dilute-phase reactor system block diagram.

Table 2. Functional description of reactor system modules developed from
          the preengineering studies.

Code	Module Name	Functional Desciption
A.	Solids delivery	Deliver a continuous stream of dry black liquor solids to the reactor. The metering system is based on pneumatic conveyance from a fluidized bed system.
B.	Liquor delivery	Deliver a continuous temperature controlled stream of black liquor to the reactor. The flow will be controlled via a metering pump which is controlled by a signal from a mass flow sensor.
C.	Air delivery	Deliver a controlled amount at temperature of clean, dry air/N_2 into the reactor.
D.	In-flight reactor	Provide a controlled temperature and gas environment for black liquor combustion studies. The vertically mounted 3-section tube will be surrounded by electrical heaters. Gas flow can either be up or down.
E-1.	Char collection	Separate char particles from reactor effluent gas, quench, and maintain absence of air.
E-2.	Phase 2 char chamber	Provide a region where char can either continue to react with combustion gases or with fresh, externally supplied air. This large, heavily insulated furnace will have preheating capability. The catch pan for the char will be of high temperature alloy for maximum experimental flexibility. Ports for observation will be available.
F.	Fume chamber	Provide a controlled region for studying fume and/or carryover from the burning processes. Flexibility will allow for optical, tube deposition, or coupon deposition studies.
G.	Incinerator	Combust any reduced species from the reactor to form only oxidized gaseous products. Fuel source will be natural gas. Controls are set to maintain a fixed discharge temperature.

Table 2 (Continued). Functional description of reactor system modules
                      developed from the preengineering studies.

H.   Gas treatment   Cool, scrub, and discharge the hot incinerator gas
                              from the system. Cooling will be with water injec-
                              tion. The Venturi scrubber will use an alkali
                              solution. The system ID fan will have a controlled
                              air bleed which varies to maintain system pressure.

I.   Alkali system   Provide a supply of alkali solution to the Venturi
                              scrubber. Sufficient storage and cooling will
                              enable the system to be closed during tests.

J.   Analog control   Housing for controllers and temperature display
         panel and   instruments. This will include relays and annun-
         annunciator   ciators.

K.   Input-output   Provide process signal conditioning to enable
         interface   process monitoring, alarming, data storage, etc.

L.   Computer system   Developed and proven hardware and software to
                              accomplish the tasks listed in K. The system also
                              includes the capability for process control.

M.   Analytical equip-   Provide real time signals from several different
         ment   gas concentration analyzers. These include O_2, CO,
                              CO_2, H_2O, and SO_2.

N.   Process safety   Enable the system to fail safely in the event of
                              power loss. The key is to maintain an inert gas
                              flow via city water pressure to the Venturi
                              scrubber.

O.   Integration   Assembly of modules into an integrated working
                              system, testing, debugging, and startup.

Figure 4. Reactor system overall schematic (down flow mode). Lower case letters refer to equipment modules described in Table 2.
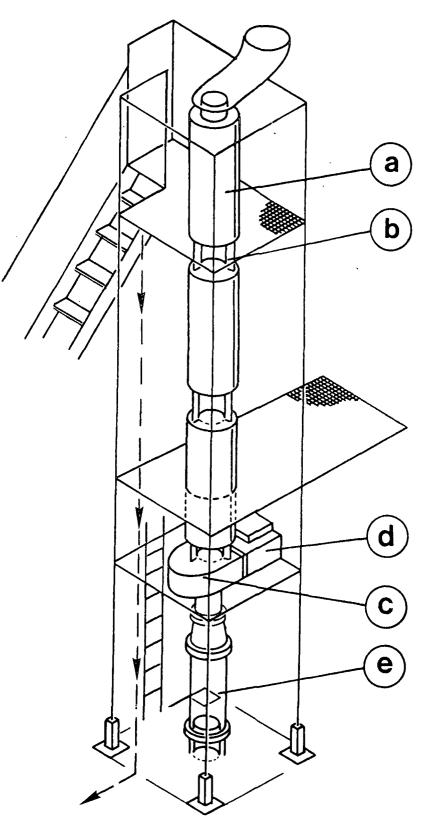
Figure 5.   IPC central units isometric.   In-flight reactor components: a.
Heater, b.   Sampling/observation section, c.   Gas/solids separator.
Air delivery: d.   Electric air heater.   e. Char collection vessel.
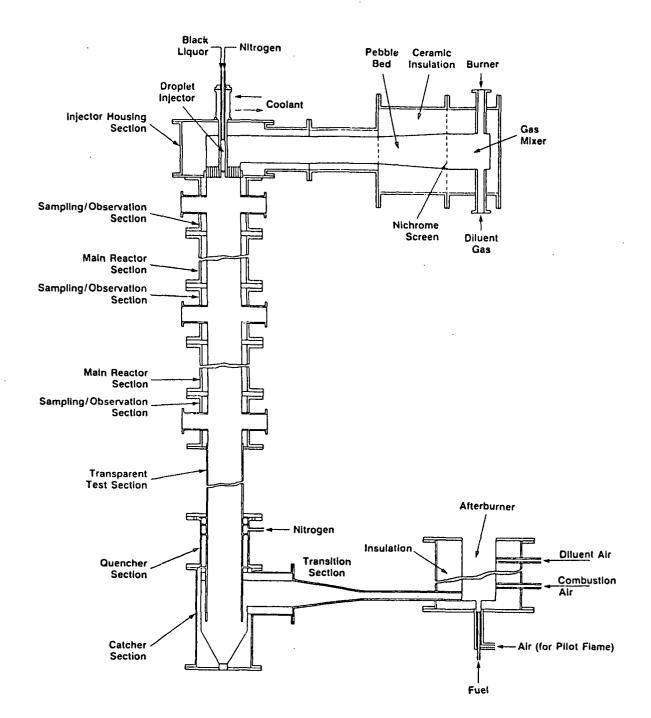
Figure 6. NBS coflow (downflow) configuration.

Figure 7. NBS initial reactor modules (IRM).

MATERIAL AND ENERGY FLOWS

Calculations for the material and energy flows around the IPC reactor are based on the following:

Liquor Composition	Wet Percent Dried Solids
C	38.7
H	3.9
O	35.2
Na	18.7
S	3.5
HHV	6100 Btu/lb BLS (14,200 kJ/kg BLS)

Gas velocity	9.8 ft/s (3 m/s)
Internal diameter	4.0 inches (102 mm)
Length	12 ft (3.7 m)
Temperature	Pyrolysis 1300°F (978°K) Gasification 1800°F (1255°K) Combustion 1800°F (1255°K)

Combustion: complete oxidation of all products, 15% excess

air above stoichiometric, all sulfur retained as

Na_2SO_4, no reduced gas species

Gasification: 40% of stoichiometric air, 100% sulfur reduction

efficiency, no sulfur volatilization, 130 Btu/scf

(4,800 kJ/Std. m^3)

Pyrolysis: N_2 feed gas at 5 times the mass flow of BLS, 100%

sulfur reduction efficiency, 50% sulfur volatized.

The mass flows are shown in Fig. 8. The gas flows and temperature in the in-flight section are for both the IPC and NBS systems. The black liquor flow and those in the other sections are only for the IPC system. The base case energy flows in the products for these three modes are:

Combustion: sensible + latent   6,100 Btu/lb BLS (14,200 kJ/kg BLS)

remaining gas HHV   0 Btu/lb BLS

Gasification: sensible + latent 1,830 Btu/lb BLS (4,260 kJ/kg BLS)

remaining gas HHV 3,800 Btu/lb BLS (8,840 kJ/kg BLS)

remaining solid HHV 470 Btu/lb BLS (1,100 kJ/kg BLS)

Pyrolysis: Heated N_2 supplied at 1,530 Btu/lb BLS (3,560 kJ/kg BLS)

These are the net energy flows in the combined solids and gaseous products leaving the in-flight reactor. The reactor was assumed to be adiabatic at the temperatures previously specified.

TESTING

The initial tests in the IPC reactors measured heatup times and temperature profiles. Subsequent tests in an N_2 atmosphere covered particle residence times and char production. The variables tested were temperature, N_2 flow, and droplet size. Current test work focuses on particle trajectories following the rapid expansion that occurs during pyrolysis.

Support testing for Phase 1 was conducted in two IPC single particle reactors (SPR). The initial work measured reaction times from ignition to maximum swollen volume and ignition to smelt bead coalescence while single droplets burned in air. Later work in the convective SPR pyrolyzed single droplets in N_2 over a temperature range of 570-1470°F (300-800°C). Changes in the mass, carbon lost

and fixed, and sulfur loss were obtained. Results of these "equilibrium" pyrolysis tests are necessary to interpret char chemistry results from the DOE reactor.

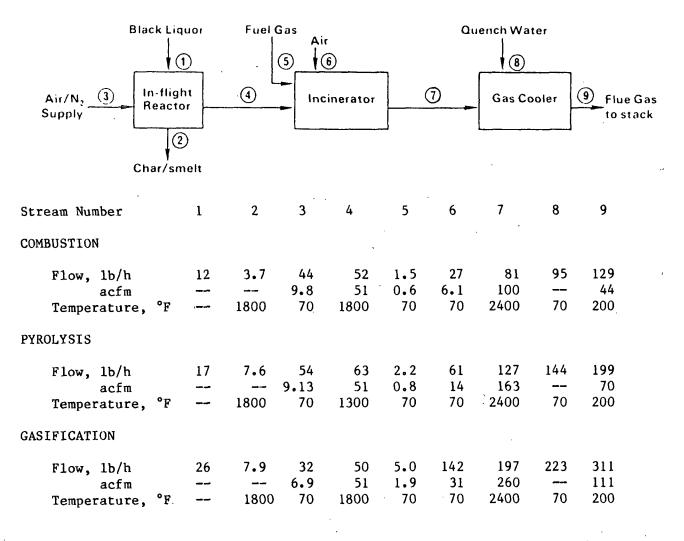| Stream Number		1	2	3	4	5	6	7	8	9
COMBUSTION										
Flow, lb/h		12	3.7	44	52	1.5	27	81	95	129
acfm		--	--	9.8	51	0.6	6.1	100	--	44
Temperature, °F		--	1800	70	1800	70	70	2400	70	200
PYROLYSIS										
Flow, lb/h		17	7.6	54	63	2.2	61	127	144	199
acfm		--	--	9.13	51	0.8	14	163	--	70
Temperature, °F		--	1800	70	1300	70	70	2400	70	200
GASIFICATION										
Flow, lb/h		26	7.9	32	50	5.0	142	197	223	311
acfm		--	--	6.9	51	1.9	31	260	--	111
Temperature, °F		--	1800	70	1800	70	70	2400	70	200

Figure 8. Design of IPC system flow rates and temperatures with full liquor firing under three burning modes.

Sulfur loss is believed to be one of the initial steps in pyrolysis. A set of tests was conducted in a radiant SPR. Off gases were measured for both reduced sulfur compounds and hydrocarbons. These initial test results gave insight into significant influencing variables and will guide test plans for sulfur loss in the flow reactor.

Two recent tests were conducted in the IPC reactor, where 65% solids content black liquor was continuously injected into the reactor. This demonstrated that reliable droplet injection into a hot gas at low liquor flow rates was possible. The injector was designed, tested, and built at NBS. The equipment to accomplish this task is being more permanently mounted before further testing.

The NBS IRM was primarily set up to test black liquor droplet injection devices and to photograph initial in-flight processes in a hot gas stream. A piezoceramic and a positive displacement injector were considered. Only the positive displacement technique has been hot tested. The injector uses a saturated jet of annularly flowing gas to dislodge the droplet from the needle tip. Figure 9 is a schematic of the inject. Video taping of droplet formation as a function of the key variables is underway.
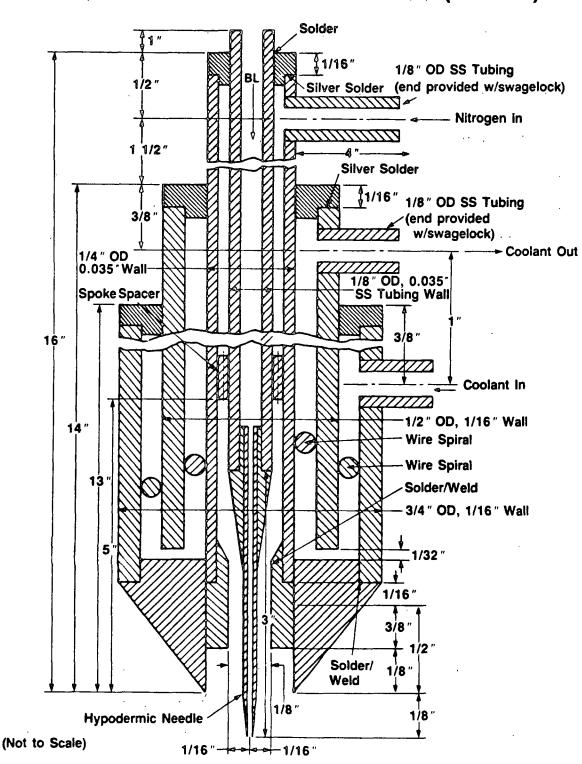
<div align="center">RESULTS</div>

SYSTEM PERFORMANCE

Heatup Rates

Heatup rates, temperature profiles, and temperature differences document the performance of the IPC Central Units. Gas temperatures in the center line of the reactor were measured by a type K thermocouple (TC). The 14 ft (4.3 m) long 1/16-inch (1.6 mm) diameter SS sheathed TC had a 1/4-inch (6.4 mm) radiation shield around 2 inches (50 mm) at the tip. The TC entered at the top of the reactor and was manually positioned at the center of each of the encasement heaters. Measurements were also made at the center of each sample/observation reaction (SOS). Since the SOS temperature values may have a substantial radiation error, they are not reported and will be remeasured. The gas temperature at the exit of the second-stage gas heater (base of the in-flight section)

BLACK LIQUOR DROPLET INJECTOR (Model II)

Figure 9. Black liquor droplet injector used in IPC continuous flow tests.

was measured with a permanently mounted 1/16-inch (1.6 mm) type K SS sheath unshield thermocouple. Figures 10 and 11 are typical heat up curves for the second-stage heater, lower, middle, and upper encasement heaters.

The upper temperature limit for the in-flight section is illustrated in Fig. 12. The gas temperature at midpoint in the in-flight section stabilized after about three hours to approximately 194°F (90°C) lower than the upper materials limit of the encasement heaters 1814°F (990°C). The major part of this temperature drop is across the 1/2-inch (12 mm) thick insulation between the 310SS housing and alumina inner lining. The insulation is necessary when full black liquor flow and combustion are established. Under the present pyrolysis test mode it could be partially removed to achieve higher gas temperatures.

Temperature Profile

Steady-state profiles, taken as described above, indicate that the encasement heater setpoints are the primary control for the gas temperature in the in-flight section. Figure 13 contains three profiles. Note that in all three plots the second stage heater exit is substantially higher, 190-235°F (88-113°C) than the center of the lower heater. Note also that with the exception of the high temperaure profile each section can be higher or lower depending on the heater setpoint. At the present time the shell temperature for each section is automatically controlled. The flowing gas temperature is controlled indirectly by setting shell setpoint temperatures.

While actual gas temperature measurements in the SOS's are in question, there is no doubt that these sections have cooler walls. Figure 14 is the medium temperature profile of Fig. 13 with the gas temperature values measured in the SOS reaction included. Erroneously low gas temperature values may have resulted

Figure 11.   IPC flow reactor heatup curves with gas at 5.5 scfm.

Figure 10.   IPC flow reactor heatup curves with gas flow at 12 scfm.

from radiation to cold walls. The walls, in any case, are no hotter than the TC

measurement. There are two 6-inch (152 mm) sections between the lower heater

and the second stage heater, lowest SOS and the support section (SS). In this

profile both the SOS and the SS were heated. Only one gas temperature measure-

ment was made in this area, center of the SOS.

DOE REACTOR HEATUP
TEST 2   AIR FLOW 5.5SCFM   2NDSTHTR SP1800F   HTR SP 1815F

Figure 12. IPC flow reactor temperature limit given an upper setpoint of
1814°F (990°C) for the encasement heaters.

The maximum gas temperature with the present configuration in the

center of the furnace sections is 1674°F (912°C). Some changes will be made to

increase this level and also to better heat the SOS sections.

Droplet Injector

The NBS droplet injector positive displacement concept was first tested

by NBS with various synthetic fluids. For an extremely wide range of fluids, a

Figure 14. Medium temperature profile which shows temperatures in center of heater sections and SOS sections.

Figure 13. IPC flow reactor temperature profile at center of the heater sections.

given tip size produced nominally the same droplet size. The data are listed in Table 3.

The droplet sizes were determined by measuring the amount of liquid displaced in the syringe and counting the number of droplets. Calculations of droplet diameters were then made on the assumption that all the droplets were spherical and of the same size.

Inspection of the data on glycerol/water mixtures in Table 3 shows that droplet size is only a weak function of viscosity. Data on other liquids tend to confirm this generalization. However, dynamics of droplet detachment are strongly affected by the viscosity; more viscous liquids require a much longer time to grow to their final size. Thus, it appears that the main controlling variable for generation of droplets of desired sizes will be the velocity of the assisting gas flow.

Table 3. Diameters of liquid droplets generated by
the positive displacement apparatus without
assisting gas stream. Tip ID was 2.9 mm cut
at an angle.

Liquid	Droplet Diameter, mm
Glycerol/water (55/45)[a]	2.26
Glycerol/water (70/30)	2.48
Glycerol/water (90/10)	2.42
Glycerol/water (100/0)	2.47
SAE 30 oil	2.29
Linseed oil	2.34
Xylene	1.94
Toluene	1.94
Cyclohexane	2.06

[a]Weight percent of the two ingredients.

Table 4 shows the variation of droplet diameter with assisting air velocity.

Table 4.   Droplet diameters of glycerol/water (55/45) solution, generated by the positive displacement apparatus with assisting air flow.

Air Velocity, ft/second	Droplet Diameter, mm
0	2.26
0.64	1.81
0.82	1.51
1.2	1.15
1.5	0.929
2.0	0.725

When black liquor was tested, rapid drying and skin formation resulted unless the assisting air flow was saturated with water vapor. This requirement plus that to cool the injector in a hot gas environment produced the injector design shown in Fig. 9. Figure 15 shows the complete NBS droplet injector system. The IPC injection system is similar except that steam is blended with hot gas for the assisting air. The present IPC system also uses a pressurized cylinder of liquor feed instead of a stepper motor. Both NBS and IPC have successfully tested the injector with nominally 65% solids content liquor.

Video taping of black liquor droplets injected into the hot NBS reactor provided data for droplet size measurements. These data are presented in Fig. 16. Additional tests showed that the size produced in the reactor was independent of gas temperature. Work will continue to further quantify drop formation from the injector in both room temperature and hot gas environments.

PROCESS TESTS

Residence Time

Procedure

The test objectives were to measure particle residence time in the in-flight section of the flow reactor with counter flowing N_2. Twenty four tests were conducted. Table 5 lists the range of conditions tested.
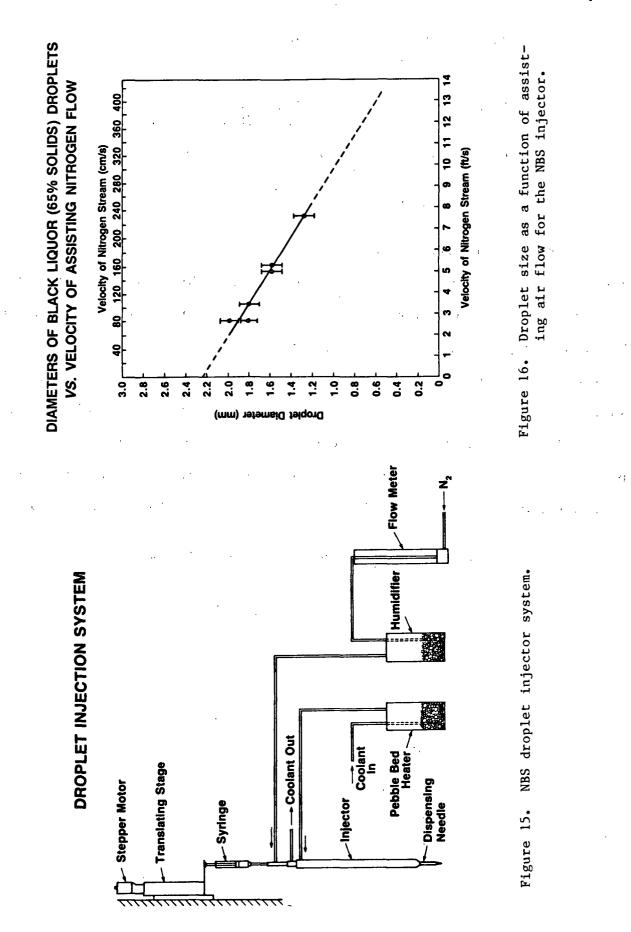
DIAMETERS OF BLACK LIQUOR (65% SOLIDS) DROPLETS VS. VELOCITY OF ASSISTING NITROGEN FLOW

DROPLET INJECTION SYSTEM

Figure 16. Droplet size as a function of assisting air flow for the NBS injector.

Figure 15. NBS droplet injector system.

Table 5. Variable ranges for residence time tests
in the flow reactor.

N_2 flow	2-14 scfm (60-400 m^3/min) 1.6-11.5 ft/s (0.5-3.5 m/s)
Gas temperature	1290-1670°F (700-910°C)
Particle mass diameter	5-30 mg 1.9-3.4 mm (nominal)

Black liquor No. 1, Table 6, at 78.4% solids content was manually formed into droplets of the desired mass using an analytical balance. These droplets, at room temperature, were dropped one at a time into the open top of the reactor. The collected particles fell through the reactor into the 36-inch (0.9 m) pyrex quench vessel at the base. A funnel directed the particles into N_2 filled sample jars. A double-switch stop watch was used to record the residence time. Its resolution was 0.01 s. A significant number of particles, 30-60%, did not make it down. There was at least one condition where no particles made it down. These times were not included. Presumably the particles stuck to the walls.

Table 6. Black liquor No. 1 analysis. Source:
Thilmany Pulp and Paper Co.

Element	Weight Percent OD Solids
C	38.6
H	2.7
O	31.7
Na	19.3
K	1.8
S	4.2
Cl	0.3
Other	1.4

The char formed was analyzed for total sulfur and sodium to determine the amount of sulfur lost. After a hot water wash the char filtrate was analyzed for total organic carbon (TOC) and inorganic carbon (IC). Any carbon that was fixed, i.e., charred, would not be present in the filtrate. Any that had formed Na_2CO_3 would have been in the filtrate. In this way a measure of carbon lost, charred, or formed into Na_2CO_3 was obtained. In all cases the small amount of sample, 100-300 mg, made the analytical measurements difficult. For some tests only single point determinations were made.

Three measurements of the expanded diameter of 10 char samples were taken. The average diameter, based on the cube, was the expanded diameter for each test.

$$\overline{D} = \left[\frac{\sum\limits_{i=1}^{3} D_i^3}{3} \right]^{1/3} \tag{1}$$

The specific swollen volume was then calculated as

$$\overline{V} = \frac{\pi}{6} \frac{\overline{D}^3}{s \cdot m} \tag{2}$$

where: $\overline{D}$ = average expanded diameter, mm

   s = initial fractional solids content

   m = initial sample mass, mg

Test data were analyzed using a statistical spreadsheet package DCS Multistat™. The test dependent variables were residence time, specific swollen volume, lost total sulfur, and fixed and lost carbon. N_2 flow, droplet initial weight, specific swollen volume, average gas temperature, droplet size, expanded droplet frontal area, and droplet expanded diameter were tested as significant independent variables.

Although the data have a lot of variability, some interesting trends are noticed that should guide future quantification of the in-flight processes.

Results

The measured particle residence times depended primarily on N_2 flow, swollen specific volume and the expanded diameter. The empirical correlation was

$$RT = 0.053 \ N_2 + 0.044 \ \overline{V} - 0.33 \ \overline{D} + 2.6 \qquad r^2 = 0.73 \qquad (3)$$

where: RT = residence time, seconds

N_2 = N_2 upflow, SCFM

$\overline{V}$ = specific swollen volume, cc/g solids

$\overline{D}$ = expanded diameter, mm

Residence time predicted via the above equation is plotted in Fig. 17 against the actual residence time. Brackets for the 95% confidence limits are also shown.

DOE PYROLYSIS
PREDICTED VS ACTUAL PARTICLE RESIDENCE TIME

Figure 17. Predicted particle residence time [Eq. (3)] <u>vs</u>. measured residence time under pyrolysis conditions.

The specific swollen volume correlated best with residence time and N_2 flow.

$$\overline{V} = 24\ RT - 0.86\ N_2 - 25.2 \qquad r^2 = 0.61 \qquad\qquad (4)$$

The predicted vs. actual swollen volume is shown in Fig. 18. There is reasonable consistency between Eq. (3) and (4) for the specific swollen volume/ residence time dependence. In both cases longer residence times occurred with higher swollen volumes and vice versa.

Of more fundamental interest is the sulfur lost during pyrolysis. The independent variables of major influence were the swollen specific volume and the expanded diameter.

$$LTS = 1.5\ \overline{V} - 14.7\ \overline{D} + 74.3 \qquad r^2 = 0.65 \qquad\qquad (5)$$

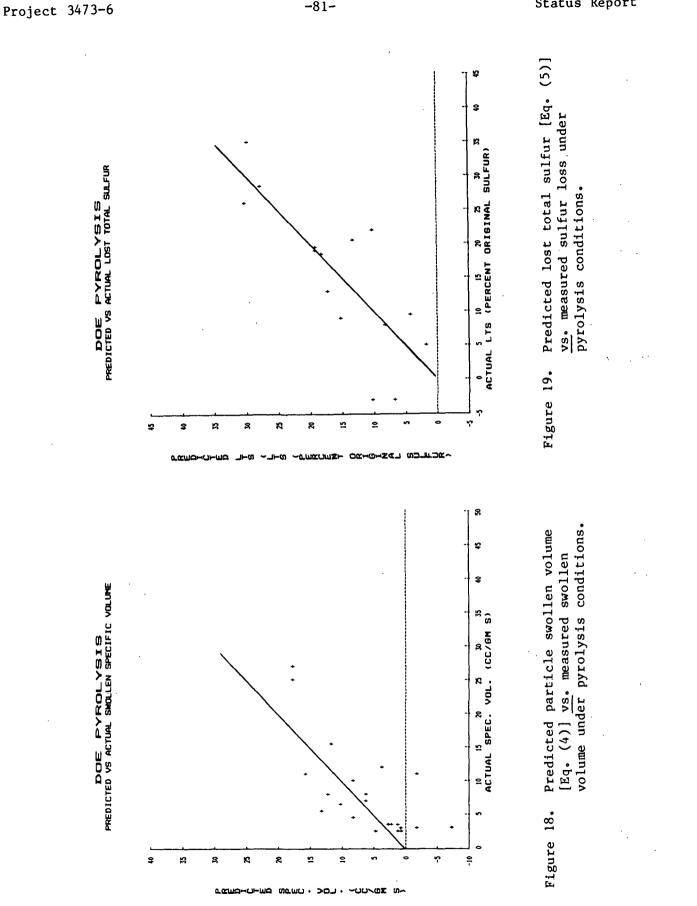where: LTS = lost total sulfur, percent of original sulfur present

The predicted lost sulfur vs. the actual, Fig. 19, shows a nominal maximum of 35% for these tests. As will be noted in the next section this level of sulfur loss implies only partial pyrolysis. The fact that reactor temperature was not a significant variable implies that the achieved particle temperature was well below the gas temperature.

The fixed and lost carbon data were very scattered and showed no significant correlation with any test variables. The variable with the highest correlation was gas temperature. The carbon measurement may be more sensitive to wall impacts, air leaks, and temperature gradients than any of the others. Higher particle temperatures may be required to get meaningful carbon results.

Equilibrium Pyrolysis

Procedure

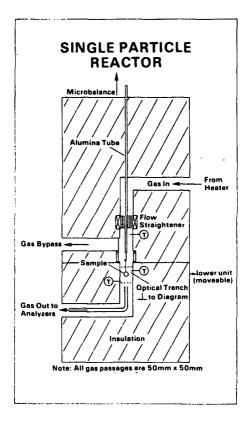The objective of this test series was to produce char particles in an N_2 atmosphere at six specific temperatures. Five char particles were produced in

Figure 19.   Predicted lost total sulfur [Eq. (5)]
             vs. measured sulfur loss under
             pyrolysis conditions.

Figure 18.   Predicted particle swollen volume
             [Eq. (4)] vs. measured swollen
             volume under pyrolysis conditions.

the convective SPR for each condition.   Figure 20 is a schematic of the convective SPR.   Table 7 lists the test conditions.

Figure 20.   IPC convective single particle reactor SPR.

Table 7.   Test conditions for equilibrium pyrolysis tests
in the convective SPR.

N_2 flow	3.5 scfm (100 sLpm)
Velocity	4.4-8.2 ft/s (1.3-2.5 m/s)
Gas temperature	570-1470°F (300-800°C)
Particle	40 mg at 78.4% solids content
	Liquor No. 1

The SPR was purged with N_2 to ensure that the O_2 content was less than 0.5% before each pyrolysis test.   After the test a separate N_2 quench from the lower half of the reactor minimized air oxidation of the hot char when the particle

was removed. In some cases white ashing was observed; these particles were dis-
carded. The upper temperature limit [1470°F (800°C)] was fixed because of this
problem.

Each droplet and corresponding char particle was weighed. The average
mass loss for the group of five particles was measured at each condition. The
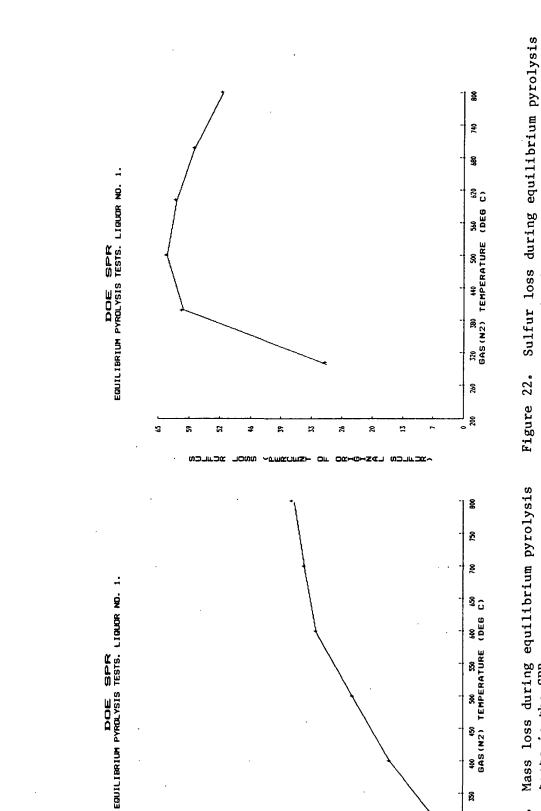five char particles were thoroughly ground, mixed, and analyzed for fixed and
lost carbon, total sulfur, and sodium as described in the Residence Time test
procedure. The small total sample size, 120-160 mg, may have again contributed
to analytical errors.

Results

Figure 21 reports the mass loss data vs. temperature. Rapid change
seems to stop at about 1110°F (600°C). The continued mass loss may be due to
minor amounts of O_2 reacting with the char.

Sulfur loss is already substantial at 570°F (300°C). Figure 22 shows a
continued steep rise between 660-750°F (350-400°C). An apparent maximum around
930°F (500°C) was measured. If these data are compared to the sulfur loss data
from the Residence Time tests, a maximum particle temperature in the flow reactor
of 660°F (350°C) is suggested. In other words, the particles were only partially
pyrolyzed.

The fixed and lost carbon results are shown in Fig. 23. The major car-
bon fixation period is between 750-930°F (400-500°C). With this in mind and the
above comment about particle temperature, it is no wonder that fixed and lost
carbon results in the DOE reactor were scattered. Carbon fixation and loss
ceases by 1290°F (700°C) in an N_2 atmosphere.

Figure 22. Sulfur loss during equilibrium pyrolysis tests in the SPR.

Figure 21. Mass loss during equilibrium pyrolysis tests in the SPR.

DOE SPR
EQUILIBRIUM PYROLYSIS TESTS. LIQUOR NO. 1.

Figure 23.   Lost plus fixed carbon measured in chars from equilibrium
             pyrolysis tests.

Continuous Liquor Feed

Procedure

Black liquor No. 1 at 68.6% solids content was continuously fed into
the reactor via the droplet injector. The NBS-developed injector was fed by a
1.1 liter heated, 140-175°F (60-80°C), pressurized, 12 psig (184 kPa), cylinder.
The target average reactor gas temperature was 1525°F (830°C). Both upflow N_2
and air were used. Air was heated and saturated in bubblers for the assisting
gas flow in Tests 36 and 37. The assisting gas was a blend of steam and air to
produce hot, humid air in Test 38.

Results

The droplet injector performed well when the assisting air flow and cooling water were operated per NBS specifications. The injector operated flawlessly for 3 hours during the test after the initial problems were resolved. The average rate over this period was 93 g/hr of black liquor or 64 grams of solids per hour. The time of droplet retention on the needle tip appears to be strongly related to the degree of saturation and/or temperature of the assisting air at a given flow. Tests 36 and 37 had both the liquor and the saturated air at approximately 160°F (70°C). The char produced was nominally 25 mg/ particle. Test 38 had a nominal 1/1 mix of steam and air at 175°F (80°C), and liquor at the same temperature. Char of 3 to 4 mg/particle was produced. The fate of the droplets fired into the reactor varied with the upflow gas velocity. Above 10 scfm in N_2 and 6 scfm in air, no particles made it to the reactor base for tests 36 and 37. The corresponding conditions for test 38 were 3 scfm in N_2 and < 1 scfm in air. Examination of particle trajectory via a mirror at the base during test 38 showed most impinging and sticking on the wall about 1 to 1.5 meters from the point of injection. This is substantially different than the manually fed 80% solids content liquor which usually made it down. There are numerous straightforward solutions to this problem which will be explored.

Pyrolysis Gases

Procedure
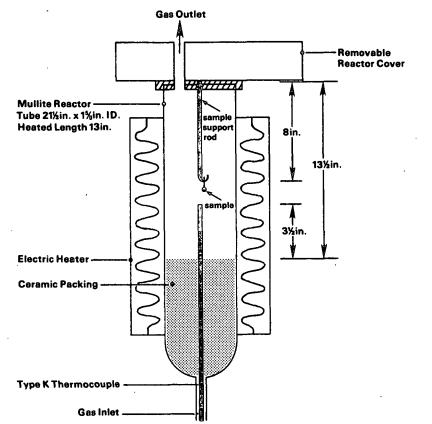
The objectives of these tests were to place into operation the process gas chromatograph (PGC) that was purchased with IPC funds, and to measure the impact of several variables on pyrolysis gas formation. Single liquor droplets were pyrolyzed in the radiant SPR, Fig. 24, with a low N_2 purge flow. During selected tests the SO_2 content of the pyrolysis gas was measured with the SO_2

analyzer. The tests were divided into two test groups. The first group of 22

tests determined the necessary system and PGC operating parameters. Many of

these are listed in Table 8 as test conditions for the second group of 70 tests.

This second test group quantitatively studied the effect of temperature, solids

content, particle size, and added sulfur on pyrolysis gas composition.

RADIANT SINGLE PARTICLE REACTOR

Gas Outlet

Removable
Reactor Cover

Mullite Reactor
Tube 21½in. x 1⅝in. ID.
Heated Length 13in.

sample
support
rod

8in.

13½in.

sample

3½in.

Electric Heater

Ceramic Packing

Type K Thermocouple

Gas Inlet

Figure 24.   IPC radiant single particle reactor.

The initial tests used 50-mL gas bags and collected samples every 15

seconds during the burn. The second test group collected one sample (500 mL)

over the entire burn. These concentration measures were then compared with the

other test variables via the DCS Multistat™ package. Models were developed to

fit the data. The models were then plotted with gas concentration vs. one of the

significant variables, all others being constant.

Table 8. Test parameter for the pyrolysis gas tests.

N_2 flow	0.01 scfm (0.3 sLpm)
Velocity	0.04 ft/s (0.01 m/s) at 930°F 500°C
Gas temperature	650-1050°F (345-565°C)
Particle mass	5-15 mg
diameter	1.9-2.7 mm nominal
Solids content	63-99%
Sulfur addition	0-3% ODS (above original in liquor)
Reduced sulfur gases	H_2S, CH_3SH, $(CH_3)_2S$, $(CH_3)_2S_2$, CS_2, COS
Hydrocarbon gases	CH_4, C_2H_6, C_2H_4, C_3H_8, C_3H_6
Other	SO_2

The liquor used for the first test series was IPC liquor No. 11. The liquor used for the second test group was synthetically produced. This is the same liquor used for the sulfur release during combustion work (Cantrell). The conditions are listed in Table 9.

Table 9. Synthetic liquor used in second group
of pyrolysis gas tests.

Loblolly pine chips

Liquor/wood	4.0
Sulfidity	25%
H-factor	1876
Time at 170°C	1 hr 57 min
Temperature rise	100°C/hr

Results

Temperature influenced pyrolysis gas release more than any other variable. Other variables of significance were particle size and solids content. Although the level and type of sulfur added did influence the release of reduced

gases, the effect was not always consistent. Sulfur addition did consistently produce higher release levels of SO_2. It was not possible to measure directly volatilized elemental sulfur.

The significant results are shown in Fig. 25 through 30. Figures 25 and 26 show that the reduced sulfur gases have a temperature maximum, while several of the hydrocarbon gases are continually increasing in the tested temperature range. Not all of the gases released depend significantly on particle size. Figure 27 shows those gases that did. Solids content of the liquor had mixed results on the reduced gases. Figure 28 reports those gases that showed a trend. Adding sulfur to the liquor did consistenly produce higher levels of SO_2. This is shown in Fig. 29. However, no significant influence was seen on most pyrolysis gases. The effect of temperature on SO_2 released is shown in Fig. 30.

These results represent the first studies of pyrolysis sulfur release. At the writing of this report the analysis is still incomplete. The analysis should be completed by the meeting date.

DISCUSSION

The tests to date suggest that sulfur is lost in the initial phase of pyrolysis. Losses began below 570°F (300°C). The primary reduced sulfur gases are H_2S, CH_3SH, $(CH_3)_2S$, and $(CH_3)_2S_2$ in decreasing order of concentration. These gases reach a maximum at approximately 725°F (385°C). Some additional testing with an SO_2 analyzer showed that SO_2 exists in substantial quantities and exhibits a similar maximum under pyrolysis conditions. More work is needed on SO_2.

Although there are hydrocarbon gases released below 570°F (300°C), actual quantities are small until the temperature reaches 750°F (400°C). In this study

Figure 26.   Hydrocarbon gases evolved from a black liquor droplet as a function of temperature under pyrolysis conditions.

Figure 25.   Reduced sulfur gases evolved from a black liquor droplet as a function of temperature under pyrolysis conditions.

Figure 28. Pyrolysis gases which vary signif-
icantly with black liquor moisture
content.

Figure 27. Pyrolysis gases which vary signif-
icantly with black liquor droplet
size.

SULFURDIOXIDE/TEMPERATURE

Figure 30. The effect of temperature on the SO2 released from a black liquor droplet during pyrolysis.

SULFURDIOXIDE/ADDED SULFUR

Figure 29. The effect of added sulfur content on SO2 evolved from black liquor droplets during pyrolysis.

neither CO, CO_2 nor H_2 were measured. All of these gases are present to some extent and will need further study. The data from all of the tests suggest that carbon lost as reduced hydrocarbons and char formation are closely coupled events. The final char fixing reactions appear to take place after the bulk of the sulfur release.

In order to do an adequate job of simulating the furnace in-flight processes in the flow reactor it as apparent that higher heat fluxes to the particle are needed. With nominally 2 mm, 80% solids content liquor droplets the particles lost only about half the potential sulfur. More recent tests with heated 65% solids content liquor suggests that a higher percent pyrolysis may have been achieved. At best, the flow reactor present temperature of 1680°F (915°C) is an acceptable maximum temperature level for some conditions. Idea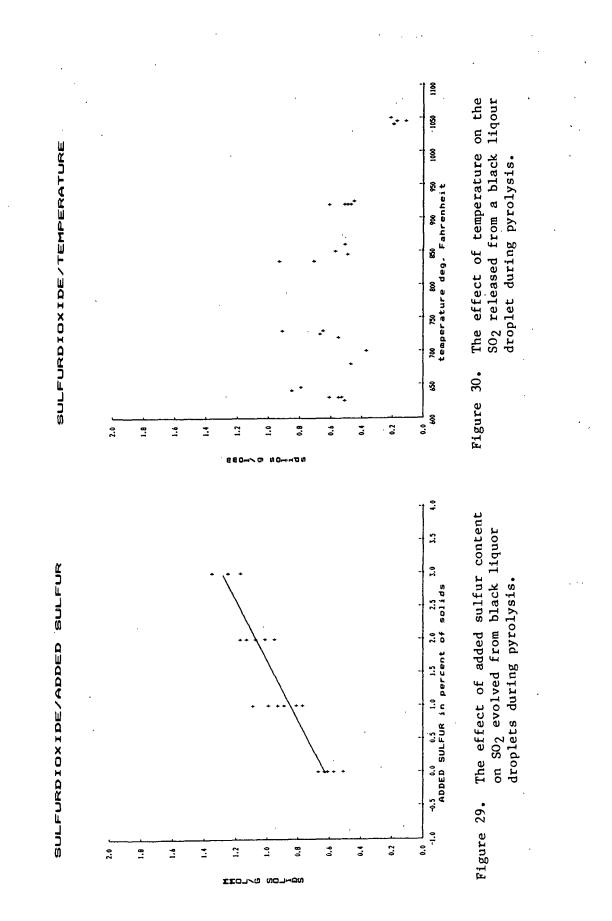lly, reactor temperatures in excess of 2010°F (1100°C) would be desirable. Practically, the system can be modified to reach 1760°F (960°C) without major changes. With internal combustion, even in the present mode, temperatures in excess of 2190°F (1200°C) will be reached with full liquor flow in the upflow mode. Many questions relating to this issue will be addressed in the near future either through tests or calculations.

Another area of concern is temperature loss in the SOS's and SS. A new heater has been designed and ordered. Based on tests with this unit and new temperature measurements a solution to this problem should be found.

The recent droplet injector tests with 65% liquor resulted in significant wall impingement under both pyrolysis and combustion conditions. Modification to the system may be needed to minimize this pattern. The effort involved should be defined in the next few weeks.

NEAR-TERM PLANS

IPC

During the next 6 months, char formation and characterization work will be done. The complete Phase 1 reactor system will also be installed.

The char formation tests on the flow reactor will look at temperature, velocity, droplet size, solids content, and oxygen level as the main test variables. The measured parameters will be expanded diameter, sulfur loss, carbon loss, and carbon fixed. The latter two will depend on the development of successful analytical procedures. Test work addressing the reactor temperature limits and particle trajectory will be done either before or in conjunction with these tests.

Char characterization tests will be done on the chars produced above. These include BET surface area, Hg pore size distribution, scanning electron micrographs, reactivity in a molten salt bath, and elemental composition. It will be essential for this work that relatively large char quantities are available.

Other items which will be addressed include analysis of pyrolysis gas data, development of a fixed carbon test, and identification of two other black liquor sources, one from a mill and the other one synthetic.

The IPC Central Units will be expanded to the Phase 1 reactor by the addition of the following modules: gas treatment, liquor feeding, downflow gas flow system, data acquisition system, gas analysis cart, and a liquor evaporator (IPC funds). The system will first be operable at low liquor flows with a continuous feed. Once the gas treatment package has been added, higher liquor flows will be possible. The downflow gas capability will be the last added feature.

NBS

The test priorities for NBS in the near term focus on variables influencing the droplet size and achievable flow rates with the present nozzle. The installation of the NBS Phase 1 reactor will also be completed.

Three variables affecting the droplet size and repetition rate to be studied are the piston movement rate, assisting gas flow rate, and the injector needle diameter. Video tape documentation will be used for this work. High speed, in-flight photography of the droplets in pyrolysis and combustion conditions will be attempted over the first meter of flight.

The first modules of the reactor will be relocated to the high bay area where other modules will be added to form the Phase 1 reactor. In addition to two more in-flight modules an afterburner and char catcher will be added. At this new location laser light scattering equipment will be assembled in preparation for particle velocity measurements.

THE INSTITUTE OF PAPER CHEMISTRY

David T. Clay
Research Associate
Recovery Group
Chemical Sciences Division

THE INSTITUTE OF PAPER CHEMISTRY

Appleton, Wisconsin

Status Report

to the

PULPING PROCESSES

PROJECT ADVISORY COMMITTEE

Project 3456-2

SMELT-WATER EXPLOSIONS

August 15, 1985

PROJECT SUMMARY FORM

DATE: August 15, 1985

PROJECT NO. 3456-2:   SMELT-WATER EXPLOSIONS

PROJECT LEADERS: T. M. Grace

IPC GOAL:

Increase the capacity potential of processes.

OBJECTIVE:

An increased understanding of the phenomena underlying recovery boiler explosions, and the application of that knowledge to reduce the hazards of operating recovery boilers.

CURRENT FISCAL BUDGET: $20,000

SUMMARY OF RESULTS SINCE LAST REPORT:

The main activity on this project is participation in BLRBAC and the API Recovery Boiler Committee. API funding covers direct costs of on-site investigations of recovery boiler explosions, attendance at API and BLRBAC meetings and participation in API's Recovery Boiler Superintendents' Seminar. The funded project covers miscellaneous costs supporting these activities. At present I am secretary of BLRBAC's subcommittee on emergency shutdown procedures, which reviews all of the reported recovery boiler incidents and chairman of BLRBAC's subcommittee on waste streams in recovery boilers.

We have completed Phase I of the project on Energetics of Smelt-Water Explosions sponsored by the Nuclear Regulatory Commission. This involved analyzing two recovery boiler explosions to determine the amount of mechanical energy accountable in the damage sustained and calculating the energy conversion efficiency by dividing the mechanical deformation energy by the thermal energy potentially releasable from the molten smelt. The best estimate of the energy conversion efficiency was 0.25% in one case and 0.6% in the second. Even though there is considerable uncertainty in these values it is considered very unlikely that the energy conversion efficiency exceeds 1% in either case. Smelt-water explosions may be characterized as weak explosions taking place in weak structures. At present, there is no reason to suspect that much more violent smelt-water explosions (say 10% efficient) are really possible. Even the most violent explosions that have occurred in recovery boilers have been low efficiency events. The risk of a high-yield fuel explosion is much greater than a high-yield smelt-water explosion.

We have made a grant to Professor Corradini at the University of Wisconsin in Madison to support work on vapor explosions as applied to the smelt-water explosion problem. He will perform a sensitivity analysis on an existing vapor explosion model, using conditions specific to the smelt-water system. The

results of the sensitivity analysis will determine what to focus on next. Professor Corradini is an expert on the theory of vapor explosions (physical explosions of the smelt-water type) and is very familiar with all of the work going on on this problem in the nuclear industry.

PLANNED ACTIVITY THROUGH FISCAL 1986:

Continuation of work with API Recovery Boiler Committee and BLRBAC.

Completion of Phase II of the NRC project which will include analysis of a dissolving tank explosion, analysis of several more recovery boiler explosions, and possibly some experiments on smelt water at Argonne National Labs.

Continuation of the collaboration with Professor Corradini.

FUTURE ACTIVITY:

Possible joint proposal with Professor Corradini for vapor explosion research in a stratified contact mode.

THE INSTITUTE OF PAPER CHEMISTRY

Appleton, Wisconsin

Status Report

to the

PULPING PROCESSES

PROJECT ADVISORY COMMITTEE

Project 3558

INCREMENTAL CAPACITY IN RECOVERY BOILERS

August 15, 1985

PROJECT SUMMARY FORM

DATE: August 15, 1985

PROJECT NO. 3558: INCREMENTAL CAPACITY IN RECOVERY BOILERS

PROJECT LEADERS: T. M. Grace

IPC GOAL:

Increase the capacity potential of processes.

OBJECTIVE:

Develop procedures for assessing the degree to which capacity increases can be
obtained by operating changes or retrofits. Evaluate approaches for gaining
incremental capacity.

CURRENT FISCAL BUDGET: $50,000

SUMMARY OF RESULTS SINCE LAST REPORT:

A review article on incremental capacity in recovery boilers was published in
the November, 1984 Tappi Journal.

No other work on the specific objectives of this project was undertaken in this
period because of the press of other activities.

Student related work in this period includes; S. Francoeur completed an M.S.
project on the conceptual design of a cyclone system for dried solids firing.
T. Cartwright initiated an M.S. project on the fluidized bed drying of black
liquor. E. Buehler has initiated an M.S. project on intensified black liquor
combustion.

PLANNED ACTIVITY THROUGH FISCAL 1986:

Prepare a detailed checklist of capacity limiting factors and methods for deter-
mining which factors govern a particular boiler.

Reach a decision regarding critical research needs for capacity improvement.

FUTURE ACTIVITIY:

When an approach is found to be feasible, we will proceed toward commercial
implementation.

THE INSTITUTE OF PAPER CHEMISTRY

Appleton, Wisconsin

Status Report

to the

PULPING PROCESSES

PROJECT ADVISORY COMMITTEE

Project 3475

FUNDAMENTALS OF SELECTIVITY IN PULPING AND BLEACHING

Delignification Reactions

Carbohydrate Reactions

September 5, 1985

PROJECT SUMMARY FORM

DATE: September 5, 1985

PROJECT NO. 3475: FUNDAMENTALS OF SELECTIVITY IN PULPING AND BLEACHING

PROJECT LEADER: D. R. Dimmel and L. R. Schroeder

IPC GOAL:

Improved process for bleached chemical pulps

OBJECTIVE:

Provide a fundamental understanding of the chemical and physical reactions that
control both (1) the rate of lignin removal, hemicellulose dissolution, and
cellulose degradation; and (2) the composition and location of lignin, hemi-
celluloses, and cellulose that remain in the pulp during pulping and bleaching.

CURRENT FISCAL BUDGET: $175,000

SUMMARY OF RESULTS SINCE LAST REPORT:

Single electron transfer (SET) reactions represent a new type of chemistry that
may be important to many organic processes, including the delignification of
wood. Room temperature electrochemical studies in organic solvents have shown
that reduced forms of anthraquinone (AQ) transfer electrons to quinonemethides,
which then rapidly fragment. Quinonemethides are important intermediates in
lignin reactions, and fragmentation reactions of these are synonymous with
delignification. Two other approaches aimed at demonstrating lignin SET reac-
tions have been completed; these employ conditions similar to pulping. While
the results of these approaches are compatible with SET reactions, they do not
definitively prove that this kind of chemistry explains the high efficiencies of
AQ pulping systems. Related student research has, however, established the
existence of quinonemethide SET reactions with reduced AQ species and with glu-
cose. A structural-reactivity study of lignin model compounds has provided
valuable insights into the general chemistry of hydroxide reactions and additive
reactions during pulping. A high temperature electrochemical cell has been
constructed and tested under mild conditions.

Studies of the effect of anthraquinone on polysaccharide degradation at alkaline
pulping conditions indicate that anthraquinone has the potential to accelerate
random chain cleavage in the wood polysaccharides. The physical structure of
cellulose prevents this reaction from causing severe pulp viscosity loss.

PLANNED ACTIVITY THROUGH FISCAL 1986: (Short Range)

Our short term goals are to produce and test an electrochemical cell which will
function at about 130°C in aqueous alkali. The cell will be used to verify the
importance of electron flux to delignification reactions and to attempt detection
of quinonemethides.

While we know that SET reactions occur with certain lignin models and pulping additives, we still do not know their importance relative to competing ionic reactions. Experimental approaches will be taken to try to provide knowledge in this area.

Mechanistic studies of cellulose chain cleavage in alkaline pulping indicate that increased ionic strength could accelerate the cleavage reaction. Thus, the effect of "dead load" (increased ionic strength) on cellulose chain cleavage during pulping will be examined.

FUTURE ACTIVITY: (Long Range)

The high temperature electrochemical studies will be expanded into evaluating methods to monitor pulping and promoting, probably indirectly, beneficial pulping reactions. Should SET reactions be shown to be important to efficient pulping, we will examine novel ways to promote these reactions in an economical manner.

Potential areas for future research include (a) investigation of the mechanism of anthraquinone oxidation of reducing end groups of polysaccharides (peeling retardation) and (b) further investigation of the mechanism of oxygen degradation of cellulose in alkaline media.

STUDENT RELATED RESEARCH:

P. Apfeld, Ph.D. - 1985; D. Smith, Ph.D. - 1985; M. Henderson, Ph.D. - 1986;
D. Geddes, Ph.D. - 1986; G. Reed, Ph.D. - 1987; J. Fitzgerald, M.S. - 1985;
M. Bovee, Ph.D. - 1986; W. Molinarolo, Ph.D. - 1987; V. Gentile, Ph.D. - 1985.

Status Report

FUNDAMENTALS OF SELECTIVITY IN PULPING AND BLEACHING

Delignification Reactions

OBJECTIVE

The goal of chemical pulping is to selectively remove lignin while retaining the carbohydrate components of wood. To improve the selectivity of pulping, we must understand the chemistry which governs the delignification and carbohydrate retention processes. The fact that anthraquinone increases pulping selectivities has generated a new interest in pulping chemistry. Is this additive interacting with lignin in a manner similar to sulfide and hydroxide, or is there a whole new chemistry involved? The goals of this project are to develop a fundamental understanding of anthraquinone's mechanism of action and the chemistry of delignification in general. With this knowledge, pulping innovations can possibly proceed by way of fundamentals rather than the empirical approach.

INTRODUCTION

We and others have shown that anthrahydroquinone (AHQ) forms "adducts," 1:1 addition products, when reacted with lignin model quinonemethides (QMs) at room temperature. Warming QM-AHQ adducts that have β-aryl ether groups leads to two phenol fragments and anthraquinone (AQ). Fragmentation of model lignin compounds in this way is taken as evidence as to how AHQ causes rapid delignification of wood during pulping.

There are, however, shortcomings of the adduct mechanism; these have been outlined in a recent review by me.[1] These shortcomings have led us to investigate the possibility that AHQ delignification reactions are single

electron transfer (SET) reactions. In a joint research effort with Helena Chum and Peter Palasz at the Solar Energy Research Institute (SERI) in Golden, Colorado, we have shown that electrochemically generated AHQ ion-radicals can cause lignin model QMs to fragment to phenolate species and AQ via a sequence of SET reactions.[2]

The electrochemical studies showed that a hitherto unrecognized type of chemistry might explain the high efficiencies associated with AQ pulping systems and might key new advances in pulping strategies. The electrochemistry experiments were, however, conducted under idealized, nonpulping conditions, namely, at room temperature and principally in organic solvents. We therefore continued more conventional studies aimed at demonstrating the feasibility of SET reactions with lignin model compounds under conditions more closely approaching normal pulping conditions.

Two approaches were taken in our project work. One approach was based on examining how bulky groups placed on lignin model compounds and on AQ analogs would affect fragmentation of the models. An adduct mechanism requires close contact, with bond-making, between AHQ and a QM and thus would be adversely affected by bulky substituents near the site of reaction. In contrast, SET mechanisms can operate without close contact between reactants and thus are not affected by steric factors.

The steric study indicated that bulky groups located near the sites for adduct formation did not seriously hinder the degree of fragmentation.[3] These results, although supportive of an SET mechanism, were not definitive. The results are being scrutinized and will appear soon as a technical paper to our member companies.

The second approach we took to establishing the existence of SET mechanisms in AHQ induced delignification-type reactions involved a structure-reactivity study. The premise of this study evolved around differences between the type of fragments initially produced by the adduct and SET mechanisms. In the adduct mechanism, the lignin model fragments to phenolate <u>ions only</u>; in the SET mechanism both phenolate <u>ions and radicals</u> are produced.

The study was principally designed to study only one of the two fragments being produced. If this fragment was lost as an <u>ion</u>, differentiation between SET and adduct mechanisms would not be possible; if the fragment was lost as a <u>radical</u>, the SET mechanism would be confirmed.

RESULTS

STRUCTURE-REACTIVITY RELATIONSHIP STUDY

Several lignin model compounds were synthesized and subjected to fragmentation by the action of NaOH (soda), NaOH/glucose, NaOH/AQ/glucose (soda/AQ), and $NaOH/Na_2S$ (kraft). The results have been gathered together in two technical papers, which are attached to this report and have recently been mailed to member companies. The study provided much information about the mechanisms of soda and soda/additive pulping reactions but did not confirm (or deny) the existence of SET reactions.

The slow step in soda induced model fragmentation appears to be the breakage of the β-aryl ether bond. The slow step in additive induced model fragmentation appears to be formation of a quinonemethide; the additive then acts on the QM. By employing competitive experiments, we were able to observe some of the chemistry which occurred after QM formation. Unfortunately, this

chemistry demonstrated that the β-aryl ether unit cleaved as a phenolate <u>ion</u> and not as a radical - so the mechanism (SET or adduct) is unresolved.

ELECTROCHEMICAL STUDIES

The joint research efforts of SERI and IPC for studying pulping mechanisms by electrochemical techniques has slowed due to the departure of postdoctoral fellow P. Palasz from the team. The low temperature studies are still continuing to a limited extent at SERI. We need an influx of government money to renew the joint venture. The money is needed to support staff personnel at SERI and to supply needed equipment at IPC. Toward this end we have submitted to the Department of Energy a proposal for a 3-year investigation of the applications of electrochemistry for monitoring and promoting pulping and bleaching reactions. The requested funds from DOE are $790,000, of which $240,000 is targeted for IPC.

Working under our normal dues-funded program, we have begun the development of an electrochemical cell which can function under high temperatures and pressures. A cell has been constructed which should meet the moderate temperatures (ca. 120°) and pressures (200 psi) that we need for the first phase of our work. The cell is capable of reproducing our early IPC-SERI cyclic voltammograms of AQ in organic solvents.

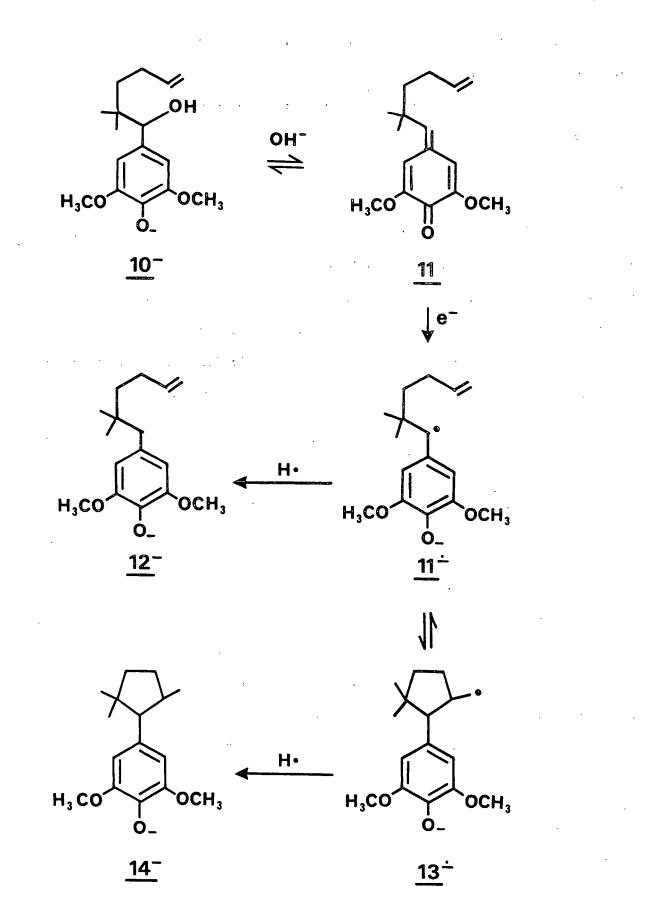The construction and startup of the new cell was no trivial task. We are rookies trying to make the big leagues. We have been helped substantially by our machine shop crew of Phat Filz, Glen Winkler, and Paul Van Rossum and by Ron Yeske and David Crowe in our corrosion group. We are presently attempting to do electrochemical measurements of aqueous solutions, first at room temperature and then at elevated temperatures.

A student, John Wozniak has elected to do a Ph.D. thesis on lignin electrochemistry. He will be doing an internship at SERI this fall. His contributions will help us pursue the area of high temperature electrochemistry at an accelerated rate.

RELATED STUDENT RESEARCH

The recent work of Ph.D. Candidate Dean Smith has produced some interesting data which relate significantly to our project goals. Dean has been studying the reactions of syringyl alcohol in alkali at 135° with and without additives present. A 3-page summary of his work is attached; the work was presented during the poster session at the 1985 International Symposium on Wood and Pulping Chemistry in Vancouver, B.C., on August 28, 1985.

The syringyl alcohol study shows that AHQ^{-2} and glucose undergo SET reactions with syringyl QM, while hydrosulfide ion (SH^-) appears to react principally _via_ an ionic mechanism. Further proof of these conclusions has come from studies involving compound **10** (the numbering system used is a continuation of Dean's 3-page abstract).

The cyclization of 5-hexen-1-yl intermediates (⟋⟍⟋⟍*) to 5-membered rings is taken as proof that radicals (* = •) existed. [A carbonium ion (* = +) would cyclize to a 6-membered ring and a carbanion (* = -) would not cyclize.] Compound **10** was specifically designated to provide QM **11** when heated in alkali. Should QM **11** accept an election in a SET reaction, the resulting ion radical **11**$^{\bullet-}$ might cyclize to a 5-membered ring ion radical **13**$^{\bullet-}$. Formation of reduction products **12** and **14** would thus indicate that radical intermediates were present.

10^-

11

$\rightleftharpoons$ OH⁻

↓ e⁻

12^-

$11^{\cdot-}$

H•

$\Updownarrow$

14^-

$13^{\cdot-}$

H•

Heating compound 10 with and without additives present has shown which additives produce radicals via SET reactions. Both AHQ^{-2} and glucose were quite good at generating radicals; AHQ^{-2} gave large amounts of 12 and small amounts of 14, while glucose did just the opposite. The yields of open side-chain product 12 and cyclized side-chain product 14 depend on the relative rates of hydrogen atom subtraction vs. cyclization. Soda "pulping" of 10 led only to recovered 10, while kraft "pulping" of 10 gave small amounts of radical derived products. Consequently, the reactions of 10 indicate the possible occurrence of SET reactions in pulping situations.

CONCLUSIONS

Through a combination of project and student research we have shown that SET reactions between lignin model QMs and certain pulping chemicals, i.e., AHQ and glucose, can occur in alkali at 135-150°C. Room temperature electrochemical studies of β-aryl ether lignin model QMs in organic solvents have shown that SET reactions can cause model fragmentation reactions analogous to delignification reactions. We still need to confirm that SET reactions are occurring in preference to ionic reactions in promoting lignin fragmentation and retarding lignin condensation reactions.

Our structure-reactivity study provided valuable information about the nature of lignin fragmentation reactions in the presence of OH^-, SH^-, glucose, and AHQ. The study pointed out the problems of defining the chemistry of additive-promoted lignin fragmentation reactions. We now have a grasp of what information can and cannot be provided by model kinetic experiments.

Our electrochemical experiments are progressing from room temperature-organic solvent systems to high temperature-aqueous solvent systems. Progress has been slow due to inexperience and other priorities.

PLANS

We will be continuing to develop an electrochemical cell that functions well under pulping conditions. The high temperature electrochemical studies should provide information about the value of SET reactions in pulping, may allow us to monitor pulping reactions, and will indicate the future feasibility of "electrochemical" pulping.

While the use of a radical probe compound (10) indicates SET reactions occur with certain pulping additives, the studies of Dean Smith do not provide a good indication of the importance of these reactions relative to adduct reactions, for example. Dean's probe compound 10 is quite sterically hindered for adduct formation and, thus, does not have too many options for reactions, other than SET reactions and reversible QM formation. Additional chemistry is needed to define the importance of SET mechanisms to lignin fragmentation reactions.

We are in the process of building model compounds which can either undergo side chain cyclization, similar to 10, or β-type elimination reactions. Attempts to prepare cyclizable probes into the pulping additive, i.e., an allylic anthrone, are also under investigation.

REFERENCES

1. Dimmel, D. R., J. Wood Chem. Technol. 5:1(1985).

2. Dimmel, D. R.; Perry, L. F.; Palasz, P. D.; Chum, H. L., J. Wood Chem. Technol. 5:15(1985).

3. Dimmel, D. R., Project 3475 Status Report, Sept. 6, 1984, and PAC oral presentation, April 1, 1985.

THE INSTITUTE OF PAPER CHEMISTRY

Donald R. Dimmel
Research Associate
Wood Sciences
Chemical Sciences Division

APPENDIX

SYRINGYL ALCOHOL CONDENSATION REACTIONS − A SEARCH FOR RADICAL REACTIONS

DEAN A. SMITH AND DONALD R. DIMMEL

THE INSTITUTE OF PAPER CHEMISTRY
APPLETON, WISCONSIN

ABSTRACT

The alkaline reaction of syringyl alcohol produced five products, of which the expected dimer was the major component. Addition of anthrahydroquinone (AHQ), glucose, or sodium sulfide resulted in changes in the product distribution. The changes appear to be indicative of (a) an increase in radical-type reactions with additions of AHQ or glucose and (b) adduct reactions with addition of sulfide.
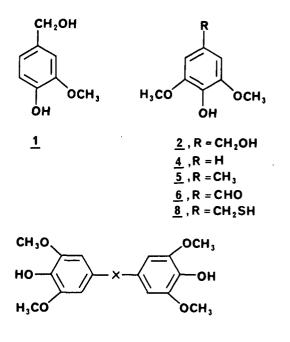
INTRODUCTION

Delignification of wood can be viewed as a competition between two reactions, one favorable and one unfavorable. The favorable one consists of fragmentation of the lignin macromolecule into water soluble components, while the latter one is condensation of water soluble lignin fragments into new lignin macromolecules. The condensed lignin is believed to have an abundance of strong carbon-carbon linkages between monomers, which stabilize the polymer toward degradation (1). Much has been assumed about condensation reactions, but little has been experimentally verified. It is important that we understand the chemistry of both fragmentation and condensation reactions if we are to achieve efficient delignification.

Previous studies (2) of the alkaline reactions of vanillyl alcohol (1) produced results which could not be explained by the generally accepted mechanism of lignin condensation, i.e., the conjugate addition of carbanions to quinone-methide (QM) structures (3). In order to explain these results, it was hypothesized that radical reactions were at least partially responsible for the alkaline condensation reactions of vanillyl alcohol (2).

RESULTS

Further investigation into defining the extent of radical condensation reactions was undertaken with a study of the alkaline reactions of syringyl alcohol (2). The advantage of syringyl alcohol over vanillyl alcohol was the

lack of polymerization, which allowed a much simpler product analysis. The reaction of syringyl alcohol in a 1N NaOH solution at 135°C (henceforth to be referred to as the system) produced five compounds. The expected dimer, disyringylmethane (3), was the major product. Three monomers, syringol (4), 4-methylsyringol (5), and syringaldehyde (6), were produced in moderate yields and a trace amount of the dimer bisyringyl (7) was also observed.
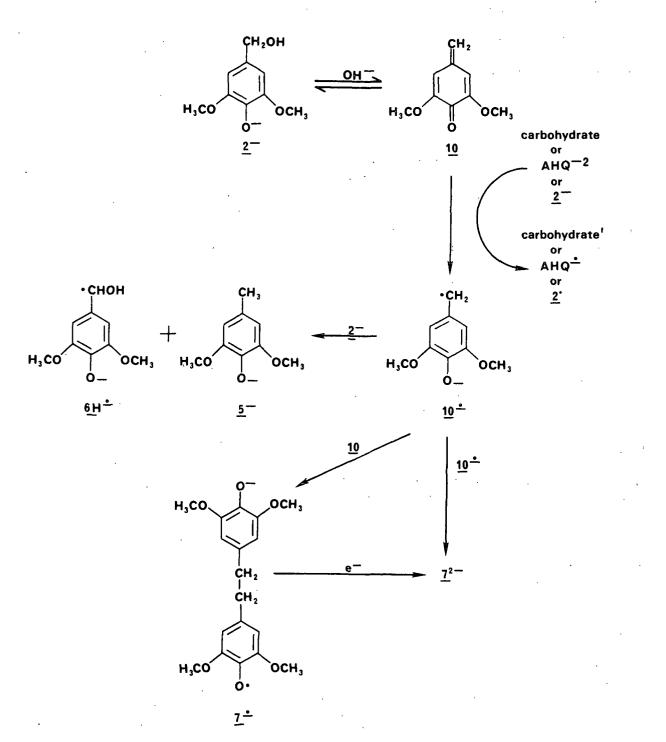

1

2, R = CH₂OH
4, R = H
5, R = CH₃
6, R = CHO
8, R = CH₂SH

3, X = −CH₂−
7, X = −CH₂−CH₂−
9, X = −CH₂−S−CH₂−

The mechanism responsible for the formation of 4-methylsyringol, bisyringyl, and syringaldehyde appears to be radical in nature. This mechanism is viewed as beginning with the transfer of an electron from a phenoxy anion to a QM resulting in the formation of a benzylic radical and a phenoxy radical (Scheme I). The resulting benzylic radical can then either form 4-methylsyringol or bisyringyl.

The 4-methylsyringol product obtained from treating α,α-dideuteriosyringyl alcohol with alkali was fully deuterated at the benzylic methyl group. This suggests that 4-methylsyringol results from transfer of a hydrogen atom (or deuterium atom) from the benzyl position of syringyl alcohol to the syringyl QM radical anion (10⁻̇). Bisyringyl probably is formed by the coupling of two benzylic radicals or the addition of a benzylic radical to a QM and the subsequent acquisition of an electron. Thus, the radical mechanisms can explain some of the

Scheme I

reactions occurring during the alkaline reaction of syringyl alcohol; 4-methysyringol and bisyringyl are the reduction products and syringaldehyde is the oxidation product.

Additional studies of the alkaline reactions of syringyl alcohol were done by adding various compounds to the system. When two molar equivalents of anthrahydroquinone (AHQ) were added, the rate of the consumption of syringyl alcohol increased and the product distribution was drastically changed. Production of 4-methylsyringol and bisyringyl was enhanced, while that of disyringylmethane was retarded. Apparently, AHQ was able to transfer electrons to QM's, resulting in an increase in the production of QM radical anions (Scheme I). The QM radical anions can then form 4-methylsyringol or bisyringyl as previously described. Anthrahydro-

quinone appears to enhance the radical reactions of syringyl alcohol by increasing the concentration of benzylic radicals.
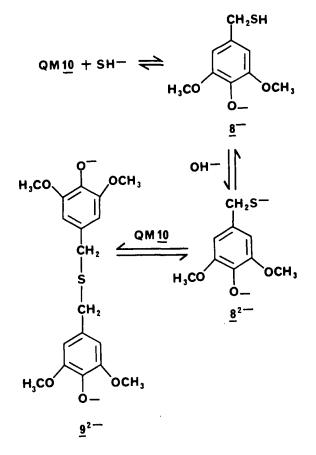
In order to simulate the presence of carbohydrates, two molar equivalents of glucose were added to the system. The presence of glucose did not change the consumption of syringyl alcohol to an appreciable degree, but it did decrease the production of disyringylmethane by half and that of syringaldehyde entirely. The production of 4-methylsyringol was nearly doubled and that of bisyringyl was also increased. Perhaps glucose or some of its alkaline degradation products can also transfer electrons to QM's and enhance the radical reactions of syringyl alcohol as does AHQ.

When two molar equivalents of sulfide were added to the system, there was an initial rapid consumption of syringyl alcohol followed by a moderate consumption. The rapid consumption of syringyl alcohol was not accompanied by an increased production of disyringylmethane. On the contrary, production of disyringylmethane was decreased; after 85 minutes the amount of disyringylmethane produced was less than half of that produced by the soda system alone. The production of syringaldehyde, bisyringyl, and 4-methylsyringol were also decreased. Analysis of the reaction solution by gas chromatography/ mass spectrometry showed the presence of two new compounds, 3,5-dimethoxy-4-hydroxybenzylthiol (8) and di-(3,5-dimethoxy-4-hydroxybenzyl)sulfide (9).

The appearance of these compounds indicates that the hydrosulfide ion in the reaction system can capture QM's to form 8 (Scheme II). Ionization of 8 allows the capture of a second QM to produce 9. Since all of these reactions are reversible, an equilibrium was probably established early. Thus, the original fast consumption of syringyl alcohol was during the establishment of the equilibrium. As syringyl alcohol was further consumed, the equilibrium shifted in the reverse direction, replenishing the syringyl alcohol and thus providing only moderate decreases of syringyl alcohol. Unlike AHQ and glucose, sulfide appeared to interact with syringyl alcohol by ionic pathways in which hydrosulfide ions add to QM's to produce "adducts."

Additional proof for the electron transfer reactions involving QM's and pulping chemicals is being sought by using radical "probes" built directly into the QM's.

Scheme II

REFERENCES

1. BRYCE, J.R.G. in: Pulp and Paper, Chemistry and Technology, New York: J. P. Casey (ed.), Wiley Interscience, 1980: 428-429.

2. DIMMEL, D.R., SHEPARD, D., AND BROWN, T.A. J. Wood Chemistry and Technology 1(2): 123 (1981).

3. GIERER, J. Svensk Papperstid. 73(18): 571 (1970).

STRUCTURAL/REACTIVITY STUDIES (I): SODA REACTIONS OF LIGNIN MODEL COMPOUNDS

Donald R. Dimmel and Lois F. Perry
The Institute of Paper Chemistry
P.O. Box 1039, Appleton, Wisconsin 54912

ABSTRACT

Lignin model compounds containing a phenolic "A" ring, α-OH, and β-aryl (ring "B") ether, with different substituents located on rings A and B, have been synthesized and degraded under a variety of conditions in sodium hydroxide-water (soda). Substituent changes on ring B had a large effect on fragmentation reactions of the models; changes on ring A showed only small effects. These substituent-reactivity relationships indicate that the slow step in the mechanism for model fragmentation under soda conditions is cleavage of the β-aryl ether bond. Vinyl ether formation, a reaction which competes with model fragmentation, is more prominent at low alkali concentration.

Resorcinol, a fragmentation product in one of the model degradations, was shown to be an effective promoter of fragmentation.

INTRODUCTION

Structure-reactivity studies consist of examining the rates of reaction of several closely related compounds and correlating the rate data with differences in structure in order to provide information on reaction mechanisms. We have synthesized and examined the rates of degradation of several related lignin model compounds. Our initial goal was to demonstrate the importance of electron transfer reaction mechanisms in pulping systems.[1,2] This report (soda reactions) and the one which follows (soda-additive reactions) describe our results with a structure-reactivity study of delignification mechanisms.

Two model series (1 and 2) were studied. Their definition and numbering system are given below. The term "fragmentation" refers to cleavage of the β-aryl ether bond. Substituents meta on ring B were chosen to minimize steric effects and ambiguous resonance effects. Should the B ring break off as a phenolate radical, all groups ortho and para can stabilize by resonance; the principal effect at the meta position is a simple polar effect.[3] Substituents located on the B ring would be expected to have a significant effect on reaction rates if cleavage of the β-aryl ether bond were the rate determining step in the mechanism. Substituents on the A ring would be expected to have little effect on the rate if the cleavage step were the slow step.

1, vary R'' (ring B), R=OCH₃, R'=H
2, vary R and R' (ring A), R''=CH₃ or CF₃

Synthesis

The synthetic steps used to prepare the m-substituted ring B models are given in Scheme 1. We employed two pathways to get to ketone **9**. The shorter pathway "a" has the following problems associated with it: the purification of bromoketone **6** is not practical (decomposes, lachrymator), a large excess of phenolate ion (**7⁻**) is needed for the coupling step (otherwise **6** can polymerize with itself), and chromatography is required to purify product **9** of the excess phenol.

The longer pathway "b" allows purification of each intermediate by simple recrystallization and does not require an excess of phenol in the coupling step. This latter advantage is important

when the phenol is expensive or hard to obtain. Route "b" has
worked well in some related studies in our laboratory and with the
preparation of nitro model **9E**, but has been less successful with
the other models. In several cases, problems arose during the
coupling step; a portion of the acyl groups would transfer from **5**
to **7** during the reaction, giving rise to lower yields, mixtures,
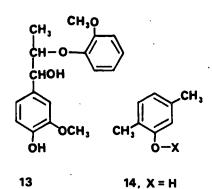and chromatography isolations. In general, the method used was
path "a".

Direct reduction of ketones **9A-F** gave the non-β-methyl (or C_2)
series of alcohols. Methylation of **9A-D** and their reduction gave
the β-methyl (or C_3) series of alcohols. The m-OH and m-NO_2 C_3-
models (**11F** and **E**) were not prepared because of both synthetic
difficulties and reactivity problems. Preliminary degradations of
C_2-alcohols **12F** and **E** indicated that these two model types would
not be of general use for all the anticipated experiments. The
nitro group was readily reduced by anthrahydroquinone (AHQ), and
phenol model (**12E**) gave undesirable by-products when degraded in
alkali. The abandonment of the m-NO_2 and m-OH series left us
without our most and least reactive models.

The methylation of chloroketone **9B** produced an unusual result:
a portion (roughly 30%) of the chloro groups were reduced, giving
rise to a product mixture composed of C_2- and C_3-chloroketones **9B**
and **10B**, along with the C_2- and C_3-unsubstituted ketones **9H** and
10H. Separation of all four components of this mixture by column
chromatography proved difficult. A sample containing 70% **10B** and
30% **10H** was obtained and reduced to a 70/30 mixture of C_3-chloro
and unsubstituted alcohols **11B** and **11H**. The latter was sub-
sequently studied as a mixture.

Except as noted above, the synthesis and product characteriza-
tions were straightforward (see Experimental Section). The C_3-
alcohols exist as four isomers, two sets of diastereomers. Attempts
to chromatographically separate these isomers were not successful.
Partial separation occurred in some cases. Degradation rates of

fractions rich in one isomer were virtually identical to the rates
of fractions rich in the other isomer. Therefore, from this point
of view, separation of isomers is not necessary. Yet with no separ-
ation, the isomer pairs form oils which are difficult to fully
purify (remove solvents, impurities, etc.) when only small amounts
are available.

Another model which was examined in this study was 13; its
synthesis has already been described.[4] Simple crystallization in
this case afforded a single pure isomer.

13   14, X = H   16, R = H   18, R = H

              15, X = Ac   17, R = CH₃   19, R = CH₃

20, R = H, R' = CH₃   23, R = H, R' = CH₃

21, R = R' = CH₃   24, R = R' = CH₃

22, R = CH₃, R' = CF₃   25, R = CH₃, R' = CF₃

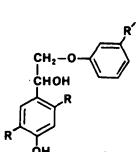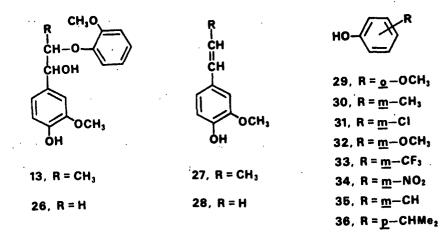Two analogs of the C_2-m-methyl alcohol **12A**, having different ring A substituents, were also synthesized; these correspond to structures **23** and **24**. Model **23** was made by brominating commercially available ketone 16 to give **18**, coupling this product with m-cresol to give **20**, and reducing the latter with NaBH$_4$. The synthesis of model **24** began with acylating 2,5-dimethylphenol (**14**), followed by a Fries rearrangement of **15** to **17**, bromination to **19**, coupling with m-cresol to ketone dimer **21**, and finally NaBH$_4$ reduction. A similar sequence was used to prepare **25**, a m-CF$_3$ analog.

Model Selection

Why two sets of β-ring analogs? Our interest was initially only in C_3-models, **11**, even though their synthesis and characterization presents more problems than the C_2-models, **12**. The larger models, **11**, have the 3-carbon side chain, as does lignin, and possibly provide more reliable product analyses; their disadvantage, however, is their lack of tendency to crystallize to pure isomers.

Previous studies with C_2- and C_3-analogs **13** and **26** demonstrated the value of using the larger model.[5] Fragmentation of the C_2-model **26** by AHQ produces vinylguaiacol (**28**) and guaiacol (**29**), which in turn react somewhat with each other, thereby interfering with quantification of fragmentation. The corresponding fragments from the C_3-model **13**, namely isoeugenol (**27**) and guaiacol are stable to each other in the presence of AHQ.

13, R = CH$_3$

26, R = H

27, R = CH$_3$

28, R = H

29, R = o-OCH$_3$

30, R = m-CH$_3$

31, R = m-Cl

32, R = m-OCH$_3$

33, R = m-CF$_3$

34, R = m-NO$_2$

35, R = m-CH

36, R = p-CHMe$_2$

The guaiacol recovery problem is, however, probably only
limited to AHQ reactions; soda model reactions should give little,
if any, styrene-type products.[6] Indeed, the C_2-m-R B-ring substi-
tuted models (12) behaved well in the soda degradations; phenol
yields were reasonable and reproducible.

Models differing in substituents on the A ring would be
expected to provide less information than B ring models concerning
the mechanism of soda promoted fragmentation. They were, however,
studied to verify the B ring model soda results and provide valuable
information in the additive experiments (accompanying paper).

Phenol Analysis

A reliable analytical procedure was needed to determine the
extent of fragmentation of the model compounds under varying con-
ditions. Analysis of changes in the level of starting material
(model compound) with time has many problems associated with it.
For example, the model can be lost via reactions, much as enol
ether formation, which are not fragmentation reactions of the β-
linkage. Also, the α-hydroxy models dehydrate easily upon gas
chromatography (GC) analysis. The simplest indicators of fragmen-
tation of the model are the phenols produced.

In general, the level of ring "B" phenol (29-33) produced is
taken to be indicative of the extent of fragmentation (or delignifi-
cation).[6] In our case, some of the ring B phenols are reasonably
water soluble - making quantification difficult when extraction
steps are involved. We therefore sought an analytical method
which could convert an alkaline phenol solution into water insol-
uble phenol derivatives. Two such methods were developed; each
involved the use of p-isopropyl phenol (36) as an internal stan-
dard (IS).

The one method consisted of treating an alkaline aqueous phenol
mixture (containing IS) with dimethylsulfate to convert phenolate

salts to methyl ethers, extracting with chloroform, and analyzing
by GC. The other method involved stirring the aqueous alkaline
phenol mixture containing IS with benzoyl chloride in toluene in
the presence of a phase transfer catalyst, separating the organic
solvent, washing, and analyzing by GC the resulting benzoate deri-
vatives. The latter method was the most reproducible but was only
successful with selected phenols. Consequently, the methylation
procedure was the one employed throughout the work, and the benzoyl-
ation method was only used as a check. The agreement between
methods was good.

Model Degradations - General

The lignin model compounds were dissolved in deoxygenated
water containing NaOH and placed in small pressure vessels along
with any additional water or water-NaOH solutions. All operations
were done in a glove bag under a nitrogen atmosphere. The
pressure vessels were sealed under nitrogen, rotated in a
prewarmed oil bath for specific time periods, cooled, opened, and
emptied. The reacted solutions were diluted with a known level of
IS, dissolved in aq. alkali, derivatized by methylation or ben-
zoation, and analyzed by GC.

Product mixtures, both before and after derivatizations, were
also examined by GC-mass spectroscopy (MS). The only volatile
products observed were starting materials (α-hydroxy models), vinyl
ethers, the ring B phenols, and guaiacol. The latter, which is
present only in small amounts, must arise from ring A by cleavage
of the C_α-ring carbon bond.

RESULTS

Model Degradations - Ring B Analogs

Models 12A-D (m-R, B ring analogs) were placed in the same
reaction vessel and heated at 170°C with high levels of NaOH to

produce the data shown in Fig. 1. The initial rate of fragmen-
tation and also the final extent of fragmentation followed the
order $\underline{m}$-CF$_3$ > $\underline{m}$-Cl > $\underline{m}$-OCH$_3$ > $\underline{m}$-CH$_3$ for the C$_2$-models of the type
12. This same order was observed at 135°C and 150°C for 12A-D
and for the C$_3$-models 11A-D at 150°C; the magnitude of the dif-
ferences was, however, much less at the lower temperatures. The
rate and extent of fragmentation also decreased substantially at
lower NaOH levels.

The data of Fig. 1 point out that there are two fragmentation
processes: a fast one, occurring in the first 20 min, and a slow
one thereafter. Analysis by GC-MS shows essentially no starting
material was left after 40 min for both the high and low NaOH level
degradations; only simple ring B phenol and cis/trans isomers of
vinyl ethers remained (Fig. 2). Vinyl ether by-products have also
been observed in the soda induced degradation of the guaiacyl B ring
model 26.[7,8]

These data indicate that H$_\beta$ attack by HO$^-$ to afford vinyl
ethers (38, path a) competes with hydroxide induced fragmentation
(path b) in the first few minutes of the reaction and that, in a
slower reaction (path c), the vinyl ethers also fragment (Scheme
2). The rate of vinyl ether fragmentation appears not to depend
on the nature of the B ring substituent, since the rates of all
four substrates are the same after about 20 min (Fig. 1).

Both vinyl ether generation and model fragmentation (paths a
and b, Scheme 2) depend on hydroxide ion attack; however, fragmen-
tation responded more to changes in the NaOH concentration. This
fact has been demonstrated by complete time vs. phenol fragment
yield studies (Fig. 1) and by observing phenol yields at specific
times when employing different levels of NaOH. The phenol yields
did not vary much when the ratio of NaOH/model were 5-25/1, but
showed significant increases at the 80/1 and 150/1 ratios. Holding
the ionic strength constant by the addition of NaCl had little
effect. Acceleration of fragmentation of β-aryl ether models by
increasing the alkali strength has also been observed by others.[7,9]

It appears that the rate of vinyl ether generation is fast and dominates at low NaOH levels. At high NaOH levels a shift in the $12^- + HO^- \rightleftharpoons 12^{-2} + H_2O$ equilibrium toward 12^{-2} probably occurs. According to Scheme 2, increasing the level of 12^{-2} in the system should favor fragmentation.

The order of reactivity at the early reaction times, namely, $CF_3 > Cl > OCH_3 > CH_3$, indicates that electron withdrawing groups aid the direct fragmentation of the models. In fact there is a good correlation between the model reactivities and the substituents' Hammett sigma values (Table 1, Fig. 3).[3]

<div align="center">

TABLE 1

Hammett σ Values[a]

</div>

Substituent	σ_m
NO_2	+ 0.71
CF_3	+ 0.42
Cl	+ 0.37
OCH_3	+ 0.12
CH_3	− 0.17
O^-	− 0.71

[a]Groups which supply electrons have negative (−) σ values; groups which withdraw electrons have positive (+) σ values. The magnitude of the σ values reflects how well they supply or withdraw electrons.

An electron withdrawing group on ring B would be expected to favor either step (b_1 or b_2) in the proposed direct fragmentation mechanism (Scheme 2). A group such as CF_3 would favor step b_1 (base abstraction) by increasing the acidity of the α-OH proton and step b_2 (β-aryl ether cleavage) by stabilizing the ring B phenolate ion fragment.[3] The fact that the ρ-value (the slope of the 10-minute line in Fig. 3) is roughly + 0.7 argues that the cleavage step is probably the rate determining step in the sequence.

The ρ-value is a measure of the sensitivity of the reaction to ring substitution.[3] Reactions performed at elevated temperatures should be influenced less by substituent changes than those done at room temperature. Consequently, the magnitude of a ρ-value should decrease with increasing temperature. Based on the temperatures employed (170°C) in the degradations and the large distance between the meta ring substituents and the α-OH group, one would expect that the ρ-value for step b_1 of the mechanism would be less than + 0.2.[3] The observed value of + 0.7 is more in accord with the generation of a phenolate ion as the slow step, since the expected ρ-value would be about + 1.0 to 2.2 at room temperature.[3]

Besides temperature effects, the magnitude of the differences (a reflection of the ρ-value) between the substituents CF_3, Cl, OCH_3, and CH_3 could be attenuated by competing vinyl ether formation reactions. If step a_1 (QM generation) was fast and step a_2 (C_β-proton abstraction) was slow in the sequence of reactions leading to vinyl ether products, then models with electron withdrawing groups on ring B would give rise to more vinyl ether products than models with electron releasing groups on ring B. When the rate of vinyl ether formation increases, there will be less direct model fragmentation. Thus, a CF_3 group could promote both rapid direct model fragmentation and rapid vinyl ether formation, with the latter reaction detracting from the overall potential yields of the former reaction.

If step a_1 (QM generation) was slow relative to step a_2 (C_β-H abstraction), substituents on ring B would have no effect on vinyl ether formation rates nor would they have any indirect effects on model fragmentation yields. Working at 143.5°C and with model 26, Gierer and Ljunggren claim that QM formation is more rapid than C_β-H abstraction; they observed only a slow disappearance of 26 with time.[9] Our results, using slightly different models at 170°C, do not distinguish which step is slower.

In summary, the ring B substituent-reactivity relationships establish that

- If C_β-H ionization is the slow step in vinyl ether production, the slow step in the direct model fragmentation cannot be C_α-OH ionization, since C_β-H is two bonds closer to the substituents than C_α-OH, and thus vinyl ether generation would dominate over fragmentation with groups such as CF_3.

- If quinonemethide formation is the slow step in vinyl ether production, either C_α-OH ionization or β-aryl ether cleavage can be the slow step in the direct model fragmentation.

- The sensitivity of the model fragmentation reactions to the nature of the substituents (even at 170°C) suggests that the substituent is heavily involved in the transition state of the rate determining step, which argues in favor of a slow β-aryl ether cleavage step as opposed to a slow C_α-OH ionization step.

Model Degradations - Ring A Analogs

A direct comparison of the aq. alkaline degradations of ring A model analogs at 170°C showed the following order of fragmentation efficiency: 2',5'-dimethyl-m-CF_3 alcohol **25** > 2',5'-dimethyl-m-CH_3 alcohol **24** > 3'-methoxy-m-CH_3 alcohol **12A** ≈ unsubstituted-m-CH_3 alcohol **23**. Actually, model **24** was nearly twice as reactive as the other two m-methyl analogs, with **12A** slightly more reactive than **23**. The observed reactivity differences probably reflect a combination of polar and steric substituent effects.

#	R_1	R_2	R_3
12A	CH_3	OCH_3	H
23	CH_3	H	H
24	CH_3	CH_3	CH_3
25	CF_3	CH_3	CH_3

Based on Hammett σ values and the probable importance of benzylic hydroxyl ionization to the reaction mechanism, the expected order of reactivity is 3'-methoxy **12A** > unsubstituted **23** > the two 2',5'-dimethyl alcohols **24** and **25**, assuming only polar effects operating. The unusually high reactivity of the dimethyl models **24** and **25** may be the result of a steric effect by the 2'-methyl group which retards vinyl ether and/or condensation side reactions; thus, fragmentation reactions take on greater prominence. Crowding effects on the β-carbon also enhance model fragmentation.[5]

CONCLUSIONS

The level of hydroxide used in soda treatments of m-R B ring substituted models **12A-D** dictates the course of degradation reactions taken, vinyl ether formation or direct fragmentation. The slow step in the direct fragmentation appears to be cleavage of the β-aryl ether bond. Vinyl ether by-products also fragment by a much slower reaction and by a mechanism which does not appear to be influenced by ring B substituents or alkali level.

EXPERIMENTAL SECTION

The equipment has been previously described.[10] All melting points are corrected. Most of the methods used to prepare the compounds described in this report were identical to procedures already published for very similar compounds and, therefore, will not be described here in individual detail. These methods include coupling of β-bromoketones with phenolate ions to give dimer model ketones **9A-D**, **9F**, and **20-22**;[4] methylation of dimer model ketones to give **10A-D**;[11] and sodium borohydride reduction of model ketones to give α-hydroxy models **11A-D**, **12A-F**, and **23-25**.[4]

The physical data and NMR data for the compounds prepared by standard methods are given in Tables 2-6. All the compounds in these tables showed infrared signals cm^{-1} at 3200-3400 (OH) and

typical aryl absorptions; compounds **9A-F, 10A-D**, and **20-22** also showed 1660-1670 (C=O).

4-Acetoxy-3-methoxy-α-bromoacetophenone (5). A sample of 15.0 g of 4-acetoxy-3-methoxyacetophenone (4)[12] was brominated using a procedure similar to that of Erdtmann and Leopold[13] to give 9.0 g (44% yield) of colorless crystals, m.p. 85.0-87.0°C from ethanol [lit.[13] m.p. 88.0-88.5°]; IR (mull) cm^{-1} 1730 (ester C=O), 1690 (ketone C=O), and 1600 (aryl); ^{1}H-NMR (CDCl$_3$) δ 2.33 (s, 3, Ac), 3.89 (s, 3, ArOCH$_3$), 4.42 (s, 2, CH$_2$Br), 7.13 (d, 1, aryl) and 7.53 (s and d, 2, aryl).

1-(4'-Acetoxy-3'-methoxyphenyl)-2-(3"-nitrophenoxy)ethanone (8E). To a stirred mixture of 4.0 g (14 mmoles) of **5**, 1.5 g (9 mmoles) of KI, 3.1 g (22.5 mmoles) of K$_2$CO$_3$, and 50 mL of dry acetone was added dropwise 2.4 g (17 mmoles) of m-nitrophenol dissolved in 40 mL of anhydrous acetone. The mixture was refluxed for 3 hr, distilled to remove most of the acetone, diluted with 100 mL of water and extracted three times with 50 mL of chloroform. The CHCl$_3$ extracts were combined, washed with 0.5M NaOH and water, dried (anhydrous Na$_2$SO$_4$) and evaporated to give a solid residue, 3.8 g (80% yield). Recrystallization from benzene-petroleum ether gave crystals (61.5%), m.p. 130-133°C; IR (mull) cm^{-1} 1760 (ester C=O) 1690 (ketone C=O) and 1600 (aryl); ^{1}H-NMR (CDCl$_3$) δ 2.35 (s, 3, Ac), 3.91 (s, 3, OCH$_3$, 5.38 (s, 2, -CH$_2$-), and 7.14-7.93 (m, 7, aryl); MS, m/e (%), 345 (M$^+$, 1) 303 (12), 151 (100), 137 (4), 123 (6), 92 (3), 76 (3), and 65 (3).

1-(4'-Hydroxy-3'-methoxyphenyl)-2-(3"-nitrophenoxy)ethanone (9E). A mixture of 0.32 g (6 mmoles) of sodium methoxide, 1.75 g (5.1 mmoles) of **8E** and 20 mL of absolute methanol was refluxed for 2 1/2 hr, cooled, diluted with water and acidified with concentrated HCl to give a precipitate. The suspension was warmed and extracted while warm with CHCl$_3$. The combined warm CHCl$_3$ extracts were washed with water twice and saturated NaCl solution twice, dried (Na$_2$SO$_4$) and concentrated. The resulting precipitate was recrystallized from absolute ethanol, 0.944 g, m.p. 187.5-189.5; other physical data are given in Tables 2 and 4.

1-(4'-Acetoxy-3'-methoxyphenyl)-2-(3"-acetoxyphenoxy)ethanone

(8G). The procedure used was similar to that for the preparation of **8E**, except **5** and m-acetoxyphenol[14] were used, along with a silica gel column chromatography product purification. The chromatography, with toluene and toluene-ethyl acetate elution, afforded m-diacetoxy-phenol, 4-acetoxy-3-methoxy-α-iodoacetophenone (m.p. 97.5-99.5 from benzene recrystallization), and **8G** (7% yield): m.p. 103.5-105.5 (benzene); IR (mull) cm^{-1} 1760 and 1740 (ester C=O), 1710 (ketone C=O), and 1600 (aryl); ^{1}H-NMR (CDCl$_3$) δ 2.28 (s, 3, Ac), 2.34 (s, 3, Ac), 3.89 (s, 3, OCH$_3$), 5.23 (s, 2, -CH$_2$-), 6.65-6.86 (m, 3, aryl), 7.10-7.36 (m, 3, aryl) and 7.53-7.62 (m, 1, aryl); ^{13}C-NMR (CDCl$_3$) ppm 20.5 and 21.0 (q, Ac methyls), 55.9 (q, OCH$_3$), 70.6 (t, -CH$_2$-), 108.4, 111.4, 112.1, 114.5, 121.0, 122.7, and 129.6 (d, aryl), 132.7, 132.9, 144.0, 151.3, 158.4 (s, aryl), 167.9 and 168.7 (s, ester C=O) and 192.3 (s, ketone C=O); MS, m/e (%), 358 (M$^+$, 3), 316 (15), 274 (9), 151 (100), 137 (5), 123 (8), 93 (3), and 65 (4).

1-(4-Hydroxy-3'-methoxyphenyl)-2-(3"-hydroxyphenoxy)ethanone

(9F). This compound has been obtained in two ways. The one way employed a procedure similar to the conversion of **8E** to **9E**, namely a hydrolysis of **8E** to **9F**; again solubility problems arose and the yield was low. The other procedure employed the standard coupling reaction of **6** with sodium m-acetoxyphenolate (**7G$^-$**) with chromatography work-up; small amounts of **9F** were obtained directly from the chromatography, meaning that a transesterification or hydrolysis reaction had occurred. Both procedures gave **9F** of m.p. 145-146 (benzene); physical data are given in Tables 2 and 4.

2,5-Dimethyl-4-hydroxy-α-bromoacetophenone (19). The standard bromination procedure[4] was used to convert 17.2 g of 2,5-dimethyl-4-hydroxy acetophenone (**17**)[15] to 20.2 g crystals, m.p. 129-131°C (ether) and 1.5 g of solid from evaporation of the ether mother liquor. A ^{1}H-NMR indicated that the crystals were a 70/30 mixture of **19/17**; physical data on **19** are given in Tables 2 and 4.

1-(4'-Hydroxy-3'-methoxyphenyl)-2-(3'-substituted phenoxy) ethanol (11A-D). The **11** series compounds were prepared by the

standard $NaBH_4$ reduction procedure applied to the corresponding ketone, **9A-D**. Spectral analysis of the crude products (oils) indicated that they were mixtures of diastereomers; infrared spectra showed no carbonyl absorptions and typical OH and aryl absorptions. The NMR spectra showed no carbonyl signals (i.e., 190-210 ppm in the ^{13}C) and no downfield proton aryl signals in the ^{1}H-NMR, which also showed the lack of a α-carbonyl. Their mass spectra all displayed prominent m/e 153 signals, indicative of fragmentation between C_1 and C_2 with charge retention on C_1.[16] Specific interpretations of the spectral data follow.

m-CH$_3$ (**11A**). Reduction of 2.0 g of **9A** with 2.6 g (40 equiv.) of $NaBH_4$ gave 2.3 g of oil, still containing small amounts of EtOH. Extensive evaporation removed nearly all of the EtOH. The oil is approximately a 60/40 ratio of isomers, based on ^{1}H-NMR. The oil was dissolved in warm toluene and placed on a silica gel column (2 x 38 cm). Elution of the column with 150 mL of toluene, 400 mL of 2% ethylacetate-toluene, 400 mL of 5% mixture and 250 mL of 10% mixture led to 18 fractions, which were combined into two main fractions, namely 1-7 and 8-16. The former was a 60/40 ratio and the latter a 30/70 ratio of isomers, based on ^{1}H-NMR. Comparison of the ^{13}C-NMR of the fractions allowed several of the signals to be assigned to each isomer. The ^{1}H-NMR (CDCl$_3$, δ) showed 1.10 and 1.18 (d, 3, J = 6 cps, C$_3$-methyls), 2.32 (s, 3, aryl methyl), 3.88 (s, 3, OCH$_3$), 4.3-4.7 (m, 2, C$_1$ and C$_2$ protons), 5.67 and 5.70 (s, 1, ArOH), 6.7-7.2 (m, 7, aryl) and 1.7, 2.6, 3.1, and 4.9 (broad s, 1.7, ROH and impurities). The ^{13}C-NMR (CDCl$_3$, ppm) showed 13.1, 15.8, and 21.4 (q, C$_3$ and aryl CH$_3$), 55.8 (q, OCH$_3$), 75.0, 77.8, 77.9, and 78.9 (C$_1$ and C$_2$ among the CDCl$_3$ signals), 108.9, 109.4, 112.9, 113.0, 114.0, 117.0, 119.2, 120.5, 122.0, 122.1, and 129.2 (d, aryl), 131.6, 132.0, 139.5, 144.8, 145.4, 146.3, 146.4, 157.2, and 157.4 (s, aryl). The MS, m/e (%), showed 288 (M, 6), 153 (100), 151 (15), 136 (42), 135 (16), 125 (21), 108 (10), 91 (26), 77 (8), 65 (20).

m-Cl (**11B**). A 0.60 g sample containing 60% **9B** and 40% **9H** was reduced with 0.88 g (14 equiv.) of $NaBH_4$ to give 0.74 g of oil.

The ^{1}H-NMR (CDCl$_3$, δ) showed 1.11 and 1.21 (d, J = 6 cps, 3, C$_3$-
methyls of the diastereomers, 60/40 ratio), 3.90 (s, 3, OCH$_3$), 4.2-
4.9 (m, 2, C$_1$ and C$_2$-protons), 5.62 and 5.69 (s, 1, ArOH, 40/60
ratio), 6.7-7.3 (m, 7, aryl) and 1.5, 2.4 and 2.9 (broad s, 1.2,
ROH and impurities). The ^{13}C-NMR (CDCl$_3$, ppm) was quite complex
with 13.2, 13.4, and 15.8 (q, C$_3$-methyls), 55.9 (s, OCH$_3$), nine
signals at 75.0-79.2 (C$_1$ and C$_2$, plus CDCl$_3$), fifteen signals at
108.8-130.1 (d, aryl) and thirteen signals at 131.2-158.1 (s, aryl).
The MS, m/e (%), showed 308 (M for 11B, 2%), 274 (M for 11H, 2%),
153 (100), 125 (10), 93 (25), 77 (12) and 65 (12).

[The presence of the H (proton) compounds in the B (m-Cl) com-
pounds was not easily seen initially. There are practically no
chemical shift differences for the ring A and aliphatic protons
and carbons in the NMR spectra; exceptions are the carbonyl car-
bons of the 9 and 10 compounds. In ^{1}H-NMR, the presence of H or
Cl on ring B also has little effect on the other ring B protons
except, of course, the number of protons differ. The real clues
that H compounds are in some B compounds come from the mass
spectral differences, the ^{13}C-NMR carbonyl differences and
increased numbers of signals, and in the ^{1}H-NMR phenolic hydroxyl
signals and aryl integration.]

m-OCH$_3$ (11C). Reduction of 1.19 g of 9C gave 1.38 g of oil,
containing some ethanol (based on NMR). Attempted recrystalliza-
tion from EtOH/H$_2$O was unsuccessful. Water was added to the re-
crystallization solvents and the product was extracted with CHCl$_3$.
The ^{1}H-NMR showed two sets of signals which indicated that the oil
was approximately a 2:1 mixture of diastereomers; these signals
were at 5.76 and 5.73 (ArOH, singlets) and 1.11 and 1.19 δ (methyl
doublets, J = 6 cps). The ^{1}H-NMR (CDCl$_3$, δ) also showed 3.77,
3.78, and 3.87 (s, 6, OCH$_3$), 4.3-4.7 (m, 2, C$_1$ and C$_2$ protons),
6.5-6.6 (m, 3, aryl), 6.8-7.0 (m, 3, aryl), 7.1-7.3 (m, 1, aryl),
2.6, 3.1, and 4.9 (broad s, 1$^+$, ROH) and residual ethanol. The
^{13}C-NMR (CDCl$_3$, ppm) showed 13.2 and 15.7 (quartets, C$_3$-methyls of
diastereomers, 35/65 ratio), 55.2 and 55.8 (q, OCH$_3$), 74.8, 77.7,

and 78.7 (C_1 and C_2-carbons mixed with $CDCl_3$ signals), 102.5, 106.5, 106.6, 108.0, 108.1, 108.7, 109.2, 114.0, 119.0, 120.3, and 129.7 (d, aryl), 131.4, 131.8, 144.7, 145.3, 146.2, 146.3, 158.3, 158.5, and 160.5 (s, aryl). The MS, m/e (%), showed 304 (m, 5), 153 (100), 152 (32), 151 (32), 125 (30), 124 (19), 123 (10), 107 (17), 93 (59), and 77 (46).

m-CF$_3$ (11D). Reduction of 0.30 g of 9D gave 0.28 g of oil. Recrystallization from EtOH/H_2O was not successful. The ^{1}H-NMR ($CDCl_3$, δ) showed 1.13 and 1.24 (d, J = 6 cps, C_3-methyls, ca. 60/40 ratio), 3.90 (s, OCH_3), 4.3-4.9 (m, C_1 and C_2 protons), 6.9-7.4 (m, aryl) and 2.0 and 5.6 (v. broad, hydroxyls). The ^{13}C-NMR ($CDCl_3$, ppm) showed 13.5 and 15.7 (q, C_3-methyls, ca. 30/70 ratio), 55.8 (q, OCH_3), 75.2, 77.6, 78.2, and 79.1 (C_1 and C_2 mixed in with $CDCl_3$ signals), 108.9, 109.2, 112.8, 112.9, 114.0, 114.1, 117.6, 117.8, 119.2, 120.2, and 129.8 (d, aryl), 131.2, 145.0, 145.5, 146.3, 146.4, and 157.5 (s, aryl), and 131.7 (q in coupled and decoupled spectra, C-CF$_3$. The MS, m/e (%), showed 342 (M, 10), 181 (11), 153 (100), 151 (9), 145 (7), 125 (14), 93 (23), and 65 (10).

Degradation Procedure. The model degradations were conducted in 4-mL capacity pressure vessels (bombs). The bombs, as many as 14 at a time, were mounted on a metal plate, which was rotated in an oil bath by means of a chain-drive system and stirring motor. The rotation could be stopped at various times to remove bombs.

The bombs were filled and sealed in a nitrogen atmosphere (glove bag). All solutions were prepared in a glove bag using deoxygenated, distilled water. All reactant solutions, IS solutions, etc., were added with an automatic pipette.

Standard solutions of sodium hydroxide and model compounds and p-isopropylphenol (IS) in aq. NaOH were prepared just prior to use. The models were present in 0.015 mmole amounts and the other reagents were adjusted to 0.015 mmole = 1 equiv.

The appropriate solutions and make-up water were added to the cool bombs. After heating for specific lengths of time, the bombs

were removed from the hot oil bath, immediately cooled in ice-water, opened, diluted with IS solution, and the contents transferred to an Erlenmeyer flask for derivatization, followed by GC analysis. Several 1M NaOH and water washes of the bombs were used to ensure quantitative transfer.

Methylation. Dimethylsulfate (1 mL, 100-350 equiv./model) was added to the product/IS mixture, and the solution was stirred rapidly for 15 min in a loosely stoppered Erlenmeyer flask. Concentrated ammonium hydroxide (4.5 mL) was thus added to quench the excess Me_2SO_4, and the solution was stirred another 15 min. Chloroform (2 mL) was added, and the solution was stirred vigorously for 2 min. The $CHCl_3$ phase was then removed with a disposable pipette, dried over Na_2SO_4 and analyzed by G.C. [Additional $CHCl_3$ extractions gave the same ratio of products to IS at a much more dilute concentration, and were thus not useful.]

Benzoylation. In this case the bombs were washed three times with 1.5 mL 1M NaOH and twice with 1.5 mL toluene. Benzoyl chloride (21 µL, roughly 5 equiv./model) and 8 mg (0.4 equiv./model) of benzyltributylammonium bromide were added to the Erlenmeyer containing the base solution, toluene and a stir bar. After stirring for 30 min, the aqueous layer was pipetted off, and the organic layer was washed twice with 3 mL 1M NaOH, twice with water, dried over Na_2SO_4, and analyzed by G.C.

Just as in the methylation procedure, reagent amounts and conditions were adjusted to give maximum, reproducible derivatization. Standard mixtures of phenols were also derivatized to give samples for determining G.C. response factors.

Analysis. Analysis of product mixtures for their phenol content was done on a 5890 Hewlett Packard gas chromatograph using a 6 foot 1/4-inch glass column packed with 3% silicone OV-17 on 100/120 chromosorb W-HP. The following temperature program was used: 65° (2 min), then 2°/min to 80° (3 min) and then 30°/min to 285° (4 min).

REFERENCES

1. D. R. Dimmel, J. Wood Chem. Technol., $\underline{5}$, 1 (1985).

2. D. R. Dimmel, L. F. Perry, P. D. Palasz, and H. L. Chum,
    J. Wood Chem. Technol., $\underline{5}$, 15 (1985).

3. J. March, <u>Advanced Organic Chemistry</u>, 3rd ed., Wiley & Sons,
    New York, 1985, 151-70, 237-50.

4. D. R. Dimmel and D. Shepard, J. Wood Chem. Technol., $\underline{2}$, 297
    (1982).

5. D. R. Dimmel and L. F. Perry, submitted for publication.

6. J. Gierer, Holzforschung, $\underline{36}$, 43 (1982).

7. J. R. Obst and N. Sanyer, Tappi, $\underline{63}$(7), 111 (1980).

8. Unpublished work, our laboratory.

9. J. Gierer and S. Ljunggren, Svensk Papperstid., $\underline{82}$, 503 (1979).

10. D. R. Dimmel, D. Shepard, and T. A. Brown, J. Wood Chem.
    Technol., $\underline{1}$, 123 (1981).

11. D. R. Dimmel and D. Shepard, J. Org. Chem., $\underline{47}$, 22 (1982).

12. H. Finnemore, J. Chem. Soc., $\underline{93}$, 1515 (1908).

13. H. Erdtman and B. Leopold, Acta Chem. Scand., $\underline{3}$, 1358 (1949).

14. Aldrich Chemical Co., Milwaukee, Wisconsin, U.S.A.

15. K. Auwers, H. Bundesmann, and F. Wieners, Ann., $\underline{447}$, 162
    (1926).

16. D. R. Dimmel and D. Shepard, J. Wood Chem. Technol., $\underline{1}$, 147
    (1981).

TABLE 2

Selected Physical Data for Synthesized Compounds

Cpd.	% Yield[a]	m.p. (°C) Solvent[b]	Mass Spectrum, m/e (%)[c]
9A	53	170.5-172.5 (aq. EtOH)	272(M,22), 151(100), 137(5), 123(8), 108 (4), 91 (7), 77 (4), 65 (7)
9B	82	118-9 (tol.)	292/294(M,12), 151(100), 137(4), 123(9), 122(3), 111(3), 108(3)
9C	75	109-10 (tol./p.e.)	288(M,16), 151(100), 137(6), 123(10), 108(6), 92(6), 77(9), 65(5)
9D	88	107.5-8.5 (benz./p.e.)	326(M,12), 151(100), 145(14), 123(13), 108(8), 77(5), 65(7)
9E	65	187.5-9.5 (EtOH)	303(M,5), 151(100), 123(12), 122(4), 108(5), 94(3), 77(3), 76(3), 65(4)
9F		145-6 (benz.)	274(M,27), 152(9), 151(100), 137(7), 123(12), 93(5), 65(9)
10A	48	86-8 (benz./p.e.)	286(M,18), 151(100), 135(23), 123(7), 108(4), 107(4), 91(15), 77(3), 65(7)
10B		117.5-9.5	306/308(M,8), 151(100), 123(10), 111(8), 108(6), 91(8), 77(6), 65(7)
10C	32	131-2 (benz./p.e.)	302(M,28), 151(100), 123(16) 77(19)
10D	12	121-3 (tol.)	340(M,10), 152(9), 151(100), 145(6), 123(8)
12A	89	94-6 (tol.)	274(M,12), 153(100), 137(13), 125(37), 122(40), 93(56), 91(29), 77(11), 65(38)
12B	88	132-4 (tol.)	294(M,6), 154(9), 153(100), 125(13), 93(30), 65(14)
12C	85	101-2.5 (tol.)	290(M,14), 166(15), 153(100), 138(26), 137(14), 125(19), 107(10), 93(35), 77(14), 65(15)
12D	93	125-5.5	328(M,17), 154(9), 153(100), 145(10), 125(15), 93(33), 65(13)

See end of table for footnotes.

TABLE 2 (Continued)

12E	98	138-40	305(M,7), 153(100), 125(21), 110(6), 93(47), 77(9), 65(20)
12F		120-3 (benz.)	276(M,5), 153(100), 137(14), 125(33), 124(22), 110(17), 93(91), 81(22), 77(17), 65(70)
17[d]	49	131-2 (benz.)	164(M,41), 150(10), 149(100), 121(17), 91(15), 77(14), 65(6)
18[e]	23	132-3 (ether)	214/216(M,16), 122(8), 121(100), 107(10), 93(14), 77(5), 65(13)
19[e,f]	62	129-31 (ether)	242/244(M,19), 164(6), 150(10), 149(100), 135(6), 121(12), 91(14), 77(10), 65(5)
20	44	170.5-2.5 (aq. EtOH)	242(M,14), 122(8), 121(100), 107(5), 93(8), 91(6), 65(11)
21	54	188.5-90.5 (acetone)	270(M,16), 150(10), 149(100), 135(3), 121(8), 91(14), 77(10), 65(8)
22	87	191-4 (tol.)	324(M,2), 150(10), 149(100), 145(9), 135(3), 121(6), 91(12), 77(9), 65(3)
23	60	94.5-6 (tol.)	244(M,6), 136(15), 123(100), 122(45), 108(13), 95(17), 91(18), 77(18), 65(11)
24	85	100.5-3.5 (tol.)	272(M,8), 152(10), 151(100), 135(11), 123(21), 122(31), 108(10), 91(19), 77(12), 65(9)
25	75	145.5-7 (tol.)	326(M,4), 175(3), 152(10), 151(100), 145(15), 123(17), 108(7), 91(7), 77(7)

---

[a]All yields are of purified products, often after column chromatography and recrystallization; omitted yields were difficult to determine (i.e., materials for more than one run combined).

[b]Recrystallization solvents: benz. = benzene, tol. = toluene, p.e. = pet. ether. The lack of indicated solvent means recryst. was not performed.

[c]M = molecular ion.

[d]Known compound;[15] lit. m.p. 130-1°C.

[e]Prepared by the standard bromination procedure.[4]

[f]A 70:30 mixture, see Exp. Section.

TABLE 3

NMR Data for Ketone Model Dimers 10[a]

Cpd.	m-R	OCH$_3$	ArOH	C$_1$	C$_2$	C$_3$	Aryl Signals[b]
10A[c]	2.26	3.89	6.23		5.40	1.69	6.6-7.2(m,5) and 7.6-7.8(m,2)
	21.5	56.0		197.6	76.6	19.4	111.0, 111.8, 114.0, 116.1, 122.2, 124.2, and 129.2(d); 126.9, 139.6, 146.8, 150.9, and 157.5(s)
10B[c]		3.90	6.29		5.42	1.69	6.65-7.25(m,5) and 7.36-7.75(m,2)
		56.0		196.3	76.6	19.1	110.6, 113.0, 113.8, 115.6, 121.3, 123.8, and 130.0(d); 126.4, 134.7, 146.5, 150.8, and 157.8(s)
10C[c]	3.83	3.91	6.24		5.43	1.72	6.8-6.9(m,5) and 7.3-7.8(m,2)
	55.1	55.9		196.9	76.3	19.0	101.5, 106.8, 106.9, 110.6, 113.8, 123.8, and 129.7(d); 126.6, 146.5, 150.6, 158.4, and 160.5(s)
10D[c]	f	3.93	6.13		5.49	1.73	6.9-7.4(m,5) and 7.6-7.8(m,2)
		56.1		196.3	76.6	19.3	110.7, 112.2, 112.5, 114.0, 117.8, 123.9, and 130.0(d); 126.5, 131.8,g 146.8, 151.1 and 157.4(s)

aSignals in δ (^{1}H) and ppm (^{13}C) are relative to TMS zero. While splitting patterns and integration areas are not indicated here, they were in accord with the assignments, i.e., OCH$_3$ appeared as a singlet (rel. area 3) in the ^{1}H-NMR and a quartet in the off-resonance coupled ^{13}C-NMR. Proton signals are given first, carbon-13 signals next.
bNumbers and letters inside the parentheses refer to relative areas and splitting, respectively: m = multiplet, s = singlet, d = doublet.
cCDCl$_3$ solvent. dAcetone-d$_6$ solvent. eDMSO-d$_6$ solvent.
fThe CF$_3$ carbon was not observed as a separate signal.
gThe splitting remains the same in the coupled and decoupled spectra, a quartet (J = 1.3 ppm), C-CF$_3$.

TABLE 4

NMR Data for Ketone Model Dimers 9[a]

Cpd.	m-R	OCH$_3$	ArOH	C$_1$	C$_2$	Aryl Signals[b]
9A[c]	2.30 / 21.5	3.92 / 56.1	6.33	193.1	5.19 / 70.6	6.7-7.2(m,5) and 7.6-7.7(m,2) 110.1, 111.5, 114.0, 115.6, 122.4, 123.4, and 129.2(d); 127.4, 139.6, 146.8, 151.0, and 158.0(s)
9B[c,d]		3.95 / 56.2	6.20	192.1	5.22 / 70.8	6.8-7.0(m,5) and 7.5-7.6(m,2) 111.3, 114.1, 115.3, 115.5, 121.4, 123.5, and 131.0(d); 127.6, 134.8, 148.1, 152.5, and 160.0(s)
9C[c]	3.78 / 55.4	3.95 / 56.2	6.12	192.6	5.20 / 70.5	6.4-7.2(m,5) and 7.5-7.6(m,2) 101.5, 106.6, 107.2, 110.1, 114.0, 123.3, and 129.8(d); 127.4, 146.8, 150.9, 159.1, and 160.7(s)
9D[c,d]	f	3.96 / 56.2	6.20	192.0	5.28 / 70.8	6.9-7.4(m,5) and 7.5-7.6(m,2) 111.2, 112.2, 115.3, 118.0, 119.1, 123.6, and 130.8(d); 127.6, 131.8,g 148.1, 152.6 and 159.4(s)
9E[c]		3.96 / 55.7	6.06	191.5	5.28 / 70.2	6.9-7.0(d,1), 7.2-7.6(m,4) and 7.7-7.9(m,2). 108.9, 111.0, 115.1, 115.6, 121.9, 122.9, and 130.4(d); 125.8, 147.6, 148.5, 152.3, and 158.5(s)
9F[c,e]	5.08	3.95 / 55.5	6.13	192.5	5.20 / 69.6	6.13(s,1), 6.4-6.5(m,3), 6.9-7.2(m,2) and 7.5-7.6(M,2) 101.7, 105.2, 107.9, 110.9, 114.9, 122.7, and 129.6(d); 126.0, 147.5, 152.1, 158.3, and 159.0(s)

a-fSee Table 3 for footnotes.

TABLE 5

NMR Data for Model Dimers of Type 12[a]

Cpd.	m-R	OCH3	ArOH	ROH	C1	C2	Aryl Signals[b]
12A[d]	2.32 21.5	3.90 56.2	5.65	2.80	4.99 72.6	4.03 74.3	6.7-7.2(m,7) 110.7, 112.3, 115.2, 116.0, 119.7, 122.0 and 129.7(d); 134.1, 139.7, 146.5, 147.8 and 159.7(s)
12B[d]		3.91 56.1	7.48	4.59	4.95 72.4	4.05 74.6	6.7-7.4(m,7) 110.6, 114.0, 115.1, 115.5, 119.6, 121.1 and 131.1(d); 133.6, 134.8, 146.5, 147.8 and 160.5(s)
12C[d]	3.78 55.4	3.91 56.2	5.64	2.75	5.04 72.5	4.02 74.4	6.5-6.6(m,3) and 6.9-7.3(m,4) 101.5, 107.0, 107.4, 110.6, 115.2, 119.6 and 130.4(d); 133.9, 146.5, 147.8, 160.8 and 161.5(s)
12D[d]	f	3.92 56.2	5.66	2.69	5.07 72.5	4.08 74.8	6.9-7.5(m,7) 110.7, 112.1, 115.2, 117.6, 119.1, 119.7 and 131.0(d); 131.2,g 133.6, 146.6, 147.9 and 160.0(s)
12E[e]		3.77 55.4	8.86	5.55	4.84 70.4	4.14 73.7	6.7-7.0(m,3) and 7.3-7.8(m,4) 108.6, 110.3, 114.7, 115.1, 118.5, 121.7 and 130.2(d); 132.5, 145.4, 146.9, 148.3 and 158.7(s)
12F[e]	8.83	3.34 55.3	9.33	5.43	4.78 70.5	3.88 72.8	6.3-6.4(m,3) and 6.7-7.0(m,4) 101.5, 104.8, 107.5, 110.2, 114.6, 118.4, and 129.4(d); 133.0, 145.3, 146.9, 158.0, and 159.3

a-f, see Table 3 footnotes.

TABLE 6

NMR Data for Substituted Ring A Models

Cpd.	ArACH$_3$	ArBCH$_3$	ArOH	ROH	C$_1$	C$_2$	Aryl Signals[b]
17c	2.26 2.49		6.49			2.56	6.66(s,1) and 7.58(s,1)
	15.2 21.8				199.8	29.0	118.4 and 133.6(d); 120.8, 129.7, 139.5, and 156.9(s)
18d			9.32			4.62	6.96(d,2) and 7.95(d,2);
					189.8	32.2	115.9 and 131.8 (d); 126.6 and 162.6(s)
19c	2.26 2.49		5.49			4.40	6.67(s,1) and 7.56(s,1)
	15.6 21.8				191.5	34.8	118.8 and 134.3(d); 122.1, 126.1, 140.8, and 159.5(s)
20e		2.25	10.44			5.39	6.7-6.9(m,6) and 7.89(d,2)
		21.3			192.3	69.6	111.5, 115.1, 115.3, 121.5, 129.0, and 130.4(d); 125.9, 138.7, 157.9, and 162.4(s)
21d,e	2.27 2.41	2.22	8.90			5.23	6.7-6.8(m,4), 7.0-7.2(m,1), and 7.77(s,1)
	15.5 21.2	21.3				70.6	111.4, 115.1, 117.8, 121.2, 128.9, and 132.4(d); 121.0, 125.1, 138.6, 157.9, and 158.8(s)

TABLE 6 (Continued)

22^d	2.22 2.42	15.4 21.3	9.01		5.47	193.9 70.6	6.77(s,1), 7.2-7.6(m,4), and 7.82(s,1) 110.8,^{h} 116.9,^{h} 117.7, 118.5, 130.2, and 132.4(d); 120.9, 124.6, 129.9,^{g} 138.6, 158.1, and 158.8(s)
23^e	2.25 21.0		9.27	5.38	4.78 70.4	3.91 72.8	6.7-6.8(m,5) and 7.0-7.2(m,3) 111.2, 114.5, 114.8, 120.8, 127.2, and 128.8(d); 132.3, 138.5, 156.2, and 158.2(s)
24^{c,d}	2.26 2.31	15.8 18.7	5.33	2.84	5.25	3.96	6.53(s,1), 6.7-6.8(m,3), and 7.1-7.3(m,2) 112.1, 115.8, 116.8, 121.8, 129.3, and 129.6(d); 121.8, 130.9, 133.8, 129.5, 154.7, and 159.5(s)
	21.4				69.0	73.4	
25^d	2.17 2.27	15.9 18.7	8.02	4.51	5.22	4.09	6.63(s,1) and 7.2-7.6(m,5) 112.0,^{h} 117.0, 117.6,^{h} 119.1, 129.3, and 131.0(d); 122.0, 130.4, 131.6,^{g} 133.9, 154.9, and 159.8(s)
					68.7	73.8	

a-f, see Table 3 footnotes.
^{g}Fine doublet (J = 0.2 ppm) in the decoupled spectrum; signals probably correspond to C_2'' and C_4''.

SCHEME 1

Steps in the Model Syntheses

#	R
A	CH₃
B	Cl
C	OCH₃
D	CF₃
E	NO₂
F	OH
G	OAc
H	H

SCHEME 2

Modes of Soda Induced Decomposition of Models 12

Figure 1. Phenol yields as a function of time in the simultaneous
           degradation of models **12A-D** at 170° in the presence
           of 150 equivalents of NaOH (upper four curves) and the
           single degradation of **12A** at 170° with 12.5 equiv. of
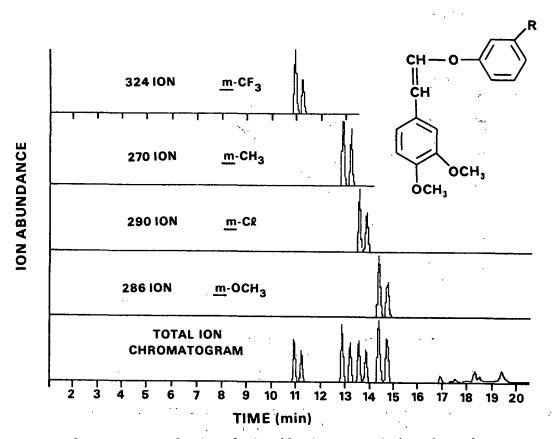   NaOH (lower curve).

Figure 2. GC-MS analysis of the 40 minute methylated product
mixture from the simultaneous degradation of models
12A-D at 170° with 150 equiv. of NaOH. Ion selection
(top portion of the figure) shows the various cis/trans
vinyl ethers (**38**) derived from **12A-D**. The bottom por-
tion of the figure displays the total ion chromato-
graph; early signals due to phenol fragments are not
present because of a time delay which was used in the
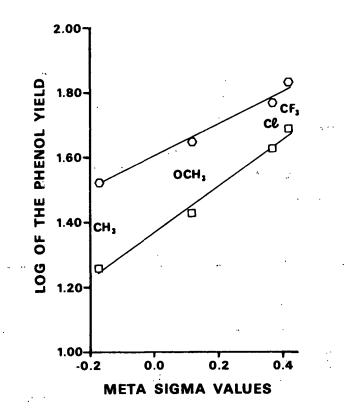analysis and the later signals correspond to dimers of
vinyl guaiacol (**28**).

Figure 3. Correlation of σ_m values with the log of the phenol
liberation yields obtained from Fig. 3: ☐ , 10 min
yields; ◯, 60 min yields.

STRUCTURAL/REACTIVITY STUDIES (II): REACTIONS OF
LIGNIN MODEL COMPOUNDS WITH PULPING ADDITIVES

Donald R. Dimmel and Lois F. Perry
The Institute of Paper Chemistry
P.O. Box 1039, Appleton, Wisconsin 54912

ABSTRACT

Lignin model compounds containing a phenolic "A" ring, α-OH, and β-aryl (ring "B") ether, with different substituents located on rings A and B, have been degraded under a variety of conditions in the presence of NaOH (soda), NaOH/Na$_2$S (kraft), NaOH/glucose, and NaOH/AHQ (soda/AQ). Substituent changes on ring B had no effect in the presence of excess AHQ and NaSH, while substituent changes on ring A had large effects under soda/AQ and kraft conditions for model degradations. These substituent-reactivity relationships indicate that the slow step in the mechanism for model fragmentation under soda/AQ and kraft conditions is quinonemethide formation. Conditions aimed at demonstrating the existence of electron-transfer fragmentation of the model compounds gave results which were inconclusive, but demonstrated that equilibrium reactions between quinonemethide intermediates exist.

INTRODUCTION

Single electron transfer (SET) reactions offer a way to remove lignin from wood.[1] We are studying ways to demonstrate the importance of these reactions in anthraquinone (AQ) pulping systems and ways to utilize this chemistry to achieve favorable pulping results. Scheme I presents a mechanism by which SET reactions from anhydroquinone (AHQ) species to lignin quinonemethide (QM) species can lead to lignin bond ruptures (and thus delignification). The reactions outlined in Scheme I have been verified by room temperature electrochemical studies of lignin QMs in organic solvents.[2]

In contrast to this "radical" view of AHQ induced delignifi-
cation chemistry, Scheme II offers a generally more accepted
"ionic" mechanism. Here AHQ^{-2} adds to the α-carbon of a lignin QM
to give an "adduct"; in a subsequent step, the adduct fragments to
AQ and two phenolate ions.[3-6] This chemistry is analogous to some
of the ionic mechanisms proposed for soda and kraft pulping
systems.[7] The superior rate of kraft vs. soda delignification
can be explained by the presence of the highly nucleophilic hydro-
sulfide ion (HS$^-$) in the former, which would favor steps 7 and 9
shown in Scheme III.

MECHANISM DIFFERENTIATION

A key difference between the pure ionic and SET mechanisms of
delignification is that the former produces only phenolate ion
fragments, while the latter gives some phenolate radical fragments.
If rupture of the β-aryl ether bonds is the slow step in delignifi-
cation, the SET and adduct mechanisms predict that substitutent
types on the aromatic fragments could have large effects on degra-
dation rates. Phenolate ions, as produced in the adduct mechanism,
are electron-rich species and thus are stabilized by electron-
withdrawing ring substituents.[8] Phenolate radicals (SET
mechanism) are electron-poor species and are therefore stabilized
by electron-releasing ring substituents.[8]

Simple fragmentations of lignin model compounds are, however,
multistep reactions, of which the fragmentation steps may not be
the slow steps in the mechanisms. In fact, quinonemethide genera-
tion is probably the slow step.[9] Miksche has shown that the rate
of isomerization of model diastereomers (step 10) is practically
the same as the rate of guaiacol (G-OH) produced (step 11) when
either diastereomer is subjected to kraft pulping conditions
(Scheme IV). These data suggest that the difficult step in the
isomerization, namely generation of the QM, is also the most

difficult step in the multistep reactions leading to fragmentation of substrates.

The very interesting data of Miksche's leave, however, some unanswered questions. For example, why is the rate of production of guaiacol from the erythro isomer only about 1/2 that of the threo isomer? Also, why is the rate of guaiacol production roughly 40% greater than isomerization from the erythro isomer, but 20% less from the threo isomer? Miksche's study does not define (nor was it intended to) the relative rates of the various steps. Quinonemethide formation may be significantly slower (Fig. 1A) or roughly comparable (Fig. 1B) to subsequent steps.

Using kinetic and competitive experiments with lignin model compounds, Gierer and Ljunggren have defined some relative rates of reactions involving quinonemethides.[10] In addition, there is evidence that AHQ^{-2} reacts faster with QMs than does SH^-, either adding to[11] or electron transferring to the QMs.[2] Although not a QM reaction, fragmentation of β-aryl ether bonds by α-O^- assistance (Scheme III, step 9, X = 0) appears to be a slow reaction relative to the various QM reactions. [Further verification of this statement is part of this present study.] Figure 2 attempts to tie all of this information together in a **hypothetical** energy diagram.

The diagram, which relates only to α-substituted, β-aryl ether lignin units, indicates that the reaction options for a soda pulping system are poor, consisting of a high energy fragmentation pathway and numerous undesirable by-product pathways (two vinyl ether generation reactions and condensation reactions). A good pulping additive, such as SH^- or AHQ^{-2}, provides a low energy route to fragmentation (delignification) which supercedes many of the undesirable reactions.

If the picture presented above is correct, studying the chemistry of additive induced delignification is a very complicated endeavor. Specifically, how do we define the chemisty of $QM-AHQ^{-2}$

interactions under pulping conditions if the reactions of importance come after the rate-determining step, namely QM generation?

Substituent effects could provide information about the mechanism of the fragmentation step, even if QM generation is the slow step. This is possible if certain steps are reversible and interaction between reactive intermediates occurs. Consider, for example, the following SET reactions which might exist during the competitive reactions of _in situ_ generated QMs which contain different substituents:

$$QM + AHQ^{-2} \rightleftharpoons QM^{\bullet-} + AHQ^{\bullet-} \tag{a}$$

$$QM' + AHQ^{-2} \rightleftharpoons QM'^{\bullet-} + AHQ^{\bullet-} \tag{b}$$

$$QM^{\bullet-} + QM' \rightleftharpoons QM + QM'^{\bullet-} \tag{c}$$

$$QM^{\bullet-} \longrightarrow ArO^- + Ar'O\cdot \tag{d}$$

$$QM'^{\bullet-} \longrightarrow ArO^- + Ar''O\cdot \tag{e}$$

If two quinonemethides (QM and QM') were generated simultaneously, AHQ^{-2} could react with either one. If one of the quinonemethides (i.e., QM') forms a more stable radical anion, one would expect AHQ^{-2} to preferentially undergo SET reactions with that quinonemethide, i.e., Eq. (b) would be preferred to Eq. (a). Many SET reactions are characterized by SET steps between species as part of a chain mechanism;[12-14] therefore, the equilibrium indicated by Eq. (c) should occur and should be shifted in the direction of the more stable species. Depending on the stabilities of Ar'O· and Ar''O·, fragmentation steps (d) and (e) would be expected to proceed at different rates.

In a competitive degradation of two models reacting via SET mechanisms the product distribution should reflect either the stabilities of the QM radical ions or the stabilities of the

resulting phenolate ion and radical fragments. Since QM-AHQ adduct reactions are reversible,[11] similar arguments apply; product distributions from competitive reactions will reflect either the stabilities of the adducts or the stabilities of the resulting phenolate ion fragments.
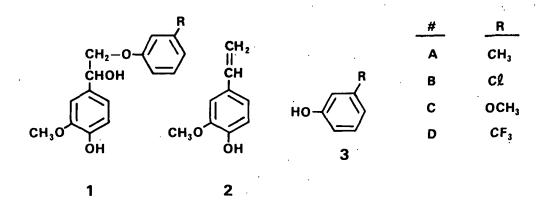
This report covers the reactions of lignin model compounds which have different ring A and ring B substituents in the presence of various pulping additives. Our goal is to detect reactivity differences which will provide information defining specific reaction mechanisms with regard to QM-additive reactions. The previous report described the model synthesis, selection, and general degradation procedure, along with the product analysis.[15] Also, that report demonstrated that the slow step in the mechanism for model fragmentation under soda conditions is cleavage of the β-aryl ether bond.

RESULTS

Degradation of Ring B Analog Models 1A-D

A mixture of models 1A-D was heated at 150°C in aq. alkali with 5 equiv. of AHQ^{-2} per model for various time intervals, and the yields of phenols 3A-D determined. The data, as seen in Fig. 3, indicate no significant differences in phenol yield (i.e., fragmentation tendencies) for the four models at short reaction times. Thus, the electron-donating or releasing powers of the B ring substituents play no role in the rate determining step of the fragmentation mechanism.

The fact that there was a yield difference at long reaction times is probably due to secondary reactions. A gas chromatography-mass (GC-MS) analysis of the product mixtures showed starting materials, vinyl ethers (dehydration products of the starting materials), phenols 3A-D, and small amounts of vinylguaiacol (2) and guaiacol (from ring A cleavage). The low levels of 2 are a

result of its tendency to polymerize in the presence of AHQ; some-
times this polymerization incorporates other phenol products[16a]
leading to an apparent lower yield of simple phenols.

#	R
A	CH_3
B	Cl
C	OCH_3
D	CF_3

In general, many data points were collected to ensure the
validity of the observed trends. The absolute yield values may
not be accurately known, but we are comfortable in comparing
degradations done under identical conditions.

Several degradations of each model with different additives
were also performed. These degradations were done at 135°C where
(a) soda reactions play less of a role and (b) reactivity dif-
ferences - as compared to 150° - will be more pronounced. We also
began employing glucose as a reagent for reducing AQ to AHQ^{-2}; the
glucose method appears to be more reliable than the AHQ-diacetate
hydrolysis method for producing known levels of AHQ.[17] The glu-
cose method involves prewarming a mixture of model, AQ, and glu-
cose in aq. alkali at 60° for 30 minutes. These conditions
promote the formation of AHQ^{-2} and the partial destruction of
glucose[18] at a temperature where QM formation should not occur.
Workup of the prewarmed solutions showed no model fragmentation.

Many model degradations were performed (an example is shown in
Fig. 4) which indicate that the order of fragmentation efficiency
in the presence of an excess additive is soda/AHQ ⪢ soda/SH⁻ >
soda/glucose > soda.

The high efficiency of the soda/AHQ is not due in part to the presence of glucose or glucose by-products in this system. This point was established by performing several control runs, including prewarming a soda/SH^- system in the presence of glucose and observing no increased phenol yields as compared to just a soda/SH^- system. Apparently, glucose is a relatively poor reactant in the presence of the much better AHQ and SH ions. Interestingly, the effectiveness of glucose alone in alkali, as a promoter of fragmentation, is only slightly reduced (ca. 10%) by the 30 minute, 60°C prewarming procedure.

A statistical analysis program[19] was applied to the 135°C model-additive reactions to help determine whether fragmentation yields were different or identical. The upper right side of Table 1 compares confidence levels of yield differences for AHQ degradations of the various models. The statistical analysis indicates a **low** degree of confidence that the AHQ runs have different rates of fragmentation; the fact that the _m_-CF₃ model (**1D**) confidence is somewhat high in two cases is probably due more to yield differences at long reaction times rather than short reaction times (i.e., such as in Fig. 3).

TABLE 1

Statistical Analysis of the Data from Kraft and AHQ Degradations
of Model **1A-D** at 135°C[a,b]

Compound	12A	12B	12C	12D
12A	0.997	0.705	0.133	0.922
12B	0.485	0.730	0.360	0.946
12C	0.137	0.412	0.910	0.511
12D	0.336	0.185	0.540	0.995

[a]The yield vs. time profiles of two runs were compared using a BMOP statistical program.[19] Numbers close to 1.00 indicate a high degree of confidence that the two sets of data are different; generally, any number below 0.90 signifies that the reaction rates are not statistically different.

[b] ⌐ ⌐ AHQ **vs.** SH   ☐ AHQ **vs** AHQ   ⌐ ⌐ SH **vs.** SH.

The statistical analysis (lower left side of Table 1) also indicates a **low** degree of confidence that the SH⁻ runs have different rates of fragmentation. There is, however, a **high** degree of confidence, in at least two cases, that AHQ degradations cause more fragmentation than SH⁻degradations (Table 1, diagonal from upper left to lower right).

Although not shown in the table, data analysis indicated that glucose induced fragmentation yields differ from model-to-model, with the $\underline{m}$-CF$_3$ model (1D) being the most reactive and the $\underline{m}$-CH$_3$ model (1A) the least reactive. The difference here probably reflects soda degradation contributions. The fact that carbohydrates can cause model fragmentation reactions has support in the literature.[20]

In summary, the nature of the substituent on the B ring has no affect on the additive-induced fragmentation reactions of models 1A-D. This fact suggests that quinonemethide formation (a process which would be insensitive to the type of $\underline{m}$-R group on ring B) is rate determining for additive reactions. Fragmentation efficiencies, when comparing different additives, probably depend on how well the additive reacts with the quinonemethide relative to competing reactions which give no fragmentation.

Kinetic Interpretation of Additive Effects

The rate of generation of fragments for a model should obey the following expression:

$$\text{Frag. Rate} = k_{HO}\,[HO^-][\text{Model}] + k_{Add}\,[\text{Add}][QM] \qquad (f)$$

where k_{HO} and k_{Add} are the rate constants for the soda induced and additive induced fragmentation reactions, respectively, and reactant orders are assumed to be 1. The concentration of the quinonemethide (QM) can be calculated by applying the steady state assumption for reactive intermediates and considering the various reactions available (Fig. 2) to the QM:

$$[QM] = \frac{k_{QM}[\text{Model}]}{k_{Add}[\text{Add}] + k_{VE}[HO^-] + k'_{VE}[HO^-] + k_{CON}[ArO^-] + k_{-QM}[HO^-]} \quad (g)$$

where k_{VE} and k'_{VE} are the rate constants for the two reactions
which produce vinyl ether by-products, k_{CON} is the rate constant
for condensation reactions involving phenols (ArO^-), and k_{QM} and
k_{-QM} are the forward and reverse rate constants for QM formation
and return to the model.

Combining Equations (f) and (g) gives:

$$\text{Frag. Rate} = k_{HO}[HO^-][\text{Model}] + k_{QM}[\text{Model}] \cdot X \quad (h)$$

where X is the fraction of reaction which is additive induced
fragmentation vs. all other reactions of the QM:

$$X = \frac{k_{Add}[\text{Add}]}{k_{Add}[\text{Add}] + k_{VE}[HO^-] + k'_{VE}[HO^-] + k_{CON}[ArO^-] + k_{-QM}[HO^-]}$$

If the k_{Add} [Add] term is large relative to the other terms
in the denominator of the X term, expression (h) reduces to:

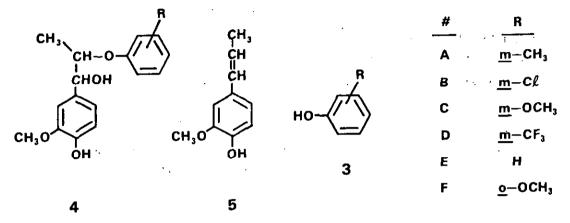$$\text{Frag. Rate} = k_{HO}[HO^-][\text{Model}] + k_{QM}[\text{Model}] \quad (i)$$

According to this expression, the rate of fragment generation
should be independent of additive concentration above a certain
level. We have observed such effects in our studies and others
have seen similar effects in kraft delignification systems.[21]

The fragmentation efficiencies which we observed for the reac-
tions of additives with models 1A-D, namely AHQ > SH$^-$ > glucose,
can be accounted for by assuming that X is largest for AHQ and
smallest for glucose. This interpretation accounts for the addi-
tive yield differences while still maintaining that QM formation
is rate determining for the additive reactions. In essence the
additive affects the product determining steps, rather than the
rate determining step.

Degradations of Ring B Analog Models 4A-D

Degradation of the β-methyl model series (4) were performed
at 150°C with pairs of models in the same reactor in the presence

of excess AHQ. One of the model pairs was generally the m-chloro compound **4B**; this provided a check on the consistency of the data. For example, the yield of m-chlorophenol from **4B** was 80-83% at an 80 min reaction time in four different runs.

#	R
A	m-CH₃
B	m-Cℓ
C	m-OCH₃
D	m-CF₃
E	H
F	o-OCH₃

The model fragmentation efficiencies as a function of time, with and without AHQ, are shown in Fig. 5. In the absence of AHQ the models displayed quite different reactivities; the meta substituent order was $CF_3 > Cl > OCH_3 > CH_3$. A similar order was observed in the soda degradations of models **1A-D**.[16b] In the presence of AHQ all models reacted at approximately the same rate after applying certain assumptions.

The main assumption relates to the fact the β-methyl models are relatively pure, but not absolutely pure compounds. Thus, the somewhat lower yields observed with m-OCH₃ model (**4C**) may be due to impurities in the substrate. The m-Cl model **4B** was known to be contaminated with unsubstituted **4E** isomers and its yields were corrected accordingly. Interestingly, the yield of phenol from degradation of the unsubstituted impurity in the m-Cl sample matched the other substituted-phenol yields.

The high yields of guaiacol observed in the degradation of the o-OCH₃ model **4F** can be attributed to some guaiacol production from ring A cleavage. Small amounts of guaiacol, which must originate from ring A, were observed in all (AHQ and soda[16b]) degradations of B ring models **1A-D** and **4A-D**.

Although the β-methyl series has its problems, the data from
this series are consistent with those of the non-β-methyl 1 series.
The most electron-withdrawing and electron-releasing substituents,
CF_3 and CH_3, respectively, displayed **similar** reactivities in the
presence of AHQ and quite **different** reactivities in the presence
of only NaOH. The phenol yields in the β-methyl series appear to
level off better than the non-β-methyl series at long reaction
times, possibly meaning less phenol losses to competing side reac-
tions. [Isoeugenol (5) has less tendency to polymerize and does
not appear to cause losses in other phenol products.[16]]

Degradation of Ring A Model Analogs in the Presence of Additives

Several models differing in their A-ring substituents were
also studied. These models would be expected to have quite dif-
ferent reactivities if a step involving the A-ring were the slow
step in the mechanism. Several steps in the proposed mechanisms
for additive induced fragmentation do involve the A-ring; QM for-
mation and addition of ions or electrons to QMs are examples.

Degradation of ring A model analogs having m-CH_3 substituents
in their B rings at 135°C in the presence of either AHQ or
SH⁻ showed the following order of fragmentation efficiency:
2',5'-dimethyl alcohol **6B** > 3'-methoxy alcohol **1A** > unsubstituted
alcohol **6A** (Fig. 6). Again, it appears that fragmentation yields
with AHQ are slightly better than with SH⁻ (confidence levels of a
significant difference were 0.989, 0.997, and 0.725).

#	R_1	R_2	R_3
1A	CH_3	OCH_3	H
6A	CH_3	H	H
6B	CH_3	CH_3	CH_3
6C	CF_3	CH_3	CH_3

The result that we had hoped for, namely a large difference
in yields between AHQ^{-2} and SH^- runs, was not realized. Large dif-
ferences in additive reactivities would have suggested mechanistic
differences. One would expect that the quinonemethides from **1A**,
6A, and **6B** would be quite different in their reactivities toward
accepting electrons and fragmenting to radicals (SET mechanism)
<u>versus</u> adduct formation and fragmenting to ions.

The observed reactivity order rules out adduct formation as
the slow step in the mechanism. Adduct formation, which develops
a full negative charge in ring A, would be expected to be slow
with the 2',5'-dimethyl models because the methyl groups are
electron feeding and would destabilize carbanions; also, the
2'-methyl is set up for steric hindrance to reaction. Instead,
the 2',5'-dimethyl analogs were the most reactive.

The results point toward a common slow step in the mechanisms
of the AHQ^{-2} and SH^- reactions. Most likely this step is QM pro-
duction. In general, highly substituted QMs are more stable than
unsubstituted QMs. Thus, the order we observed for ease of
fragmentation fits an order for ease of QM generation. The order
does not, however, rule out single electron transfer to the QM as
the slow step. The radical nature of $QM^{\cdot-}$ might derive some stabi-
lization from electron releasing ring methyl groups.

With the proper substituents on the A ring, QM formation may
become so easy that this step would no longer be the rate limiting
step, and the chemistry of subsequent reactions might be observable.
Therefore, the degradations of two 2',5'-dimethyl ring A models,
having different ring B substituents ($\underline{m}$-CH$_3$, **6B**, and $\underline{m}$-CF$_3$, **6C**),
were compared. As can be seen in Fig. 7, the $\underline{m}$-CF$_3$ model is more
reactive than the $\underline{m}$-CH$_3$ model (100% confidence level). However,
the difference was not substantial and may only reflect differen-
ces in NaOH-induced fragmentation (**6C** > **6B**). Again, in this
series, AHQ was better than hydrosulfide ion at inducing fragmen-
tation (99.96% confidence of a difference).

Competitive Model Degradations

Competitive degradations with limited amounts of additives offer
a possible way to distinguish SET and adduct mechanisms (see discus-
sion associated with Eq. a-e). The best models to compare would be
the ones having potentially the greatest reactivity differences.
In our case this would be C_2-models such as 1A ($\underline{m}$-CH$_3$) and 1D ($\underline{m}$-CF$_3$).

In the adduct mechanism case, both 1A and 1D should form adducts
at the same rate, but the $\underline{m}$-CF$_3$ model 1D should fragment faster
since it has the better ring B phenolate ion leaving group. In
the SET mechanism case, both the $\underline{m}$-CF$_3$ model 1A and the $\underline{m}$-CH$_3$ model
1D should accept electrons at the same rate, but they should
fragment at different rates. There are two ways the quinone-
methide radical anions could fragment (Scheme I). The one way
produces ring B phenolate ions, meaning the $\underline{m}$-CF$_3$ model 1D will be
more reactive than $\underline{m}$-CH$_3$ model 1A; the other way produces ring B
phenolate radicals, meaning 1A will be more reactive than 1D.

Therefore, in competitive degradations of 1A and 1D with
limited amounts of AHQ, unusually high yields of $\underline{m}$-cresol would
signify that equilibrium reactions, such as (c), are occurring and
that an SET mechanism prevails. Unusually high yields of $\underline{m}$-
trifluoromethylphenol would indicate that equilibrium reactions
between reactive intermediates are occurring, but the nature of
the mechanism would still not be defined.

Data from the competitive degradations of 1A and 1D are shown
in Table 2. The degradations employed 1 equiv. of each model in
aq. alkali in the presence of 0.8 equiv. of an additive (SH$^-$ or
AHQ). Under these conditions, NaOH-induced fragmentation reac-
tions will compete; therefore, the "net" yield caused by additive
induced fragmentation was calculated (columns 5 and 8 of the table).

At reduced AHQ levels, the $\underline{m}$-CF$_3$ model 1D appears to be more
reactive than the $\underline{m}$-CH$_3$ model 1A in net yield; with SH$^-$ the differ-
ence between 1A and 1D is small, probably within the experimental
errors of the measurements. Over a series of six time measurements,

1B ($\underline{m}$-Cl) was consistently more reactive than 1A ($\underline{m}$-CH$_3$) in net yield in the presence of 0.8 equiv. of AHQ at 150°C.

TABLE 2

Phenol Yields from Competitive Model Degradations Performed with Limited Amounts of Additive[a]

Volume[b]	Time, min	Phenol Yield from 1A (%)			Phenol Yield from 1D (%)		
		SH⁻/OH⁻	OH⁻	SH⁻	SH⁻/OH⁻	OH⁻	SH⁻
Low	20	25.5	- 1.1	= 24.4	29.7	- 5.0	= 24.7
Low	40	35.7, 34.9	- 2.6	= 32.7	43.8, 45.7	- 10.1	= 34.7
High	20	18.4	- 0.8	= 17.6	22.6	- 3.4	= 19.2
High	40	29.6	- 1.9	= 27.7	35.2	- 7.0	= 28.2
		AHQ/OH	OH⁻	AHQ	AHQ/OH⁻	OH⁻	AHQ
Low	20	16.2	- 1.2	= 15.0	23.9	- 4.4	= 19.5
Low	40	19.4, 18.2	- 2.4	= 16.2	30.1, 30.6	- 8.6	= 21.8
High[c]	20	11.3	- 1.0	= 10.3	18.1	- 4.1	= 14.0
High[c]	40	15.5	- 2.1	= 13.4	26.8	- 8.1	= 18.7

[a]One equiv. of models 1A and 1D was mixed with 0.8 equiv. of additive and 25 equiv. of NaOH and heated at 135° for 20 or 40 min.
[b]Low and high refer to 1.5 and 3.5 mL volumes.
[c]Fifty equiv. of NaOH were used in this case.

The data, in at least the AHQ cases, indicate that equilibria between reactive species is being established to some extent and that the mechanism is of an adduct type or an SET type in which the fragmentation generates a B ring phenolate ion and an A ring phenolate radical.

The data in Table 2 point out some other interesting trends. The more concentrated the solution, the more soda induced fragmentation occurs - an observation which confirms our previous work.[16b] Also, the more concentrated the solution, the more additive induced fragmentation occurs. Under the conditions of limited additive levels, SH⁻ induces more fragmentation than AHQ. The reason for this is not obvious. One possible explanation is that the concentration of AHQ^{-2} is less than anticipated because of

nonquantitative reduction by glucose or reaction with residual oxygen; the reactions were performed with extremely low levels of reactants, levels where even trace amounts of oxygen could have an effect.

Finally, competitive degradations of the $\underline{m}$-CH$_3$ model 6B and the $\underline{m}$-CF$_3$ model 6C were conducted. Each of these models has the 2,5-dimethyl substitution pattern on ring A which facilitates fragmentation. Consequently, lower temperatures can be used, thereby extending the lifetimes of the reactive intermediates and allowing a better establishment of equilibrium reactions.

Figure 8 shows a comparison of the phenol yields from models 6B and C when degraded simultaneously at 120°C in the presence of a limited amount of AHQ. The $\underline{m}$-CF$_3$ model was substantially more reactive than the $\underline{m}$-CH$_3$ model in the presence of AHQ. The reactivity differences in the presence of AHQ can not be accounted for by differences in soda control rates, which (as can be seen in Fig. 8) are small at 120°C. Clearly, the AHQ differences must be due to the establishment of equilibrium reactions between reactive species, QMs, QM$\overset{\bullet}{-}$ and/or QM-AHQ adducts, with a preference for fragmentation of the QM having the $\underline{m}$-CF$_3$ group.

Limited amounts of NaSH have the same effect as limited amounts of AHQ for competitive degradations of 6B and C at 120°C. The $\underline{m}$-CF$_3$ model was substantially more reactive than the $\underline{m}$-CH$_3$ model. The reactivity differences must reflect the preference for fragmentation of $\underline{m}$-CF$_3$ phenolate ions after establishing equilibrium reactions between reactive species, probably QMs and QM-SH adducts.

CONCLUSIONS

Additive induced model fragmentation reactions appear to have a common slow step, presumably formation of a quinonemethide, which is sensitive to substituents located on ring A but not to substituents on ring B. Our results indicate that the slow step in

additive induced fragmentation of lignin model compounds cannot be
nucleophile addition to a quinonemethide or fragmentation of the
β-aryl ether bond.

The close similiarities in the rates of AHQ and SH⁻ degrada-
tions suggests a common slow step, namely quinonemethide genera-
tion. The effectiveness of an additive (AHQ^{-2} > SH^- > glucose)
can be accounted for based on the efficiency by which the additive
fragments the model vs. competing side-reactions.

In the direct competition of two models with a limited amount
of AHQ^{-2} or SH^-, the model with the best phenolate ion ring B
leaving group is the more reactive. This result indicates that
reactions between QMs and QMs°, QM-AHQ adducts, and/or QM-SH
adducts occur. Most likely, the fragmentation step is slower
than the established equilbria between QM species, especially for
stabilized QMs (6B and C type).

<center>EXPERIMENTAL SECTION</center>

The synthesis of the compounds, the general degradation proce-
dure, and methods of analysis were previously described.[15] Specific
changes in the degradation procedure are described below.

Degradation Procedure. Except for AQ and AHQ-diacetate, which
had to be weighed into each bomb (small pressure vessel), all
reactant solutions, IS solutions, etc., were added to the bombs
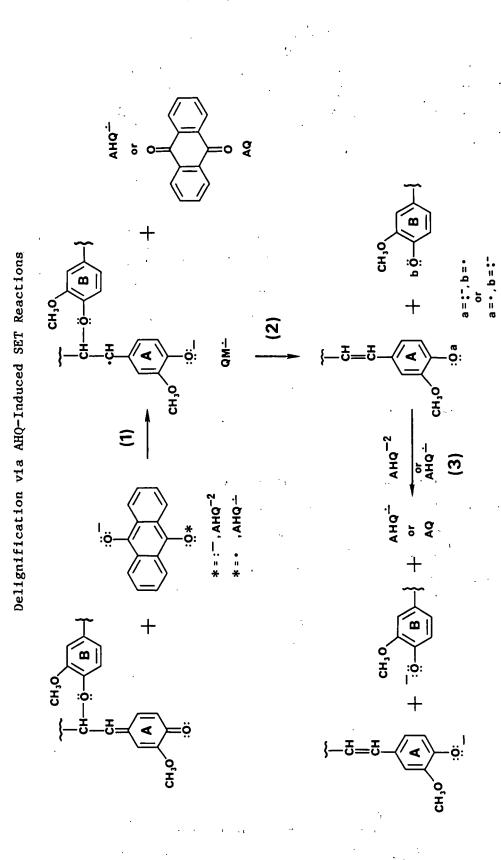with an automatic pipette.

Standard solutions of glucose, sodium hydroxide, and sodium
sulfide in water, and model compounds and p-isopropylphenol (IS)
in aq. NaOH were prepared just prior to use. The models were
present in 0.015 mmole amounts, and the other reagents were
adjusted to 0.015 mmole = 1 equiv. Generally, this meant the use
of 25 equiv. of NaOH and 5 equiv. of additive/model. The amount
of NaOH solution used was adjusted to compensate for additive con-
sumption (i.e., 4 equiv./AHQ-diacetate) or additive liberation
($Na_2S + H_2O \rightleftharpoons NaSH + NaOH$).

The appropriate solutions and make-up water were added to the cool bombs. For degradations involving AQ/glucose and AHQ-diacetate, the bombs were prewarmed along with soda controls at 60° for 30 min prior to immersion in the oil bath. This prewarming helped to give a high concentration of AHQ^{-2} prior to immersion. No model fragmentation (even for the most reactive models, **24** and **25**) occurred as a result of prewarming in the presence of NaOH or NaOH/additive solutions.

After removal from the hot oil bath, the bombs were immediately cooled in ice-water, opened, diluted with IS solution, and the contents transferred to an Erlenmeyer flask for derivatization, followed by GC analysis.

REFERENCES

1. D. R. Dimmel, J. Wood Chem. Technol., 5, 1 (1985).

2. D. R. Dimmel, L. F. Perry, P. D. Palasz, and H. L. Chum, J. Wood Chem. Technol., 5, 15 (1985).

3. J. R. Obst, L. L. Landucci, and N. Sanyer, Tappi, 62(1), 55 (1979).

4. L. L. Landucci, Tappi, 63(8), 95 (1980).

5. J. Gierer, O. Lindeberg, and I. Noren, Holzforschung, 33, 213 (1979).

6. H. Aminoff, G. Brunow, G. E. Miksche, and K. Poppius, Paperi Puu, 61, 441 (1979).

7. J. Gierer, Holzforschung, 36, 43 (1982).

8. J. March, Advanced Organic Chemistry, 3rd ed., Wiley & Sons, New York, 1985, 151-70, 237-50.

9. G. E. Miksche, Acta Chem. Scand., 26, 4137 (1972).

10. J. Gierer and S. Ljunggren, Svensk Papperstid., 82, 503

11. D. R. Dimmel and D. Shepard, J. Wood Chem. Technol., 2, 73 (1982).

12. N. Kornblum, Angew. Chem. Int. Ed., 14, 734 (1975).

13. G. A. Russell, Chem. Stosow, 26, 317 (1982).

14. J. March, Advanced Organic Chemistry, 3rd ed., Wiley & Sons, New York, 1985, 582-3.

15. D. R. Dimmel and D. Shepard, J. Wood Chem. Technol., $\underline{2}$, 297
     (1982).

16. D. R. Dimmel and L. F. Perry, submitted for publication: (a)
     forthcoming, (b) preceding article.

17. Unpublished data from our laboratory.

18. J. W. Green, I. A. Pearl, K. W. Hardacker, B. D. Andrews,
     and F. C. Haigh, Tappi, **60**(10): 120 (1977).

19. BMDP Statistical Software, UCLA, Calif., 1983.

20. (a) L. J. Wright and T. J. Fullerton, J. Wood Chem. Technol.,
     $\underline{4}$, 61 (1984); (b) T. J. Fullerton and L. J. Wright, Tappi,
     $\underline{67}$(3), 78 (1984); (c) T. J. Fullerton and A. L. Wilkins, J.
     Wood Chem. Technol., $\underline{5}$, 189 (1985).

21. (a) L. Olm and G. Tistad, Svensk Papperstid., $\underline{82}$, 458 (1979);
     (b) P. Axegard and J.-E. Wiken, Internat. Sym. Wood Pulping
     Chem., Stockholm, June 9-12, 1981, Abstracts Vol. 2, 23;
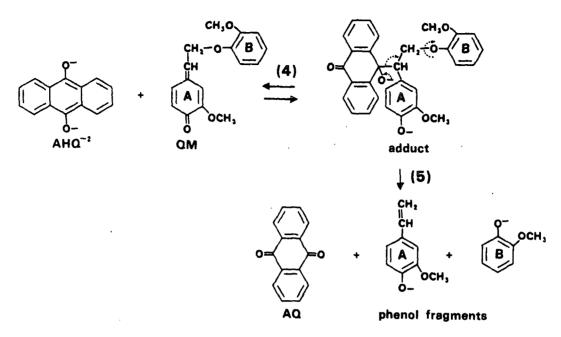   (c) R. Kondo and K. V. Sarkanen, Holzforschung, $\underline{38}$, 31 (1984).

SCHEME I

Delignification via AHQ-Induced SET Reactions

SCHEME II
Delignification via AHQ Adduct Reactions
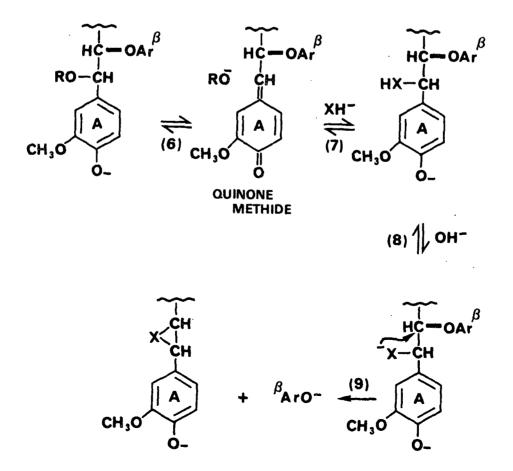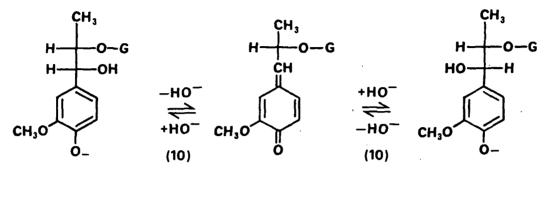

SCHEME III
β-Aryl Ether Cleavage of Phenolic Lignin End Units

where X = O or S

SCHEME IV
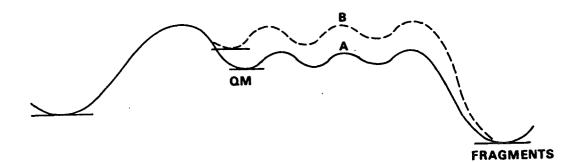### Model Isomerization and Fragmentation by Miksche[9]

$-HO^-$
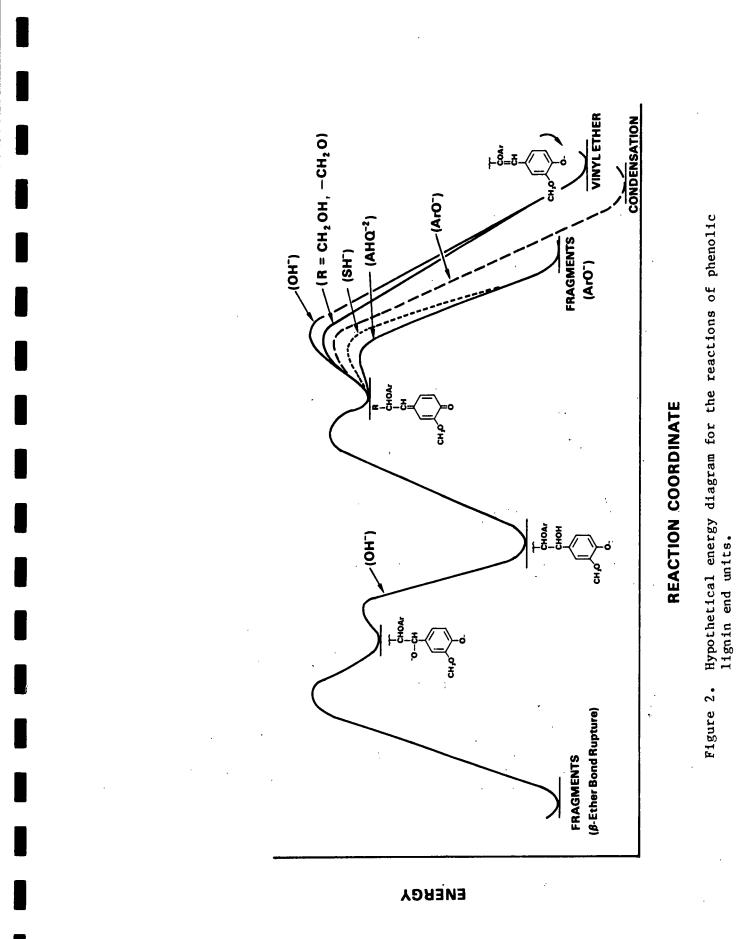$+HO^-$
(10)

$+HO^-$
$-HO^-$
(10)

(11) $\downarrow SH^-$

$\downarrow$

G-OH

$G = $ (structure)

Figure 1. Hypothetical partial energy diagrams for fragmentation of a model by way of a QM.

Figure 2. Hypothetical energy diagram for the reactions of phenolic
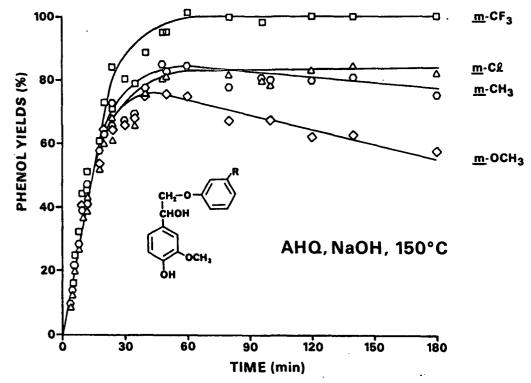   lignin end units.

Figure 3. Phenol yields as a function of time for degradations
          of models 1A-D (1 equiv. each, in the same reactor) at
          150°C in the presence of 180 equiv. of NaOH and 20
          equiv. of AHQ diacetate. At the start of the reaction
          there should be 100 equiv. of NaOH (25/model) and 20
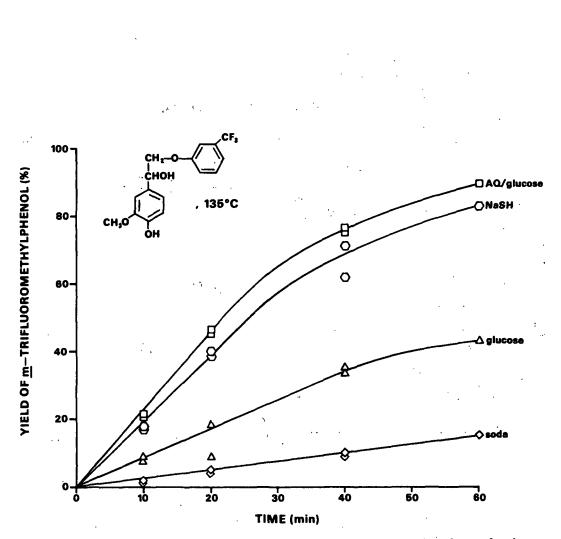   equiv. (5/model) of AHQ^{-2} available.

Figure 4. Phenol yield as a function of time for the degradation of model 1D in the presence of different additives at the 5 equiv. level at 135°C.
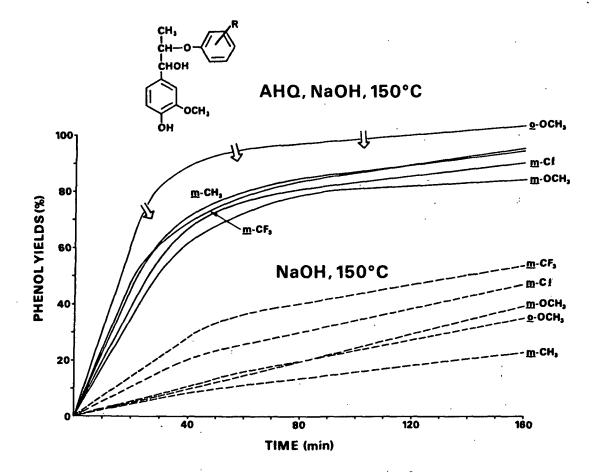
Figure 5. Phenol yields as a function of time (5, 10, 15, 20, 30,
           40, 60, 80, and 160 min) for the degradation of models
           4A-D,F (done as 1 equiv. pairs in the same reactor) at
           150°C in the presence of 75 equiv. of NaOH and 6 equiv.
           of AHQ diacetate (——) and in the presence of 50 equiv.
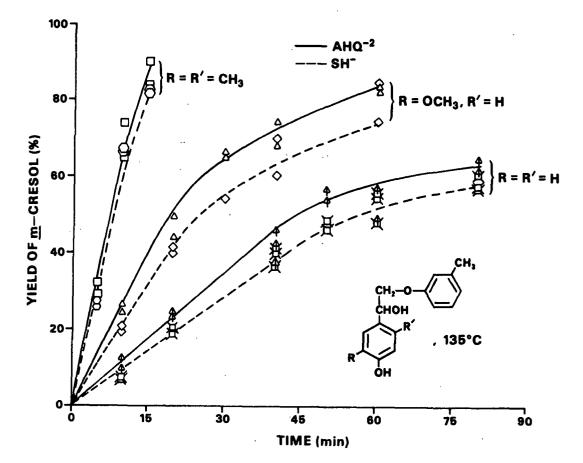   of NaOH (- -). Data points have been omitted for
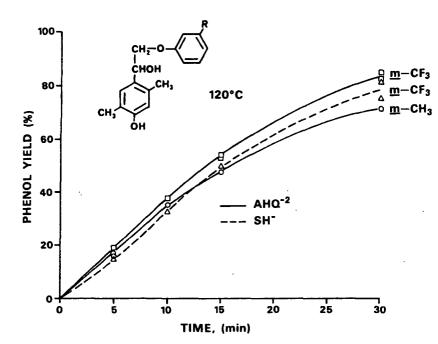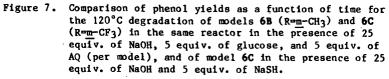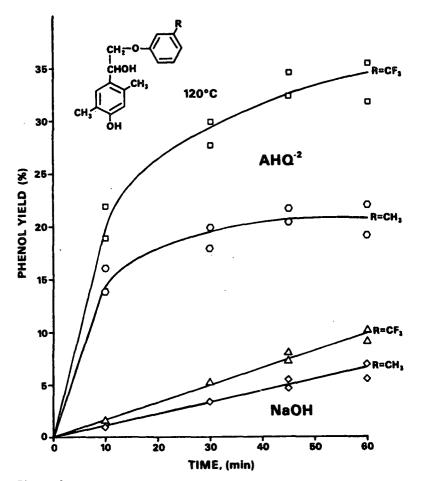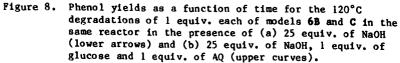   clarity reasons.

Figure 6. Phenol yields as a function of time for the degradations
of models differing in their ring A substituents in the
presence of excess levels of AHQ (—) and SH⁻ (- -) at
135°C in aqueous alkali.

Figure 7. Comparison of phenol yields as a function of time for
the 120°C degradation of models 6B (R=m-CH₃) and 6C
(R=m-CF₃) in the same reactor in the presence of 25
equiv. of NaOH, 5 equiv. of glucose, and 5 equiv. of
AQ (per model), and of model 6C in the presence of 25
equiv. of NaOH and 5 equiv. of NaSH.

Figure 8. Phenol yields as a function of time for the 120°C
degradations of 1 equiv. each of models 6B and C in the
same reactor in the presence of (a) 25 equiv. of NaOH
(lower arrows) and (b) 25 equiv. of NaOH, 1 equiv. of
glucose and 1 equiv. of AQ (upper curves).

Status Report
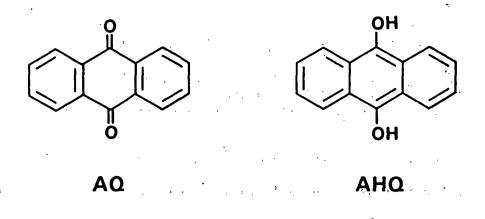
FUNDAMENTALS OF SELECTIVITY IN PULPING AND BLEACHING

Carbohydrate Reactions

OBJECTIVE

The ultimate goal of chemical pulping is to liberate cellulosic fibers from wood through delignification without degrading or removing the wood polysaccharides. Unfortunately, the alkaline pulping processes are not selective for delignification. For example, in kraft pulping the loss of carbohydrate material may be comparable to, or even exceed, the lignin removal.[1-2] In addition, reduction of the polysaccharide DP, leading to decreased pulp viscosity and product strength, also occurs.[1-3] The fact that anthraquinone (AQ) increases pulping selectivity has stimulated interest in the chemistry of the interaction of anthraquinone with wood components.

The objective of this project is to elucidate the mechanism of carbohydrate degradation during pulping and bleaching to facilitate their ultimate control. An immediate goal is to understand what role anthraquinone plays in random glycosidic bond cleavage of wood polysaccharides.

AQ   AHQ

INTRODUCTION

In a previous study of the effect of anthraquinone on alkaline degradation of polysaccharides, it was discovered that anthraquinone causes DP loss in amylose.[4,5] The potential implications of this finding with respect to reactions of hemicelluloses and cellulose led to a subsequent study of the effect of anthraquinone on the DP of cellulose in soda and kraft cooking.[2]

Yield data for kraft and soda cooking of cotton linters with and without anthraquinone are presented in Table 1. The kraft liquors were $1.0\underline{M}$ NaOH and $0.15\underline{M}$ Na$_2$S. Soda liquors were $1.15\underline{M}$ NaOH to give the same effective alkali as the kraft liquor. Anthraquinone, when used, was added such that its concentration would be $0.0048\underline{M}$ if totally soluble.

Table 1. The effect of anthraquinone (AQ) and yield in kraft and soda cooking of cotton linters.

Temperature, °C	Time, h	Yield, %			
		Kraft[a]	Kraft–AQ[a,c]	Soda[b]	Soda–AQ[b,c]
140	--	96.4	99.5	96.6	99.2
170	0.0	95.3	98.1	95.3	98.7
170	0.5	94.9	95.1	94.4	96.2
170	1.0	92.4	93.0	92.0	94.1
170	2.0	89.5	90.2	90.4	87.5
170	4.0	83.5	83.9	84.4	84.5
170	8.0	73.7	73.6	75.0	75.0

[a] $1.0\underline{M}$ NaOH, $0.15\underline{M}$ Na$_2$S, 25:1 liquor-to-cellulose ratio.
[b] $1.15\underline{M}$ NaOH, 25:1 liquor-to-cellulose ratio.
[c] $0.0048\underline{M}$ AQ, comparable to 0.5% addition at 5:1 liquor-to-wood ratio.

The protective action of the anthraquinone toward the peeling reaction is reflected in the increased yields in both the soda and kraft cooks with anthraquinone, particularly during the heatup period. On reaching the final

cooking temperature, both the kraft-anthraquinone and soda-anthraquinone cooks
had approximately 3% higher yields than the corresponding cooks without anthra-
quinone. Surprisingly, the yield advantage in the anthraquinone-spiked cooks
diminished during the cook, and at longer cooking times the yields of the anthra-
quinone cooks and the control cooks were essentially equal. This convergence of
yield at longer cooking times is probably related to the types of acid end
groups formed on the cellulose with and without anthraquinone in the alkaline
treatments. Although extremely stable compared to reducing sugar end groups,
the aldonic acid end groups are subject to isomerization[6] and possibly cleavage[7]
under the severe cooking conditions. In alkali without anthraquinone, the
peeling reaction is partially stopped through formation of 3-deoxyhexonic (meta-
saccharinic) acid and 2-C-methylglyceric acid end groups.[8] These end groups
would be relatively stable and not easily cleaved from the cellulose chain. How-
ever, if the action of anthraquinone parallels that of sodium anthraquinone-2-
sulfonate with hydrocellulose[9] and glucose[10] in alkaline media, a substantial
number of pentonic acid end groups will form. Such end groups, in which the
polysaccharide chain is β to the carboxyl group and an abstractable proton is on
the α carbon atom, would be subject to cleavage from the cellulose,[7,11] thereby
allowing the peeling reaction to resume. This effect could be accentuated in
the current system because the anthrahydroquinone (AHQ) formed from anthraquinone
in oxidizing the cellulose end groups, both those present initially and those
formed as a result of chain cleavage, is not being recycled to anthraquinone
through oxidation. Thus, in the latter stages of the reaction, the protection
against the peeling reaction afforded by anthraquinone is diminishing.

The effect of anthraquinone on polysaccharide chain cleavage in the
soda and kraft cooks was, at most, very small. This is illustrated by the $\overline{DP}_w$

vs. time and viscosity vs. time curves in Fig. 1-4. The DP_w and viscosity curves

for both the soda and kraft cooks with anthraquinone are essentially identical

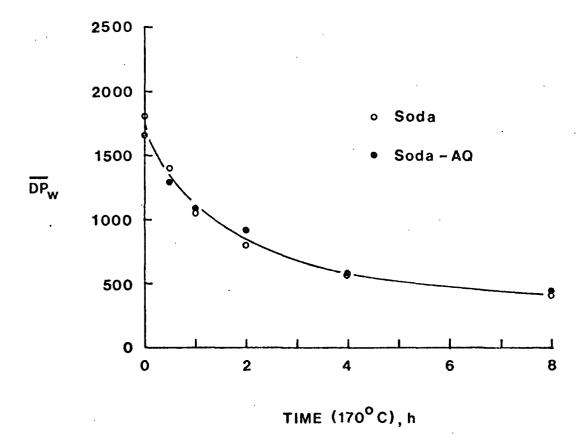to those for the cooks without anthraquinone.

Figure 1. Effect of anthraquinone (0.0048M) on $\overline{DP}_w$ in soda (1.15M NaOH)
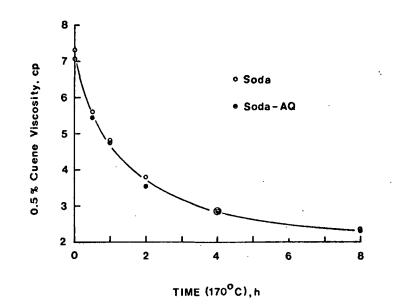cooking of cotton linters.

Figure 2.   Effect of anthraquinone (0.0048M) on cuene viscosity in
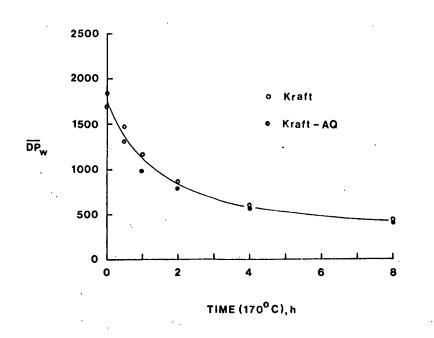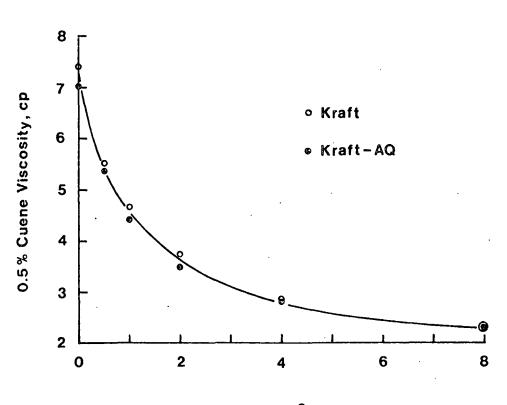   soda (1.15M NaOH) cooking of cotton linters.

Figure 3.   Effect of anthraquinone (0.00048M) on $\overline{DP}_w$ in kraft (1.0M NaOH,
            0.15M Na₂S) cooking of cotton linters.

Figure 4.   Effect of anthraquinone (0.0048$\underline{M}$) on cuene viscosity in kraft
            (1.0$\underline{M}$ NaOH, 0.15$\underline{M}$ Na$_2$S) cooking of cotton linters.

CURRENT EFFORT

Current research is being directed toward the question of why amylose
and cellulose differ in their reactivity toward anthraquinone.

Amylose and cellulose are both 1,4-linked polymers of glucopyranose.
The differences between the two polymers are the stereochemistry of the gluco-
sidic linkage and the degree of intermolecular association. Amylose has α-1,4
glucosidic bonds between glucose units, whereas cellulose has β-1,4 glucosidic
bonds. Cellulose exhibits considerable crystallinity, which varies depending on
the cellulose source and the prior treatment of the cellulose. Cellulose does
not dissolve in aqueous alkali. Amylose has only very limited crystallinity
unless it is retrograded. In addition, amylose will dissolve in alkaline media.

Thus, the differences in reactivity of amylose and cellulose toward anthraquinone could result either from differences in the stereochemistry of the intermonomeric bonds or intermolecular association (crystallinity and solubility).

The potential role of the stereochemistry of the glucosidic linkages in cellulose and amylose in the reaction with anthraquinone has been addressed through a study of reactions of 1,5-anhydrocellobiitol (I), a model for cellulose, and 1,5-anhydromaltitol (II), a model for amylose. The syntheses of I and II were outlined in a previous report.[12]

I

II

1,5-Anhydrocellobiitol (I) contains the β-1,4 glucosidic linkage found in cellulose and has been used previously as a cellulose model in studies of alkaline cleavage of glycosidic bonds.[13,14] 1,5-Anhydromaltitol (II) contains the α-1,4 glucosidic linkage found in amylose. Both I and II are incapable of undergoing the peeling reaction, and hence any degradation of these compounds reflects reactions which may account for random chain cleavage in cellulose and

Table 3. Degradation of 1,5-anhydromaltitol
(0.01$\underline{M}$) in 0.984$\underline{M}$ NaOH at 169.9°C.

$10^6 k_r$, s^{-1}[a]

No additive   1.12 (0.02)[b]

Anthraquinone (0.00480$\underline{M}$)[c]   1.65 (0.06)[b]

Anthrahydroquinone (0.00480$\underline{M}$)[c]   1.20 (0.06)[b]

---

[a]Pseudo-first-order rate constant for degradation.
[b]Average of duplicates; figure in parentheses is
the range of the duplicate determinations.
[c]AQ or AHQ addition is comparable to 0.5% addition
at a 5:1 liquor-to-wood rato. Molarity figure
assumes total solubility.

While the increase in k_r for the model compounds ($\sim 0.50 \times 10^{-6}$ s^{-1}) is

not huge, it can be calculated from Eq. (1)[15] that it could cause amylose or

cellulose (assuming total accessibility and solubility) of initial $\overline{DP}_n$ 1000 to

degrade to $\sim \overline{DP}_n$ 220 in 2h.

$$\ln \left(1 - \frac{1}{P_o}\right) - \ln \left(1 - \frac{1}{P_t}\right) = kt \qquad (1)$$

where P_o = initial number-average degree of polymerization ($\overline{DP}_n$)

$P_t = \overline{DP}_n$ at time t, and

k = first-order rate constant for chain cleavage

The fact that anthraquinone accelerated the degradation of both model

compounds indicates that the physical structure of cellulose controls its degra-

dation. To demonstrate this we are currently degrading amorphous cellulose[16] in

1.0$\underline{M}$ sodium hydroxide with and without anthraquinone. The $\overline{DP}_w$ of the reactions

is being followed as a function of time by gel permeation chromatography.[17]

An initial experiment has indicated that the amorphous cellulose may be too reactive at 170°C to demonstrate the effect of anthraquinone, but this experiment is being duplicated. Additional degradations are being studied at lower temperatures.

Preliminary experiments also indicated that the greater susceptibility of the amorphous cellulose to the peeling reaction would cause problems. Thus, the amorphous cellulose is reduced with sodium borohydride to prevent primary peeling and put the emphasis on chain cleavage reactions.

FUTURE WORK

The study of the effect of anthraquinone on random chain cleavage will center on the role that the cellulose physical structure plays in the reaction.

Mechanistic studies of cellulose chain cleavage in alkaline pulping indicate that increased ionic strength could accelerate the cleavage reaction. Thus, the effect of "dead load" (increased ionic strength) on cellulose chain cleavage during pulping will be examined.

REFERENCES

1. Matthews, C. H., Svensk Papperstid. 77:629(1974).

2. Schroeder, L. R. Alkaline degradation of polysaccharides in pulping and bleaching. Project 3284, Interim Report to the Program Committee, March 17, 1980.

3. Schroeder, L. R.; Wabers, B. A. Fundamentals of selectivity in pulping and bleaching - carbohydrate reactions. Project 3475-1, Interim Report to the Program Committee, September 10, 1982.

4. Arbin, F. L. A.; Schroeder, L. R.; Thompson, N. S.; Malcolm, E. W., Tappi 63(4):152(1980).

5. Arbin, F. L. A.; Schroeder, L. R.; Thompson, N. S.; Malcolm, E. W., Cellulose Chem. Technol. 15:523(1981).

6. Alfredsson, B.; Samuelson, O., Svensk Papperstid. 65:690(1962).

7. Thompson, N. S.; Corbett, H. M.; Green, J. W., Trans. Tech. Sect. (Can. Pulp Paper Assoc.) 7(1):TR26(1981).

8. Johansson, M. H.; Samuelson, O., J. Applied Polymer Sci. 19:3007(1975).

9. Heikkila, H.; Sjöström, E., Cellulose Chem. Technol. 9:3(1975).

10. Vuorinen, T., Carbohyd. Res. 116:61(1983).

11. Szabo, I.; Teder, A., Svensk Papperstid. 72:68(1969).

12. Bovee, M. J.; Blythe, D. A.; Schroeder, L. R.; Wabers, B. A., IPC Technical Paper Series No. 144, August, 1984.

13. Brandon, R. E.; Schroeder, L. R.; Johnson, D. C., ACS Symp. Ser. 10:125 (1975).

14. Blythe, D. A.; Schroeder, L. R., J. Wood Chem. Technol. 5:313(1985).

15. Sharples, A. In Cellulose and cellulose derivatives, Part V, p. 991, N. M. Bikales and L. Segal (ed.), Wiley-Interscience, New York, 1971.

16. Schroeder, L. R.; Gentile, V. M.; Atalla, R. H., IPC Technical Paper Series No. 152, March, 1985.

17. Schroeder, L. R.; Haigh, F. C., Tappi 62(10):103(1979).

THE INSTITUTE OF PAPER CHEMISTRY

Leland R. Schroeder
Professor of Chemistry and
Associate Dean

THE INSTITUTE OF PAPER CHEMISTRY

Appleton, Wisconsin

Status Report

to the

PULPING PROCESSES

PROJECT ADVISORY COMMITTEE

Project 3477

DEVELOPMENT AND APPLICATION OF ANALYTICAL TECHNIQUES

Analysis of Pulping and Bleaching Liquors by Ion Chromatography

Sources of Error in the Amalgam Method for Determining
Polysulfide in Kraft White Liquor

September 15, 1985

PROJECT SUMMARY FORM

DATE: August 20, 1985

PROJECT NO. 3477: DEVELOPMENT AND APPLICATION OF ANALYTICAL TECHNIQUES

PROJECT LEADER: D. B. Easty

IPC GOAL: N/A

OBJECTIVE:

Evaluate and/or develop analytical techniques which are required to meet demands of both Institute and member company activity.

CURRENT FISCAL BUDGET: $65,000

SUMMARY OF RESULTS SINCE LAST REPORT:

Analysis of Pulping and Bleaching Liquors by Ion Chromatography

A method for determining chlorine dioxide in bleach liquors by ion chromatography (IC) has been developed and tested. It is based upon a chlorite response in the IC conductivity detector found to be proportional to the ClO_2 injected. Chlorine dioxide contents of liquors determined by IC were in close agreement with values obtained by the tyrosine and iodometric procedures. A ten-fold excess of chlorine was found not to interfere with the ClO_2 determination, apparently because the chlorine was reduced to chloride by the organic resin in the IC.

Chlorite-ClO_2 mixtures are analyzed by IC in two steps. The first result represents chlorite plus ClO_2. In the second step, chlorite alone is determined following removal of ClO_2 with nitrogen sparging. This technique was demonstrated by successful analysis of mixtures of known concentration.

In pH 10.8 eluent, chlorine is converted to hypochlorite and determined by IC using the electrochemical (amperometric) detector. Ion chromatographic results agreed with those from iodometric titration. Chlorine dioxide did not interfere with the IC determination of chlorine.

Quantitative spike recovery values documented the validity of IC for determining oxalate in bleaching effluents.

Results of our studies of IC analysis of bleaching liquors were reported to the membership in May (IPC Technical Paper Series No. 153) and were submitted for publication in Paperi ja Puu.

Determination of Polysulfide in Kraft Pulping Liquors

A brief study has revealed the following sources of error in the amalgam method for determining polysulfide in kraft white liquor (TAPPI Test Method T 694 pm-82): liquor dilution, sample volume placed on amalgam, and contact with air during amalgam treatment. These findings were recently submitted as a Note to the Editor of Tappi Journal. This work was prompted by a method comparison conducted as a part of our earlier (1984) development of a gas chromatographic method for polysulfide.

PLANNED ACTIVITY THROUGH FISCAL 1986:

Studies of lignin determination in unbleached pulps by diffuse reflectance Fourier transform infrared spectrometry will be resumed. This had been interrupted for a year due to manpower and workload considerations. The investigation will involve analysis of more pulps and rigorous evaluation of the data obtained.

Also planned are brief studies of the decomposition of bleaching liquors and chlorine dioxide solutions which have been diluted extensively for ion chromatographic analysis.

FUTURE ACTIVITY:

Future work will involve continued studies of pulp and liquors by chromatographic and spectrometric techniques. Likely topics are: improved material balance in unbleached pulp analysis, pyrolysis gas chromatography, and determination of volatiles by headspace analysis.

Status Report

DEVELOPMENT AND APPLICATION OF ANALYTICAL TECHNIQUES

Analysis of Pulping and Bleaching Liquors by Ion Chromatography

INTRODUCTION

Ion chromatography (IC) is a type of liquid chromatography most commonly used for separation and determination of ionic species in aqueous solutions. The principal use envisioned for IC in the pulp and paper industry is determination of inorganic anions in pulping and bleaching liquors. Ion chromatographic methods found applicable for liquor analysis should also be useful for less complex samples such as white waters. Measurements utilizing IC should be easier, quicker, and more accurate than wet chemistry.

In an ion chromatograph, ions are separated on an ion-exchange column, eluted by an ionic eluent, and detected most commonly by an electrolytic conductivity detector. The two basic types of ion chromatographs differ in how the signals due to the ions of interest are enhanced relative to the conductivity of the eluent. In suppressed ion chromatography, a second column (or fiber) in series, called the suppressor, chemically reduces the eluent's conductivity (e.g., by converting sodium carbonate to carbonic acid). Single-column IC uses low-conductivity eluents and electronic suppression, i.e., subtraction of background conductivity from the sample signal before the signal is amplified. Studies at the Institute have employed suppressed ion chromatography.

The Institute's ion chromatograph was delivered in the spring of 1982, and studies of its use for pulping liquor analysis were begun shortly thereafter. Requests for IC analyses from the industry and the Institute have limited the time available for research on methodology to a few man-weeks per year.

PROCEDURES

ION CHROMATOGRAPHY

Apparatus and reagents are listed in TAPPI T 699 pm-83 and in our earlier report on IC analysis of black liquor.[1] Essential details and modifications for bleach liquor analysis are described below. The ion chromatograph is a dual-channel Model 2020i equipped with electrolytic conductivity and electrochemical (amperometric) detectors (Dionex Corporation, Sunnyvale, CA, U.S.A.). Bleach liquor analysis was performed on an HPIC AS-3 column followed by an anion fiber suppressor. Eluent used for chlorine-containing species was $0.002\underline{M}$ Na_2CO_3; for oxalate the eluent was $0.003\underline{M}$ $NaHCO_3$, $0.0024\underline{M}$ Na_2CO_3. All ions except hypochlorite were detected by electrolytic conductivity; hypochlorite was detected with the electrochemical detector with a platinum electrode, applied potential -0.20 V. The electrochemical detector was placed ahead of the separator column to avoid loss of hypochlorite due to its decomposition by the ion-exchange resin.

Because distilled water produced an interference equivalent to about 0.7 ppm hypochlorite at the hypochlorite retention time, eluent rather than water was used to dilute samples in which hypochlorite was determined. Use of formaldehyde solution (1 mL/L) as diluent has been suggested in T 699 for preserving hypochlorite samples and standards. This was found to produce a negative interference equivalent to about 2.5 ppm hypochlorite. Therefore, formaldehyde was not used to preserve hypochlorite.

IODOMETRIC AND SPECTROMETRIC METHODS

Determinations of chlorine-containing oxidants in water and bleach liquors by iodometry have been reported by several authors.[2-4] Aieta's procedure,[4] which employs five iodometric titrations, was used in this study for measuring chlorine dioxide, chlorine, chlorite, and chlorate. The strength of hypochlorite solutions was determined by iodometric titration at pH 2.

Spectrometric and other procedures for determining chlorine dioxide have been reviewed by Masschelein.[5,6] Two spectrometric methods were used in this investigation. The Acid Chrome Violet K (ACVK) method[5,7] is sufficiently sensitive to determine chlorine dioxide in solutions diluted for injection into the IC. Decolorization of ACVK (Color Index Code 61710) is proportional to chlorine dioxide content; it was measured at 550 nm in 5-cm cells. In a less-sensitive but more convenient method, chlorine dioxide oxidizes tyrosine to dopaquinone, measurable at 490 nm.[5,8] Interference due to chlorine was removed by reaction with ethylamine.

<div align="center">RESULTS AND DISCUSSION</div>

CHLORINE DIOXIDE

Bleach liquors are known to change in composition during storage, and ion chromatography should be able to characterize the decomposition by simultaneous determination of chlorine-containing anions. To test this ability, a laboratory-prepared chlorine dioxide liquor was diluted 1:2500 with distilled water, and aliquots of dilute liquor were injected into the IC as a function of storage time at room temperature. At each time interval a duplicate sample was taken for chlorine dioxide determination by the ACVK method. The liquor

initially contained 7.0 g/L chlorine dioxide and 0.52 g/L chlorite (iodometric titration); its pH after dilution was 5.67. Results of the analyses are shown in Fig. 1.
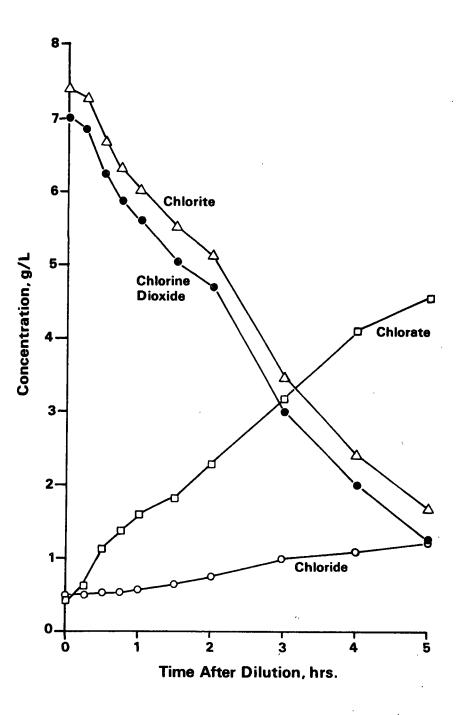

Figure 1. Analysis of dilute chlorine dioxide liquor. Anions determined by ion chromatography, chlorine dioxide by ACVK method.
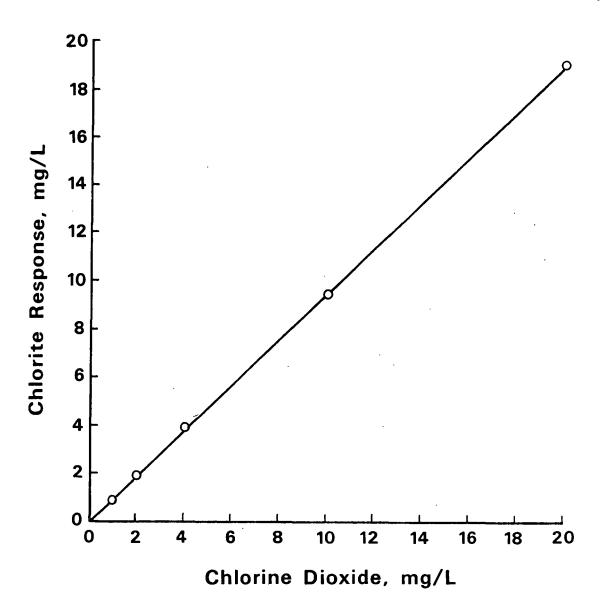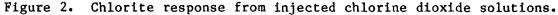
The data in Fig. 1 indicate that the chlorine dioxide was converted to chlorite upon injection into the IC, presumably by reaction with the ion-exchange resin. Thus a liquor's chlorite response in the IC reflects the chlorite originally present in the liquor plus the chlorine dioxide. Data obtained after several hours' storage indicate that the chlorine dioxide had decomposed to chlorate and chloride prior to injection; the original chlorite content of the liquor did not change significantly. Approximately 80% of the chlorine from decomposed chlorine dioxide is accounted for in chlorate and chloride. The chlorate/chloride mole ratio varied from 2 to 4. A ratio of 5 would be expected if decomposition followed the equation below, proposed for chlorine dioxide disproportionation in neutral media.[9] This will be studied further.

$$6 \; ClO_2 + 3 \; H_2O \longrightarrow 5 \; HClO_3 + HCl$$

The unanticipated behavior of chlorine dioxide in the IC was tested further by injecting a series of chlorine dioxide solutions and measuring the chlorite response. As shown in Fig. 2, the chlorite response was proportional to the chlorine dioxide injected. This provides the basis for an IC method for determining chlorine dioxide in bleach liquors. In this procedure, chlorite serves as a surrogate for chlorine dioxide, and Fig. 2 shows the calibration line. Data in Table 1 show that chlorine dioxide contents determined by IC were in excellent agreement with values from the tyrosine and iodometric methods.

Because the IC responds (as chlorite) to the sum of chlorite and chlorine dioxide, an additional step is necessary to determine a liquor's chlorite content. The original chlorite may be determined by injecting a second aliquot of sample from which the chlorine dioxide has been removed by nitrogen sparging. This technique was used to obtain the data in Table 2, in which measured chlorine dioxide and chlorite concentrations match well the known contents of prepared mixtures.

Figure 2. Chlorite response from injected chlorine dioxide solutions.

Because chlorine and chlorine dioxide are often used in the same

bleaching stage, possible interference by chlorine in the chlorine dioxide

determination was a concern. Values in Table 3 did not reveal any interference,

even when chlorine was present in a ten-fold excess. Data in Table 4 suggest

that chlorine did not interfere because it was reduced to chloride in the IC,

probably by reaction with the organic resin. Note that chlorine dioxide

(chlorite) is determined with the conductivity detector, which does not respond

to chlorine (hypochlorite).

Table 1. Comparison of methods for determination
of chlorine dioxide.

Method	Result, g/L
IC	3.87 ± 0.04[a]
Tyrosine	3.85 ± 0.03[a]
Iodometric	3.78[b]

---

[a]95% Confidence limits for the mean of eight
determinations.
[b]Iodometric determinations were performed daily.
Result decreased from 4.30 to 3.78 g/L in two
weeks due to slow decomposition of the ClO_2
stock solution.

Table 2. Ion chromatographic analysis of chlorine dioxide-
chlorite mixtures.

Prepared Mixture, ppm		Measured Concentration, ppm	
ClO_2	Chlorite	ClO_2	Chlorite
1.93	1.00	1.92	1.00
1.93	1.00	1.95	1.00
1.93	2.00	1.92	2.00
1.93	2.00	1.95	1.97
0.96	3.00	0.96	2.97
0.96	3.00	0.98	2.94

Table 3. Analysis of chlorine-chlorine dioxide mixture.

Time, min[a]	Method	ClO_2, g/L	Cl_2, g/L
--	Prepared conc.	0.100	1.00
2	IC (conductivity)	0.101	--
30	Tyrosine	0.102	--
90	Iodometric	0.099	0.99
150	IC (conductivity)	0.100	--

---

[a]Minutes after preparing sample. Sample pH 1.98.

Table 4. Reduction of Cl_2 in ion chromatograph and noninterference
with ClO_2 determination.

	ClO_2, g/L	Cl_2, g/L	Cl^-, g/L
Prepared conc.[a]	0.50	0.49	0.050
IC (conductivity)[b]	0.50	--	0.55
Prepared conc.	0.50	1.00	0.046
IC (conductivity)	0.50	--	1.03
Prepared conc.	0.50	2.00	0.037
IC (conductivity)	0.50	--	2.00

[a]From IC and titrimetric analysis of individual chlorine water
 and ClO_2 solutions.
[b]IC analysis of ClO_2-chlorine water mixture.

CHLORINE

The sodium carbonate eluent used for IC analysis of bleach liquors has
a pH of 10.8. At that pH the hypochlorous acid formed by the hydrolysis of
chlorine in water would be essentially all converted to hypochlorite:

$$Cl_2 + H_2O \rightleftharpoons HOCl + HCl$$

$$HOCl \rightleftharpoons H^+ + OCl^-$$

These equations are the basis for an IC method for the determination of chlorine
in bleach liquors. Tables 5 and 6 indicate that the IC and iodometric analysis
of chlorine water and tap water yielded comparable results. Because the
chlorine (hypochlorite) was measured with the electrochemical detector, there
was no interference from chlorine dioxide (Table 6). Installation of the
electrochemical detector before the separator column permitted the chlorine to
be measured before it was reduced to chloride. Solutions containing chlorine
dioxide, chlorite, chlorate, and chloride were run through the electrochemical
detector to confirm that these species were not electroactive under the con-
ditions of this analysis.

Table 5. Determination of chlorine.

| Method | Chlorine Water Samples | | Tap Water, mg/L |
	A, g/L	B, g/L	
IC (electrochemical)	0.75	0.81	1.3
Iodometric	0.77	0.80	1.2

Table 6. Analysis of chlorine-chlorine dioxide mixtures.

Method	ClO_2, g/L	Cl_2, g/L
Prepared conc.	0.050	0.50
IC (electrochemical)	--	0.50
Iodometric	0.049	0.50
Approximate conc.	0.50	0.50
IC (electrochemical)	--	0.44
Iodometric	0.50	0.44

CHLORATE AND CHLORITE

Values for chlorate in bleach liquors determined by IC are compared with those from the iodometric method in Table 7. Results are similar from the two methods. The iodometric method for chlorate also detects chlorine, chlorine dioxide, and chlorite. Accurate chlorate values depend, therefore, on accurate determination of and correction for these other chlorine-containing species. Thus, use of IC rather than iodometry for measuring chlorate should lead to enhanced speed, ease, specificity, and accuracy in the determination.

A spike recovery study was performed to confirm the validity of the IC method for determining chlorate and chlorite. A chlorine dioxide liquor was diluted 1:2500 and allowed to stabilize overnight. Spiking solution containing chlorate and chlorite was added, and six replicate determinations of these ions were performed by IC. Results shown in Table 8 indicate nearly quantitative spike recoveries.

Table 7. Determination of chlorate in bleach liquors.

	Chlorate, mg/L	
	Iodometry	IC
C_D influent	N.D.	16
C_D effluent	49	66
D_1 influent	331	260
D_1 effluent	307	294
D_2 influent	50	52
D_2 effluent	78	93

N.D. = none detected.

Table 8. Recovery of chlorite and chlorate added to a chlorine dioxide liquor.

	Original, ppm	Added, ppm	Expected,[a] ppm	Found,[b] ppm	Recovery, %
Chlorite	N.D.[c]	1.00	0.50	0.495	99
Chlorate	1.18	1.00	1.09	1.06	97

[a]Spiked sample prepared by mixing 1 part spiking standard plus 1 part diluted ClO_2 liquor.
[b]Mean of six replicate determinations.
[c]None detected.

OXALATE

The formation of oxalic acid during bleaching of kraft pulp has been demonstrated.[10] In that study the oxalic acid was esterified and measured by gas chromatography. Oxalate was determined in the current work by ion chromatography without derivatization. Spent liquors from chlorine and chlorine dioxide stages were diluted, and their oxalate contents were measured before and after addition of oxalate spikes. Quantitative spike recovery values in Table 9 document the value of IC for this analysis.

Table 9. Recovery of oxalate added to bleaching effluents.

Sample	Original, ppm	Added, ppm	Total Found, ppm	Recovery, %
C Stage, diluted 1:10	0.20	1.0	1.20	100
	0.20	1.0	1.20	100
	0.20	2.0	2.15	98
	0.20	2.0	2.15	98
D Stage, diluted 1:100	0.20	2.0	2.19	99
	0.20	2.0	2.10	95
	0.20	3.0	3.20	100
	0.20	3.0	3.30	103

ACKNOWLEDGMENT

LITERATURE CITED

1. Easty, D. B.; Borchardt, M. L.; Webb, A. A., Paperi Puu, in press.

2. Rapson, W. H.; Anderson, C. B., Pulp Paper Mag. Can. 67:T54(1966).

3. Eriksson, B.; Sjöström, L., Svensk Papperstid. 79:570(1976).

4. Aieta, E. M.; Roberts, P. V.; Hernandez, M., J. Am. Water Works Assoc. 76(1):64(1984).

5. Masschelein, W., J. Am. Water Works Assoc. 76(3):80(1984).

6. Masschelein, W. J. Chlorine dioxide: chemistry and environmental impact of oxychlorine compounds. Ann Arbor, MI, Ann Arbor Science Publishers, 1979:89-107.

7. Masschelein, W., Anal. Chem. 38:1839(1966).

8. Lepeintre, M.; Dupuy, J.; Ouviand, J., Chemie Analytique 10:498(1960). (In French.) The method has been outlined in English by Masschelein, Ref. 5.

9. Reference 6, p. 51.

10. Krasowski, J. A.; Marton, J., J. Wood Chem. Technol. 3(4):445(1983).

THE INSTITUTE OF PAPER CHEMISTRY

Dwight B. Easty
Group Leader
Analytical Sciences
Chemical Sciences Division

Status Report

DEVELOPMENT AND APPLICATION OF ANALYTICAL TECHNIQUES

Sources of Error in the Amalgam Method for Determining Polysulfide
in Kraft White Liquor

INTRODUCTION

In 1982, a provisional method, TAPPI Test Method T 694, was adopted for
determining polysulfide in kraft white liquor. This method is based upon the
potentiometric titration of sodium sulfide before and after reduction of the poly-
sulfide with sodium amalgam. More recently, a new method for polysulfide based
on gas chromatography was developed in this laboratory.[1] Part of the method
development involved a comparison of results obtained by the GC and amalgam pro-
cedures. In the course of this work, a critical evaluation of the amalgam
method revealed several unanticipated sources of error, described in this report.

PROCEDURES

Details of the sodium amalgam method are provided in TAPPI Test Method
T 694 pm-82. Deoxygenated water was used for liquor dilution; all analyses on a
diluted sample were completed within 1 hour. A fresh portion of regenerated
amalgam was used for each sample. In order to exclude air from samples during
amalgam treatment, a hose from a nitrogen cylinder was connected to a vinyl
glove fitted over the modified plastic beaker. Sulfide was determined by manual
potentiometric titration with mercuric chloride using a silver-sulfide ion-
selective electrode and double junction reference electrode.

RESULTS AND DISCUSSION

SAMPLE DILUTION AND QUANTITY ON AMALGAM

Dilution of white liquor (20 mL ——> 100 mL) and the amount of diluted
liquor placed on the amalgam (10 mL) are clearly specified in T 694. Our

investigation has shown that use of different dilutions and sample quantities significantly affected results of the determination (Table 1). This finding has prompted two concerns: (1) The conditions specified in T 694 might not be those which yield the correct polysulfide value. No study of sample dilutions and quantities, which might resolve this question, is referenced in the Test Method. (2) Despite the warning note in T 694, analysts might use other liquor dilutions and volumes of sample on amalgam without realizing that these are critical quantities. It is not intuitive that sample dilution and volume on amalgam can affect analytical results; the subtle importance of these factors detracts from the ruggedness[2] of the method. An unsuspecting analyst might assume that sample amounts are specified in order to simplify calculations, as in other TAPPI Test Methods.

Table 1. Effect on measured polysulfide of sample
          volume and concentration in contact with
          amalgam[a].

Liquor Dilution	Volume of Diluted Liquor Placed on Amalgam, mL	
	5	10
20 mL —> 100 mL	16.7	16.0
	16.7	16.0
	16.7	16.1
	16.7	15.9
10 mL —> 100 mL	15.6	15.1
	16.0	15.2
	15.9	15.1
	15.9	15.1

[a]Polysulfide values are in g/L. Fifteen mL of amalgam
was used for each sample.

CONTACT WITH AIR DURING AMALGAM TREATMENT

In Test Method T 694, diluted liquor is swirled with sodium amalgam in a modified plastic beaker to reduce the polysulfide sulfur to sulfide. Because sulfide is susceptible to oxidation in air, oxidative losses during swirling

were suspected. This was tested by swirling 10-mL quantities of several diluted polysulfide liquors for two minutes in the modified plastic beaker without amalgam. Titrations revealed that sulfide losses during swirling amounted to 0.3-1.1 g/L. When swirling was performed in a nitrogen atmosphere, sulfide losses from the same liquors were reduced to approximately 0.1 g/L. These results suggest that two reactions may occur when polysulfide liquor is swirled on amalgam: reduction of polysulfide by amalgam and oxidation of sulfide by air.

The effect of exposure of diluted liquor to air during swirling was next tested with amalgam in the modified beaker. Polysulfide determinations were performed with and without a nitrogen atmosphere over the sample during reduction. Sulfide losses would produce lower polysulfide values in the determination. Results are shown in Table 2. Polysulfide values were consistently lower when samples were swirled on amalgam without nitrogen protection. Thus, exposure of samples to air during amalgam treatment appears to contribute significantly to errors in the determination.

EXTENT OF AMALGAM TREATMENT

Prolonged contact of samples with amalgam can cause reduction of thiosulfate in the liquor to sulfide, as noted in T 694. To minimize this reaction as well as air oxidation of sulfide, samples should be swirled with amalgam no longer than is required to just reduce the polysulfide. To test the time required, a polysulfide liquor was swirled on amalgam, and aliquots were withdrawn every half minute. Polysulfide was measured in each aliquot by the triphenylphosphine GC method.[1] Polysulfide did not decrease significantly after one minute of swirling. A one-minute contact time of liquor with amalgam appeared adequate for polysulfide reduction.

Table 2. Polysulfide determinations run with and without nitrogen
          protection during reduction on amalgam.

Liquor	N$_2$ Protected, g/L	Not Protected, g/L
1	15.9	14.9
	16.0	14.6
2	6.2	5.6
	6.1	5.3
3	7.7	6.8
	7.6	6.8
4	14.5	14.0
	14.6	14.1
5	13.7	12.2
	13.8	12.3

CONCLUSIONS

This investigation has shown that liquor dilution, volume placed on
amalgam, and contact with air during amalgam treatment are sources of error in
the polysulfide determination. The study has also raised the possibility of
inherent errors in the procedure; these could occur if liquor dilution, volume
on amalgam, and time of swirling have not been optimized. These errors can be
averted by use of the GC procedure.

LITERATURE CITED

1. Borchardt, L. G.; Easty, D. B., J. Chromatogr. 299:471(1984).

2. Cardone, M. J., J. Assoc. Off. Anal. Chem. 66:1257(1983).

THE INSTITUTE OF PAPER CHEMISTRY

Dwight B. Easty
Group Leader
Analytical Sciences
Chemical Sciences Division

THE INSTITUTE OF PAPER CHEMISTRY

Appleton, Wisconsin

Status Report

to the

PULPING PROCESSES

PROJECT ADVISORY COMMITTEE

Project 3288

FINE STRUCTURE OF WOOD PULP FIBERS

Project 3521-2

RAMAN MICROPROBE INVESTIGATION OF MOLECULAR STRUCTURE
AND ORGANIZATION IN THE NATIVE STATE OF WOODY TISSUE

September, 1985

PROJECT SUMMARY FORM

DATE: September, 1985

PROJECT No. 3288: FINE STRUCTURE OF WOOD PULP FIBERS

PROJECT LEADER: R. H. Atalla

IPC GOAL:

Develop relationships between the critical paper and board property parameters
and the way they are achieved as a combination of raw materials selection, prin-
ciples of sheet design and processing.

OBJECTIVE:

Define the structure of wood pulp fibers and relate to ultimate web properties.
Emphasis is on full chemical pulps.

CURRENT FISCAL BUDGET: $45,000

SUMMARY OF RESULTS SINCE LAST REPORT:

Solid state ^{13}C NMR studies have shown native celluloses to be composites of two
crystalline forms, I_α and I_β. Their Raman spectra show them to have the same
molecular conformation, but to have different hydrogen bonding patterns. The
distribution of cellulose between the two forms varies over a wide range among
native celluloses. There are indications that the two forms differ in their
susceptibilities to swelling and chemical reaction. The relative amounts of the
two forms are therefore important determinants of properties.

In studies of pulp refining we have applied the method developed by W. Platt in
his thesis studies to other types of pulp and found it sensitive to subtle dif-
ferences in the nature of the pulps. The key measurements are the relaxation
times of the protons in proton NMR spectra of water bound in the pulps and the
variation of these relaxation times with moisture content.

We have also made progress in improving the methodology for quantitative charac-
terization of wood pulps using Raman spectroscopy. We have extended studies
previously carried out in collaboration with Dr. V. J. Pohjola of the Helsinki
University of Technology to establish the confidence limits on our quantitative
analyses and their dependence on the standards used.

PLANNED ACTIVITY THROUGH FISCAL 1986:

1. Use solid state ^{13}C NMR and Raman spectroscopy to investigate differences in
   the response of celluloses I_α and I_β to chemical reactions and pulping con-
   ditions.

2. Develop mild chemical procedures to isolate cellulose from woody sources to
   establish the range of variation of cellulose crystallinity and its distri-
   bution between the two native crystalline forms.

3. Study the intramolecular and intermolecular interactions which dominate the
    aggregation of cellulose and related cell-wall polysaccharides.

FUTURE ACTIVITY:

Progress on several projects, including the new areas of high-yield pulping and
moisture tolerant webs, will benefit from a better understanding of the relation
between fiber and product properties. New information on cellulose and fine
fiber structure will be useful in guiding activity. Future work will focus on
the structure of native wood fibers and its modification in both conventional
chemical and high-yield pulping processes. Particular attention will be given
to factors which control papermaking properties.

PROJECT SUMMARY FORM

DATE: September, 1985

PROJECT No. 3521-2: RAMAN MICROPROBE INVESTIGATION OF MOLECULAR STRUCTURE
                     AND ORGANIZATION IN THE NATIVE STATE OF WOODY TISSUE

PROJECT LEADER: R. H. Atalla

IPC GOAL:

Develop relationships between the critical paper and board property parameters
and the way they are achieved as a combination of raw materials selection, prin-
ciples of sheet design and processing.

OBJECTIVE:

In conjunction with work sponsored by the DOE, use the Raman Microprobe to develop
a better understanding of wood fiber structure. Establish by Raman microprobe
spectroscopy the variability of molecular structure and organization in cell
walls of native woody tissue. Also, by the same methods, explore the effects of
mechanical and chemical treatments on structure and organization in high-yield
pulp fibers. Finally, upon installation of the new microprobe system, explore
the photophysics of lignin and lignin residues in high-yield pulp. (This work
is also supported by DOE under Project 3521-3 with a Fiscal 1985/1986 budget of
$49,000. This is in addition to the DOE grant of $194,000 toward the acquisi-
tion of the new Raman microprobe system.)

CURRENT FISCAL BUDGET: $40,000

SUMMARY OF RESULTS SINCE LAST REPORT:

Optimization of the Raman microprobe, together with the new techniques we devel-
oped, have permitted acquisition of high quality spectra that clearly indicate a
high level of organization of lignin in the cell walls. The spectra show lignin
to be oriented with respect to the plane of the cell-wall surface and to vary
in amount relative to the cellulose from point to point within the secondary
wall.

Success in our initial efforts in this area has enabled us to compete success-
fully in the DOE University Research Instrumentation Program for award of the
funds for a new Microprobe system which, with multichannel detection, will
enable us to expand the scope of our program and to include in it studies on
the photophysics of lignins related to brightness stability in high yield pulps.

PLANNED ACTIVITY THROUGH FISCAL 1986:

Exploration of the spectra of different woods and native fibers will be con-
tinued. The effects of mechanical and chemical treatments on the architecture
of the cell walls will be investigated in conjunction with our high-yield
pulping program. A substantial effort will also be devoted to design, acquisi-
tion, and assembly of the new microprobe system.

FUTURE ACTIVITY:

Continuation of the program in conjunction with the DOE supported effort is anticipated through Fiscal 1986/1987.

FINE STRUCTURE OF WOOD PULP FIBERS

INTRODUCTION

An important part of our program under Project 3288 has been the continuation of the studies of polymorphy in native celluloses. In this context the question of polymorphy is confined to the differences between the I_α and I_β forms which we have detected on the basis of solid state ^{13}C NMR. Our results are summarized in the preprint prepared for the Daicel Symposium, a copy of which is attached to this report as Appendix I. This paper also is an abridgment of the manuscript submitted for the Fundamental Research Symposium of PIRA held at Oxford, England.

In addition to our studies on the polymorphy of native cellulose our effort under Project 3288 has concentrated on two areas. The first was concerned with analysis of the methods we have been using to quantify conformational distribution in pulpwood samples on the basis of their Raman spectra. We have continued our efforts to establish the confidence limits one can assign to our calculated distributions, and to understand the factors related to the nature of the samples as well as to the standards used, which are the key ones in determination of the limits.

The second area of concentration is related to our continuing effort to understand the nature of molecular level transformations in fiber architecture which accompany mechanical refining. We have extended the methods developed by W. Platt in his doctoral dissertation, which are based on the proton NMR of water bound in the fibers, to investigations of loblolly pine. The contrast with his results on spruce pulps has added insight concerning the phenomena involved in the transformations. Furthermore, they have helped us to understand

what previously had seemed to be divergences between the results of proton NMR studies and our Raman spectroscopic studies of refining.

In addition, under Project 3288, we have completed and published our study of the factors which influence the regeneration of cellulose in the cellulose I lattice.

Under Project 3521 we have continued studies in a number of areas that exploit the capabilities of the Raman microprobe. In addition we have successfully competed in the DOE University Research Instrumentation Program, and have a grant of $194,000 toward the acquisition of a new Microprobe system equipped with multichannel detection and pulsed laser excitation.

The areas of concentration were the further development of information concerning the molecular architecture of native wood and, in relation to our academic program, the studies associated with the doctoral dissertation of James Wiley. The latter have been directed at enhancing our understanding of the spectrum of cellulose, exploring molecular orientation in native fibers, and seeking further evidence concerning the differences between the two crystalline forms of native cellulose which we have previously identified as I_α and I_β.

In the following sections overviews will be provided, together with abstracts of preprints which are in preparation for publication. The complete publication will be transmitted to the membership as part of the Institute Technical Paper Series.

OVERVIEW - PROJECT 3288

The current status of our studies on polymorphy in native cellulose is best summarized in the following abstract from the manuscript attached as Appendix I.

Abstract: Our studies of cellulose structure based on X-ray diffractometry, Raman spectroscopy, and Solid State ^{13}C NMR have lead us to propose two stable ordered states of cellulose chains, k_I and k_{II}, predominant in celluloses I and II, respectively, both having the dimeric anhydrocellobiose as the basic repeating unit. The disordered state, k_o, has less coherence between the orientations of adjacent anhydroglucose rings.

Our model recognizes two crystalline forms within the native state, identified as I_α and I_β. I_α is dominant in bacterial and algal celluloses, I_β in celluloses from higher plants. These two forms contain chains possessing the same molecular conformation, k_I, but with different patterns of hydrogen bonding. Cellulose II contains chains predominantly in the k_{II} conformation.

Conformational Analyses

As we have previously reported on many occasions and in a number of publications, we have been able to resolve the Raman spectra of most chemical pulps into linear combinations of the spectra associated with the three distinct conformational states that are postulated in our model of cellulose structure. These states are the ordered conformation k_I which is dominant in native celluloses, the order conformation k_{II} which is dominant in mercerized celluloses and some regenerated celuloses, and the disordered state k_o which is associated with amorphous celluloses. The analyses in terms of these conformations have been used primarily for qualitative comparisons of celluloses from different sources, or subjected to different preparative processes.

During the academic year 1983/1984 we had as a member of our group Dr. Viekko Pohjola of Helesinki University of Technology. In a collaborative effort we carried out a more rigorous analysis of the mathematical bases and procedures

that we had been using. The analysis, summarized in the abstract attached in

Appendix II, confirmed the validity of our model, but it raised questions con-

cerning the influence of the standards used in the spectral analyses on the

quality of the fit to the experimental spectra. In particular, it indicated that

the use of highly crystalline celluloses to generate the standard spectra was

resulting in estimates of error that were excessively inflated. This conclusion

was derived from the observation that the error spectra were quite similar to

derivative spectra. Such an effect points to standards with typically narrower

bandwidths than those in the samples under analysis.

In the work undertaken since the studies with Pohjola, we have investi-

gated the use of alternate standards and found that the estimates of error were

indeed more reassuring. In essence our key conclusion is that it is inappropriate

to use cotton based standards when analysing celluloses from wood pulps. Instead,

we have now established standard spectra derived from Avicel, which is a micro-

crystalline cellulose derived from a high-alpha pulp. The bandwidths in the

spectra of the new standards are clearly more representative of those expected

from ordered domains in wood pulp celluloses.

Studies on Refining

In his doctoral research program, summarized in the abstract attached

as Appendix III, Platt investigated the effect of refining on the state of mole-

cular aggregation in pulp fibers by monitoring the mobility of water bound in

the fibers using proton NMR. The thesis underlying his method is that water

absorbed on a cellulosic surface has lower mobility than bulk water, and that

the relaxation time in proton NMR measurements would reflect the distribution of

mobilities. Thus, if one measures the average spin-lattice relaxation time as a

function of moisture content, one would find it declining at first and then

rising to approach that of bulk water. The nature of the minimum in plots of

relaxation time vs. moisture content would thus reflect the manner in which the

water within the fibers is distributed.

The key effect of refining which he observed was a broadening of the

minimum and a shift to higher moisture contents. Thus, it was argued that new

surfaces capable of binding water were generated in the course of refining.

Whereas Platt worked with black spruce, in our extension of the work we

have studied the effects of refining on the internal structure of loblolly pine

fibers. We have found that in addition to broadening of the minima, the minimum

relaxation time is significantly reduced. Such an effect suggests that the new

surfaces generated in the refining of loblolly pine may bind the water more

tightly than surfaces available prior to refining. Our tentative conclusion at

this time is that in the case of spruce, while new surface is generated during

refining, it is basically similar in site energy distribution to surfaces

available prior to refining. In the case of loblolly pine, on the other hand,

it appears that the new sites generated during refining have an energy distribu-

tion differing from that of sites available prior to refining.

The finding based on the proton NMR studies correlates with an earlier

finding based on Raman spectroscopic studies. In those studies it was found

that refining had little effect on the susceptibility of spruce pulp fibers to

mercerization, whereas the effect on loblolly pine fibers was to somewhat

increase the susceptibility to mercerization. We are continuing to assess the

implications of these findings and to consider additional studies that add

clarity to the broader view of the effects of refining.

Future Work

In our future work we expect to continue our efforts in the areas outlined above, and to pursue further the implications of our previously reported findings concerning the two crystalline forms of native cellulose, I_α and I_β.

The proton NMR studies will be continued to enable us to identify more specifically those characteristics of pulp fibers which determine the energy site distributions which control relaxation times. We expect then to be able to clarify our picture of the molecular transformations caused by refining.

The program directed at improving our quantitative analysis of conformational distributions in cellulose will be continued until we have identified the most suitable set of standards for analyses of pulp fiber samples, and until the methodology for quantitative analysis is well established.

One of the central parts of our program will be directed at further development of our understanding of the differences between the I_α and I_β forms of cellulose and the degree to which such differences may have implications concerning the response of wood celluloses to chemical treatments. We expect to continue studies of the response of algal celluloses to chemical treatments to establish whether the higher susceptibility of the I_α form to acid hydrolysis has parallels in differences in reactivity in other environments.

We also plan to devise mild chemical or enzymatic etching procedures to try to isolate the fundamental cellulose fibrils from wood pulp fibers to enable us to assess the true nature of wood celluloses. In the past it has generally been thought that the wood celluloses are less crystalline than celluloses from the algae or from cotton or ramie. It now appears to us that there is a possibility that cellulose fibrils in wood are equally crystalline, but that the

encrusting materials have prevented adequate resolution in the usual methods of characterizing crystallinity. Furthermore, traditional methods for removing the encrustants are severe enough to disrupt any crystallinity that may be present in cellulose. We believe that new procedures are necessary if we are to be able to establish the true distribution of crystalline wood cellulose between the I_α and I_β forms. Furthermore, answers to these questions are central to our pursuit of new insights concerning the response of pulp fibers to process conditions.

Finally, we also expect to begin an effort to understand the dominant intermolecular interactions responsible for the aggregation of cellulose with other cell wall polysaccharides.

OVERVIEW - PROJECT 3521

(Excerpted and revised from the Annual Report to DOE)

In our previous report we gave an account of the development of the Raman microprobe technique for studies on native woody tissues and included preprints of preliminary reports on our first explorations and some initial drafts of more extended reports on our findings. The key findings were that lignin was more highly organized in native woody tissue than had heretofore been recognized and that the Raman microprobe can reveal valuable new information concerning many aspects of cell wall architecture in plant tissue.

The present report includes abstracts of completed papers on three studies previously described in preliminary form (Appendices IV, V, and VI). The first is a more detailed discussion of spectroscopic evidence for lignin and cellulose orientation in woody tissue, as well as evidence for compositional variation within the walls of individual cells and between the walls of adjacent cells. The second is a report on Raman microprobe studies of orientation and

organization in native celluloses from ramie fibers and from the alga <u>Valonia</u> <u>ventricosa</u>. The third is a more extensive report describing the techniques developed for acquiring spectra from sections of woody tissue; this manuscript has been accepted for publication in the Journal of Raman Spectroscopy.

In addition the report includes brief summaries of work we have undertaken to explore possible modifications in our techniques which could enhance our capacity to record spectra from a wider variety of samples and to record useful spectra in shorter intervals of time. We also summarize our efforts to culture algae capable of producing highly crystalline cellulose for use as a spectral standard; some of these efforts have included adaptation of the algae to growth in D_2O.

Future Work

Although we are continuing with our program as initially set forth in our proposal for the present grant, we are currently actively reassessing our plans in light of our successful application for funding for a new Raman Microprobe system with multichannel detection and pulsed laser excitation. Under the DOE University Research Instrumentation Program we have been awarded funds to assemble a system which would enable us to expand the scope of our investigations and to initiate collaborative studies with other investigators in the area of cell wall architecture.

EXPANSIONS OF RESEARCH PROGRAMS THAT WOULD BE POSSIBLE WITH THE NEW INSTRUMENT

In addition to enabling significant expansion of the scope of our primary program under our present DOE Grant (DE-FG02-84ER13189), acquisition of the new instrument will make possible other research programs both in collaboration with colleagues at the Institute and in collaborations with investigators at

other institutions. In all of these instances, we have carried out or are

currently carrying out exploratory studies. Further work in all of these areas

is limited at present by available instrument time.

The programs contemplated in collaboration with other faculty at IPC

include

1. <u>Characterization of cell wall structure in tissue generated in an</u>

<u>extensive program in tissue culture ongoing at the Institute</u>. The program is

concerned with embryogenesis in the wild carrot model system. Its longer term

objective is embryogenesis from tissue derived from conifer hybrids. We believe

<u>in situ</u> spectral characterization of cell-wall structure and composition will be

helpful in characterizing the response of cultured cells to the variables under

study.

2. <u>The response of cell-wall structure to various chemical treatments</u>.

Preliminary work has been carried out using acid-chlorite delignification.

Mapping of the spectra of cell-wall structures subjected to different reagents

for varying periods would vastly expand our knowledge of variability in cell-

wall structures and would add to our understanding of many industrial processes

utilizing biomass as a basic feedstock.

Another study that could be undertaken with the new system is an

assessment of the potential of Raman spectroscopy for <u>measurement of lignin con-</u>

<u>tent in pulps</u>. This possibility is given a high priority in the Advanced Sensor

Program of the Industrial Processes Section of DOE.

EXPLORATORY STUDIES

Additional exploratory studies were carried out in four areas. These

included

    A.   Effects of higher laser power

    B.   Studies on cellulose orientation in delignified tissue

    C.   Bound water in the cell walls

    D.   Algal celluloses

A. Laser Power Effects. Because of the extended data acquisition times found necessary, the possibility of using higher laser powers was explored. Higher powers had been found undesirable in our earlier studies carried out on dry samples. It was thought that the water immersion technique might allow the use of higher powers.

Secondary cell walls from black spruce were studied in both longitudinal and transverse sections. Lignin was monitored at the 1600 cm^{-1} band, and cellulose at the 1098 and 2900 cm^{-1} bands. It was found that at higher irradiance the lignin band appeared to decay under some conditions, while the cellulose bands remained unchanged. The tendency of the 1600 cm^{-1} band to decay seemed to vary. This may be correlated with differences in the composition of the lignin suggested by variability of the ratio of the alpha carbonyl band to that of the aromatic rings at 1600 cm^{-1}.

A number of possible mechanisms were considered. The first was the possibility of thermal degradation. This was ruled out because comparisons of the Stokes and anti-Stokes lines indicate a maximum temperature of 50°C. Neither cellulose nor lignin are expected to decompose at such temperatures. The second possibility considered was that of photochemical decomposition. This seemed unlikely primarily because the majority of lignin fragments absorb only in the ultraviolet. This possibility will be assessed further, however. The most plausible interpretation at the present time is that the warming of the immediate

environment near the focused laser beam may result in slow extraction of some of the hemicellulose fragments with some lignin fragments attached. Experiments to assess these possibilities are currently in progress.

B. <u>Cellulose Orientation</u>. Experiments were carried out at a level of resolution corresponding to 2 micrometers to attempt to detect differences that might be attributed to differences in cellulose organization in different morphological features. Spectra were recorded for three different domains in both longitudinal and cross sections of black spruce. The domains consisted of 1. the middle lamella + the primary wall + the S_2 layer of the secondary wall; 2. the S_2 layer of the secondary wall; 3. the S_3 layer + part of the S_2 layer of the secondary wall. Unfortunately the signal to noise ratio was not sufficient to allow confidence that any observed differences were significant. It is anticipated that this problem will be overcome with the new spectrometer system.

C. <u>Bound Water in the Cell Wall</u>. In observations of the bands associated with the O-D stretching vibration in studies of samples immersed in D_2O, some orientation sensitive intensity variations have been noted. These can be attributed to bound water held in a specific orientation by strong interactions with the hemicelluloses in the cell walls. These observations are quite preliminary and need further assessment.

It is anticipated that the new multichannel detection system will enable us to pursue the questions arising in all three areas outlined above, and to do so much more expeditiously.

D. <u>Algal Celluloses</u>. Our initial studies on algal celluloses grew out of our desire to have a readily cultured organism capable of producing highly crystalline cellulose so that the spectral features of cellulose can be readily

separated from those of other components of cell walls. Although our earliest efforts were directed at culturing Valonia ventricosa and Valonia macrophysa, the difficulty of duplicating an optimum marine environment limited the productivity of this approach. When it was discovered that celluloses of equal crystallinity could be obtained from the Alga Rhizoclonium heiroglyphicum, the possibilities of using fresh water algae as a source of crystalline cellulose were explored.

Since our early findings on the cellulose from Rhizoclonium heirglyphicum we have found a number of other algae that produce crystalline cellulose similar to that from Valonia. After much experimentation we have developed procedures and media that have enabled us to culture species of Rhizoclonium, Cladophera, and Pithophora algae. We have also made considerable progress toward adapting some of these strains to growth in D_2O. Success in this latter effort will enable us to produce perdeuterated cellulose that will be of great value in structural studies on cellulose, as well as in interpreting its Raman spectra more completely.

The Institute of Paper Chemistry

Rajai H. Atalla
Chemical Sciences Division

APPENDIX I

STUDIES ON POLYMORPHY IN NATIVE CELLULOSE

by

Rajai H. Atalla
The Institute of Paper Chemistry
Appleton, Wisconsin 54912, U.S.A.

ABSTRACT

Our studies of cellulose structure based on X-ray diffractometry, Raman spectroscopy, and Solid State ^{13}C-NMR have led us to propose two stable ordered states of cellulose chains, k_I and k_{II}, predominant in celluloses I and II, respectively, both having the dimeric anhydrocellobiose as the basic repeating unit. The disordered state, k_o, has less coherence between the orientations of adjacent anhydroglucose rings.

Our model recognizes two crystalline forms within the native state, identified as I_α and I_β. I_α is dominant in bacterial and algal celluloses, I_β in celluloses from higher plants. These two forms contain chains possessing the same molecular conformation, k_I, but with different patterns of hydrogen bonding. Cellulose II contains chains predominantly in the k_{II} conformation.

INTRODUCTION

Earlier studies led us to propose a model of cellulose structure in which anhydrocellobiose, with nonequivalent anhydroglucose units, is the basic repeat unit. The nonequivalences between the adjacent anhydroglucose units were found to be different in celluloses I and II. Thus, the two most common polymorphs possess different molecular conformations as well as different unit cells in their crystalline domains.

Later high resolution ^{13}C NMR studies on crystalline native celluloses

showed that they are composites of two distinct crystalline modifications, and

that the relative proportions of the two modifications are different in dif-

ferent native forms. In this report we review our model of structure, with par-

ticular attention to the native state, and discuss our most recent findings.

STRUCTURAL MODEL

Molecular Conformations

Our first detailed comparison of the Raman spectra of celluloses I and

II led us to conclude that the molecular chains possess different conformations

(1). To identify the differences between the two conformations, we pursued

information from a number of sources. We examined the results of conformational

energy calculations (2,3); they indicate that two different states of the glyco-

sidic linkage are stable. These are represented as relatively small left-handed

and right-handed departures from the twofold helix conformation, and are well

approximated, respectively, by the crystal conformations of the model disaccharides

cellobiose (4) and methyl-β-cellobioside (5). The vibrational spectra in the OH

stretching region for the disaccharides and for celluloses I and II led us to

suggest that nonequivalent glycosidic linkages alternate along the molecular

chains (6). The multiplicities of chemically equivalent carbons in the solid

state ^{13}C NMR spectra confirmed this conclusion, and the chemical shifts were

consistent with a difference between the skeletal conformations in celluloses I

and II. Finally, the Raman spectra showed the C-6 carbons to be nonequivalent

in cellulose I but equivalent in cellulose II (7).

The observations outlined above and the constraints imposed by packing

of the chains in the lattice, lead to a model incorporating features of both

disaccharide structures. It consists of a cellulose chain with alternating gly-
cosidic linkages corresponding alternately to small left-handed and right-handed
departures from the twofold helix conformation. This feature is taken as common
to both polymorphs.

        The difference between molecular conformations in the two polymorphs is
related to the nonequivalence of C-6's in cellulose I and is illustrated in
Figure 1. The vibrational spectra in the OH stretching region indicated that
alternate C-6's in cellulose I have their primary hydroxyl groups participating
in bifurcated intramolecular hydrogen bonds similar to the one known to occur in
crystalline methyl-beta-cellobioside. In this disaccharide the dihedral angles
at the glycosidic linkage correspond to a relatively small right-handed depar-
ture from the twofold helix for cellulose. In this conformation the positions
of the ring oxygen and the primary hydroxyl oxygen on C-6 are such that they can
both function as electron donors in the hydrogen bond with the hydroxyl group on
C-3 of the adjacent ring. The conformation of cellobiose, which is equivalent
to a small left-handed departure from the twofold helix, does not allow the
oxygen on C-6 to participate in the bifurcated bond, and the intramolecular
hydrogen bond remains an isolated one. We believe that the participation of
alternate primary hydroxyl groups in bifurcated intramolecular hydrogen bonds
is the key factor stabilizing the glycosidic linkages of cellulose I in posi-
tions where their nonequivalence is less pronounced than in cellulose II.

        In terms of the new model, the mechanism of conversion of cellulose
from polymorph I to polymorph II is simple. It involves removal of the primary
hydroxyl on every other C-6 from the bifurcated intramolecular hydrogen bonds.
This allows the glycosidic linkages to relax into the more distinct positions
characterisitic of cellulose II and permits the C-6's to move into approximately

equivalent positions. The small contraction of the unit cell in the chain direction when cellulose I is converted to cellulose II is a logical consequence of the relaxation of the glycosidic linkages.

The two ordered states were identified as k_I and k_{II} on the basis of their predominance in celluloses I and II, respectively. In addition, a disordered state, identified as k_o, has been defined as corresponding to the molecular organization dominant in the most amorphous celluloses. Our model permits use of Raman spectra for quantitative characterization of the structure of native and processed celluloses, most of which are not pure polymorphic forms (8,9).

Crystalline Forms

In our work with VanderHart (10,11) a number of crystalline celluloses were investigated using (CP/MAS) ^{13}C NMR spectroscopy. Spectra were recorded for Acetobacter xylinum, Valonia ventricosa, cotton linters and ramie, and for regenerated celluloses I and II of pure polymorphic form (12,13). The spectra of the native celluloses and of the regenerated cellulose I are shown in Figure 2, together with the accepted assignments.

Although the spectrum of cellulose II was consistent with a unique unit cell, those of the native celluloses revealed multiplicities, indicating a more complex architecture. The sharper components of the C-4 and C-6 resonances, as well as the C-1 resonance arise from magnetically nonequivalent sites within crystalline domains. The relative intensities of the multiplet components are not constant, nor are they in the ratios of small whole numbers. A model based on two independent crystalline forms provided the most plausible decomposition of the spectra.

The approximate spectra of the two forms are illustrated in Figure 3, and designated I_α and I_β. The spectra were obtained by taking appropriate linear combinations of the spectrum of the regnerated cellulose I and that of the cellulose from Acetobacter xylinum, which are the closest to the two extremes of a two component model. Comparison of the I_α and I_β spectra with the spectrum of cellulose II, which is included in Figure 3, clearly shows that the multiplicity of I forms is quite distinct from the well established polymorphic variation.

The spectra in Figure 2 and those recorded for many other native celluloses persuade us that all native celluloses are composites of the two distinct forms. We believe that our finding confirms earlier reports (14) that Acetobacter and Valonia cellulose are structurally different from that of cotton and ramie. A very crude estimate based on our model suggests that Acetobacter cellulose is 60 to 70% I_α, whereas cotton is 60 to 70% I_β.

CONFORMATIONAL VARIATION AND POLYMORPHY

The SS ^{13}C NMR spectra indicate that polymorphy occurs within the cellulose I subset of structures, in addition to, and clearly apart from the well recognized cellulose II form. The Raman spectral studies, on the other hand, show that two distinct ordered states of the cellulose chains are stable. The question thus arose whether the two forms I_α and I_β represent true solid state polymorphs with molecules possessing identical conformations, or whether, like celluloses I and II, they contain molecules with different conformations.

Our earlier analysis indicated that comparison of the Raman spectra of the different native forms would resolve this question. Our earlier studies of Raman spectra had concentrated on celluloses from higher plants where I_β is the

dominant component. We, therefore, extended our investigations to include the Raman spectra of bacterial and Valonia celluloses.

The Raman spectra of the native celluloses are shown, together with a spectrum of cellulose II, in Figure 4. The region shown, between 250 and 1500 cm^{-1}, is dominated by the skeletal motions most sensitive to molecular conformation. The spectra of the three native celluloses are very similar. The spectrum of cellulose II is in sharp contrast, however; most of its features, particularly in the region below 600 cm^{-1}, are quite different from those of the native celluloses. We conclude, therefore, that the same conformation, k_I, occurs in the three native celluloses, and a distinctly different conformation, k_{II}, in cellulose II.

When these results are considered together with the ^{13}C NMR results shown in Figure 3, we conclude further that the molecular conformation k_I can aggregate to form two different crystalline lattices, I_α and I_β. Cellulose II, in contrast, is an aggregate of molecules in the conformation k_{II} in yet a third distinct lattice. A similar pattern has been observed among the polymorphs of amylose (15).

The chemical shift variation in the ^{13}C NMR spectra also indicates the same conformation, k_I, for celluloses I_α and I_β, and a different one, k_{II}, for cellulose II. On the average, the chemical shifts in cellulose II differ from those of celluloses I_α and I_β more than the shifts of the latter two differ among themselves.

To further explore the difference between I_α and I_β forms, we investigated the Raman spectra in the OH stretching region. Marrinan and Mann (14) had

detected the differences between native celluloses from their infrared spectra in the OH region. In our experiment the Raman microprobe was used to record spectra of parallel aggregates of elementary fibrils from the cell walls of Valonia ventricosa and for individual ramie fibers. Spectra were recorded with the electric vectors of the exciting radiation parallel and perpendicular to the direction of the fibrils.

The spectra in the CH and OH stretching regions are shown in Figure 5. They are best resolved in the parallel mode, where the bands are also more intense. The differences between the ramie and Valonia celluloses are that the latter possesses an OH band at lower frequency than any in the ramie spectrum, while the ramie spectrum has one somewhat broader band at higher frequencies than any in the Valonia spectrum. Thus each of the two forms of cellulose has at least one hydrogen bond that does not occur in the other form. These obser-vations, together with the similarity of the Raman spectra in the skeletal region, lead us to the conclusion that the difference between the I_α and I_β forms resides in the patterns of intermolecular hydrogen bonding. Such dif-ferences can account for the differences in the SS ^{13}C NMR spectra of the two forms.

REFERENCES

1. R. H. Atalla, Proceedings of the 8th Cellulose Conference, Appl. Polymer Symp. 28:659(1976).

2. D. A. Reese and R. J. Skerrett, Carbohyd. Res. 7:334(1968).

3. S. Melberg and K. Rasmussen, Carbohyd. Res. 71:25(1979).

4. S. S. C. Chu and G. A. Jeffrey, Acta Crystallogr. B24:830(1968).

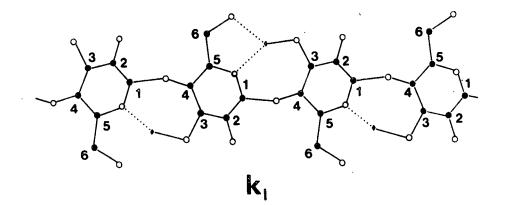5. J. T. Ham and D. G. Williams, Acta Crystallogr. B29:1373(1970).

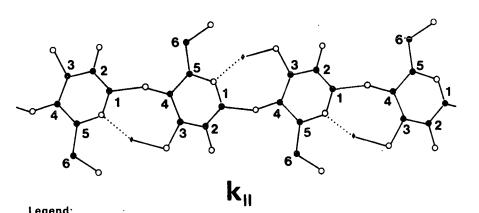6. R. H. Atalla, Advances in Chemistry Series, No. 181, 1979, p.55.

7. R. H. Atalla, Proceedings of the International Symposium on Wood and Pulping Chemistry, Stockholm, June 1981. SPCI Report No. 38, Vol.1, 1981, p.57.

8. R. H. Atalla, Proceedings of the 9th Cellulose Conference, Appl. Polymer Symp., No. 37, 1983, p. 295.

9. R. H. Atalla, J. Ranua, and E. W. Malcolm, Tappi J. 67:96(1984).

10. R. H. Atalla and D. L. VanderHart, Science, 223:283 (1984).

11. D. L. VanderHart and R. H. Atalla, Macromol., 17:1465 (1984).

12. R. H. Atalla and S. C. Nagel, Science, 185:522 (1974).

13. R. E. Whitmore and R. H. Atalla, Int. J. of Biol. Macromol., in press.

14. H. J. Marrinan and J. Mann, J. Polym. Sci. 21:301(1956).

15. A. Sarko and P. Zugenmaier, ACS Symposium Series, No. 141, 1980, p. 459.

FIGURE CAPTIONS

Figure 1.   Schematic representation of conformations k_I and k_{II}.

Figure 2. ^{13}C CP-MAS spectra of various celluloses: A –
            Ramie; B – cotton linters; C – regenerated cellulose
            I; D – Acetobacter xylinum cellulose; E – Valonia
            ventricosa cellulose. The "X" marks the small first
            spinning side band of linear polyethylene added as
            an internal standard; its centerband at 33.6 ppm is
            not included in this display.

Figure 3.   Comparison of the ^{13}C CP-MAS spectra of cellulose II
            and the spectra of the two proposed crystalline
            forms of cellulose I, namely, I_α, and I_β. An "X" or
            a gap mark locations of the first spinning sideband
            of the linear polyethylene chemical shift standard.

Figure 4.   Raman spectra of Valonia ventricosa cellulose,
            Acetobacter xylinum cellulose, Microcrystalline cot-
            ton cellulose, and high-crystallinity cellulose I.

Figure 5.   Raman microprobe spectra in the CH and OH stretching
            regions for ramie and Valonia ventricosa celluloses.
            The spectra were recorded for fibrillar aggregates
            of Valonia cellulose and for on individual fiber of
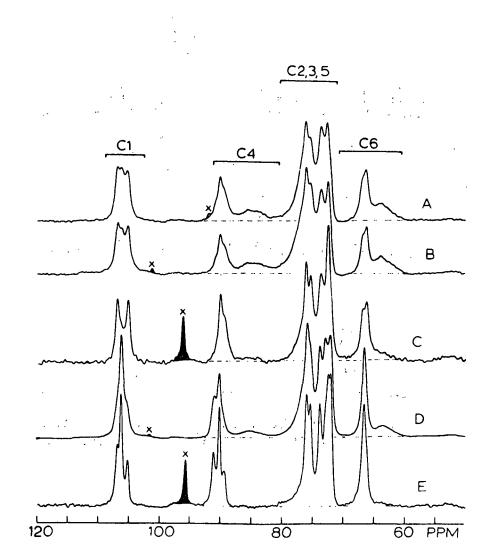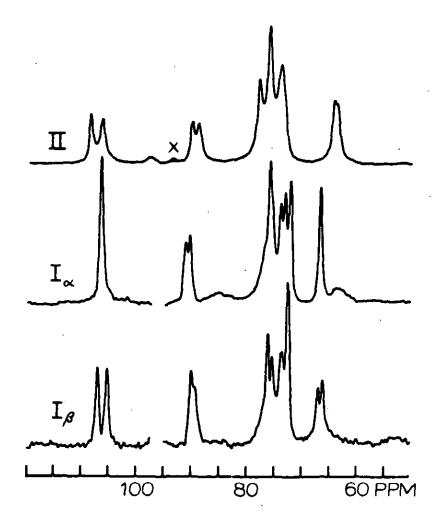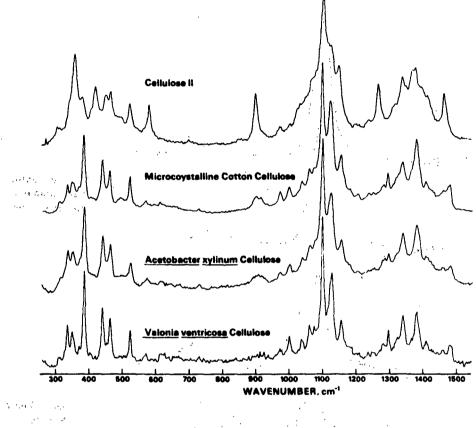   ramie.

k_I

k_{II}

Legend:
- ● = Carbon
- ○ = Oxygen
- ✦ = Hydrogen
- —— = Covalent bond
- ······ = Hydrogen bond

C2,3,5

C1 C4 C6

A

B

C

D

E

120 100 80 60 PPM

Cellulose II

Microcoystalline Cotton Cellulose

Acetobacter xylinum Cellulose

Valonia ventricosa Cellulose

WAVENUMBER, cm⁻¹

Ramie

Valonia

Electric Vector
Perpendicular
to Fiber Axis

Ramie

Valonia

Electric Vector
Parallel
to Fiber Axis

2600   2800   3000   3200   3400   3600

Wavenumbers, (cm^{-1})

APPENDIX II
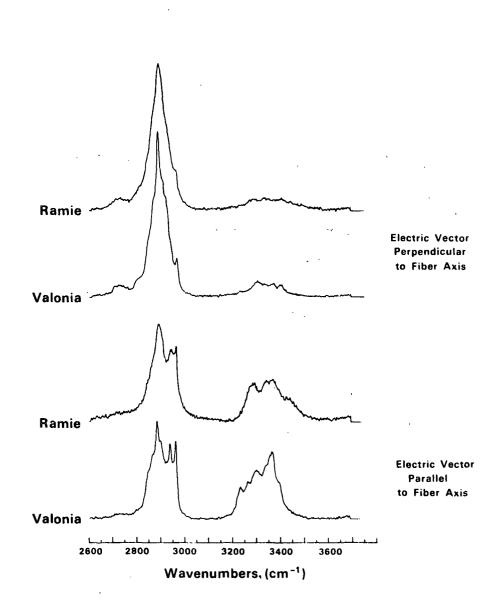
Statistical Interpretation of Raman Spectra of Cellulose Pulps

V. J. Pohjola[*] & R. H. Atalla
The Institute of Paper Chemistry
Appleton, WI 54912
*Present address: Helsinki University of Technology
SF-02150 Espoo 15, Finland

Abstract

Raman spectrum of cellulose was modelled by a linear combination of three standard spectra representing the three cellulose conformations (Atalla's cellulose model) and a straight line representing fluorescence background. By minimizing the sum of squares of the errors, estimates for the regression coefficients and for their confidence limits were obtained. The regression coefficients of the standard spectra represent the mutual proportions of the three cellulose conformations in the sample examined.

The conformational compositions of cellulose in a kraft pulp and in three ASAQ pulps were determined. According to reported data there were significant differences in some properties such as tensile strength and bleachability of the pulps. The conformational compositions, instead, were very similar when interpreted in terms of the 95% confidence limits of the regression coefficients. The slight differences that were observable in the bleached samples were found to be paralleled by differences in the bleaching conditions. On that basis the factors which favor reduction of viscosity and removal of noncarbohydrate components during bleaching seem to favor formation of molecular chains typical for amorphous celluloses, mostly at the expense of chains typical for cellulose II during mercerization of the bleached samples.

The error spectrum was found to be characterized by a nonrandom pattern, which was similar for all the samples. The difference in bandwidths of the

recorded spectra and the standard spectra is suggested to be the origin of the pattern.

The overall fit of the regression model to the recorded Raman spectra was very good. This reflects simultaneously the success of the fit of the cellulose model to the Raman features and the fit of straight line to fluorescence background in the relatively narrow wave number range in question.

APPENDIX III

Proton NMR Relaxation Studies of Water in Pulp Fibers

by

William Neil Platt
Rajai Hanna Atalla

ABSTRACT

This work presents a new, valuable technique for quantifying and characterizing the surface present in a pulp sample at the molecular level. It is precisely this level that must be further understood to advance our understanding of pulping, bleaching and refining and their subsequent efects on the sheet properties.

Proton NMR spin-lattice relaxation times (T_1) of water in a pulp system allow detection of the local molecular environment. Molecules moving either faster or slower than the resonance frequency create inefficient relaxation processes.

Molecular motion of the proton ensemble average as described by a correlation time, τ_c, changes with temperature and/or distribution of the population. The latter approach was used by varying the moisture present in each sample. Samples at low moisture content have impeded molecular motion of the water, whereas samples at higher moisture content have rapid bulk water motion. There exists an optimal moisture content where τ_c gives a minimum relaxation time.

Proton T_1 values of water were measured by inversion recovery methods, whereas the spin-spin relaxation times were approximated by measuring the width at half of the spectral height. Results are presented for unbleached and bleached

bisulfite pulps; unbleached, bleached and refined bleached kraft samples; all samples were from the same northern spruce chip source.

Results are presented in terms of T_1 versus moisture content. The absolute depth, width and moisture content where the T_1 minima occur are discussed in terms of the strength of the molecular interactions, the distribution of the molecular environments and the quantity of pulp surface present.

Data indicate differences arise with the pulping process used which are overcome by the bleaching process. Mechanical refining increases the pulp surface area, which can and does interact with water.

APPENDIX IV

IN SITU RAMAN MICROPROBE STUDIES OF PLANT CELL WALLS: MACROMOLECULAR ORGANIZATION AND COMPOSITIONAL VARIABILITY IN THE SECONDARY WALL

U. P. Agarwal and R. H. Atalla[*]
Division of Chemical Sciences
The Institute of Paper Chemistry, Appleton, WI 54912

ABSTRACT

Native state organization and distribution of cell wall components in the secondary wall of woody tissue from Picea mariana (Black Spruce) have been investigated using polarized Raman microspectroscopy. Evidence for orientation is detected through Raman intensity variations resulting from rotations of the exciting electric vector with respect to cell wall geometry. Spectral features associated with cellulose and lignin were studied. The changes in cellulose bands indicate that the pyranose rings of the anhydroglucose repeat units are in planes perpendicular to the cross section, and can occur parallel to both tangential and radial planes, while methine C-H bonds are in planes parallel to the cross section. Changes in bands associated with lignin suggest that the aromatic rings of the phenyl propane units are most often in the plane of the cell wall surface. However, regions where lignin orientation departs from this pattern also occur. These results represent the first direct evidence of molecular organization with respect to cellular morphological features in woody tissue, and suggest that cell wall components are more highly organized than had heretofore been recognized. Studies carried out in order to establish the usefulness and sensitivity of the Raman technique to differences of composition within the cell walls provide evidence of variations in the distribution of cellulose and lignin. Such compositional differences were more prominent between the walls of different cells than within a particular cell wall.

APPENDIX V

RAMAN SPECTRA OF CELLULOSES

James H. Wiley and Rajai H. Atalla

ABSTRACT

The Raman microprobe has made new information accessible for the assignment of the vibrational spectrum of cellulose and the study of cellulose polymorphy and orientation. Spectra were recorded from ramie fibers, mercerized ramie fibers, ramie cross sections, and oriented aggregates of Valonia cellulose by varying the polarization of the incident light relative to the geometry of the samples. Based on an analysis of intensities in the spectra of native ramie fibers and Valonia aggregates, the vibrational bands were divided into two groups. In the first group, the bands are most intense when the electric vector of the exciting light is either parallel or perpendicular to the fiber axis. The group 1 bands result from displacements which are predominantly either parallel or perpendicular to the fiber axis. In the second group, the bands are most intense when the electric vector is between 0 and 90 degrees to the fiber axis. Less is known about the directionality of the displacements which result in group 2 bands. The new information about the directional character of the vibrational modes was used with information from spectra of deuterated celluloses and normal coordinate analyses of model compounds to make band assignments.

Cellulose polymorphy was studied by comparing the spectra of Valonia, ramie, and mercerized ramie. The similarity of the Valonia and ramie spectra in the low frequency region indicates that the conformation of the cellulose backbone is the same. The frequency pattern in the OH stretching regions, however, differs significantly, suggesting distinct hydrogen bonding patterns in ramie and Valonia celluloses. The spectra of mercerized and native celluloses differ in

both low frequency and OH stretching regions. Therefore, the conformation of
the cellulose backbone, as well as the hydrogen bonding pattern in cellulose II,
is distinct from native cellulose.

Cellulose orientation in the plane perpendicular to the chain axis was
studied by recording spectra of ramie cross sections with different polariza-
tions of the incident light relative to the cell wall surface. The intensities
suggest nonrandom orientation of the cellulose.

APPENDIX VI

RECORDING RAMAN SPECTRA FROM PLANT CELL WALLS

R. H. Atalla[*] and U. P. Agarwal
Division of Chemical Sciences
The Institute of Paper Chemistry
Appleton, WI 54912

Abstract

A Raman microprobe system has been successfully utilized to obtain luminescence free spectra from sections of woody tissue. The procedures for optimizing the microprobe and the sample mounting techniques are described. Spectra from the secondary wall of black spruce (_Picea mariana_) indicate that both lignin and cellulose can be studied in their native state.

THE INSTITUTE OF PAPER CHEMISTRY

Appleton, Wisconsin

Status Report

to the

PULPING PROCESSES

PROJECT ADVISORY COMMITTEE

Project 3474

IMPROVED PROCESS FOR BLEACHED PULP

Low-Lignin Pulps

Nonchlorine Bleaching

September 9, 1985

PROJECT SUMMARY FORM

DATE: September 9, 1985

PROJECT NO. 3474:   IMPROVED PROCESS FOR BLEACHED PULP

PROJECT LEADERS: T. J. McDonough and N. S. Thompson

IPC GOAL:

Improved process for bleached chemical pulp.

OBJECTIVE:

Define pulping and bleaching technology that will decrease the number and size
of the required process stages, including reduced needs for effluent treatment.

CURRENT FISCAL BUDGET: $130,000

SUMMARY OF RESULTS SINCE LAST REPORT:

An empirical model describing the behavior of both the kraft and kraft-
anthraquinone pulping processes has been derived and used in conjunction with
the MAPPS computer simulation system to evaluate the economics of pulping to low
lignin contents in these processes. It was concluded that low-lignin kraft
pulping is both economically and environmentally beneficial. These results have
been presented to the management of a large bleached kraft market pulp mill with
an expressed interest in reducing bleaching costs and bleach plant effluent
generation.

Studies of the kinetics of sulfite-anthraquinone (SAQ) pulping as a route to
modifications of that process for achieving low kappa numbers have been con-
tinued. Effects of Na_2SO_3 have been delineated and the activation energies and
stoichiometries have been determined. Rates of removal of individual carbohydrate
components have been determined in addition to delignification rates. The data
obtained to date will form the basis of a kinetic model capable of predicting
the effects of process modifications on delignification rate, yield selectivity
and viscosity selectivity. Analysis of the data and construction of such a
model are now in progress.

In collaboration with the Systems Group, and with the aid of two Master's Degree
candidates, Arlene Heaster and Scott Dibbs, a Mapps simulation of SAQ pulping
has been constructed. This will be useful in evaluating proposed operating
alternatives and process modifications, particularly when the complete kinetic
description referred to above becomes available.

Research on the fundamentals of oxygen bleaching has been redirected. Following
earlier efforts to identify effective cellulose protectors, additional antioxi-
dants (chosen for configuration and reactivity) were tested. Although some
preserved cellulose better than the controls, none exceeds the benefits obtained
from magnesium ion. As a result we conclude that although radicals are present
during oxygen bleaching, we cannot control them. Thus research emphasis was
changed from attempts to stabilize cellulose against degradation to developing
techniques to enhance lignin removal relative to cellulose degradation.

PLANNED ACTIVITY THROUGH FISCAL 1985/1886

A kinetic model of SAQ pulping will be constructed on the basis of the data
obtained so far and the results of a limited number of further experiments. The
model is expected to be capable of predicting pulp composition as a function of
cooking time for a variety of conditions of liquor composition and pH. It will
be used to define optimum conditions for producing low-lignin bleachable SAQ
pulps.

The possibility of a mill trial of low-lignin kraft pulping will be pursued with
the mill already identified.

It is also planned to determine whether or not pretreatment of lignin to modify
its chemical nature will affect its response during oxygen bleaching. These
results will be compared with the corresponding posttreatments. Posttreatments
of pretreated pulps will also be checked. The pretreatments will include a
variety of oxidative treatments to destroy lignin aromaticity with the hope this
structure will initiate different antioxidative reactions.

FUTURE ACTIVITY

The predictions of the kinetic model will be confirmed by experiment and process
modifications suggested by it will be developed.

Experiments will be carried out to identify the radicals that are present during
oxygen bleaching and how they are affected by the proposed pretreatments. The
effect of radicals during other pulping and bleaching reactions will be explored,
and the chemical mechanism by which fibers are degraded by superoxide will be
pursued.

IMPROVED PROCESS FOR BLEACHED PULP

Low-Lignin Pulps

INTRODUCTION

This project is directed toward the development of technology for eco-
nomically producing strong alkaline pulps at very low unbleached kappa numbers.
This would substantially reduce both chemical costs and pollutant generation in
the bleach plant. It would also have a positive impact on pulp mill energy re-
covery and reject levels and may be expected to reduce capital costs by permitting
shorter and/or more environmentally acceptable bleaching sequences to be used.

Significant results achieved to date include the following:

1. Demonstration of the ability of the kraft and kraft-anthraquinone
processes to achieve significant unbleached kappa number reductions relative to
conventional practice. An appropriate choice of pulping conditions and good
control allows these reductions to be achieved with little or no loss in yield,
pulp strength or bleachability. These conditions may include various combina-
tions of high sulfidity, low effective alkali, low temperature, and anthraquinone
addition. For example, an existing mill that wishes to reduce unbleached kappa
number without changing digester capacity or production rate might increase both
sulfidity and temperature and, optionally, add anthraquinone.

2. Demonstration of the feasibility of bleaching low-lignin pulps to
very high brightness levels in only three stages. A brightness of 90 is
achievable in the C_DED sequence after oxygen predelignification and a brightness
of at least 86 can be obtained in the same sequence with no oxygen pretreatment.

3. Demonstration of the additivity of the beneficial effects of low-
lignin pulping and oxygen bleaching on bleach plant effluent pollutant levels.

4. Development of a simulation model to allow the economics of low-lignin pulping to be critically evaluated and optimized.

5. Identification of promising conditions for pulping to very low lignin contents in the alkaline sulfite-anthraquinone system.

Recent activity has been directed toward two objectives. One is to gain a fundamental understanding of the sulfite-anthraquinone (SAQ) pulping process, with a view to modifying it for pulping to low lignin contents. This is justified by the known ability of SAQ pulping to achieve higher selectivity than the kraft process, the fact that it produces pulps equivalent to kraft in strength properties, and its compatibility with existing kraft operations, albeit at the expense of additional equipment for the recovery system. The other short-term objective has been to evaluate, by computer simulation, the economics of low-lignin kraft and kraft-anthraquinone (kraft-AQ) pulping. This is now complete.

The present report is divided into two major sections. The first deals with the simulation of kraft and kraft-AQ low-lignin pulping operations. The second reports on the status of our investigations of SAQ pulping.

SIMULATION OF KRAFT AND KRAFT-AQ LOW-LIGNIN OPERATIONS

Earlier work under this project has demonstrated that there are many benefits associated with pulping to lower kappa numbers prior to bleaching. It has also been shown that the required kappa number reductions can be achieved by relatively simple changes in mill practice and without extensive equipment changes. For example, an increase in temperature and sulfidity in an existing continuous digester would lead to a beneficial kappa number reduction with no significant loss in bleached yield or pulp strength.

Changes in mill practice that result in brownstock kappa number reductions entail both costs and economic benefits. This raises the questions of whether the benefits outweigh the costs and whether some operating strategies have significant economic advantages over others. To provide answers to these questions, we conducted a parametric simulation study of the effect of digester conditions and brownstock kappa number on kraft pulp mill operation and economics.

Another factor motivating this work is the possibility of a mill trial. We have identified a large bleached kraft market pulp mill that has an active interest in reducing bleaching costs and bleach plant effluent generation. The management is therefore investigating oxygen bleaching, modified kraft pulping (as developed at the Swedish Forest Products Research Laboratory) and our approach to low-lignin pulping. We felt that an economic analysis based on computer simulation would be an effective way of demonstrating the expected benefits of low-lignin pulping.

The simulation was based on a laboratory pulping study in which we pulped loblolly pine chips under systematically varied sets of conditions in the kraft and kraft-anthraquinone (kraft-AQ) processes. Some of the data appeared in an earlier report;[1] the remainder were obtained more recently. Three sets of pulping experiments, each based on a different experimental design, were done. Two were central composite rotatable designs, one for the kraft process and one for the kraft-AQ process. The other one was designed to delineate the effect of very small levels of AQ addition. In all, 116 cooks were done. The resulting data were described by the regression equations laid out in Table 1. These equations were fitted to the data by K. Saffran, who used them in a related optimization study.[2] As indicated by the high values of the multiple correlation coefficient (R^2) in the table, the equations accurately represent the behavior of the system. Figure 1 illustrates this for kappa number. The only

significant deviations of the predicted values from the observed ones occurred

at kappa numbers so high as to be outside of the range of interest for low-

lignin pulping.

Table 1. Pulping equations.[a]

<div align="center">Equation</div> R^2

$$\log_{10}Y_T = 1.561 + 0.3529*A_s + 2.020*T + 0.7730*E - 0.1327*S - 0.4343*L$$
$$+ 0.1410*H + 0.05024*A - 1.812*A_s*T - 0.1356*A_s*L - 10.87*T*E$$
$$+ 2.085*T*L - 3.758*T*H + 1.046*E*L + 0.3111*S*H \qquad 0.95$$

$$\log_{10}Y_s = 1.548 + 0.3190*A_s + 1.805*T + 0.7928*E - 0.06551*S$$
$$- 0.3613*L + 0.1963*H + 0.04812*A - 1.621*A_s*T - 0.1258*A_s*L$$
$$- 10.64*T*E + 2.143*T*L - 3.228*T*H + 0.9443*E*L \qquad 0.94$$

$$\log_{10}K = 1.120 + 0.2730*A_s + 7.481*T - 4.572*E - 1.348*S + 2.282*L$$
$$+ 0.2182*H - 6.588*A_s*T + 1.773 + A_s*E + 0.9294*A_s*S$$
$$- 0.6266 A_s L + 1.169*A_s*H - 20.23*T*H + 1.059*S*S - 1.578*S*L$$
$$+ 2.134*S*H - 4.241*L*H + 5.574*H*H \qquad 0.97$$

$$\log_{10}V = 1.923 + 1.221*A_s - 3.920*T - 2.663*E + 1.188*S + 2.178*L$$
$$+ 1.550*H + 0.2806*A - 8.444*A_s T - 7.015*E*S + 6.872*E*L$$
$$- 16.76*E*L - 2.662*L*L \qquad 0.94$$

$$\log_{10}R = - 0.7870 - 0.1419*A_s + 5.723*T + 14.40*E + 3.694*S - 2.069*L$$
$$- 1.789*H + 1.226*A_s*H - 19.24*T*S - 20.79*E*E - 6.505*E*S$$
$$+ 1.344*S*L + 1.860*S*H + 1.537*L*L - 2.258*L*H + 3.169*H*H \qquad 0.94$$

---

[a]Independent variables and their transformations:

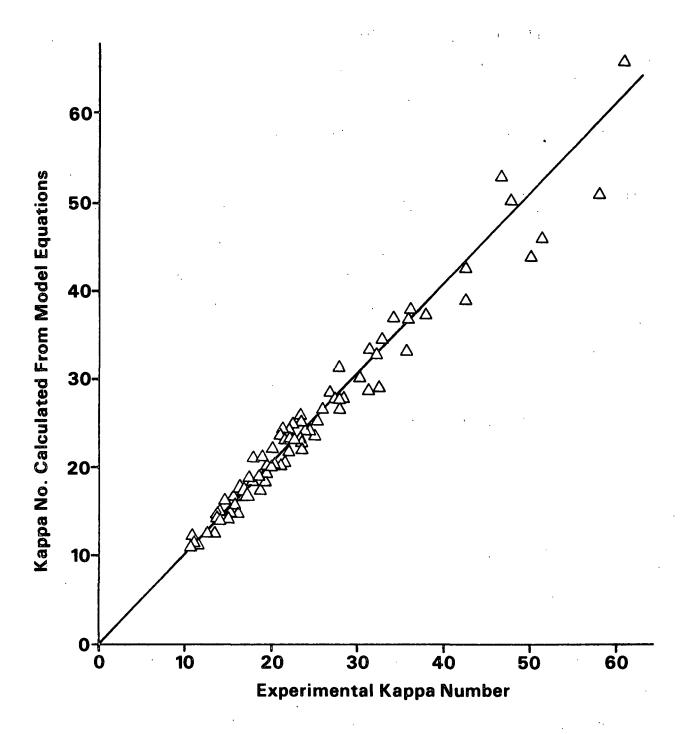| AQ	= Anthraquinone charge, percent on dry wood	A	= AQ * 1.0
		A_s	= $\sqrt{AQ}$
Temp.	= Cooking temperature, °C		
		T	= Temp. * 0.001
EA	= Effective alkali charge, percent on wood		
		E	= EA * 0.01
Sulf.	= Sulfidity, percent	S	= Sulf. * 0.01
LW	= Liquor-to-wood ratio (weight of water/weight of wood	L	= LW * 0.1
		H	= HF * 0.0001
HF	= H factor		

Figure 1.   Predicted vs. actual kappa number.

An important consideration in applying these equations is their range

of applicability.   Because they are empirical polynomial equations rather than

theoretically based ones, they are valid only over the independent variable

ranges investigated in the experiments on which they are based.   This range is

difficult to define in simple terms because the data came from three different
sets of experiments. It can be expressed in terms of a constraint on the sum of
squares of the transformed independent variables, as shown in Table 2. A subset
of the points for which the equations are applicable is made up of all com-
binations of levels of temperature, H factor, sulfidity, effective alkali,
liquor-to-wood ratio and AQ charge over the following ranges:

Temp.: 166-180°C   EA: 16-20%, o.d. wood basis

HF: 1540-2600   LW: 3.2-5.0 mL/g. o.d. wood

Sulf.: 18-35%, active alkali basis   AQ: 0-0.2%, o.d. wood basis

The total range of applicability of the equations is greater; the effect of an
individual variable can be predicted over a range that is approximately twice as
great as that given above if the remaining variables are maintained at the center-
points of their ranges.

For the purpose of the simulation, the equations were incorporated into
a digester model which is one of a series of "modules" employed by the system, a
steady state simulator called MAPPS (Modular Analysis of Pulp and Paper Systems)
developed at The Institute of Paper Chemistry. The input to the model consists
of the flow rates, temperatures and pressures of all components of the process
streams going to the digester (wood, white liquor, black liquor, recycled knots)
and process parameters (operating temperature, digester volume). Execution of
the module gives values for the flow rates, temperatures and pressures of the
outlet streams. These are then supplied as inputs to the next module in the
sequence. Since the process is cyclic, sequential execution of all modules in
the flowsheet provides new values for the digester inlet streams. The calcula-
tion is continued until successive iterations give essentially the same values

for these streams, at which point the simulation is said to have converged. The

resulting stream compositions and enthalpies then define a complete process mass

and energy balance which can be combined with variable cost and revenue infor-

mation to determine the profitability of the mill when it is run under the con-

ditions simulated.

Table 2. Transformation of independent variables for
defining range of applicability of pulping
equations in Table 1.[a]

$$T_1 = \frac{\log HF - 3.3}{0.11}$$

$$T_2 = \frac{\log LW - 0.6}{0.097}$$

$$T_3 = \frac{\log Sulf. - 1.4}{0.15}$$

$$T_4 = \frac{\log EA - 1.26}{0.046}$$

$$T_5 = \frac{Temp. - 173}{7}$$

$$T_6 = \frac{\log AQ + 1}{0.3}$$

$$\text{If } AQ < 0.1\%, \ T_6 = 0.0$$

[a]The equations are applicable over the region defined
by $T_1{}^2 + T_2{}^2 + T_3{}^2 + T_4{}^2 + T_5{}^2 + T_6{}^2 < 5.7$.

In the present case, a flowsheet was constructed to represent a single-

line bleached kraft pulp mill and the simulator was run under various conditions

of alkali charge, sulfidity and anthraquinone charge in the digester. In addi-

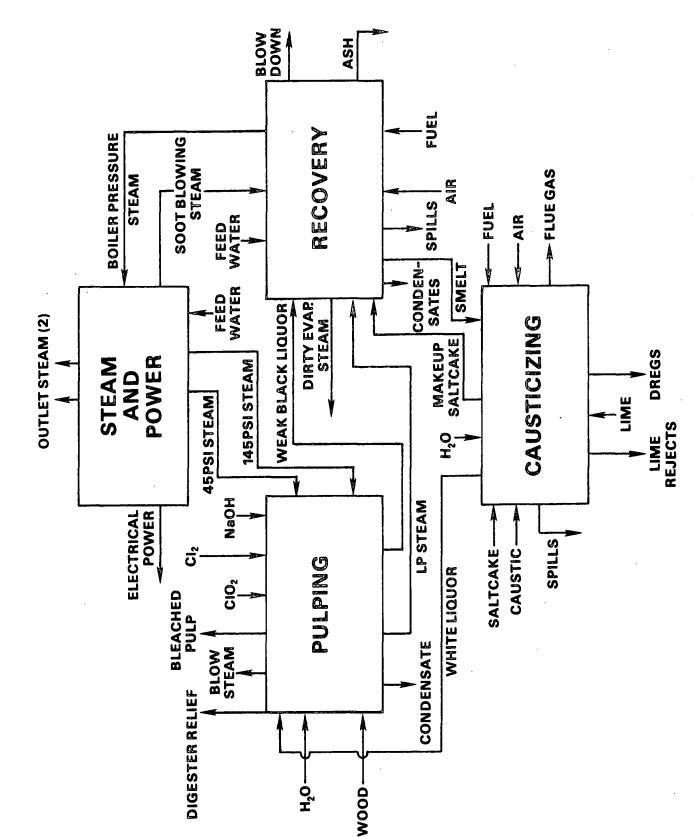tion, the H-factor was varied to give a range of brownstock kappa numbers for

each of the liquor compositions given by these variables. The liquor-to-wood

ratio was held constant at 4 mL/g. o.d. wood. The flow of wood to the digester

was chosen to maintain bleached pulp production constant, and the cooking tem-

perature was determined as the value necessary to provide the specified H-factor

in the time calculated from the wood flow rate and a fixed digester volume. In

other words, the simulation was appropriate for an existing mill contemplating a

decrease in kappa number with no change in production rate or digester capacity.

The flowsheet simulated is shown in Fig. 2-6. Figure 2 subdivides the

process into 4 areas: pulping and bleaching, chemical recovery, causticizing,

and steam and power generation. The subsequent figures show the modules that

constitute the simulation of each of these areas and give the module numbers,

MAPPS module type names, and stream numbers. Also, each module is labelled with

the name of the equipment it represents.

Some of the simulation results are presented in Fig. 7 to 11, showing

the simulator's predictions of the effects of changing digester conditions and

brownstock kappa number on some important factors. Wood cost increases slightly

as kappa number is reduced, owing to a reduction in fully bleached yield, as

shown in Fig. 7. At a given kappa number, wood cost is decreased by increasing

sulfidity or by adding AQ. Reducing the effective alkali charge also decreases

wood cost, except at very low kappa numbers where yield is adversely affected by

alkali depletion.

Figure 8 shows that the rate of steam generation is increased by decreas-

ing the kappa number, decreasing the sulfidity, or decreasing the effective

alkali charge. Decreasing the kappa number results in increased organics flow

to the recovery furnace; decreasing sulfidity decreases the amount of heat used

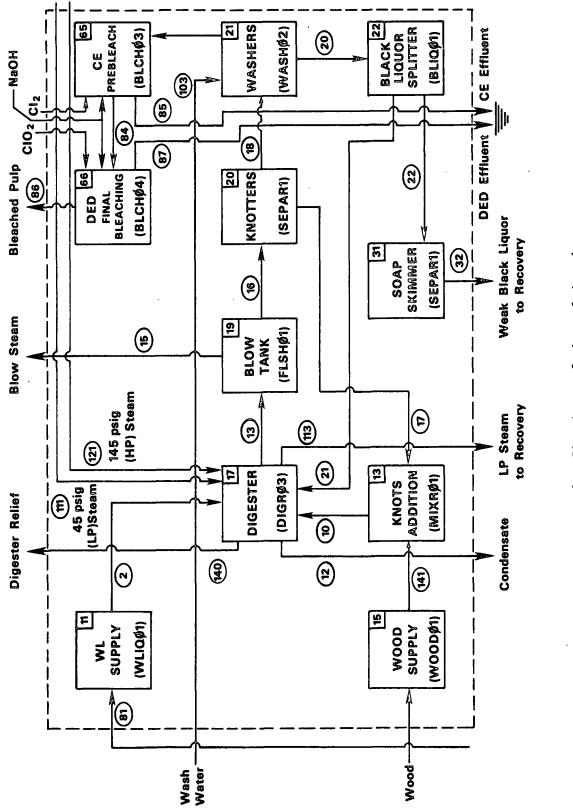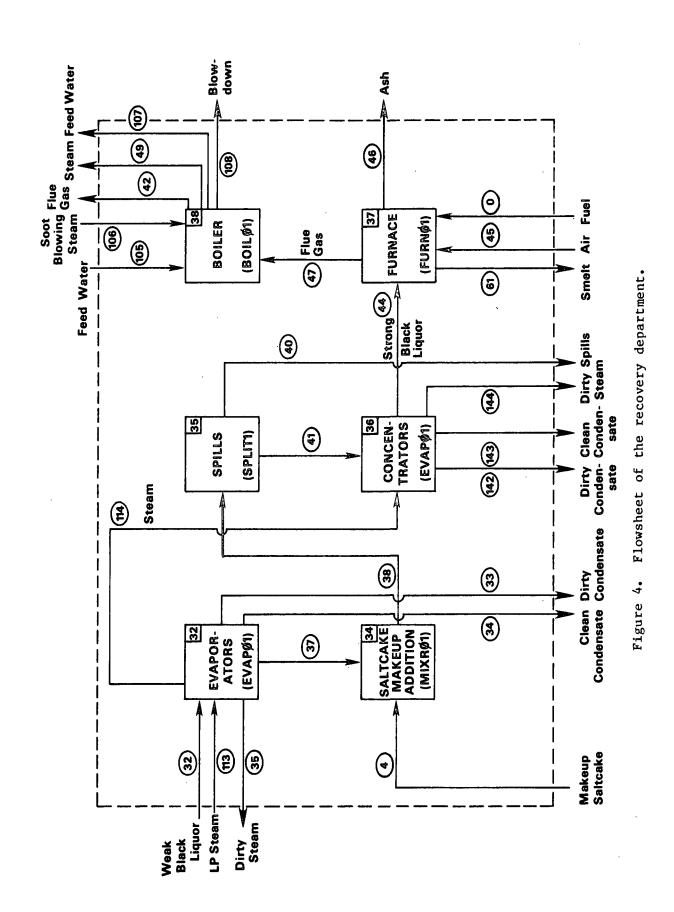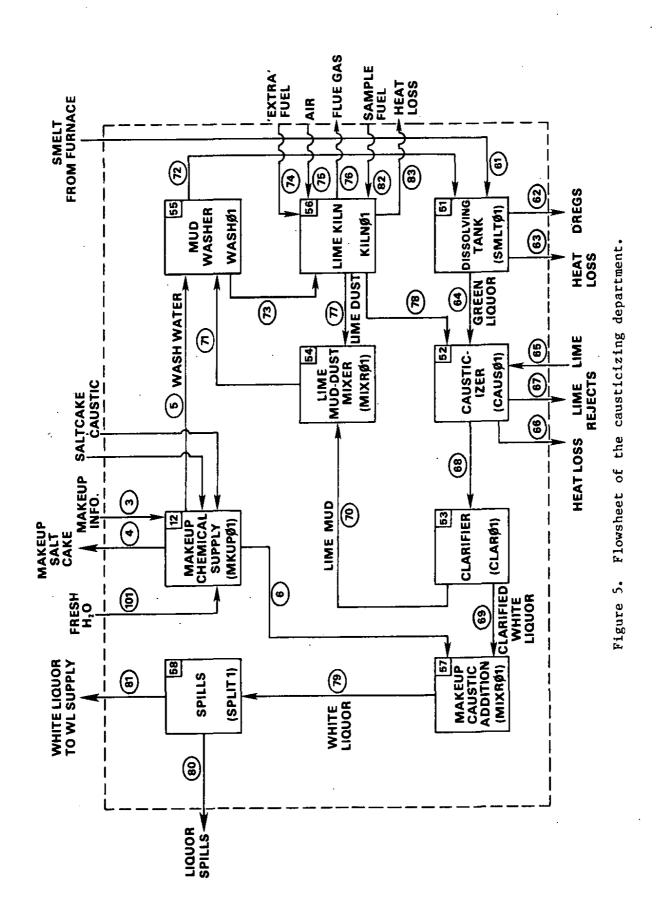Figure 2. General flowsheet of the mill simulated, showing interconnections between departments.
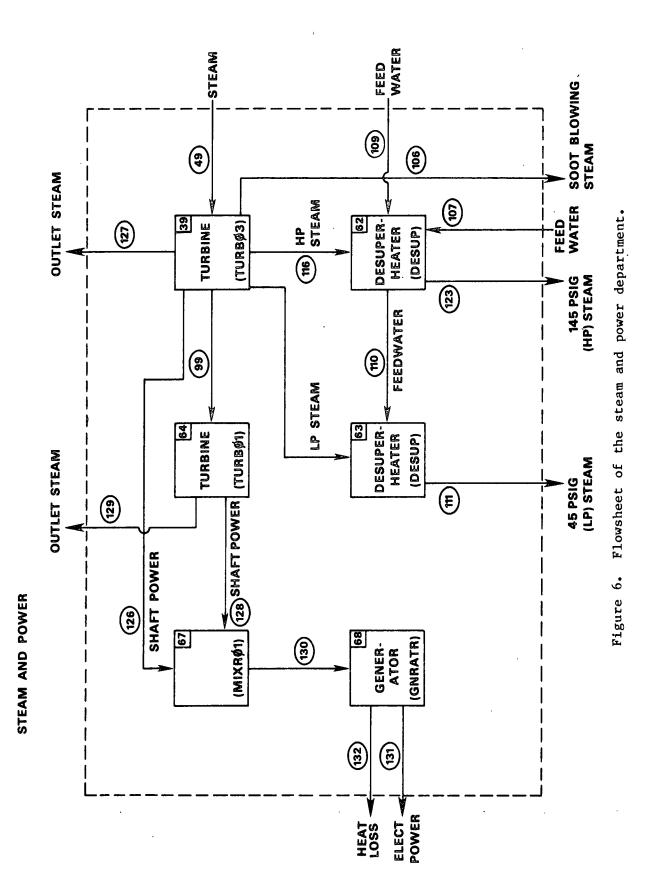
Figure 3. Flowsheet of the pulping department.

Figure 4. Flowsheet of the recovery department.

Figure 5. Flowsheet of the causticizing department.

Figure 6. Flowsheet of the steam and power department.

Figure 7. Effects on wood cost. Basis: 20 tons bleached pulp.

Figure 8. Effects on steam generated (lb). Basis: 20 tons bleached pulp.

Figure 9. Effects on power credit. Basis: 20 tons bleached pulp.
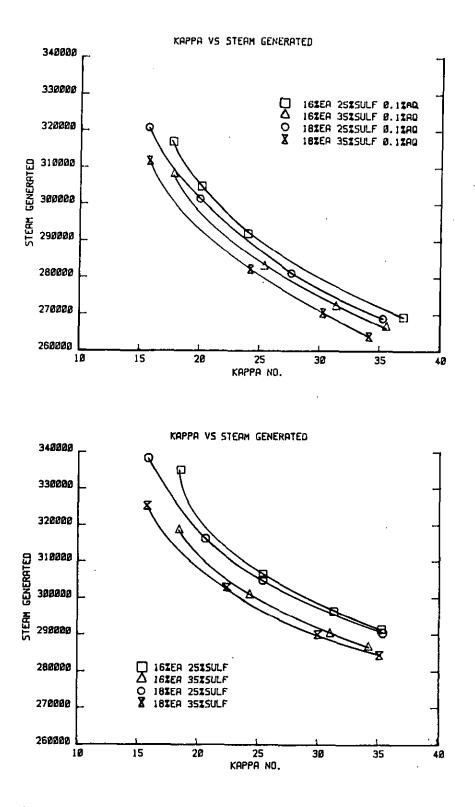
Figure 10.   Effects on revenue.   Basis: 20 tons bleached pulp.

KAPPA VS VISCOSITY

KAPPA VS VISCOSITY
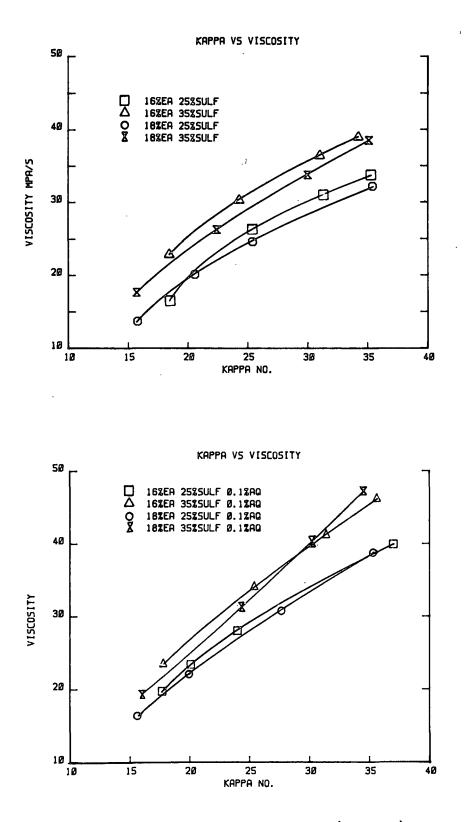
Figure 11.   Effects on pulp viscosity (mPa • s).

to satisfy the sulfate reduction endotherm. Decreasing the effective alkali charge may be expected to decrease steam generation by increasing pulp yield and thereby decreasing the flow of organic material to the furnace. However, this effect is small compared to the combined effects of increased water flow to the furnace at constant strong black liquor solids concentration and increased sulfate reduction. AQ addition decreases steam generation by increasing yield.

Under the assumptions of the simulation, the pulp mill is a net producer of power. The effects of the pulping variables on the associated credit closely parallel the effects on steam generation rate, as illustrated in Figure 9.

Two obvious beneficial effects of decreasing brownstock kappa number are decreased costs for bleaching chemicals and for effluent treatment. Both the requirement for bleaching chemicals in the first two stages and the production of BOD are nearly proportional to the kappa number of the unbleached pulp. The bleaching chemical savings are readily estimated by assuming a direct proportionality, and also assuming no change in the chlorine dioxide requirements in the latter stages of the bleach sequence. The value of reduced effluent loading is more difficult to estimate. For a mill with adequate secondary treatment facilities it would amount to the variable cost of BOD removal and would be modest; for a mill with overloaded secondary treatment contemplating expansion it would be increased by the amortized capital cost of expensive new treatment facilities which would otherwise be required and might be quite high. In the present study the cost of removing 1 lb of BOD was assumed to be $0.29, a figure believed to correspond to the latter situation.

The effect of the variables studied on overall mill profitability was estimated by assuming unit costs for chemicals, energy and product. These were

used to calculate net revenue for each condition simulated. The unit costs
assumed are collected in Table 3, and the results of the net revenue calcula-
tions are shown in Figure 10. For all conditions, net revenue is predicted to
be highest when the brownstock kappa number is in the neighborhood of 20. At a
given kappa number, it can be increased by increasing sulfidity or decreasing
effective alkali charge and is lower when AQ is used.

Table 3. Assumed unit costs.

BLEACHED SLUSH PULP	375 $/T
SOFTWOOD	72
Na_2SO_4	55
NaOH	171
LIME	7
Cl_2	157
ClO_2	802
FUEL OIL	171
STEAM (70 psi)	6
ANTHRAQUINONE	3600
ELECTRICAL ENERGY	1.7¢/kw·h

The calculations that resulted in the data of Figure 10 were made
without consideration of pulp quality. Figure 11 shows the predicted effects of
the variable changes on pulp viscosity. Depending on how low a viscosity is
considered acceptable, the degree to which maximum revenue operation can be
approached may be limited by the effect of the indicated operating condition
changes on viscosity. At a given kappa number, viscosity is increased by
increasing sulfidity or adding anthraquinone. Under some conditions it is also
increased by reducing effective alkali charge.

On the basis of the analysis described above, several interesting cases
were chosen for more detailed study. These were designated as the Base Case,
Case 1 and Case 2, and may be described as follows:

Base Case - a typical set of operating conditions for making

bleachable grade pulp from southern pine; the un-

bleached kappa number target was assumed to be 30.

Case 1 - conditions chosen to give near-maximum revenue within

the range studied; low effective alkali and high sulfidity

are used to pulp to kappa number 20. No AQ added.

Case 2 - same as case 1, except 0.1% AQ added.

Table 4 compares the 3 cases with respect to some important variables.

Table 4. Case comparison.

CASE	BASE CASE	1	2
EA, %	16	16	16
AQ, %	0	0	0.1
SULFIDITY, %	25	35	35
DIG. TEMP., °F	343.6	350.1	343.3
KAPPA NO.	30	20	20
YIELD, %	46.2	44.2	45.3
VISCOSITY, mPa·s	30.0	24.9	26.7
ORGANICS TO RECOVERY, T/HR	23.9	25.4	24.3
STEAM GENERATED, T/HR	149.1	157.0	150.6
STEAM TO EVAPS, T/HR (EV + CON)	27.6	27.5	27.6
PULP PRODUCED, T/HR	20	20	20

As shown in Table 5, lowering the unbleached kappa number from 30 to 20 without using AQ (Case 1 vs. Base Case) increases pulping costs slightly. The increase in wood cost is small in spite of a substantial difference in the yield of unbleached pulp. Fully bleached yield is about the same in the two cases because of the greater shrinkage of the higher kappa number pulp during bleaching. The requirement for makeup chemical is reduced by virtue of the reduced capacity of low kappa pulp for sorption of sodium. Adding AQ causes wood cost to drop below that of the Base Case, but the saving is more than offset by the cost of the AQ.

Table 5. Pulping costs.

$/HR

CASE	BASE	1	2
EA/AQ/S	16/0/25	16/0/35	16/0.1/35
KAPPA NO.	30	20	20
WOOD	3322	3380	3290
MAKEUP	44	31	31
AQ	0	0	165
	3366	3411	3486

Case 1 enjoys slightly lower energy and recovery costs than the base case, as shown in Table 6, principally because of its higher sulfidity. At the same effective alkali charge there is less sodium hydroxide and therefore a smaller load on the causticizing system, which results in a slightly smaller kiln fuel requirement. The savings are increased by adding AQ because of the reduction in wood flow to the digester and the consequent reduction in the amount of alkali at fixed alkali charge.

Table 6. Energy and recovery costs.

$/HR

CASE	BASE	1	2
EA/AQ/S	16/0/25	16/0/35	16/0.1/35
KAPPA NO.	30	20	20
KILN FUEL	212	209	202
LIME	7	7	6
	219	216	208

The largest economic impact of unbleached kappa number reduction is felt in the bleach plant, as illustrated by the figures in Table 7. The requirements for chlorine and caustic in the first two bleaching stages are

reduced approximately in proportion to the kappa number reduction. The amount of chlorine dioxide needed for final bleaching is assumed to be unaffected by unbleached kappa number.

Table 7. Bleaching costs, $/hr.

CASE	BASE	1	2
EA/AQ/S	16/0/25	16/0/35	16/0.1/35
KAPPA NO.	30	20	20
Cl_2	195	118	118
NaOH	117	75	75
ClO_2	312	312	312
	624	505	505

Total credits are slightly increased by decreasing brownstock kappa number (Table 8). There is an increase in power credit because more steam is generated by burning more organic material in the recovery furnace. The steam credit decreases because more steam is needed to heat the digester contents to a higher cooking temperature. An environmental credit is given to the low-lignin cases to reflect the decreased cost for treatment of the smaller amount of BOD discharged from the bleach plant.

Table 8. Credits, $/hr.

CASE	BASE	1	2
EA/AQ/S	16/0/25	16/0/35	16/0.1/35
KAPPA NO.	30	20	20
PULP	7500	7500	7500
POWER	275	288	277
STEAM	239	236	218
EFFLUENT SAVINGS	0	43	43
	8014	8067	8038

When total costs and credits are viewed together, as in Table 9, it becomes apparent that pulping to 20 kappa number results in higher net operating revenue than pulping to 30 kappa number. It is not economical to use AQ to accomplish this, unless the increased viscosity obtained with AQ can be given a substantial economic value. The calculated profit advantage of Case 1 over the base case amounts to $6.50/o.d. ton of bleached pulp. This can be attributed mainly to savings in bleaching chemical and effluent treatment costs.

Table 9. Summary, $/hr.

CASE	BASE	1	2
EA/AQ/S	16/0/25	16/0/35	16/0.1/35
KAPPA NO.	30	20	20
PULPING	3366	3411	3486
BLEACHING	624	505	505
RECOVERY	219	216	208
TOTAL COSTS	4209	4132	4199
PULP	7500	7500	7500
POWER	275	288	277
STEAM	239	236	218
EFFLUENT SAVINGS	0	43	43
TOTAL CREDITS	8014	8067	8038
NET REVENUE	3805	3935	3839
NET REVENUE, $/T	190.25	196.75	191.95

The above analysis assumes that no equipment would be required to shift to low-lignin pulping. To check the validity of this assumption, equipment capacities were estimated from appropriate throughput rates for both test cases. These are shown in Table 10, as ratios to the base case capacities. The largest predicted change is a 5% increase in recovery boiler steam generation for Case I.

Table 10. Equipment capacities relative to the BASE CASE.

	BASE CASE T/HR	CAPACITY RELATIVE TO BASE CASE	
		1	2
WOOD HANDLING	46	1.02	1.00
BROWNSTOCK WASHERS	231	1.01	1.00
BLACK LIQUOR OPERATIONS	209	1.02	1.01
RECOVERY BOILER	149	1.05	1.01
WHITE LIQUOR CLARIFIER	133	1.02	1.01
LIME KILN	9	0.98	0.95

A further assumption is that operation at 35% sulfidity is not precluded by considerations such as recovery boiler corrosion or emissions. It seems likely that this is the case except where boiler operating pressures are high or where the liquor is also heavily contaminated by such impurities as potassium and chloride. Under these conditions, composite boiler tubes would be required.

It should be noted that Scandinavian mills typically operate at sulfidities of 35% or higher. It is also notable that they maintain high kappa number targets even under these conditions. The reasons for this are not entirely clear, but they probably arise from a competitive advantage enjoyed by market pulps possessing very high viscosity. In an integrated mill, or a market pulp mill selling on strength specifications, such high viscosities are of little value.

SULFITE-ANTHRAQUINONE PULPING

A significant part of the current activity on Project 3474 deals with fundamental studies of the sulfite-anthraquinone (SAQ) process, with the objective

of developing a low-lignin version of it. Such a process would be capable of pulping to very low kappa numbers at high yield and strength levels and would produce a readily bleachable pulp. SAQ pulping in its present form is highly selective, producing good yields of strong, easily bleachable pulp, but it cannot be used to pulp to low lignin content (kappa numbers of 25 or less). Below a kappa number of about 40 it slows down markedly and loses selectivity. This is illustrated by Fig. 1 and 2 of the attached reprint.[3] Varying the relative concentrations of Na_2SO_3, Na_2CO_3 and NaOH in the pulping liquor affords some degree of control over rate and selectivity (Fig. 3-6 of the reprint) but this is not sufficient to allow selective pulping to low kappa numbers at a reasonable rate.

The rate and selectivity of a pulping process are determined by either or both of two kinds of fundamental rate phenomena, depending on the conditions. These are the rates of diffusion of pulping chemicals and reaction products through the chip and the rates of the various chemical reactions occurring within the chip. If it is assumed for the moment that limitations associated with diffusion rates can be rendered unimportant by reducing chip thickness, the rates of the chemical reactions will control the rate of pulping and their relative rates will control the selectivity of pulping. If the rates of the individual classes of reactions (delignification, carbohydrate dissolution and cellulose chain cleavage) have composition or temperature dependencies that differ from one another (as seems likely), knowing their rate laws would suggest ways in which the selectivity of the process and its ability to pulp to low kappa numbers can be improved. For this reason, a major objective of our recent and current work is to separately determine rate laws for delignification, carbohydrate dissolution and cellulose chain cleavage.

EXPERIMENTS

Four sets of experiments have been performed, all with southern pine wafers or shavings as raw material. In the first, a liquor-to-wood ratio of 20:1 was used to minimize the degree to which consumption of pulping chemicals changed their concentration in the bulk liquor during the cook. This makes it easier to analyze the data and gives a rate expression which is expected to be equally applicable to low liquor-to-wood ratio cooks, an assumption which will be verified in confirmatory experiments. Runs were carried out under varied conditions of liquor alkalinity, sulfite concentration and AQ concentration. Kappa number, yield and viscosity were measured at various times, beginning when the digester had been at the maximum cooking temperature for 30 minutes. These results were used to derive the following preliminary model:

$$-\frac{dL}{dt} = 0.416 \cdot c_{OH^-}^{0.038} \cdot c_{AQ}^{0.059} \cdot c_{S}^{0.127}$$

for $t < 30$ min at 180°C, and

$$-\frac{dL}{dt} = 2.15 \cdot 10^{-3} \cdot c_{OH^-}^{0.18} \cdot c_{AQ}^{0.121} \cdot c_{S}^{1.00} \cdot (L - 1)$$

for $t > 30$ min at 180°C, where

L = lignin yield, g lignin/100 g wood

c_{OH^-} = Concentration of hydroxide ion inferred from cold liquor pH

c_{AQ} = Initial AQ concentration g/L liquor

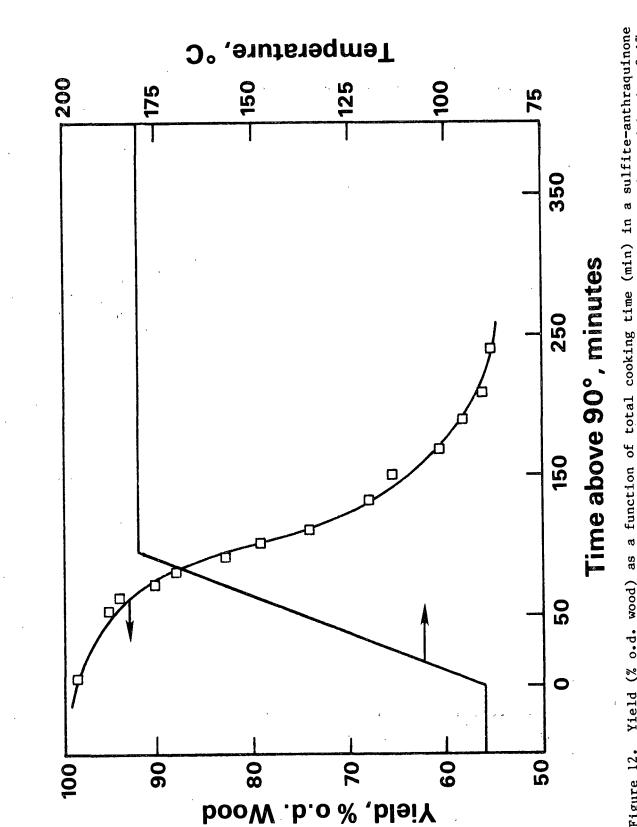c_{S} = Total concentration of Na_2SO_3 and $NaHSO_3$, g Na_2O/L liquor
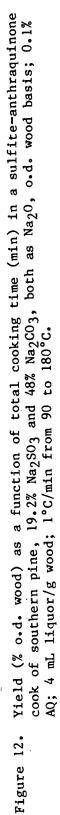
t = time in minutes

This model was used to construct a MAPPS simulation of SAQ pulping. The simulator has been used to make some initial estimates of the feasibility of SAQ pulping at high liquor-to-wood ratio on a commercial scale.

Analysis of the data from these experiments, which spanned the latter part of the bulk delignification phase and the first part of residual delignification, led to the conclusion that the variables investigated were affecting the selectivity of the latter stages of pulping through their influence on the initial stage. This, together with the fact that the preliminary model described above provided an inadequate picture of the early phase of pulping, prompted experiments aimed at understanding the influence of pulping variables during the first part of the cook. In addition, the need for more detailed information was recognized at this point, and it was decided to directly determine the lignin content and the carbohydrate composition of the partially cooked chips.

In the second set of experiments, the sequence of events during the early part of the cook was characterized by determining, in normal, low liquor-to-wood ratio cooks, the composition of the chips and liquor as a function of time from the point at which the temperature rise of the digester contents was begun. This provided a set of reference data for checking the applicability of candidate models derived from high liquor-to-wood ratio cooks, and guiding the choice of conditions to be used in those cooks. Figures 12 through 18 exemplify the data yielded by these experiments.

The third set of experiments was conducted at a liquor-to-wood ratio of 40:1 and was designed to elucidate the effects of sodium sulfite concentration, AQ concentration and pH on the rates of removal of individual wood components (lignin, extractives, glucomannan, arabinoxylan and cellulose) during the very

Figure 12. Yield (% o.d. wood) as a function of total cooking time (min) in a sulfite-anthraquinone cook of southern pine, 19.2% Na_2SO_3 and 48% Na_2CO_3, both as Na_2O, o.d. wood basis; 0.1% AQ; 4 mL liquor/g wood; 1°C/min from 90 to 180°C.

Figure 13. Lignin yield (% o.d. wood) vs. total cooking time (min) in a sulfite-anthraquinone cook of southern pine. Conditions as in Fig. 12.

Figure 14.   Arabinoxylan yield (% o.d. wood) vs. total cooking time (min) in a sulfite-anthraquinone cook of southern pine. Conditions as in Fig. 12.

Figure 15. Galactoglucomannan yield (% o.d. wood) vs. total cooking time (min) in a sulfite-anthraquinone cook of southern pine. Conditions as in Fig. 12.

Figure 16. Cellulose yield (% o.d. wood) vs. total cooking time (min) in a sulfite-anthraquinone cook of southern pine. Conditions as in Fig. 12.

Figure 17. Pulp viscosities (mPa · s) vs. total cooking time (min) in a sulfite-anthraquinone cook of southern pine. Conditions as in Fig. 12.

Figure 18. Na2SO3 concentration (g/L) in spent liquor vs. total cooking time (min) in a sulfite-anthraquione cook of southern pine. Conditions as in Fig. 12.

early part of the cook (initial or heat-up phase). Figures 19-21 are typical of

the data obtained, and show that the initial rate of delignification depends on

both concentrations.

The activation energy of the delignification reaction was the subject

of the fourth set of experiments, conducted by A. Eagle, a special student. They

included preliminary determinations of the sensitivity of the rate of the process
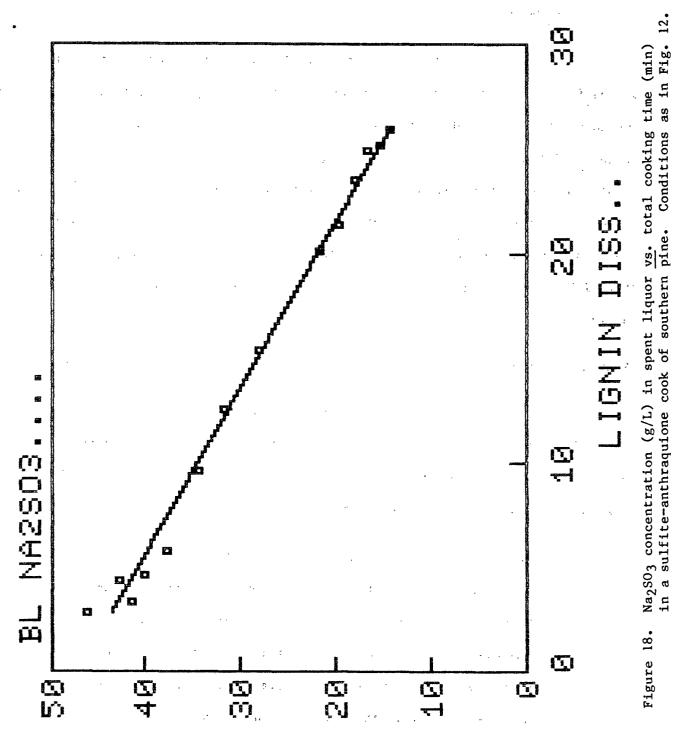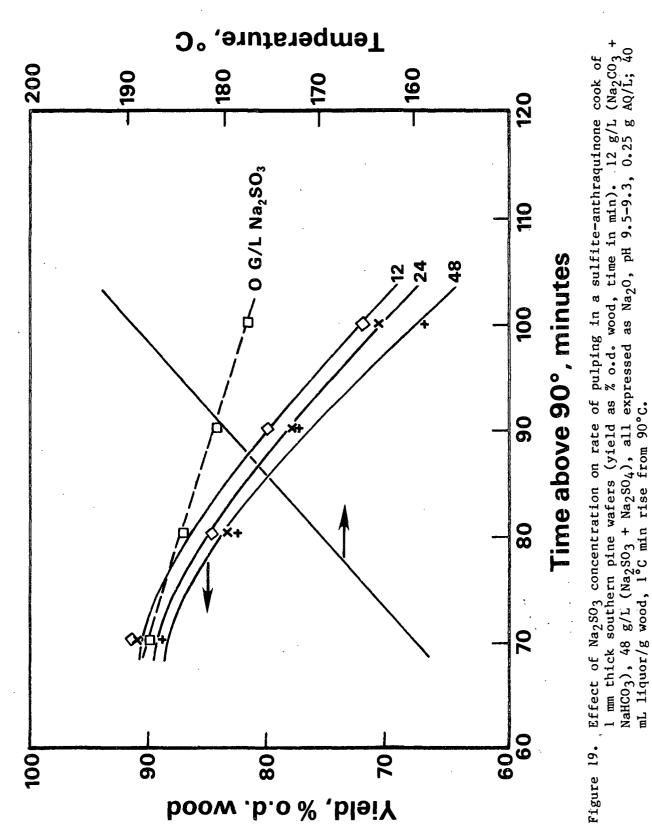
to chip thickness (Fig. 22) and AQ charge (Fig. 23). In accordance with the

results of these preliminary runs, subsequent work was done using thin shavings

instead of chips, with an AQ charge of 1% based on the o.d. weight of the wood.

The result of the activation energy determination was 35,250 cal., a value some-

what higher than the generally accepted value of about 32,000 cal. for kraft

pulping.

ANALYSIS OF DATA AND MODELLING

The experiments described above have yielded a substantial body of

data. It will form the basis of a kinetic model of the process comprising rate

laws for delignification, carbohydrate degradation and cellulose chain cleavage.

This analysis is now in progress according to the following plan:

1. Review literature on sulfite pulping kinetics and

    kinetics of wood sulfonation in chemimechanical pulping.

2. Graphically examine the data and list its major features.

3. Postulate various plausible sets of important reaction

    steps for removal of each wood component. For lignin for

    example, one such set might turn out to be

    $$L + AQ + SO_3^= \longrightarrow L\text{-}SO_3^= + AQ$$

    $$L\text{-}SO_3^= \text{ (solid)} \longrightarrow L\text{-}SO_3 \text{ (dissolved)}$$

Figure 19. Effect of Na_2SO_3 concentration on rate of pulping in a sulfite-anthraquinone cook of 1 mm thick southern pine wafers (yield as % o.d. wood, time in min). 12 g/L (Na_2CO_3 + $NaHCO_3$), 48 g/L (Na_2SO_3 + Na_2SO_4), all expressed as Na_2O, pH 9.5-9.3, 0.25 g AQ/L; 40 mL liquor/g wood, 1°C min rise from 90°C.

Figure 20. Effect of Na2SO3 concentration on delignification rate in a sulfite-
anthraquinone cook of 1 mm thick southern pine wafers. (Lignin
yield 25% o.d. wood, time in min.) Conditions as in Fig. 19.

Figure 21.   Effect of AQ concentration on delignification rate in a sulfite-anthraquinone cook of 1 mm thick southern pine wafers (lignin yield as % o.d. wood, time in min). Conditions as in Fig. 19, except initial Na_2SO_3 concentration constant at 48 g/L and AQ concentration varied.

Effect of Chip Thickness on Hypo No. of Pulp
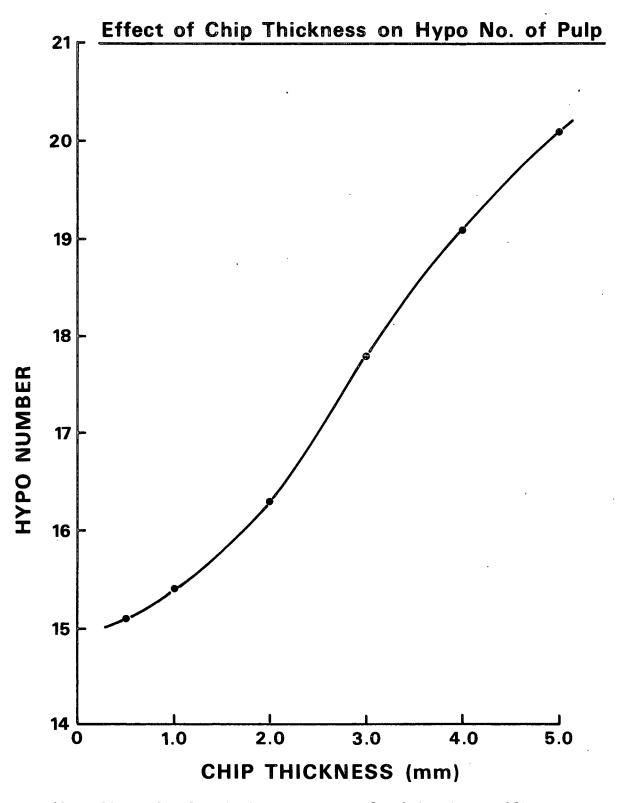

Figure 22. Effect of wafer thickness on rate of pulping in a sulfite-
anthraquinone cook of southern pine. 48 g/L Na_2SO_3, and
12 g/L Na_2CO_3, both as Na_2O, pH 10.0-9.8 0.5 g AQ/L; 20 mL
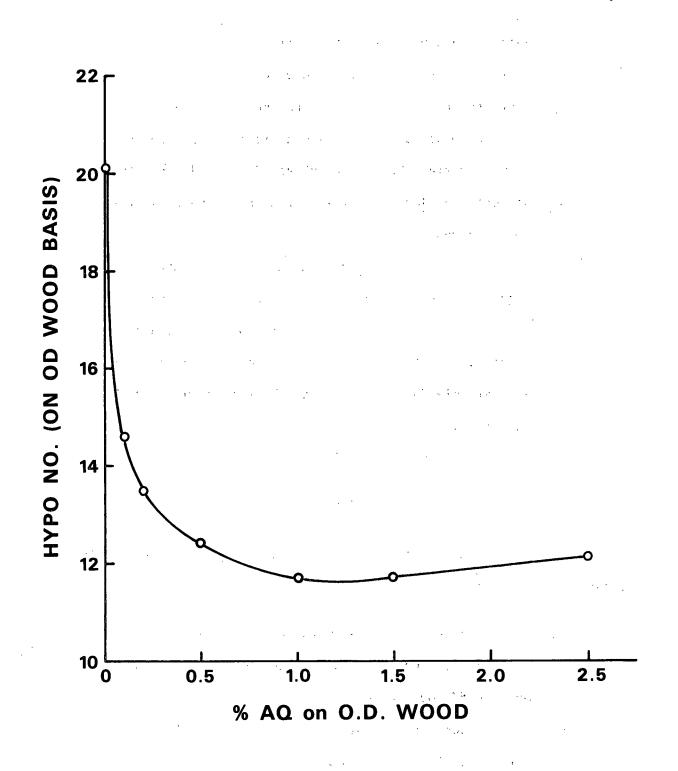liquor/g wood, 2°C min from 90 to 177°C.

Figure 23.   Effect of AQ concentration on rate of pulping in a sulfite-
anthraquinone cook of southern pine shavings. Conditions as
in Fig. 22.

4. Assign rate constants, activation energies and reaction orders to each step of each reaction scheme; numerically integrate, manually adjusting parameters to see if the predicted behavior can be made to resemble the observed behavior during the initial phase. If not, discard the model.

5. Use nonlinear least squares to fit the parameters of the remaining candidate models.

6. Apply the model discrimination-parameter estimation technique of Hill et al. (x) to arrive at the final model for the initial phase (with some further experiments).

7. Attempt to fit the initial phase model to the bulk phase data; if this fails, repeat the above procedure for the bulk phase.

8. Extend to include the residual phase.

CONCLUSIONS

1. In a typical kraft mill pulping southern pine, lowering the unbleached kappa number target from 30 to 20 would

- increase operating revenue by approximately $7/ton
- require the recovery boilers to burn more black liquor, generating 5% more steam
- decrease brownstock viscosity by 5 mPa·s (5 cp.)
- require operation at 35% sulfidity.

2. Adding AQ in conjunction with the kappa number decrease is unlikely to be profitable. It would, however, result in increased brownstock viscosity and reduced steam consumption by eliminating the need to increase the digester temperature.

3. Currently available kinetic data for the SAQ pulping process, when supplemented by the results of a limited number of additional experiments, is expected to form the basis of a fairly complete kinetic description of the process.

PLANS

The following activities are planned:

1. Complete the derivation of a kinetic model for SAQ pulping according to the plan outlined above.

2. Continue to work toward a mill trial of low lignin kraft pulping at the mill already identified. The next step contemplated is to propose, on a contract research basis, a pulping and bleaching study of their wood raw material. This will allow us to tune our existing MAPPS simulation to their conditions and to perform additional simulations and economic analyses in ranges of particular interest.

3. Tuning our model to a new wood supply would be greatly facilitated if the present multiparameter polynomial model could be replaced with a theoretically based model with fewer parameters. Efforts to do this will continue.

4. Establish the catalytic activity of recycled SAQ pulping liquor.

5. As opportunities arise, seek more information on the relationship between viscosity and strength for SAQ pulps.

ACKNOWLEDGMENTS

REFERENCES

1. Project 3474-1 Interim Report to the Program Committee, Sept. 24, 1980.

2. Saffran, K. E. The development of a simulation-optimization program for the pulp and paper industry. Doctoral Dissertation, The Institute of Paper Chemistry, 1984.

3. McDonough, T. J., Van Drunen, V. J., and Paulson, T. W. Sulfite-anthraquione pulping of southern pine for bleachable grades. 71st Annual Meeting of the Technical Section, CPPA, Preprints, p. A161. Montreal, 1985

THE INSTITUTE OF PAPER CHEMISTRY

Thomas J. McDonough
Group Leader, Pulping/Bleaching
Pulping Sciences
Chemical Sciences Division

APPENDIX

SULFITE-ANTHRAQUINONE PULPING OF SOUTHERN PINE
FOR BLEACHABLE GRADES

T. J. MCDONOUGH, V. J. VAN DRUNEN, AND
T. W. PAULSON

The Institute of Paper Chemistry
P.O. Box 1039
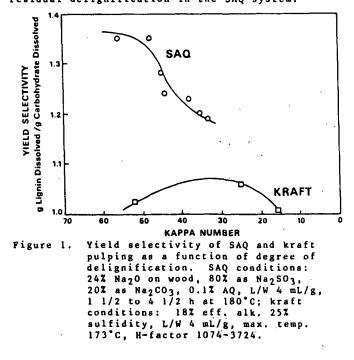Appleton, WI 54912

ABSTRACT

Sulfite-anthraquinone (SAQ) pulping was in-
vestigated as a process for the manufacture of
bleachable pulp from southern pine. The effects
of the relative proportions of Na_2SO_3, Na_2CO_3,
and NaOH on rate, selectivity and pulp composi-
tion were systematically studied. Additional
pulping experiments at constant chemical concen-
tration demonstrated that the rates of removal
of both lignin and carbohydrates increase with
increasing liquor alkalinity. By contrast, pulp
viscosity retention passes through a maximum at
intermediate alkalinities. Compared to kraft,
the SAQ pulps had 5-8% higher carbohydrate yield
(o.d. wood basis), were more easily bleachable,
lost slightly more yield upon bleaching and were
at least as strong. In separate experiments,
the SAQ process was shown to be capable of
pulping to very low kappa numbers while
retaining high viscosity and acceptable yield.
This can be achieved by employing high liquor-
to-wood ratio and correspondingly high chemical
charge. Current kinetic studies are expected to
identify other routes to the same end.

KEYWORDS: Sulphite pulping, alkaline pulping,
anthraquinone, bleached pulps,
mechanical properties, selectivity

INTRODUCTION

Since its introduction in the late 1970's,
the potential benefits of sulfite-anthraquinone
(SAQ) pulping have been well established (1-6).
Relative to kraft and kraft-AQ pulping, SAQ
pulping under mildly alkaline conditions
(terminal pH about 9) possesses advantages in
terms of yield, pulp beatability, pulp bleach-
ability, elimination of causticizing, and re-
duced potential for odor emissions. It also has
the disadvantages of a slower pulping rate, po-
tential for increased recovery boiler corrosion,
and the need for chemical conversion and liquor
regeneration systems. The strength properties
of the pulp are similar to those of kraft,
although it has been found, at least in some
cases, to have slightly lower tear strength.

Compared to the kraft process, SAQ pulping
under mildly alkaline conditions is very selec-
tive, giving both a higher yield and a higher
viscosity at a given lignin content or kappa
number. This would make it attractive for the
production of bleachable grades of low kappa
number and correspondingly low bleaching chemi-
cal requirements were it not for the fact that
the process slows down and loses selectivity at
a kappa number somewhat above the usual 30-35
level. This is illustrated in Fig. 1 by data
from laboratory cooks of southern pine. The
ordinate, yield selectivity, is defined as the
mass of lignin dissolved since the beginning of
the cook per unit mass of carbohydrate dis-
solved. It is a quantity that should obviously
be maintained at as high a value as possible.
When plotted against kappa number it passes
through a maximum at the point of transition
from bulk delignification to the relatively
slower residual delignification. Beyond this
maximum, selectivity suffers because carbo-
hydrate dissolution undergoes no corresponding
rate decrease and continues unabated. It is
apparent that, at kappa numbers above 50, SAQ
pulping displays a pronounced selectivity advan-
tage over kraft pulping. It can also be seen
that as delignification is continued this advan-
tage diminshes, owing to the earlier onset of
residual delignification in the SAQ system.

Figure 1.   Yield selectivity of SAQ and kraft
pulping as a function of degree of
delignification. SAQ conditions:
24% Na_2O on wood, 80% as Na_2SO_3,
20% as Na_2CO_3, 0.1% AQ, L/W 4 mL/g,
1 1/2 to 4 1/2 h at 180°C; kraft
conditions: 18% eff. alk. 25%
sulfidity, L/W 4 mL/g, max. temp.
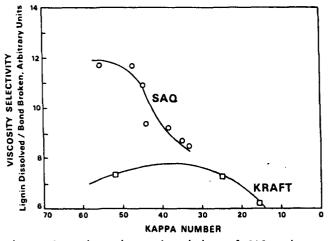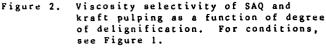173°C, H-factor 1074-3724.

Another factor which may limit the degree
of delignification that can practically be
achieved in the pulping step is loss of pulp
strength, which is associated with the cleavage
of glycosidic bonds in cellulose. If allowed to
proceed far enough, the resulting reduction in

cellulose chain length manifests itself as a loss in pulp strength. Pulp viscosity is a good indicator of the extent of chain breakage and can be used for an approximate calculation of the number of bonds broken. Figure 2 shows that cellulose chain shortening exhibits the same type of dependence on degree of delignification as dissolution of cellulose (a different process) and other carbohydrates. Again the pronounced advantage of SAQ pulping diminishes as delignification is extended below a kappa number of about 50.

Figure 2. Viscosity selectivity of SAQ and kraft pulping as a function of degree of delignification. For conditions, see Figure 1.

If the reason for this behavior can be determined, it may become possible to modify or redesign the SAQ process to make it a very attractive alternative to kraft for the production of bleached grades. We are currently investigating this possibility by studying the kinetics of SAQ pulping. In the meantime, the good bleachability of the pulp and the high selectivity of the process at moderate degrees of delignification make it a candidate for the production of bleachable grades in its present form. Accordingly, we have conducted an experimental study of its applicability to southern pine. We have also done some experiments to demonstrate that, surprisingly, SAQ processes are capable of selectively pulping to very low kappa numbers.

EFFECTS OF LIQUOR COMPOSITION

The effects of varying the initial liquor composition, although they have been the subject of considerable research, are not well delineated in the literature. Data are available on the effect of varying the sulfite content at constant total chemical charge (1,5,6,9) but not on the effect of varying the ratio of Na_2CO_3 to NaOH. Table I contains the results of a series

of experiments systematically designed to define both types of effects. Pulping conditions were maintained constant and were chosen to characterize the period preceding the transition to residual delignification. The wood pulped was in the form of thin (1 mm) wafers to minimize mass transfer effects. In all cases the total chemical charge was 24% Na_2O, based on o.d. wood weight. Liquor composition was varied over the ranges 60 to 100% Na_2SO_3, 0 to 40% Na_2CO_3, and 0 to 40% NaOH, all expressed as Na_2O. The compositions were chosen to form a simplex lattice design of the special cubic type described by Gorman and Hinman (8), and all cooks but one were duplicated to improve precision. Regression analysis of the data gave equations that were used to plot the contour diagrams shown in Fig. 3 to 5.

Chemical Charges, % o.d. wood, as Na2O			Total Yield, % o.d. wood	Kappa Number[a]	Viscosity,[b] mPa·s	pH at 25°C	
Na2SO3	Na2CO3	NaOH				Initial	Final
24.0	0	0	68.7	93.0	28.7	10.3	8.7
			68.7	97.8	27.0	10.3	8.5
14.4	9.6	0	57.7	67.8	74.3	11.7	9.4
			56.7	71.0	80.3	11.8	9.4
14.4	0	9.6	48.5	30.4	23.9	13.5	12.3
			47.6	27.4	28.7	13.4	12.3
19.2	4.8	0	57.6	52.1	61.8	11.8	9.4
			56.9	55.0	71.2	11.6	9.3
19.2	0	4.8	54.0	52.2	57.8	13.4	10.5
			54.3	52.8	72.7	13.4	10.1
14.4	4.8	4.8	55.9	76.5	46.8	13.4	10.3
			55.6	71.4	59.0	13.3	10.2
17.6	3.2	3.2	54.8	58.8	51.4	13.3	10.0
			54.4	57.0	76.3	13.2	9.8
20.8	1.6	1.6	56.5	49.1	59.4	13.1	9.6
			56.2	52.0	61.8	13.0	9.5
16.0	6.4	1.6	55.6	61.7	60.2	13.0	9.5
16.0	1.6	6.4	52.9	55.8	44.9	13.4	10.7
			52.6	52.3	53.1	13.4	10.8

[a]The cooked wafers were fiberized in a blender (2 minutes, high speed), screened on a 0.006-inch cut flat screen, and the kappa number determined on the accepts. The percentage rejects was 1% or less in all but one case, where it was 1.6%.
[b]Viscosity was measured after delignification with sodium chlorite in acetic acid for 20 hours at room temperature.
[c]Cooking conditions: 24% total Na2O based on o.d. wood wt.; 0.1% AQ; liquor-to-wood ratio 4.1 mL/g; vacuum preimpregnation; 90 minute linear temperature rise from 90 to 115°C; 3 hours at 175°C.

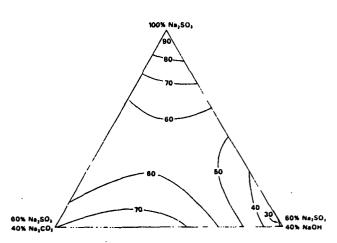Table I. Experimental Sulfite-Anthraquinone Pulping Data: Effects of Liquor Composition[c].

Figure 3. Contours of constant kappa number.

Since pulping conditions were constant, the kappa number attained in liquor of a given

composition is an indicator of the rate of pulp-
ing in that liquor. Thus, compositions giving
equal rates are found on the same contour lines
in Fig. 3, and regions of low kappa number
define liquor compositions that give high rates.
It is apparent that pulping is fastest in NaOH-
rich liquors and slowest in 100% Na_2SO_3, with
Na_2CO_3-rich liquors being intermediate. In
liquors containing 0 to 10% NaOH, a maximum rate
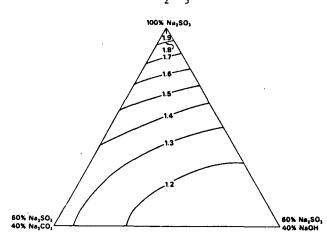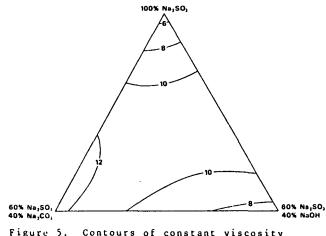is found at about 75% Na_2SO_3.

Figure 4. Contours of constant yield selec-
tivity (g lignin dissolved/g carbo-
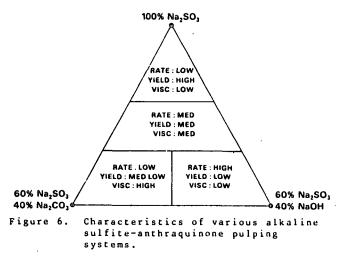hydrate dissolved.

Figure 5. Contours of constant viscosity
selectivity (10^{-4} x g lignin dis-
solved/mole glycosidic bonds broken
in cellulose).

The yields in Table I are not directly
comparable with one another because of the dif-
fering degrees of delignification. Yield selec-
tivity, the mass of lignin dissolved per unit
mass of carbohydrate dissolved, is less depen-
dent on degree of delignification and therefore
is more comparable. Figure 4 shows that yield
selectivity is best in pure sodium sulfite and
poorest in liquors rich in NaOH, with Na_2CO_3-
rich liquors being intermediate but relatively
poor. In liquors containing 75 to 80% Na_2SO_3,
yield was moderately good and insensitive to the
ratio of Na_2CO_3 to NaOH. Note that all of the

liquor compositions of Fig. 4 gave yield selec-
tivities that were better than typical kraft
values (about 1.0).

Viscosity retention is best in Na_2CO_3-rich
liquors, as shown in Fig. 5. Pure Na_2SO_3 gave
the lowest viscosity selectivity, and the
strongly alkaline liquors were intermediate. In
liquors containing about 80% Na_2SO_3, viscosity,
like yield, was moderately high and was insensi-
tive to the ratio of Na_2CO_3 to NaOH. All com-
positions, with the exception of pure or nearly
pure Na_2SO_3, were equal to or better in this
respect than kraft (about 8).

The effects of varying the liquor composi-
tion at constant total Na_2O concentration are
summarized in Fig. 6. A choice must be based on
the best compromise among the 3 factors dis-
cussed above.

Figure 6. Characteristics of various alkaline
sulfite-anthraquinone pulping
systems.

Removal of Individual Wood Components

Further insight into the effects of liquor
composition on the rates of dissolution of the
various wood components is provided by Table II,
which also contains analytical data for a com-
parable kraft pulp and the wood from which the
pulps were made. Under the pulping conditions
used, the liquor containing only sodium sulfite
removed no cellulose, about one third of the
glucomannan, about one quarter of the arabino-
xylan and about two thirds of the lignin. The
residual lignin was heavily sulfonated, con-
taining 4% sulfur (about one sulfonic acid group
for every 3 C_9 units).

Table II. Effect of Liquor Composition on Yields of Pulp Components.

Replacing 20% of the Na_2SO_3 with Na_2CO_3 (Na_2O basis) had no effect on cellulose but nearly doubled the amount of glucomannan removed and reduced the residual lignin content by 50%. The sulfur content of the residual lignin was also decreased, indicating that the added Na_2CO_3 functioned by extracting sulfonated lignin. Replacing an additional 20% of the Na_2SO_3 with Na_2CO_3 caused a slight decrease in the amount of lignin removed and a slight increase in the amounts of carbohydrates removed, including cellulose. A simultaneous increase in residual lignin content and decrease in sulfur content suggests that the main effect of the additional replacement was to reduce the Na_2SO_3 charge below the level required for complete lignin sulfonation.
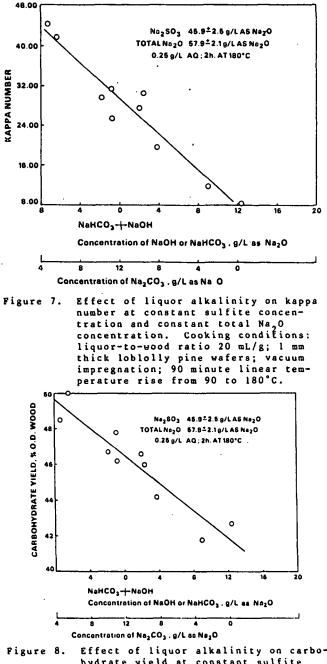
Replacing Na_2SO_3 with NaOH instead of Na_2CO_3 gave more efficient lignin removal but also resulted in the removal of larger amounts of all carbohydrate components.

Isolating the Effects of Alkalinity

To better characterize the effect of liquor alkalinity, a second series of laboratory cooks was done under conditions which resulted in all other variables being maintained approximately constant. These cooks differed from those already described by being conducted at a high liquor-to-wood ratio (and correspondingly high chemical charge). This was done so that the concentrations of chemicals in the liquor would remain nearly constant throughout the cook.

Figures 7-9 show the effect of increasing alkalinity at a fixed concentration of Na_2SO_3 and fixed total Na_2O concentration. In other words, they show the effect of varying the composition of the nonsulfite component of the cooking chemical without varying its amount. It consists of a mixture of Na_2CO_3 with either $NaHCO_3$ or NaOH, depending on whether the liquor pH is below or above the value marking complete conversion of bicarbonate to carbonate ions (about 12). At one end of the range studied it was a mixture of 8 g $NaHCO_3$/L and 4 g Na_2CO_3/L, while at the other end it was 12 g NaOH/L.

The effects on kappa number and yield were observed to be quite nonlinear in liquor pH. Both were insensitive to pH over the range 10-13, but strong pH effects were evident above and below this range. When plotted against alkalinity, both were approximately linear. The rate of pulping increases continuously with liquor alkalinity, as shown by the decreasing kappa numbers of Fig. 7. The rate of carbohydrate dissolution is similarly affected, as is evident from Fig. 8.

Figure 7. Effect of liquor alkalinity on kappa number at constant sulfite concentration and constant total Na_2O concentration. Cooking conditions: liquor-to-wood ratio 20 mL/g; 1 mm thick loblolly pine wafers; vacuum impregnation; 90 minute linear temperature rise from 90 to 180°C.

Figure 8. Effect of liquor alkalinity on carbohydrate yield at constant sulfite concentration and constant total Na_2O concentration.

Unlike delignification and carbohydrate dissolution, cellulose chain cleavage is slowest at intermediate pH values, as shown by the viscosity maximum in Fig. 9. The maximum occurs when the pulping liquor contains a small amount of free sodium hydroxide; larger amounts result in a precipitous drop in viscosity. Liquors containing no free sodium hydroxide but increasing proportions of sodium bicarbonate also give progressively lower viscosity. The latter effect has also been observed by Thompson (10); its mechanism is not known.

These relationships between liquor alkalinity and the rates of delignification, carbohydrate dissolution and cellulose chain cleavage

4

help to explain the effects of liquor composi-
tion on the outcome of the pulping process under
conditions of low liquor-to-wood ratio and chem-
ical charge. When the proportion of nonsulfite
alkali is low, the products of the delignifica-
tion and carbohydrate dissolution reactions
neutralize a sufficiently large fraction of it
to cause a rapid pH drop into the region where
the liquor is effectively buffered by dissolved
lignin, the carbonate-bicarbonate system, or
both. Under these conditions, the alkalinity
prevailing during most of the cook is insen-
sitive to the initial ratio of NaOH to Na_2CO_3.
This is why neither rate nor selectivity is much
affected by the nonsulfite alkali composition
when the Na_2SO_3 charge is in the neighborhood of
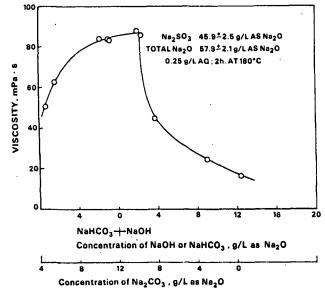80% of the total alkali charged (Fig. 3-6).

Figure 9. Effect of liquor alkalinity on pulp
viscosity at constant sulfite con-
centration and constant total Na_2O
concentration.

As the proportion of Na_2SO_3 is reduced to
about 60% of the total alkali charged, there is
sufficient nonsulfite alkali present for its
composition to have a substantial effect. NaOH-
rich liquors remain strongly alkaline throughout
the cook, while Na_2CO_3-rich liquors quickly be-
come buffered in the 9-10 pH range. Consequent-
ly, kappa number, yield and viscosity decrease
as Na_2CO_3 is replaced by NaOH.

It has been stated that, unlike kraft pulp-
ing, sulfite anthraquinone pulping is acceler-
ated by Na_2CO_3. At first sight, the data in
Fig. 7 seem to bear this out, inasmuch as they
show that kappa number decreases with increasing
Na_2CO_3 concentration in the absence of free
NaOH. However, it should be noted that the
experimental relationships shown in Fig. 7, 8
and 9 were obtained under conditions of constant
total nonsulfite alkali composition and must be

interpreted in this light to avoid erroneous
conclusions. Thus an increase in Na_2CO_3 con-
centration implies a corresponding decrease in
the concentration of $NaHCO_3$ and an increase in
pH. If the pH (and therefore the ratio of
Na_2CO_3 to $NaHCO_3$) is held approximately constant
and the Na_2CO_3 concentration is increased, it is
found that the pulping rate is decreased, not
increased as may be expected (Fig. 10). Na_2CO_3
serves as a buffer, not as an active pulping
chemical.

COMPARISONS WITH THE KRAFT PROCESS

In considering sulfite-anthraquinone pulp-
ing as an alternative to the kraft process, it
is of interest to compare the two with regard to
pulping rate, selectivity, pulp quality and pulp
bleachability.

Selectivity and Rate

Selectivity, as already discussed, is
better in the case of SAQ pulping, but the ad-
vantage diminishes with decreasing kappa number
(Fig. 1 and 2). If pulping is terminated at
a kappa number of 40 or above, SAQ pulping
possesses significant yield and viscosity advan-
tages. This is apparent from the data of Table
III, which were obtained by laboratory pulping
of southern pine chips from two different
sources. The SAQ process gave carbohydrate
yields that were respectively 6 and 8 percentage
points higher. The latter figure represents a
potential for obtaining 18% more pulp from the
same amount of wood, although bleach plant
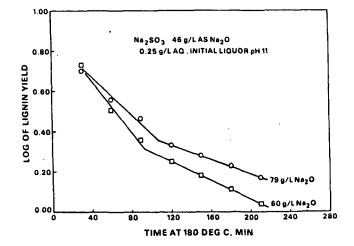losses would reduce this figure somewhat, as
described below.

Figure 10. Effect of total Na_2O concentration
on delignification rates at constant
concentrations of Na_2SO_3 and anthra-
quinone and constant total pH.

Wood Source	1			2		
Process	Kraft	SAQ		Kraft	SAQ	
Cook no.	159	190	167	2	3	4
Chemical charges, as Na2O, % o.d. wood						
Na2SO3	0	19.2	19.2	0	19.2	19.2
Na2CO3	0	4.8	4.8	0	4.8	2.4
NaOH	15	0	0	13.7	0	2.4
Na2S	5	0	0	4.6	0	0
Anthraquinone charge, % o.d. wood	0	0.1	0.1	0	0.1	0.1
Maximum temperature, °C	165	175	180	173	175	175
Time at maximum temperature, min.	121	240	210	88	240	160
Total yield, % o.d. wood	46.7	53.6	51.9	47.7	57.0	57.4
Rejects, % o.d. wood	0.4	2.8	2.2	0.4	2.9	2.7
Kappa No.	38.8	44.3	41.0	35.0	41.7	47.3
Carbohydrate yield, % o.d. wood	44.0	50.0	48.7	45.2	53.4	53.3
Viscosity, mPa·s	37.4	72.1	52.5	31.1	77.5	117
Spent liquor pH	~13	9.3	9.0	~13	9.0	9.4
Brightness	22.5	44.9	36.0	23.8	34.8	32.3

[a] All pulps were prepared in a 50-L digester equipped with external circulation and indirect heating at liquor-to-wood ratios in the range 3.8-4.1.

Table III. Kraft and SAQ Pulping of Southern Pine.

Wood Source	1		2	
Process	Kraft	SAQ	Kraft	SAQ
Cook no.	159	167	11[a]	12[b]
Kappa no.	38.8	41.0	30.8	43.0
Viscosity, mPa·s	37.4	52.5	29.7	77.3
Chlorination[c]				
Total Cl2, %	9.70	9.22	7.07	11.06
Residual Cl2, %	0.53	0.20	0.04	0.19
Extraction				
NaOH, %	4.85	4.61	3.54	5.53
Kappa no.	4.7	4.8	4.5	2.3
Viscosity, mPa·s	28.8	54.3	24.2	57.5
Chlorine dioxide				
ClO2, %	0.8	1.0	1.0	1.0
Residual ClO2, %	0.004	0.13	0.00	0.21
Brightness	79.2	89.3	80.6	90.8
Viscosity, mPa·s		46.3		54.9
Extraction				
NaOH, %	0.5		0.5	
Chlorine dioxide				
ClO2, %	0.2		0.4	
Residual ClO2, %	0.02		0.05	
Brightness	89.8		89.8	
Viscosity, mPa·s	24.9		20.0	

[a] Same pulping conditions as cook 2; see Table III.
[b] Same pulping conditions as cook 3; see Table III.
[c] Includes 15% ClO2 as available Cl2 based on total available Cl2.
[d] All chemical percentages based on o.d. unbleached pulp weight.
[e] Conditions (stage no.; consistency, %; time, min.; temp., °C): 1,3,45,25; 2,10,60,60; 3,6-10,80,70; 4,10,60,60; 5,6-10,180,70.

Table IV. Bleaching of SAQ and Kraft Pulps[d,e].

SAQ pulping also gives very much higher pulp viscosity than kraft pulping, as is also apparent from Table III. On the basis of the available information on the relationship between strength and viscosity for SAQ pulps, it seems likely that it is similar to the corresponding relationship for kraft pulps. If this is true, the implication is that the SAQ pulps can be treated more severely in subsequent processing, for example, by extensive oxygen bleaching, without incurring strength loss by reducing the viscosity below a critical value.

The rate disadvantage of SAQ pulping can be diminished by raising the temperature, but the yield and viscosity advantages are somewhat reduced at the higher temperature. Another way of accelerating the cook is to use NaOH as makeup chemical. The effect shown in Table III is somewhat greater than anticipated on the basis of the results of the experiments on liquor composition effects described above. This may be due to beneficial effects of NaOH on swelling and mass transfer. The earlier experiments were designed to eliminate the influence of mass transfer limitations and were accordingly conducted with wood in the form of thin wafers; the data of Table III were obtained on chips.

Bleachability

SAQ pulp bleachability differs from that of kraft pulp in two important respects: the higher lignin content of the unbleached pulp and the greater ease of bleaching the chlorinated and extracted pulp to high brightness. Thus, previous studies of Canadian and Scandinavian softwoods have shown that although SAQ pulps require higher charges of chlorine and caustic in the first two bleaching stages, they can be fully bleached with chlorine dioxide in only one additional stage. The data of Table IV show that the same is also true of southern pine pulps.

Their high chlorine requirement and exceptionally high viscosity make SAQ pulps natural candidates for oxygen bleaching. Our studies have shown that, like pulps from other species, southern pine SAQ pulps respond normally to oxygen bleaching. For example, the kappa number of pulp from cook 167 (Table III) was reduced from 41 to 20 by oxygen bleaching with 2.5% NaOH to give pulp having a viscosity of 32 mPa.s at a yield of 49.4% based on o.d. wood.

Bleaching Yield

The literature provides little information on the relative yield losses in the bleaching of SAQ and kraft pulps. Ingruber et al. (6) determined shrinkages in the bleaching of pulps made from an eastern Canadian softwood mixture. Their results, expressed as yield reduction (based on unbleached pulp) per unit of kappa number reduction, were 0.216 and 0.167 for SAQ and kraft pulps, respectively. Finnish workers (5,9) concluded that shrinkage was no worse for SAQ than kraft pulps, but they reported high levels for both.

The results of our determinations are presented in Table V. For pulps from both wood sources SAQ pulp suffered a greater yield loss than kraft pulp. Nevertheless, the major part of the unbleached yield advantage of the former remained after bleaching.

Wood Source	1		2	
Process	Kraft	SAQ	Kraft	SAQ
Cook no.	159	167	11	12
Kappa no.	36.8	41.0	30.8	43.0
Unbl. yield, % o.d. wood	46.7	51.9	48.7	57.0
Bleaching yield, % o.d. unbl. pulp	93.57	91.71	93.55	89.03
	93.34	91.86	93.66	89.50
	93.22	92.19	94.21	89.83
Average	93.4 ± 0.5	91.9 ± 0.5	93.8 ± 0.5	89.7 ± 0.5
Yield loss per kappa unit, %	0.170 ± 0.013	0.198 ± 0.012	0.201 ± 0.015	0.240 ± 0.011
Bleached yield, % o.d. wood	43.6	47.7	45.6	51.1

*SAQ pulps bleached in CED sequence, kraft in CEDED; bleaching conditions as in Table IV.

Table V. Bleaching Yield Data*.

Bleached Pulp Strength

Bleached SAQ pulps from southern pine are slightly superior in strength to the corresponding kraft pulps. Data to support this statement are presented in Table VI and Fig. 11 and 12. The SAQ pulps have a higher ultimate tensile strength and a higher tensile strength at a given degree of refining. Equivalently, they require less refining energy to attain a given strength. At a given tensile strength, the tear strengths are the same as the corresponding kraft pulp values.

THE FUTURE - LOW-LIGNIN SAQ PULPS

In spite of the natural tendency for SAQ pulping to slow down and lose selectivity at rather high kappa number levels, we have found that the process is capable of pulping to very low kappa numbers with good selectivity. This can be achieved by using high liquor-to-wood ratios and correspondingly high chemical charges, as illustrated by the data of Table VII. High liquor ratio SAQ pulping may be conducted in either moderately alkaline ($HLS_{10}AQ$) or strongly alkaline ($HLS_{13}AQ$) liquors. (In these designations, the subscript refers to the terminal pH of the pulping liquor.) At the lower pH low kappa numbers can be obtained at very high viscosity levels and carbohydrate yields that are better than the corresponding kraft yields. Operating at the

higher pH level accelerates the process and gives extremely low kappa numbers with acceptable viscosities but at the cost of about 2% yield. Both types of pulp are as strong as or stronger than kraft.
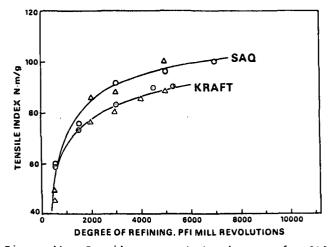

Figure 11. Tensile strength development for SAQ and kraft pulps from two wood sources. Circles and triangles represent data from wood sources 1 and 2, respectively. Open symbols represent SAQ pulp data; filled symbols are for kraft pulps.
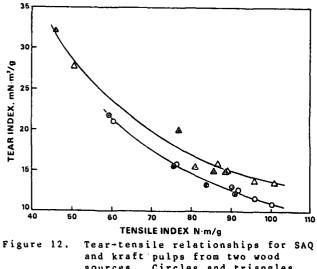
The marked beneficial effect of increasing liquor ratio and chemical charge is characteristic of the SAQ process. The data in the table show that there is no corresponding effect on the selectivity of the kraft or kraft-AQ processes when the liquor ratio and chemical charge is increased.

These results suggest two different possibilities. One is the development of a process based directly on the use of high liquor ratios. It would involve efficient separation of spent liquor from the chips at the end of the cook, followed by fortification and reuse. Although the total charge of pulping chemicals would be very high in such a process, the actual

Wood Source	Process	Cook No.	PFI Revs.	CSF, mL	Density, g/cm³	Burst Index, kPa·m²/g	Tear Index, mN·m²/g	Tensile Index, Nm/g	Zero-span Breaking Length, km	log₁₀ (MIT Fold)	Bendtsen Porosity, mL/min	Scattering Coefficient, cm²/g
1	Kraft	159	500	725	0.587	4.69	21.7	59.3	17.2	2.88	>3000	200
			1500	665	0.631	6.44	15.5	75.4	17.9	3.10	2849	165
			3000	560	0.653	7.21	13.5	83.8	18.2	3.27	1245	151
			4500	455	0.677	7.36	13.2	90.0	18.2	3.31	421	141
			5250	380	0.680	7.88	12.1	90.6	21.4	3.42	190	140
1	SAQ	167	500	735	0.600	4.86	21.2	60.1	17.5	2.94	3188	186
			1500	660	0.648	6.43	15.6	75.9	19.2	3.13	2008	156
			3000	585	0.673	7.46	12.7	92.0	19.8	3.30	896	130
			5000	480	0.688	8.00	11.6	95.7	20.4	3.45	304	124
			7000	370	0.702	8.36	10.9	100.1	19.4	3.46	130	118
2	Kraft	11	500	700	0.575	3.29	32.1	46.1	17.7			
			2000	630	0.628	5.92	19.9	76.9	19.3			
			3000	490	0.649	6.56	15.6	81.0	20.5			
			4000	365	0.655	6.83	15.1	85.5	19.0			
			5000	280	0.685	7.14	15.0	88.4	19.9			
2	SAQ	12	500	730	0.583	3.60	28.0	50.3	17.7			
			2000	600	0.648	6.63	16.1	86.7	19.4			
			3000	500	0.654	7.72	15.0	88.9	19.0			
			4000	350	0.677	8.00	13.8	95.9	19.1			
			5000	315	0.693	7.90	13.6	100.4	19.6			

Table VI. Physical Properties of Bleached Pulps.

7

consumption of chemicals would be limited to that required to fortify the liquor prior to reuse. A precedent for this approach is the SCMP chemimechanical pulping process, which employs a very concentrated pulping liquor and therefore a high chemical charge (11).

Figure 12.   Tear-tensile relationships for SAQ and kraft pulps from two wood sources. Circles and triangles represent data from wood sources 1 and 2, respectively. Open symbols represent SAQ pulp data; filled symbols are for kraft pulps.

Process	HLS₁₀AQ	HLS₁₃AQ	K	HLK	HLKAQ
Cook no.	161	160	159	189	192
Initial concentrations, g Na₂O/L					
Na₂SO₃	48	48	0	0	0
Na₂CO₃ + NaOH	12	12	37.5	37.5	37.5
Na₂S	0	0	12.5	12.5	12.5
Initial AQ concentration, g/L	0.25	0.25	0.00	0.00	0.25
Maximum temperature, °C	180	180	165	165	165
Time at max. temp., min	210	120	121	118	120
Liquor-to-wood ratio, mL/g	20	20	3.8	20	20
Initial pH	11.0	13.6	n.d.ᵃ	n.d.	13.5
Final pH	10.0	13.1	n.d.	n.d.	n.d.
Total yield, % o.d. wood	46.8	43.5	46.7	40.2	40.2
Rejects, % o.d. wood	1.1	0.1	0.4	0.1	0.0
Kappa no.	22.8	12.9	38.8	16.8	13.5
Carbohydrate yield, % o.d. wood	45.2	42.6	44.0	39.2	39.6
Viscosity, mPa·s	51.9	25.0	37.4	16.1	13.6
Unbleached brightness	42.2	42.7	22.5	40.9	43.0
No. of bleaching stages	3	3	5	n.d.	n.d.
Bleaching chemical cost index	51	44	100	n.d.	n.d.
Bleached yield, % o.d. wood	44.0	41.8	43.6	n.d.	n.d.
Tensile index at 4000 PFI rev., N·m/gᵇ	90	93	86	75	n.d.
Tear index at 80 tensile index, mN·m²/gᵇ	16.2	14.6	14.5	14.8	n.d.

ᵃn.d. = not determined.
ᵇPhysical properties given were determined after bleaching except in the case of the HLK pulp.
ᶜProcess designations: HLS₁₀AQ, HLS₁₃AQ - high liquor-to-wood ratio sulfite-anthraquinone (subscript density terminal liquor pH); K - kraft; HLK - high liquor-to-wood ratio kraft; HLKAQ - high liquor-to-wood ratio kraft-AQ.
ᵈAll pulps prepared from chips in a 50-L digester equipped with external circulation and indirect heating.

Table VII. Comparison of high liquor ratio SAQ pulping with kraft variants ᶜ,ᵈ.

A second possibility is that determining the mechanism of the selectivity improvement will provide the insight needed to achieve the same end by other means. For example, a knowledge of the relative concentration dependencies of delignification, cellulose chain cleavage, and carbohydrate dissolution will allow optimal liquor concentration - time profiles to be specified and suggest ways of achieving them, such as staging and liquor injection. This is the objective of our current studies of the kinetics of the process.

EXPERIMENTAL

Materials

Bolts of southern yellow pine, believed to be loblolly pine, were chipped in a Carthage

chipper or, in some cases, sawn into discs from which 1 mm thick wafers were subsequently cut. Wood from two different sources was used. Both were characterized by chemical analysis and determination of specific gravity. The results are summarized in Table VIII.

Source	Cellulose	Galactogluco-mannan, %	Arabino-xylan, %	Lignin, %	Extractives, %	Specific Gravity
1	37.6	17.0	8.4	31.8	4.5	0.411
2	38.8	17.9	8.4	30.8	2.6	0.505

Table VIII. Wood furnish characteristics.

Pulping liquors were prepared from reagent grade sodium sulfite, sodium hydroxide and sodium sulfide. SAQ liquors were made by absorbing carbon dioxide in sodium sulfite-sodium hydroxide solutions until the desired pH was reached. Liquor concentrations were checked by acidimetric titration. The kraft pulping liquors contained no sodium carbonate.

Pulping

The cooks done to determine liquor composition effects were carried out in 500-mL bomb microdigesters heated by rotating them in an oil bath. To eliminate mass transfer effects, these cooks were conducted with 1-mm thick wood wafers as raw material. Before cooking, the wafers were impregnated by submerging them in the pulping liquor and applying a vacuum. At the end of the cook the bombs were removed from the oil bath and cooled, first with steam and then in a shower of cold water.

The cooked wafers were fiberized in a blender and washed with deionized water. The pulp pad was dewatered, air-dried, weighed and sampled for moisture to determine yield. The remaining sample was reslushed in a Tappi disintegrator and screened on a 0.006-inch cut flat screen. Kappa number was determined on the screened pulp by the standard TAPPI procedure.

Larger scale cooks were carried out in a stainless steel vessel of about 50-L capacity fitted for external circulation and indirect steam heating. In these cases the wood pulped was in the form of chips screened to pass a 3/4-inch opening and to be retained on a screen with 1/4 inch openings. The chips were charged to a stainless steel basket which closely matched the interior contours of the digester and which could be removed with the contents following the cooks. After charging with chips and liquor the digester was evacuated to assist chip impregnation with the SAQ liquor. Subsequently, the temperature-time profile was controlled by manually regulating the steam input to the heat exchanger. Pulping conditions are appended to the data tables.

At the end of the cook the blow valve was opened to expel the spent liquor through a cyclone separator into a muslin-covered wash box where any entrained fibers were collected. The cooked chips were washed and fiberized in a Williams disintegrator.

The pulp was screened through a 0.006-inch cut screen plate on a Valley flat screen. The rejects were oven dried, weighed, and discarded. The accepted pulp was dewatered by centrifugation, mechanically subdivided, weighed and sampled for moisture to determine yield.

Bleaching

Oxygen bleaching was done at 100 psia O_2 and 25% consistency in a reactor equipped with stainless steel mesh trays and heated by direct steam. Chlorination and chlorine dioxide stages were done either in a 30-gallon glass-lined stirred reactor or in polyester bags. Caustic extraction was accomplished by mixing caustic with the pulp at 10% consistency in a Hobart mixer and transferring the pulp to polyester bags, which were then placed in a thermostat.

Testing and Analysis

All pulp testing was conducted according to TAPPI standard methods as follows:

    Kappa number - T236 os-76
    Viscosity of pulp - T230 om-82
    Brightness of pulp - T452 om-83
    Physical testing - T220 om-83
    Extractives - T204 os-76
    Klason lignin - T222 os-74
    Acid-soluble lignin - Useful Method 250

Viscosity was determined after overnight treatment with sodium chlorite in acetic acid solution at room temperature or below.

Carbohydrates were determined by acid hydrolysis followed by conversion of the resulting sugars to alditol acetates and analysis by gas chromatography (12).

CONCLUSIONS

1. In the pulping of southern pine, the sulfite-anthraquinone process possesses a marked selectivity advantage over the kraft process in terms of both yield and viscosity. Under normal conditions, the advantage diminishes rather rapidly as the kappa number at which the comparison is made is decreased below 40.

2. For a given degree of delignification, pulping in liquor containing only Na_2SO_3 results in very slow lignin removal and poor viscosity

but good carbohydrate retention. Replacement of 20% of the Na_2SO_3 with Na_2CO_3 accelerates lignin removal and improves viscosity retention but gives a somewhat lower yield. Further replacement slows down the cook and reduces yield but improves viscosity. Analysis of the pulp suggests that Na_2CO_3 functions by extracting sulfonated lignin, but that too high a level of replacement of Na_2SO_3 impairs the ability of the liquor to sulfonate lignin.

3. Partial replacement of Na_2SO_3 with NaOH instead of Na_2CO_3 gives more efficient lignin removal but reduces pulp viscosity and carbohydrate retention.

4. Cooks conducted under conditions of constant chemical concentration show that the rates of removal of both lignin and carbohydrates increase with increasing alkalinity. Pulp viscosity, on the other hand, passes through a maximum as liquor alkalinity is increased. The maximum occurs at an alkalinity slightly higher than necessary to convert all bicarbonate ions to carbonate ions.

5. At constant pH, increasing the concentration of Na_2CO_3 retards delignification. The apparent activity of Na_2CO_3 as a pulping chemical in SAQ systems is related to its buffering ability.

6. The rate disadvantage of SAQ pulping relative to kraft can be diminished by raising the pulping temperature or by using NaOH as makeup chemical. In the former case, its selectivity advantage is also diminished.

7. Bleaching of SAQ pulps in conventional sequences requires more chlorine and caustic in the first two stages than kraft pulps. Subsequently, however, they can be fully bleached in only one stage, while kraft pulps require 3 additional stages.

8. The bleaching yield of SAQ pulps is lower than that of kraft pulps, but the difference is not great enough to seriously erode the overall yield advantage of the former.

9. Bleached SAQ pulps from southern pine are as strong as or stronger than the corresponding kraft pulps. They exhibit a higher ultimate tensile strength and equal tear at a given tensile level.

10. The SAQ pulping process is capable of pulping to very low kappa number levels while retaining high viscosity and acceptable yield. Currently, this can be achieved by using high liquor-to-wood ratio and correspondingly high chemical charge. Ongoing kinetic studies are

expected to identify other routes to the same
end.

ACKNOWLEDGMENTS

The pulping of wood from source 2 and
analysis of the corresponding pulps (Tables
III - VI) were conducted under the sponsorship
of MEI Systems Inc. That company's assistance is
gratefully acknowledged.

We thank Mr. Art Webb of the IPC Analytical
Group for performing the pulp analyses, and
members of the IPC Paper Testing Group for the
physical test data.

REFERENCES

1. KETTUNEN, J., VIRKOLA, N., AND YRJALA, I.
   The effect of anthraquinone on neutral
   sulphite and alkaline suphite cooking of
   pine. Paperi ju Puu 61(11): 685 (1979).

2. RAUBENHEIMER, S. AND EGGERS, S.H.
   Zellstoffkochung mit Sulfit und
   Anthrachinon. Das Papier 34(10A): V19
   (1980).

3. CAMERON, D.W., FARRINGTON, A., NELSON,
   P.F., RAVERTY, W.D., SAMUEL, E.L., AND
   VANDERHOEK, N. The effect of addition of
   quinonoid and hydroquinonoid derivatives in
   NSSC pulping. Appita 35(4): 307 (1981).

4. VIRKOLA, N., PUSA, R., AND KETTUNEN, J.
   Neutral sulfite AQ pulping as an alter-
   native to kraft pulping. Tappi 64(5): 103
   (1981).

5. OJANEN, E., TULPPALA, J., AND VIRKOLA, N.
   Neutral sulphite anthraquinone (NS-AQ)
   cooking of pine and birch wood chips.
   Paperi ja Puu 64(8): 453 (1982).

6. INGRUBER, O.V., STRADAL, M., AND HISTED,
   J.A. Alkaline suphite-anthraquinone
   pulping of eastern Canadian woods. Pulp
   Paper Canada 83(12): T342 (1982).

7. INGRUBER, O.V. AND ALLARD, G.A. Alkaline
   sulphite pulping. Can. Pat. 847,218(July
   21, 1970).

8. GORMAN, J.W., AND HINMAN, J.E. Simplex
   lattice designs for multicomponent systems.
   Technometrics 4: 463 (1962).

9. TIKKA, P., TULPPALA, J., AND VIRKOLA, N.
   Neutral sulfite AQ pulping and bleaching of
   the pulps. International Sulfite Pulping
   Conference, Toronto, 1982.

10. THOMPSON, N.S., AND KAUSTINEN, O. A study
    of certain carbohydrate degradations during
    sulfite pulping. Tappi 49(12): 550 (1966).

11. MUTTON, D.B., TOMBLER, G., GARDNER, P.E.,
    AND FORD, M.J. Sulfonated chemimechanical
    pulping process. Pulp Paper Can. 83(6):
    T189 (1982).

12. BORCHARDT, L.G., AND PIPER, C.V. A gas
    chromatographic method for carbohydrates as
    alditol acetates. Tappi 50(2): 257-61
    (1970).

Status Report

IMPROVED PROCESS FOR BLEACHED PULP

Nonchlorine Bleaching

INTRODUCTION

Our previous research has shown that cellulose degradations need not parallel lignin removal during oxygen bleaching. (For example excessive cellulose degradation is not necessarily accompanied by extra lignin removal and the converse has also been observed to occur.) Although free radicals were found to be present in pulp lignin, additional radicals were produced during oxygen bleaching, suggesting that radical processes play a part during bleaching. Bleached pulps, on the other hand, contain few if any radicals. The chemical nature of these radicals cannot yet be determined, and the part they play in the degradation of pulp remains to be proven.

We concluded that although radicals are present during oxygen bleaching and probably adversely affect pulps, we have not been able to control them. Therefore, the research emphasis of this project on oxygen bleaching is changed from attempts to stabilize cellulose against degradation by these radicals to developing techniques to enhance the extent of lignin removal relative to cellulose degradation.

NATURE OF LIGNIN IN PULPS

There are two general classes of lignin in low-yield, unbleached pulps. One is that material which has been rendered soluble in the pulping process but which has not been removed either because of incomplete washing or because of entrapment within the fiber structure. The other component is that lignin which

has not been dissolved but which may have been chemically modified as a result

of the cooking process. Both these lignins contain functional groups which

should affect bleaching reactions, as they are a source of radicals when they

interact with oxygen. Some of these functional groups should be amenable to

chemical alteration with the possibility of introducing a different sequence of

lignin-oxygen interactions. This in turn could alter the extent of lignin

removal relative to cellulose degradation.

A comparison of the amounts of some of these groups in spruce wood and

kraft pulp (see Table 1) was calculated from data provided by Falkehag et al.[1]

The data show the number of functional groups in a theoretical lignin fragment

composed of 23 phenyl propane units. The numbers show that for an equal number

of aromatic nuclei, kraft lignin is richer in phenolic groups (due to

demethylation), unsaturation and various types of carbonyl groups. Thus kraft

lignin should be more reactive toward oxygen than unmodified lignin. These

reactive phenolics yield quinones (with the production of superoxide radicals),[2]

and quinone formation results in several alternative possibilities for reaction

with oxygen. Thus, conflicting tendencies result when lignin is modified. The

introduction of phenolic groups should increase the ability of lignin to react

with oxygen. On the other hand, the production of superoxide by their reaction

with oxygen should be detrimental to the cellulosic component of fibers. This

phenol-rich lignin configuration has been investigated previously in this

research and so far it has not been proven possible to control the reactions

satisfactorily to maximize lignin removal or to minimize cellulose degradation.

It is conjectured that chemical modifications of the functional groups of kraft

lignin might alter its interactions with oxygen and produce more satisfactory

results after oxygen bleaching.

Table 1. Some functional groups of kraft and native lignins.[a]

	Spruce Wood	Softwood Kraft
Aromatic nuclei	23	23
Phenolic hydroxyl	7	18
Aliphatic hydroxyl	23	10
Carboxyl groups	1	5
Carbonyl groups	2	3
Quinone groups	0	1.5
Unsaturation	5	8

[a]The number of functional groups for 23 aromatic nuclei.

It has been shown by many investigators that unsaturated compounds are very reactive toward oxygen and degrade by complex radical mechanisms (for a review see Mittet).[3] These reactions are different than those involving phenolics, since a greater participation by organic peroxides is usually observed. The reactions generally go at lower temperatures and the resultant peroxides cleave rapidly, break C-C bonds and generate solubilizing carboxyl groups. In contrast (by analogy to phenolics such as BHT), the reaction of phenolics leads to quinones which frequently form stable intermediates because of their antioxidant characteristics.

The reaction of unsaturated fatty acids with oxygen during bleaching was recently investigated by Mittet.[4] By analogy with his results, a nonaromatic, unsaturated lignin derivative would degrade by different pathways than the aromatic lignins. They would tend to be broken into smaller fragments rich in carboxylic acids and would produce less potential aromatic chromophores than unmodified kraft lignins. This possibility of lignin degradation was investigated briefly in past projects,[5] and additional experiments have been conducted

as time permitted. I would like to review some of this reported and unreported

data as an introduction to our new experimental approach.

INVESTIGATIONS FROM PROJECT 3092[5]

The effect of extraction of a well washed commercial southern pine

kraft pulp with dilute alkali and its subsequent treatment with reducing agents

is shown in Table 2. The data show that extraction of pulp with mild alkali

does not affect the properties of the bleached pulp significantly. It does

diminish the quantity of oxygen needed to bleach the pulp by about 10%. Thus,

contaminants wasteful of oxygen can be removed by alkaline preextraction, although

other properties are not changed.

Table 2. Effect of pretreatment on the bleaching properties of a commercial
southern pine kraft pulp.[a]

| | Original Pulp | Untreated Pulp | 0.1N NaOH Extracted | Reduced Pulp | |
				$NaBH_4$	$Na_2S_2O_4$
O_2 consumed, g O_2/100 g pulp	—	1.50	1.34	1.35	1.18
Yield, %	—	93.4	92.3	94.6	94.4
Viscosity, cp	29	13.6	13.9	13.6	14.7
K-number	20.5	6.6	6.4	6.7	6.1
Brightness	25.0	45.4	48.4	49.0	50.2
Zero-span, km	14.1	13.6	13.7	14.2	14.1

[a]100°C, 130 psig O_2, 6% NaOH on pulp, 25% consistency, 1 hour.

Alkaline sodium borohydride reduces carbonyl groups and quinones but

does not affect double bonds. Quinones are converted to phenols by this reduc-

tion but they are easily reoxidized again when the pulp is bleached with oxygen.

The unchanged oxygen consumption after borohydride reduction suggests quinones are the principal group involved in the reduction by borohydride.

Alkaline hydrosulfite treatment, on the other hand, does not reduce most carbonyls, but it does reduce quinones quantitatively.[5] It also adds to double bonds, a reaction which may contribute to the difficulty of reoxidizing phenols to quinones again.

The results in Table 2 are limited in extent and they suggest that more drastic alterations must be made in lignin composition if bleaching improvements are to be achieved. In attempting to do this, early work in Project 3092 used acid chlorite treatments to modify lignin in a more drastic but uncontrolled manner. The results are shown in Table 3.

Table 3. The effect of mild chlorite treatments[a] on kraft pulp.

	Control	Chlorited Pulp
Time of chloriting, days	0	3
K-number	20.5	18
Brightness	25.0	32.1
Viscosity, cp	29.0	26.2
Ca++, ppm	1700	884
Cu++, ppm	3.6	52
Fe+++, ppm	70	22

[a]10% $NaClO_2$ on pulp, 10% consistency, pH 4, room temperature, 3 days.

A small quantity of lignin was removed from the treated pulp, making subsequent interpretation of the bleaching results difficult. This omission was compounded by the lack of yield data. Even the lignin estimations using K-number are uncertain because of the altered chemical nature of the chlorited lignin.

The results after oxygen bleaching comparing controls and these treated pulps is shown in Table 4.

Table 4. The effect of O_2 bleaching on chlorited pulps.[a]

	Controls		Chlorited Pulp
Alkalinity, % of pulp	6.4	1.7	1.7
O_2 consumed, g/100 g pulp	1.5	0.2	0.12
Yield[a], %	93.4	99	96.2
Viscosity, cp	13.5	22.2	18.6
K-number	6.1	13.8	6.0
Brightness	45.5	28.6	43.0
Zero-span, km	13.6	14.7	13.9

[a]100°C, 130 psig, 60 minutes, 100 g pulp.
[b]Unbeaten.

A small quantity of lignin was removed from the treated pulp by the chloriting process and the copper content was inadvertently increased during washing. Although similar, the lignin estimations using the K-number test are uncertain because of the altered chemical nature of the chlorited lignin. Better estimations will have to be employed in the future. A more rapid conventional chlorine dioxide stage will probably duplicate the effects of the prolonged low temperature chloriting procedure and eliminate the harmful effects chlorous acid has on carbohydrate.

The comparison between controls and the chlorite treated pulp after oxygen bleaching is shown in Table 4. The mild partial removal of lignin with chlorite is beneficial as far as pulp brightness, yield and oxygen consumption are concerned. The zero-spans are not adversely affected at similar kappa numbers while pulp viscosities are significantly better. The chloriting procedure

does destroy original phenolic units, does introduce new phenolic units, quinones and does ultimately produce unsaturated carboxylic acids and lactones. These changes must contribute to the interaction of oxygen derivatives with cellulose.

FURTHER EXPERIMENTS TO MODIFY LIGNIN

The possibility of using other reagents for the selective and controlled destruction of phenolic units with little loss of lignin has also been investigated. The experiments were very limited in scope but do provide some insight. Sodium peroxide and peroxyacetic acid were used to oxidize phenolic units to varying and unknown extents. Only small quantities of the oxidant were used with the hope that lignin would be altered without great loss of the carbon content.

PEROXIDE PRETREATMENTS

Peroxide was first chosen as a pretreating agent because it is a commonly used bleach in the paper industry and because it does not provide products that might prove detrimental to waste liquor recovery. Under mild conditions, peroxide probably attacks chromophores associated with extended conjugated bonding systems. These are thought by Gellerstedt[6] to be cinnamaldehyde type structures and quinones. Under more drastic conditions, phenolic components are attacked and the aromatic ring is cleaved by reactions believed to involve the hydroxyl radical.[7] The lower temperatures involved in peroxide bleaching (compared to oxygen bleaching) may minimize this potential hazard. The effect of a peroxide pretreatment on southern pine kraft pulp is shown in Table 5.

The peroxide treatments have removed significant quantities of lignin, increased brightness and have left the zero-span tensile strength of the resulting paper unchanged. After bleaching with oxygen (Table 6), the brightnesses of the pulps were greatly increased by the treatments, while the zero spans were

unaffected. These preliminary results indicate that properties of pulps after
oxygen bleaching can be influenced by mild pretreatments but they do not predict
which properties can ultimately be affected if the bleaching conditions are
optimized. The research was terminated before analyses were completed.

Table 5. The effect of a peroxide[a] bleach on southern pine kraft pulp.

Quantity of Peroxide, % on pulp	K-Number	G.E. Brightness	Zero Span Tensile, km[b]
0	20.1	28.1	15.3
0.3	18.6	28.4	15.2
0.75	17.0	34.0	15.4
1.0	16.8	35.0	14.9

[a]Conditions of bleach.
[b]Unbeaten.

Table 6. The effect of peroxide pretreatments on the properties
of oxygen bleached pulps.[a]

Quantity of Peroxide, % on pulp	G.E. Brightness	Zero-Span Tensile, km
0	48.6	10.2
0.3	52.6	11.7
0.8	56.2	12.1
1.0	54.9	11.9

[a]100°C, 130 psig O_2, 6% NaOH (on pulp) 25% consistency, 1 hour.

In all instances, oxygen bleaching resulted in about 20 units increase
in brightness. The percentage increase decreases with increasing initial bright-
ness. These conditions obviously affect chromophores but have not altered pulp
strengths appreciably. The low zero-span tests result from the use of a contam-
inated pine kraft pulp and circumstances did not permit repeating the experiment.

These results suggest that peroxide as well as chlorite can modify the response
of pulp to oxygen. Because of the limited analyses and the great differences
between the pine kraft pulps employed, no conclusions can be drawn concerning
the relative merits of the pretreatments at this time.

PERACETIC ACID PRETREATMENTS

In many ways, peroxyacetic acid is a more desirable pretreating chemi-
cal than peroxide or chlorite. It reacts readily with phenols by hydroxylating
them, converting them to quinones and ultimately to muconic acid derivatives.[8]
The nature of the attacking species depends upon the pH of the reaction system.[7]
Since the hydroxyl radical is not thought to be involved in these reactions,[9]
some side effects should be minimized. Significant oxidation of carbohydrate
(measured as carbonyl) does occur and is particularly apparent for those reac-
tions conducted at low pH.[10] It seems likely that experimental conditions will
have to be carefully controlled and monitored in the case of peroxyacetic acid
pretreatments.

According to model experiments, the ultimate lignin reaction product
will contain varying degrees of unsaturation and muconic acid derivatives.
These will provide an alternate pathway for oxygen delignification. An examina-
tion of the pyrolysis products of peracetic acid pretreated lignins by Fleck[10]
showed a fast initial reaction which did not degrade aromatics. When the yield
diminished to 97%, pyrolysis examinations showed that aromatic cleavages pre-
dominated. Thus the aromatic units of lignin can be destroyed without excess
lignin loss and with only a small consumption of peroxyacetic acid. Prolonged
treatment of pulp would probably consume excessive oxidant, dissolve much lignin
and leave a "holocellulosic" residue.

A significant increase in pulp brightness occurs as a result of peracetic acid treatment of unbleached kraft pulp. The K number has been diminished significantly, although not to the same extent as was observed for pulps after acid chlorite pretreatments (Table 7). Because of the drastic alteration of lignin structure as a result of the pretreatment, K number is not an accurate measure of lignin content. Little increase in zero-span tensile was observed, and the small change that is evident may result from a loss of lignin content.

Table 7. The effect of peracetic acid pretreatments[a] on southern pine kraft pulp.

Pulp	Pretreatment	G.E. Brightness	$KMnO_4$ K-Number	Zero-Span Tensile, km	Buf & pH
MAL	SO_2	25.0	19.5	14.1	8.5
MAM	Acetic acid	28.5	21.6	14.6	8.5
MAN	0.42% PAA[a]	31.2	20.2	14.9	8.5
MAP	0.88% PAA[a]	33.2	19.2	15.4	8.5
MAR	3.0% PAA[a]	39.6	17.8	15.1	8.5
MAT	7.0% PAA[a]	47.2	14.5	15.5	8.0

2.38%

[a]5% consistency, SO_2 pretreated, pH 8-8.5, 40°C, 2 hours.

The results of oxygen bleaching the peroxyacetic acid pretreated pulps are shown in Table 8. The pulp employed in this group of experiments was a commercial southern pine kraft which had inadvertently been contaminated with 40-50 ppm copper ion during washing at the Institute. Thus the oxygen bleach of the contaminated pulp gave a lower brightness and a poorer zero span tensile than the control pulps which had been washed with either SO_2 or acetic acid to eliminate the contamination. Increasing the amount of pretreating agent resulted in marked increases in brightness with little change in zero span tensile.

Table 8. The effect of peracetic acid prebleaching on some properties
of oxygen bleached pulp.[a]

Pulp	Pretreatment	G.E. Brightness	$KMnO_4$ K-Number	Zero-Span Tensile, km
MA	none	48.6	5.3	10.2
MAL	SO_2	52.9	8.0	13.9
MAM	Acetic acid	53.6	7.9	14.2
MAN	0.42% PAA	54.8	7.8	14.0
MAP	0.88% PAA	56.8	6.9	13.6
MAR	3.0% PAA	60.8	5.8	13.9
MAT	7.0% PAA	65.1	5.6	14.1

[a]$100°C$, 130 psig, O_2, 60 minutes, 6% NaOH on pulp, 25% consistency.

It is not known whether a peroxyacetic acid posttreatment after a con-
ventional oxygen bleach would achieve these same brightnesses while maintaining
zero-span strengths. This survey suggests that chemical modification of pulp
with peroxyacetic acid before oxygen bleaching may also be a useful direction to
pursue if one is to attain more rapid or complete removal of lignin without
incurring excessive loss of paper properties. These preliminary experiments
suggest that the brightness and perhaps the K-number of the resulting pulps are
most affected, but the experiments do not define precisely the reasons for these
alterations. Only additional research exploring pretreatment parameters can
determine whether these treatments are truly effective.

SUMMARY

This group of experiments shows that modification of kraft lignin by
oxidative pretreatments can alter the properties of the oxygen bleached pulps
derived from them. The results suggest that chlorite treatments (or chlorine
dioxide) might be more beneficial than peroxyacetic acid and peroxide as far as

lignin removal is concerned. This may be a premature conclusion, since optimized pretreatment and bleaching conditions have not yet been achieved. Because of the similarity of attack by chlorine dioxide and peroxyacetic acid on lignin, (destruction of aromatics and production of muconic acid derivatives), it is possible the two reagents might be equivalent when optimized. A drawback to the chlorine dioxide treatment would be the production of chlorinated effluents, while the peroxyacetic acid treatment would introduce ketones and alkaline lability into polysaccharides.

It is likely that pretreatment of pulp before oxygen bleaching may be a fruitful technique to increase brightness and speed of lignin removal without incurring excessive cellulose damage. Current industrial practice also lends support to this approach. It is postulated that those pretreating agents that demethylate, hydroxylate, and convert the aromatic components of lignin to unsaturated acids and lactones will be the most effective pretreating chemicals. They will achieve this ability because they will interact with oxygen in a different manner than aromatic lignins.

<div align="center">PROJECTED RESEARCH PROGRAM</div>

Reagents leading to the destruction of phenolic units will be tested as pretreating agents to improve the properties of oxygen bleached pulps. The changes in the chemical characteristics of the lignin component brought about by the pretreatment will be related to the behavior of the pulp during bleaching. The desired characteristics are high brightness, and satisfactory viscosity and zero-span strength. Those sequences giving satisfactory criteria will be subject to further papermaking tests after it has been shown that the sequence is better than the converse employing a posttreatment with the same reagents.

Secondary pretreatments will also be employed if necessary to understand and control the final product.

REFERENCES

1. Falkehag, S. I.; Maron, J.; Adler, E., Adv. Chem. Ser. 59:75-89(1966).

2. Pal'mova, S. B.; Bagomolov, B. D., Izv, Vysh. Vched., Les. Zh., 12(4):102-5(1969).

3. Kerber, R.; Starnide, J., Ber. 104(7):2035(1971).

4. Mittet, G., Ph.D. Thesis, The Institute of Paper Chemistry, Appleton, WI, 1979.

5. Thompson, N. S.; Corbett, H. M., Report One, Project 3092, Oct. 5, 1973.

6. Gellerstedt, G.; Pettersson, I.; Sundin, S., Int. Symp. on Wood and Pulping Chemistry, Stockholm, June 9-12, 1981. p. 120-4.

7. Norman, R. O. C.; Smith, J. R. L. In Oxidases and Related Redox Systems, Vol. 1, T. J. King and M. Morrison, eds., J. Wiley, New York, 1965. p. 131-55.

8. Johnson, D. C. Lignin reactions in delignification with peroxyacetic acid. UNI Publishing Co., Tokyo, Japan, 1980. p. 217-28.

9. Suss, H. U.; Kruger, H., Tech. Papers, Int. Symp. on Wood and Pulp Chem., Vancouver, B.C., August 26-30, 1985. p. 13-20.

10. Fleck, J. A., Ph.D. Thesis, The Institute of Paper Chemistry, Appleton, WI, 1975.

THE INSTITUTE OF PAPER CHEMISTRY

Norman S. Thompson
Senior Research Associate
Wood Sciences
Chemical Sciences Division

THE INSTITUTE OF PAPER CHEMISTRY

Appleton, Wisconsin

Status Report

to the

PULPING PROCESSES

PROJECT ADVISORY COMMITTEE

Project 3524

FUNDAMENTALS OF BRIGHTNESS STABILITY

September 5, 1985

PROJECT SUMMARY FORM

DATE: September 5, 1985

PROJECT NO. 3524: FUNDAMENTALS OF BRIGHTNESS STABILITY

PROJECT LEADER: W. F. W. Lonsky

IPC GOAL:

A significant increase in yield of useful fibers.

OBJECTIVE:

Elucidate mechanism for brightness loss in high-yield pulps.

CURRENT FISCAL BUDGET: $110,000

SUMMARY OF RESULTS SINCE LAST REPORT:

Free singlet oxygen is not involved in the yellowing reaction of high-yield pulps. Mechanisms for singlet oxygen formation and reactions are valid only for the homogeneous model studies in solution but are not applicable to the heterogeneous reactions occurring in a sheet.

Oxygen does not participate in the rate determining step of the reaction. The partial pressure of oxygen can be varied over a wide range without affecting the rate of the yellowing reaction. It is shown that oxygen is enriched on the fiber surface. Two mechanisms are proposed and discussed leading to the formation of ortho- and para-quinones. They provide a basis for the possible explanation of how the same quinonoid products can originate from softwood and hardwood lignin structures but at different rates.

A UV monochromator has been set up to evaluate the photoactivity of narrow UV wavelength ranges on paper (290 to 400 nm in 4 to 10 nm intervals). The highest photoactivity was found in the wavelength range around 310 nm.

By stepwise increase of the light flux in a set of irradiation experiments, light saturation of the sheet was observed. A maximum rate of the color reversion is reached that cannot be exceeded upon further increase of the flux.

The effect of heavy metals on light induced color reversion has been found to be insignificant for the concentration levels found in commercial pulps. However, an effect on the thermal aging reaction was observed.

The effect of the sheet pH on the rate of color reversion has been determined. The pH range 3 to 7 is the most appropriate for future determination and comparison of the rates of reversion of bleached and unbleached pulps.

PLANNED ACTIVITY THROUGH FISCAL 1986:

Demonstrate suppression of yellowing by lignin modification, including clarification of the organic peroxide structures formed during alkali/peroxide

bleaching and how they affect brightness stability. Factors limiting the
brightness of high-yield pulps will be defined.

FUTURE ACTIVITY:

Development of new bleaching methods leading to brightness stable high-yield
pulps. Evaluate the effect of sizing and filler materials on brightness stabi-
lity. Determine best light stability possible based on combination of factors
such as light absorption, photobleaching, and lignin modification. Define the
effect of treatments used to improve the physical strength of high-yield pulp on
brightness level and stability.

FUNDAMENTALS OF BRIGHTNESS STABILITY

SUMMARY

Evidence from theory and practice is provided that the interaction of free singlet oxygen in the photoyellowing reaction does not occur.

The enrichment of oxygen on the surface of high-yield pulp has been demonstrated. Oxygen is bound by dipole-induced dipole interaction (charge transfer) with electron rich structures of the wood components.

The effects of the light flux on the yellowing reaction are discussed.

The experimentally determined relationship between the rate of the yellowing reaction and the logarithm of light exposure time has been theoretically derived. In practice, an increase of the rate of yellowing with increasing light flux is observed. The rate approaches a maximum value that cannot be exceeded by a further increase of the flux.

The kinetics have been applied to determine the rate of yellowing with dependence on the sheet pH. Softwood and hardwood high-yield pulps darken at almost constantly decreasing rates with increasing pH within the pH-range 3 to 7. A significantly lower rate is observed in the pH range 9 to 10.

REMARKS

Last year's report included investigations of the reversion of high-yield pulps at high brightness levels. It was shown that the chemical reactions in both high and low brightness pulps are of the same general class, i.e., both concern the reactions and development of quinonoic structures. However, the high brightness pulps yellowed at a faster rate, apparently due to an increase in carbonyl

content of the lignin after peroxide bleaching. This brightness reversion in
bleached pulps may be viewed as a combination of the reaction of the unbleached
material overlaid with the chemical changes that occur as a result of bleaching.
Any bleaching sequence must be designed not only to increase whiteness, but also
to change the chemical structure in a manner that will increase, not decrease,
light stability. To do this we need to establish a knowledge of the basic light
interactions with unbleached pulps to decide on modifications that will lead to
improved bleached pulps. Therefore, we continue to study the photochemistry of
both bleached and unbleached high-yield pulps.

INTRODUCTION

A general research outline is shown in Fig. 1. The first part of
this report discusses the pros and cons of the chemical, photochemical, and phy-
sical interactions of the principal components of high-yield pulp yellowing:
lignin, light, and oxygen. The status of the research with UV-absorbing
fluorescent additives to achieve brightness stabilization is summarized. The
second part discusses the effects of pulpwood types and sheet pH on the rate of
yellowing. Possible ways to reduce the rate of yellowing are presented.

The last section addresses theoretical considerations regarding the
rate of yellowing, the formation of chromophores and their measurement.

PART I: INTERACTION OF LIGHT, LIGNIN, AND OXYGEN

Is Singlet Oxygen Formed During Light-induced Color Reversion?

Our research activity was concentrated on the question, "Does oxygen
react with high-yield pulps in the singlet or triplet state?" Only if free
singlet oxygen is formed is the application of singlet oxygen quenchers meaning-
ful. Literature provides support for the presence of singlet oxygen during

Figure 1. Research outline: color reversion and brightness stability.

light-induced yellowing. In general, an energy-transfer mechanism involving

light absorption by arylcarbonyl groups is the widely accepted mechanism. How-

ever, no one was ever able to show the formation of singlet oxygen on a pulp

sheet. We tested various quenchers without a single positive result. From

discussion with other researchers in this field, I learned that at least 50

substances have been tested on pulp with the same result. These substances are

known to be good singlet oxygen quenchers, but none of them - with the exception

of TBH (2,6 ditert. butyl cresol) showed the expected effect.

Other experiments have not proceeded as expected if singlet oxygen is

involved. Elmer Ogryzlo (Prof. of Chemistry at the University of British

Columbia at Vancouver, Canada), a specialist in singlet oxygen research,

discussed a cooperative research project in which he was involved around 1970.

TMP sheets were placed into a stream of singlet oxygen for 15 hours. Neither

yellowing nor bleaching was observed. However, we determined that one probably

essential component was not present in the reactor: water. In some orienting

yellowing experiments with sunlight we recognized the importance of humidity.

(Presently we have only qualitative results, which show that increasing humidity

increases the rate of yellowing. Much lower rates were observed when the light-

induced color reversion was carried out at $10 \pm 2\%$ relative humidity in a

temperature-humidity controlled room.) Humidity was completely excluded in

Ogryzlo's experiments to avoid quenching by water.

In a cooperative research project we are repeating these experiments in

the presence of water in the gas stream (2% water, 5% singlet oxygen in oxygen).

The preliminary results indicate that singlet oxygen under these conditions does

not yellow spruce or aspen TMP sheets. The reduced pressure (10 Torr.) can also

be excluded as a cause of inhibited reactivity, since experiments by Van den

Akker et al. are reported in which light-induced yellowing of MP sheets was
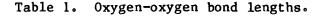
observed at such pressures. The reversion was found not to be markedly reduced. Based on these results we can rule out singlet oxygen as a responsible intermediate in the yellowing reaction. The oxidation mechanisms as suggested by Gellersted and Nimz are certainly valid for reactions of model substances in solution but are not applicable to the heterogeneous (gas-solid) interactions of light, lignin, and oxygen in paper.

Our present experience and accumulated knowledge suggest that we look for an alternative pathway that includes the interaction of triplet oxygen (as present in air) with lignin radical structures as primary reaction products after the absorption of UV radiation.

The Effect of Heavy Metals on Brightness and Color Reversion of High-yield Pulps

Heavy metals are known catalysts in oxidation reactions. During the past decade intensified research has taken place to understand their catalytic action. In essence, a heavy metal ion is surrounded by a ligand field of certain geometry. Ligands occupy particularly spaced positions. Some of these ligands are only weakly bound and can easily be exchanged and substituted by other ones which form stronger, more stable bonds. An exchange can also be caused by an increase of the concentration of this particular ligand. Ligands can be simple, small inorganic compounds like water, ammonia, oxygen, hydrogen, and so forth, or they can be large organic molecules which contain strong polarizable groups, such as amines, alcohols, phenols, carbonyls, C-C double bonds, etc.

When an oxygen molecule enters a ligand field and becomes part of the inorganic heavy metal complex, its electrons are redistributed. Consequently, bond distances are changed (Table 1). This is what we understand as "activation" of the oxygen molecule. It is now in a more reactive state than before and can cause oxidation of a substrate. If it has nothing to react with, it can

occasionally leave the ligand field and be replaced by another ligand, thereby gaining back its original electron distribution.

Table 1. Oxygen-oxygen bond lengths.

Compound	Type	Structure	O–O, Å
O_2	Free molecule	O=O	1.2074
KO_2	Superoxide	$\cdot O_2^-$	1.28
H_2O_2	Peroxide	O_2^{2-}	1.453
$Co(bzacen)pyO_2$	Reversible O_2 complex	Co–O\O·	1.26
"Picket-fence porphyrin"–Fe(II)(methylimidazole)O_2	Reversible O_2 complex	Fe–O\O·	1.24
$[(NH_3)_5CoOOCo(NH_3)_5]^{4+}$	μ peroxo complex	Co–O\O–Co	1.47
$[(NH_3)_5CoOOCo(NH_3)_5]^{5+}$	Oxidized μ peroxo complex	Co–O\O–Co	1.31

The bond distances for structurally investigated and defined ligands are listed in Table 1 together with those of defined salts of the stepwise reduced forms of oxygen. Oxidation is defined as electron withdrawal from a substrate. If an oxygen molecule withdraws one electron from a substrate, the oxygen is reduced to superoxide, which in turn is capable of withdrawing a second electron and becoming reduced to hydrogen peroxide. Comparing the O–O bond distances in heavy metal ion complexes with those of the oxygen molecule, of superoxide, and of peroxide show indeed the reorganization of the electrons in the oxygen molecule when it becomes part of a heavy metal complex ion. Heavy metal ions in pulp could theoretically undergo similar reactions with air oxygen. Photodecomposition or thermal activation of the metal-peroxide intermediates could initiate lignin or cellulose oxidation, enhancing the light-induced or thermal aging reactions.

In an effort to clarify the impact of heavy metals on brightness stability, William Welsh (M.S. degree, 1985, IPC) investigated their effect in commercial high-yield pulps. The concentrations of heavy metals were changed by column chromatography of the pulp with sequestering reagents in deionized water. The results are summarized in Tables 2-4. At the concentration levels in which the heavy metals occur in commercial high-yield pulps they do not affect brightness or color reversion by light. There is, however, an effect on the thermal reversion of the pulp. This relates to the yellowing that occurs during the drying operation of the sheet on the paper machine.

Table 2. Metal analyses of handsheets used in yellowing experiments.
Heavy metal concentrations in ppm (O.D. basis).

Handsheets	Cu	Fe	Mn
Unbleached-untreated	261	24.9	51.0
Unbleached-heavy metal free	33.6	11.1	0.56
Peroxide bleached-untreated	446	38.2	1.09
Peroxide bleached-metal free	28.0	10.6	0.32

Table 3. Brightness stability of spruce TMP: light-induced reversion.

Pulp Handsheets	k^a	$B_1{}^b$	Correlation
Unbleached-untreated	-7.53	49.7	0.996
Unbleached-heavy metal free	-7.36	51.9	0.995
Peroxide bleached-untreated	-16.2	63.2	0.997
Peroxide bleached-heavy metal free	-15.7	64.4	0.999

[a]K as slope from plotting ΔR_∞ vs. ln t.
[b]Brightness value after 1 hour exposure to sunlight.

Table 4. Brightness stability of spruce TMP: thermally aged.

Pulp	Brightness Before Aging	Brightness After Aging	Brightness Drop
Unbleached-untreated	53.1	51.2	1.9
Unbleached-heavy metal free	56.0	53.8	2.2
Peroxide bleached-untreated	77.6	71.2	6.4
Peroxide bleached-heavy metal free	75.4	70.9	4.5

Thus, I do not consider the heavy metal ions to cause a significant problem in the area of light-induced color reversion.

The Preferred Absorption of Oxygen on Pulp

The idea of oxygen activation through ligand bonding in heavy metal complexes initiated the idea of possible interactions of the polarizable oxygen molecule of the air with pulp constituents. Nitrogen, of which air consists about 80% by volume, is normally not bound as a ligand to heavy metals due to the low polarizability of its triple bond. Searching the literature for indications on increased oxygen solubility resulted in some interesting findings.

It is a well known fact that oxygen is present in water at a higher concentration than nitrogen. Gas solubilities are usually expressed as mole fractions of the gas (1 atm, 25°C). The values for oxygen and nitrogen are 0.17×10^4 and 0.13×10^4, respectively. The reason why oxygen is more soluble than nitrogen has to originate in its different dipole-induced dipole interactions with water. This in turn means that the oxygen's electrons are more mobile than those in nitrogen. This is usually expressed by the biradical oxygen structure and the tight triple bond structure of nitrogen (Fig. 2). It should also find its expression in the specific molar heat contents, since, besides identical contributions for the degrees of freedom for translation and rotation (5/2 R), the vibrational energies should differ largely due to the different bond types of the molecules. In fact, the Cp value of oxygen is 0.219 and of nitrogen 0.249 cal $\times$ g^{-1} $\times$ $°K^{-1}$. In the last decade research has been going on dealing with the dipole-induced dipole interaction between organic molecules and gaseous oxygen. Compounds containing polar functional groups (alcohols, carbonyl compounds, amines) form loosely bonded complexes with oxygen. Alkenes and aromatics do also, due to the high electron density of these bond types. In particular, the charge-transfer complex formed from benzene and oxygen as reported by D. F. Evans[1] appears to be interesting.

Its existence was spectroscopically demonstrated. If those organic compounds are able to form weak complexes (weaker than Van der Waals forces) with oxygen, then pulp components containing those structures should be able to do the same. A dry TMP sheet consists of a large number of free hydroxyl groups which are not involved in hydrogen bridging. It has aromatic rings, hydroxyl and carbonyl groups in the surface lignin. The absorption-desorption theory of gas absorption kinetics on solid surfaces predicts that oxygen and nitrogen would be on the surface in the same concentration as there is in the gas phase (20 parts oxygen and 80 parts nitrogen). However, if we invoke our dipole-induced dipole interaction theory, the result should be far from that value. The oxygen molecules, forming weak intermolecular bonds, would be retained for a much longer time than the nonpolarizable nitrogen molecules.

Figure 2. Polarizability of oxygen vs. nitrogen.

This idea has been experimentally verified. A preparative gas chromatography column was filled with fluffed and air dried TMP. Dry argon gas was used to remove the residual water, and as a monatomic noble gas (Cv 3/2R), it served as carrier gas for the GC analysis. A thermoconductivity cell was the detector. It responds to the different specific heat capacities of the by-passing fractionated gases. Nitrogen, oxygen, and air were injected. In Fig. 3 the three gas chromatograms are plotted on the same scale. It is evident that nitrogen has the shortest retention time on the TMP column; the peak form is symmetric.

Oxygen is retained longer; the peak shows tailing, which indicates that the weak

oxygen-pulp bond was slowly broken and the oxygen was eluted with the carrier

gas. The results of these experiments are exactly as we expected them according

to our theoretical considerations.

Figure 3. GC with TMP column.

From this result we may conclude that oxygen is enriched in a sheet of

paper above the value of its proportion in air. The polar groups of the nonbonded

fiber surface of a TMP sheet can be pictured as centers of preferred oxygen absorp-

tion. An increase of the oxygen concentration by replacing the surrounding air

with pure oxygen should not significantly increase the concentration of absorbed

oxygen molecules per unit of surface area at room temperature. This can explain

why the rate of the yellowing reaction does not increase when the UV irradiation

of a sheet is done under oxygen instead of air as observed in our experiments.

Status of the Research with Brightness Stabilizing Additives

Two UV-absorbing additives have been tested as brightness stabilizers. Laser grade α-NPO (2-(1-Naphthyl)-5-phenyloxazole) and Coumarin 120 (unknown structure) absorb UV radiation strongly in the range 300-330 nm and emit visible light in the blue region (λ_{max} 420-440 nm). Both dyes are extremely stable toward UV radiation in air.

α-NPO fluoresces strongly in the solid state, whereas Coumarin 120 does so only in solution. It was observed that the fluorescence of α-NPO was quenched when applied to spruce or aspen TMP, and no brightness stabilizing effect was noticed when the sheets were exposed to sunlight. Absorption of α-NPO on a pure cellulose sheet did not suppress the fluorescence. I intend to follow up on this unusual quenching phenomenon, since it could lead to a new selection method for additives in the future.

Summary of the Current Status of the Studies
on the Mechanism of Color Reversion

The wavelength of 310 nm has been identified as the most efficient UV wavelength for the yellowing reaction of high-yield pulps caused by quinone formation. Lignin structures containing α-carbonyl groups have their absorption maximum at this particular wavelength.

Since we disproved the generally assumed participation of singlet oxygen as an intermediate in the light-induced color reversion reaction (see Fig. 1: 4-5-6 and 6-7-8), alternative pathways have to be considered.

UV absorption by aryl α-carbonyl groups causes $(n-\pi^*)$ or $(\pi-\pi^*)$ excitation of the carbonyl group (see Fig. 4). The excited species [I] can then abstract a hydrogen atom from surrounding molecules (D-H) and generates two radicals D· and [II]. The experimentally observed quinone absorption band suggests that

Figure 4. Possible light-induced oxidation of lignin to quinones by triplet oxygen.

secondary hydrogen abstraction by D· occurs preferentially from phenolic species [III], which gives the lignin its well known antioxidant property. The resonance stabilized forms of the phenoxy radical [IV] can then react with the triplet oxygen and form quinones. A second energetically less favorable pathway would include one of the "Norrish Type" processes which are essentially photodissociation processes occurring on [I] either directly or after intramolecular hydrogen abstraction. The product would be exclusively of the p-quinone type [V].

The elucidation of these mechanisms is the near-term goal of our investigations.

Both mechanisms suggest radical mechanisms for the reaction. Strong antioxidants - compatible with the antioxidant properties of lignin - should show a brightness stabilizing effect.

We shall also check on a possible side effect that could be caused by the use of high-powered light sources: most of the light energy is converted into thermal energy. Our improved techniques indicate that some of the decrease of reflectivity could be due to heat buildup in the sheets. This seems not to be affecting measurements at 420 and 457 nm, to which we normally refer. However, there is indication of unexpected reflectance decrease in the ranges of 500 nm and above.
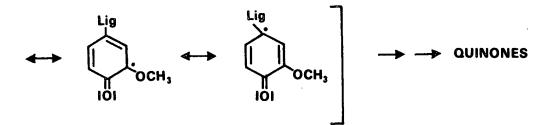
PART II: THE EFFECT OF MATERIAL PROPERTIES ON THE
           RATE OF THE LIGHT-INDUCED COLOR REVERSION

The Effect of Pulpwood Type on the Rate of Yellowing

Since the rate constant for yellowing is a function of the precursor (lignin) concentration (see the following section: "The kinetics of the brightness loss of high-yield pulps"), pulpwood with a higher lignin content will revert faster than that with a lower lignin content. Thus, softwood high-yield pulps, in general, will revert faster than hardwood high-yield pulps.

The chemical difference in the basic lignin units of the two lignin types is certainly the dominant factor for the different rate of yellowing. The soft-wood lignin structure (A) in Fig. 5 can react in the indicated position much faster than the hardwood lignin structure (B). The oxygen attack on structure (B) is sterically hindered, and a methoxy group has to be displaced. Hardwood lignin contains a certain amount of guaiacyl units (A), generally about 25%. If only structures (A) of hardwood formed quinones, a quick estimation using the rate equation discussed in section III (assuming all other parameters are identical for both pulps) gives for the ratio of the rate constants, k(softwood)/k(hardwood) the value 2.1. Thus, softwood would yellow twice as fast as hardwood.

The reaction scheme in Fig. 5 reveals how one and the same quinone type can be formed from softwood and hardwood structures.

Structure A

fast reaction
(softwood)

Structure B

slow reaction
(hardwood)

Figure 5.   Formation of 3-methoxy-o-benzoquinone structures from softwood and hardwood lignin radicals.

Although the lignin structures are different, the analyses of reverted pulp sheets of softwood and hardwood high-yield pulps do not show a significant difference in the product distribution. In both cases the light-induced formation of quinonoid structures within the lignin is the cause of the yellow discoloration. The solid state difference reflectance spectra show only an insignificant shift of the maximum absorption band (Fig. 6). o-Quinones, which are only moderately stable in solution and convert into colored materials mainly by unknown reactions, appear to be stabilized against secondary reactions through charge-transfer complex formation in the solid lignin matrix.

Figure 6. Solid state difference reflectance spectra of aspen and spruce TMP handsheets (sunlight exposed minus unexposed sheet reflectance).

Besides the difference in lignin structure, softwood and hardwood high-yield pulps differ in physical properties. Paper physicists use the terms K (absorption coefficient) and S (scattering coefficient) of the Kubelka-Munk equation to characterize the optical properties of a sheet. K is related to the concentration of the chromophores, while S is related to the free (nonbonded) fiber surface. Figure 7 shows the plots of S and K, respectively, vs. the wavelengths for typical spruce TMP. While the S and K curves of the cellulose sheet are almost horizontal lines, the presence of lignin in the spruce sheet diminishes the S value as soon as absorption occurs and K increases. At wavelengths shorter than 380 nm the determination of K and S becomes meaningless because of the extremely strong absorption in the UV range. Solid state reflectance analysis depends on reliable K values. We plan to build a scanning spectrophotometer with an integrating sphere that is equipped with a high-power UV light source. We should be able to analyze the UV range for spectral changes with higher accuracy.

Figure 7. S and K values of spruce TMP.

When yellowing experiments are done with the same type of pulp, K will decrease in the wavelength region of the formed chromophore absorption band (o-quinone), since the light absorption increases. S, however, will hardly change as long as the chromophore concentration is small, since the scattering coefficient is a material constant and the sheet is the same as before the radiation. K/S values at a give wavelength can be effectively used for monitoring the progress of the yellowing reaction.

The Effect of Sheet pH on the Rate of Color Reversion

One of the important parameters for the brightness of pulp sheets and the rate of brightness loss is the pH. Any chemical pretreatment prior to the mechanical fiberization of the wood chips affects the lignin, possibly by increasing its phenolic group content. Hydrolysis of ester bonds can occur during TMP production, adding additional acidic groups to the pulp. Similar effects will happen during bleaching of high-yield pulps. Therefore, we determined the rate of yellowing as a function of pH. In earlier reports we demonstrated the dependence of brightness on the pH of the sheet. Aspen and spruce TMPs have been soaked overnight in buffer solutions of pH 2 to 12. Handsheets were formed and the brightness was measured. The brightness dropped with increasing pH. Then the sheets were exposed to simulated sunlight for varying time periods. The rates of the reversion were characterized by the slopes of the plots of ΔR vs. ln t.

For a given pulp the rate of reversion almost constantly decreases with increasing pH of the sheet within the pH range 3 to 7. The rate of reversion slows down significantly as soon as the pH exceeds 9. The results are shown in Fig. 8.

We are presently investigating the pH range 9-12. We shall report on further results at the meeting. Tables 5 and 6 show the original brightness values (R_∞ 457 nm), the reflectance at the maximum of the quinone absorption band (R_∞ 422 nm), and corresponding slopes of the plots ΔR <u>vs.</u> ln t. The pH range of 3 to 7 appears to be most appropriate for the future determination and comparison of the rates of color reversion of bleached and unbleached pulps, since a linear relationship between rate and pH has been established.

Figure 8. The change of the rate of the brightness loss with the pH.

Table 5. The effect of sheet pH on the rate of light-
          induced color reversion of Aspen TMP.

pH	R(457)	$\frac{\partial(\Delta R)}{\partial(\ln t)}$	R(422)	$\frac{\partial(\Delta R)}{\partial(\ln t)}$
2	56.20	-2.26	47.87	-3.09
3	56.71	-2.50	48.24	-3.57
4	57.68	-2.36	49.38	-3.30
5	57.43	-2.39	48.93	-3.19
6	58.05	-2.24	49.70	-3.07
7	56.04	-2.28	47.90	-3.13
8	54.42	-2.21	46.48	-3.00
10	51.49	-0.92	43.49	-1.79
11	52.58	-1.81	45.11	-2.85
12	46.32	-1.28	38.45	-2.26

Table 6. The effect of sheet pH on the rate of light-
          induced color reversion of Spruce TMP.

pH	R(457)	$\frac{\partial(\Delta R)}{\partial(\ln t)}$	R(422)	$\frac{\partial(\Delta R)}{\partial(\ln t)}$
2	53.84	-3.53	44.96	-4.29
3	52.80	-3.35	44.47	-4.08
4	53.25	-3.41	43.60	-3.93
5	53.72	-3.35	44.92	-4.03
6	52.82	-3.22	43.56	-4.00
7	51.71	-3.25	42.57	-3.85
8	51.28	-3.95	42.92	-4.43
10	44.40	-1.84	35.98	-2.52
11	45.51	-2.55	37.45	-3.13
12	39.18	-1.39	30.82	-2.40

Summary Remarks on the Effect of the Material Properties
on the Rate of Color Reversion

Although softwoods and hardwoods have different lignin structures, they
produce the same chromophores at different rates. From a photochemical point of
view it is not likely that only guaiacyl structures - occurring in both lignin
types - can form quinones. The major reason for the observed different rates
seems to be the different attack of oxygen on syringyl and guaiacyl radical
structures.

We will focus on the identification of the various quinone types, the
range of their absorption bands, and the structures from which they are origi-
nating.

PART III: THEORETICAL CONSIDERATIONS ON THE RATE OF
            LIGHT-INDUCED COLOR REVERSION

The Effect of Light Flux Increase on the Rate of Reversion

Experiments in the laboratory are usually performed with high-power lamps
to simulate the outdoor experiments in a much shorter time under controllable at-
mospheric conditions. Diffuse or direct radiation is used in the experiments.
Changes are generally recorded in terms of brightness losses, that is, the drop
of the reflectance measured at an infinitely thick sheet before and after irra-
diation with light.

The questions arise, "What effect does the increase of the light flux
have on the rate of yellowing? Are we approaching the highest possible reaction
rate when we try to speed up the photoinduced reactions by increasing the fluxes
more and more? Do we light saturate a sheet?"

With these questions in mind, Stuart Lebo (Ph.D. candidate) varied the
light flux of monochromatic UV radiation (310 nm) over a wider range: 4.95 x
10^{12}, 9.63 x 10^{12}, 1.57 x 10^{13}, and 2.36 x 10^{13} photons x cm^{-2} x sec^{-1} in a set

of experiments. He monitored chromophore formation by measuring R_∞ at 410 nm
after 15, 30, 120, and 240 minutes. Figure 9 shows the greatly increasing
brightness loss when the flux is doubled and tripled. However, increasing the
flux again does not increase the rate of yellowing. This means that the last
increase of the flux has exceeded the light saturation value of the sheet.
Figure 9 shows that light saturation was just about obtained at a flux of 1.57 x
10^{13} photons x cm^{-2} x sec^{-1}. Any higher photon flux will not increase the
rate of reversion of this particular sheet.

Irradiated: 310 nm
R_∞ : 410 nm
Humidity : $12 \pm 2\%$

Figure 9. Light saturation of a spruce TMP sheet.

"What happened to the excess photons?" is the next question. Light saturation means that all possible absorbing structures interacted with a photon and are in an energetic higher state, the "excited state". The excessive amount of photons must have been absorbed by "something" without enhancing the yellowing reaction. Ajait Singh (Nuclear Energy Research Institute, Canada) suggested during a discussion of this topic that the excited state of carbonyl groups after the abstraction of a hydrogen atom from surrounding molecules (compare mechanism in Fig. 4) has a UV absorption band similar to that of the ground state but lower in intensity. Therefore, the molecule in the excited state is capable of absorbing radiation of the same wavelength as the ground state (310 nm) and uses the absorbed energy to redissociate the abstracted hydrogen atom and thereby returns to the ground state. It is ready now to absorb the next incoming UV quantum again.

The observation of light saturation should caution us against using too high a flux in our yellowing experiments, since this can falsify kinetic data. First, a heat buildup can occur that causes "thermal aging" of the sheet, which in turn affects the reflectance and brightness measurements done in the visible light region. Second, to compare yellowing rates of experiments done with different light fluxes it is necessary to relate the brightness loss to the product of time x flux, which is the total number of photons that struck the sheet surface during the time of the experiment. (This correlation is essential when the results of indoor and outdoor experiments are compared.)

At regular light fluxes a certain fraction of the incoming photons are absorbed and initiate photoreactions. The major part of the light absorbing molecules is in the ground state, however. Fluxes, close in magnitude to that of light retention, cause most of the molecule to be in the excited state and

the population of the ground state is low. This causes deviations from regular
photochemical reaction kinetic considerations.

An Approach to Develop the Kinetics for Light-induced Color Reversion

The Kubelka-Munk theory is widely used to determine the physical and
optical properties of paper. It considers the most important interactions of
light with the fiber layer structure of a sheet: reflectance, scattering, and
absorption. The chemist runs into trouble soon when he tries to follow chemical
changes which are not occurring evenly throughout the sheet. We ask, "What are
we really measuring when we measure reflectances of light exposed and nonlight
exposed sheets and compare them? Can we determine the concentration or rela-
tive concentration of a chromophore after a certain time of light exposure?"

A. M. Scallan[2] recently published an alternative approach to the Kubelka-
Munk theory. His model is based on Stoke's theory for calculating the light
reflectance of a stack of translucent layers. He considers any layer of finite
thickness as being built up of many infinitesimally thin, identical layers. He
assumes that within a fiber layer all physical and optical properties are evenly
distributed. I extend this concept of a "homogenizing process" throughout the
sheet.

I treat a sheet of paper as a homogeneous medium regarding the light
absorption and the photochemical properties. I average and distribute evenly
the inherent discontinuities in the paper: the change of refractive indices and
the consequences. Scattering and multiple reflections extend the pathway of the
light between two points to a multiple of the geometric distance. They change
the direction of a particular photon train and are the origin of the backscat-
tered light flux. The single fluxes can be summarized as light vectors in

forward and backward directions. Beer's Law can then be applied to calculate the "locally absorbed light flux" for an infinitesimally thin layer.

Absorption of light is one of the requirements for a photoinduced reaction. But not every adsorption act produces a chemical conversion. Some groups will absorb the radiation and dissipate the energy as heat; some will emit fluorescent light. From the total amount of absorbers only a fraction is assumed to be able to undergo photochemical reactions.

The amount of absorber degraded per unit time will be proportional to the concentration of light absorber and to the locally absorbed light flux. The product concentration can then be calculated. A high flux of UV radiation is applied to yellow a sheet through the formation of chromophores from lignin. The sheet surface shows the discoloration, whereas the backside appears visually unchanged.

The chromophore formation is followed by spectral reflectance analysis of the visible region. Approximately 1000 times smaller fluxes are used then. The determination of R_∞ requires at least 7 to 8 backup sheets to obtain a constant reflectance value that will not further increase when more sheets are added to the stack. It means that visible light is penetrating a stack of 5 to 6 sheets (the extinction coefficient, ε is relatively small). At wavelengths shorter than 400 nm (UV) no difference is noted if one backup sheet is used. The UV radiation does not penetrate a single sheet (ε is extremely large).

To derive the rate of yellowing of a sheet we measure the reflectivities of the sheet prior to and after exposure to (monochromatic) UV radiation for which ε is constant. We use visible light (422 or 457 nm) to determine the progress of yellowing for which ε' is constant but different from ε. Beer's Law can be applied in an analogous manner to determine the backscattered light flux.

The mathematical treatment of this model will be presented in the next report.

FUTURE WORK

The identification of the various quinonoid structures during light-induced discoloration of softwood and hardwood high-yield pulps will be undertaken, and the proposed mechanisms clarified. For this purpose we shall build a scanning UV-visible spectrophotometer with integrating sphere that is equipped with a high-power UV light source.

The suppression of yellowing by lignin modification will be demonstrated. The presence and reactivity of peroxide structures in alkali-peroxide bleached pulps will be studied as well as how they affect brightness stability.

Factors limiting the brightness of high-yield pulps will be defined.

REFERENCES

1. Evans, D. F., J. Chem. Soc., 1953. 345 p.

2. Scallan, A. M., J. Pulp Paper Sci. 11(3):J80(1985).

THE INSTITUTE OF PAPER CHEMISTRY

Werner F. W. Lonsky
Research Associate
Wood Sciences
Chemical Sciences Division

THE INSTITUTE OF PAPER CHEMISTRY

Appleton, Wisconsin

Status Report

to the

PULPING PROCESSES

PROJECT ADVISORY COMMITTEE

Project 3566

STRONG, INTACT, HIGH-YIELD FIBERS

September 6, 1985

PROJECT SUMMARY FORM

DATE: September 6, 1985

PROJECT NO. 3566: STRONG, INTACT, HIGH-YIELD FIBERS

PROJECT LEADERS: T. J. McDonough, S. Aziz

IPC Goal:

Significant increase in the yield of useful fibers.

OBJECTIVE:

Identify or develop methods of wood fiber separation which will allow the pro-
duction of separated fibers having the same physical strength and geometrical
form possessed when bound in the orignal wood matrix.

CURRENT FISCAL BUDGET: $170,000

SUMMARY OF RESULTS SINCE LAST REPORT:

Determinations of fiber strength in unpulped pine and spruce woods have been
completed. Spruce and pine wood chips have been mechanically and chemimechani-
cally treated in the Sprout-Waldron refiner and the Asplund mill. Single fiber
and handsheet testing have been partially completed.

PLANNED ACTIVITY THROUGH FISCAL 1986:

Continued investigation of the effects of fiberization variables on fiber
strength and integrity is expected to provide information on the fiberization
mechanism and allow the identification of conditions that maximize fiber
strength. The properties of artifically bonded paper made from these fibers
will be compared with those of similar paper made from unbeaten kraft fibers.
The feasibility of increasing fiber strength by selective wall component modifi-
cation will be investigated.

FUTURE ACTIVITY:

Activity in the following areas will be planned and initiated: (a) correlation
of wood properties and fiberization behavior, (b) alternative fiber separation
methods, and (c) biological pretreatment of wood.

Status Report

STRONG, INTACT, HIGH-YIELD FIBERS

OBJECTIVES

The objective of this project is to identify or develop methods of wood fiber separation which will allow the production of separated fibers having the same physical strength and geometrical form as they possessed when bound in the original wood matrix. The current short term goals are to identify the factors governing retention of fiber strength and integrity during fiber separation and to develop methods for controlling them.

INTRODUCTION

Earlier work on this project showed that the major factors preventing state-of-the-art chemimechanical pulps from being as strong as kraft pulps are fiber strength and fiber conformability. We chose the first as the target of our initial efforts in a program to develop very strong high-yield pulps. There are two reasons for concentrating on fiber strength first. One is that we have prepared pulps with yields greater than 80% in which the strength of the sheet is limited by the strength of the fibers - increased densification beyond a certain point has no effect on sheet strength. The other is that control of fiber strength will probably be achieved by some means (chemical pretreatment or adjustment of refining conditions) that will also affect conformability. If the two problems are to be attacked separately, as seems highly desirable, solving the fiber strength problem first will define the starting material for solving the conformability problem; imparting conformability to fibers that have been treated to preserve or enhance their strength may be a different problem from imparting conformability to ordinary mechanical pulp fibers. Also, since the

manner in which the wood is fiberized affects fiber length retention, fiber con-
formability and energy consumption, it was decided to direct the project toward
improving all aspects of the fiberization process, not just fiber strength
retention. This reasoning established the goals of the current project, the
initial emphasis being placed on the fiber strength aspect.

Our first report[1] described project goals and proposed activity, as
well as collection of the wood to be used and initial results on its charac-
terization. Early work on the development of a method for in situ measurement
of wood fiber strength was also described. The second report[2] described comple-
tion of work on development of the method and its application to earlywood and
latewood from well characterized locations within one of two loblolly pine trees
collected for the project.

Since the work described in the second report was completed we have
completed a similar characterization of spruce wood and have begun work on wood
fiberization and characterization of the resulting coarse pulps, especially with
regard to the strength of their fibers. Mechanical, thermomechanical and
chemithermomechanical fiberization of both pine and spruce are being investi-
gated. In addition, we have completed experiments designed to determine the
effect of sulfonation per se on the strength of the fibers in southern pine
earlywood, as well as its effect on fiber strength retention during subsequent
mechanical and chemimechanical pulping.

Another component of our effort in recent months has been a preliminary
assessment of the feasibility of initiating research at IPC on applications of
biotechnology to high-yield pulping. This assessment, which included a litera-
ture survey, was prepared for us by a private consultant, Dr. J. V. Maxham. It
is appended to this report.

ZERO-SPAN TESTING OF THIN WOOD SECTIONS

Disks taken from the butt log of a white spruce tree collected in northern Wisconsin were mapped, sawn and sectioned with a microtome to give thin sections measuring approximately 25 mm in the longitudinal direction, 20 mm in the tangential direction and 0.10-0.15 mm in the radial direction. Sections were cut from the earlywood, latewood and transition wood parts of each of three annual rings in each of 7 different radial locations in the disk. Each group of early-wood sections (from a given annual ring at a given location) consisted of about 10 specimens; fewer transition wood and latewood sections could be cut from any one annual ring, so these groups were somewhat smaller. All specimens were broken in a Pulmac zero-span tester, the load being applied in the longitudinal direction (parallel to the fiber axes). The fragments were retested to give a total of 6 measurements per section; these were averaged after discarding any obvious outliers and converted to breaking lengths with the aid of measurements of specimen dimensions and weight. The zero-span breaking lengths (ZSBL) for all specimens within a group were then averaged to give a single entry in Table 1 or 2.

Table 1. Spruce Earlywood ZSBL, km.

Location	Annual Ring		
(Angle in Degrees)	12	18	26
0	31		27
45	32		
90	33	37	35
180	32	32	36
225	30	30	30
270	32	32	33
Average		32	
Std. Dev.		2.5	

Table 2.   Spruce Latewood ZSBL, km.

Location	Annual Ring		
(Angle in Degrees)	12	18	26
0	33		
90	44	44	42
180	49	52	45
225		46	
270	54	48	54
Average		46.4	
Std. Dev.		6.1	

These tables show that, as previously observed for pine wood, latewood fibers are stronger than earlywood fibers, even when the strengths are expressed as breaking lengths, which tends to remove the effect of wall thickness. (In calculating the breaking length, the breaking load is divided by the weight of the specimen.) This may be due to the smaller proportion of presumably weak middle lamella in latewood, larger proportion of S_2 wall layer, fewer and smaller pits in the fiber wall, or differences in fibril angle. Another point of similarity with the pine results is the absence of any marked systematic variation of the strength of a given fiber type with position across or around the tree.

Table 3 compares data for spruce and pine. The spruce fibers are about 50% stronger than their pine counterparts; this probably accounts in part for the higher tensile strength of papers made from spruce pulps.

Table 3.   Summary: Wood ZSBL, km.

		Earlywood	Transition Wood	Latewood
Pine	Average	20		31
	Std. dev.	3		6
Spruce	Average	32	34	46
	Std. dev.	2	3	6

FIBER STRENGTH IN RMP AND CMP

As a first step toward understanding the effect of mechanical and chemimechanical separation on fiber strength we undertook a study[3] in which refiner mechanical pulp (RMP) and sulfonated chemimechanical pulp (SCMP) were prepared in the laboratory from characterized southern pine and the resulting fibers were subjected to single fiber load-elongation testing.

As a preliminary experiment, thin pine earlywood sections were sulfonated and tested to determine whether sulfonation itself has any effect on the strength of unseparated fibers, apart from any effect it may have on the mechanism and consequences of subsequent fiber separation in the refiner. Table 4 is typical of the data obtained and shows that the effect of sulfonation is to slightly increase section breaking length. The effect on the load bearing ability of the fiber is, however, negligible; the increase in breaking length is due to a slight yield decrease during sulfonation.

Table 4. Axial zero-span tensile strength of ultrathin wood sections, km.

	Disk 1		
Region	Before Sulfonation	After Sulfonation	Increase
1	22.1	26.2	4.1
2	23.6	24.6	1.0
3	22.7	26.2	3.5
4	24.3	24.6	0.3
5	24.7	24.8	0.1
6	22.4	24.4	2.0
7	26.4	23.4	-3.0
			+1.14

Two different samples of SCMP were prepared and compared with RMP. The first, designated SCMP1, was made under conditions known to give very strong pulps from spruce. Classification and testing of handsheets showed that this pulp, which had a yield of 98%, was actually poorer than RMP (Tables 5 and 6). Consequently, SCMP2 was prepared with NaOH added to the pretreatment liquor, in an effort to obtain improved properties. The resulting pulp had a yield of 85% and was higher in burst and tensile, but showed no tear improvement over RMP. Southern pine was not expected to perform nearly as well in the SCMP process as spruce, but this near total failure of the process to produce a better pulp than RMP was surprising.

Table 5. Bauer-McNett classification.

Pulp type	On 28-mesh, %	On 48-mesh, %	On 60-mesh, %	On 100-mesh, %	Through 100-mesh, %
RMP	16.8	24.9	10.9	9.5	37.9
SCMP1	5.9	32.2	18.4	13.8	29.7
SCMP2	10.4	45.0	8.8	18.1	17.7

Table 6. Handsheet properties.

Pulp Type	Pretreatment Yield, % o.d. wood	CS Freeness, mL	Density, g/cm^3	Burst index, $kPa \cdot m^2/g$	Tear index, $mN \cdot m^2/g$
RMP	—	110	0.26	0.54	3.84
SCMP1	98	235	0.28	0.33	2.01
SCMP2	85	325	0.33	0.63	2.97

Pulp Type	Extensional Stiffness, kN/m	Breaking Length, km	Tensile Index, Nm/g	Breaking Length, Zero-span, km
RMP	185.6	1.78	15.80	7.71
SCMP1	181.1	1.35	11.90	8.38
SCMP2	—	—	18.90	—

Fibers taken from the 28 and 48 mesh fractions of the above pulps were individually tested on the IPC load-elongation recorder. The results are laid out in Table 7. The SCMP fibers were similar to those of RMP in both breaking load and cross-sectional area, with the result that the breaking stresses of the two types of pulp were similar. This conclusion held true for both SCMP pulps. The three pulps were also similar with respect to modulus.

Table 7. Single fiber test results and their 95% confidence intervals.

Fraction (mesh size)	Pulp Type	No. of Fibers Tested	Load, g	C.S.A., um^2	Stress, kg/mm^2	El. Modulus, kg/mm^2	Strain, %
28	RMP	43	32 ± 4	582 ± 73	59 ± 8	1111 ± 274	7.2 ± 0.9
28	SCMP1	42	32 ± 4	534 ± 57	62 ± 7	1196 ± 209	6.8 ± 0.7
28	SCMP2	40	34 ± 4	588 ± 62	59 ± 4	1351 ± 161	7.8 ± 0.8
48	RMP	35	28 ± 4	557 ± 83	54 ± 6	1427 ± 200	7.0 ± 0.8
48	SCMP1	39	28 ± 5	522 ± 58	52 ± 6	1399 ± 174	6.8 ± 0.6
48	SCMP2	41	28 ± 4	591 ± 56	47 ± 4	1283 ± 148	6.3 ± 0.6
	Kraft[a] whole	127	15 ± 1	250 ± 9	62 ± 3	580 ± 30	18.3 ± 0.9

[a]Hardacker and Brezinski, Tappi 56(4):154(1973).

Fibers taken from the 48 mesh fraction were weaker than those from the 28 mesh fraction. One interpretation is that the same processes which result in fiber shortening also result in fiber weakening. Another is that fibers that become shortened during refining tend to be those that were initially weaker.

To allow a rough comparison of RMP and SCMP fiber strength with that of kraft, we retrieved from the literature data on a southern pine kraft pulp. These results, published in 1973 by Hardacker and Brezinski, are shown as the last row of entries in Table 7. The breaking stress of the kraft fibers was

about the same as we obtained for RMP and SCMP. However, closer examination of
the data showed that it was obtained as the quotient of a 50% smaller breaking
load and a 50% smaller cross-sectional area. The implication is that kraft
fibers have only half the load bearing capacity, on an individual fiber basis,
of high yield pulps such as the ones tested. This cannot be viewed as a firm
conclusion until measurements are made on a kraft pulp prepared from the same
wood supply that gave the high yield pulps.

Another interesting comparison can be made with the thin wood section
data of Table 3. Pine earlywood and latewood sections had breaking lengths of
20 and 31 km, respectively. If it is assumed that a value of 25 represents an
average for the mixture of earlywood and latewood in the chips used to make the
pulps, this value may be compared with a fiber breaking length calculated from
the single fiber data of Table 7. Approximating the fiber strengths in this
table by a value of 60 and dividing by an assumed cell wall density of 1.5 gives
a single fiber breaking length of 40. This gives rise to the seeming paradox
that the pulp fibers are stronger than the fibers in the wood from which the
pulp was made. A number of interpretations are possible. One is that the wood
zero span test data do not truly reflect fiber strength because of stress con-
centration during the test. Another is that single fiber data are censored
because the fibers tested were selected on the basis of their being long enough
to easily mount in the testing jig. Longer fibers are likely to be stronger
ones as discussed above with reference to Table 7. It seems likely that both
factors come into play; all that can be concluded now is that at least some of
the fibers in the high-yield pulps tested have strengths that are high in
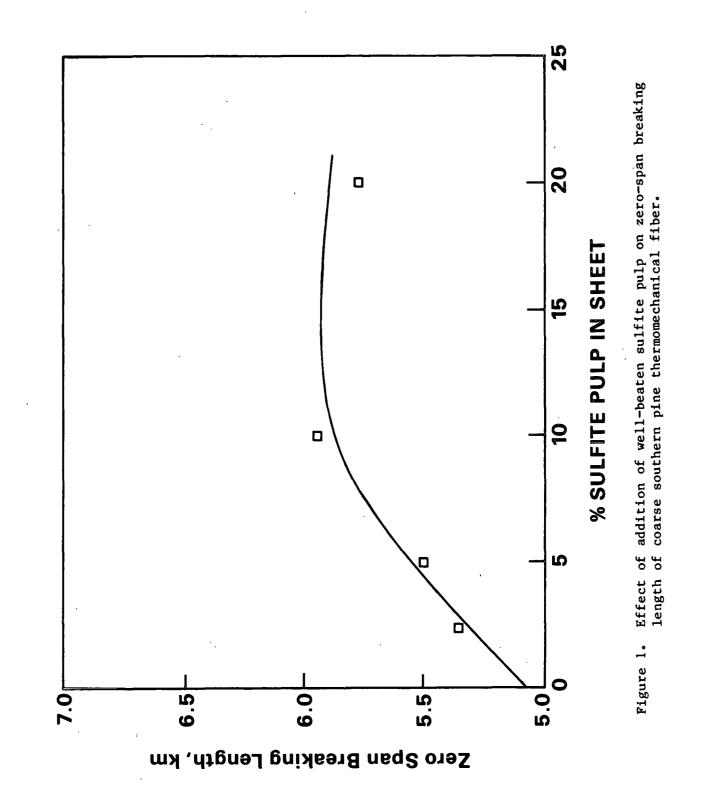relation to the strength they once possessed as part of the original wood struc-
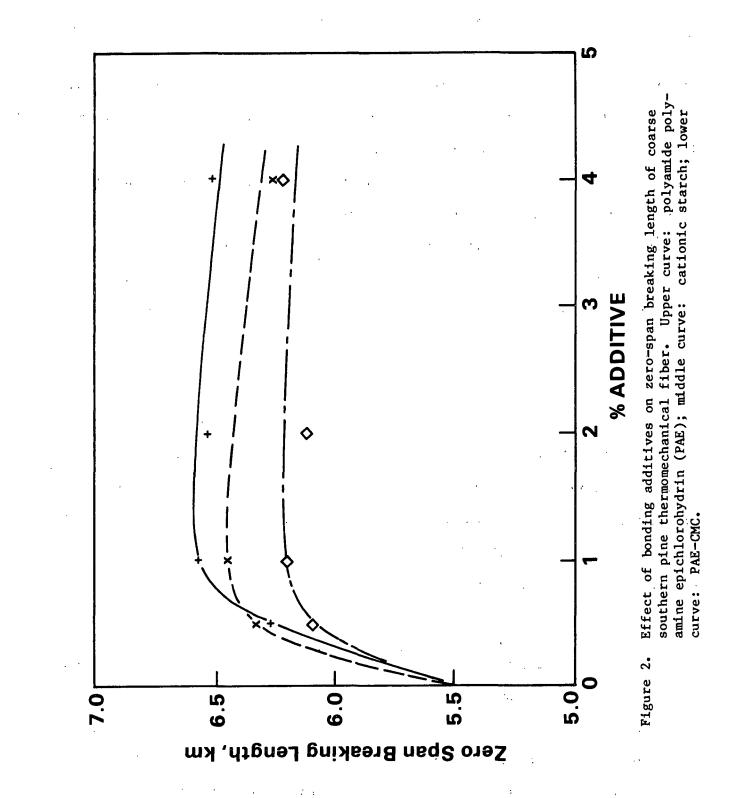ture.

FIBERIZATION AND FIBER PROPERTIES

One of our objectives is to relate fiber properties to fiberization variables. Accordingly, we have begun to experiment with the preparation and evaluation of fibers separated under various conditions. A guiding principle in this work is that the experiments should be conducted in such a way as to allow the effects of the mechanical action that results in fiber separation to be separated from the effects of mechanical action applied to the fiber after separation. Accordingly, relatively mild conditions are used and fiberization is far from complete. The resulting material is separated into fibrous and non-fibrous fractions on a 0.006 inch cut flat screen.

The first experiments were done with southern pine chips in the Asplund mill. 300 Grams of chips were charged to the mill and fiberized for 2 minutes at a temperature of 120°C and a consistency of approximately 37%. Screening yielded 140.7 grams of accepts and 136.1 grams of rejects.

A property of primary concern was the zero-span strength of the accepts, but this proved difficult to measure because of the difficulty of forming handsheets from such coarse material. This was first circumvented by adding small amounts of well beaten sulfite pulp as a bonding agent, which gave the results shown in Fig. 1. In later experiments, other bonding additives were used to obtain the results shown in Fig. 2. In later experiments, improvements in technique, including the use of sailcloth as a forming medium, resulted in our being able to form sheets without bonding additives. These sheets had breaking lengths as high as 7.0 km. The conclusion was that the zero-span breaking length of sheets of the fibrous material was at least 7.0 km. For comparison with the wood section and single fiber data, this may be multiplied by 8/3 to correct for the random orientation of the fibers in the sheet, giving a value of

Figure 1. Effect of addition of well-beaten sulfite pulp on zero-span breaking
length of coarse southern pine thermomechanical fiber.

Figure 2.   Effect of bonding additives on zero-span breaking length of coarse
southern pine thermomechanical fiber. Upper curve: polyamide poly-
amine epichlorohydrin (PAE); middle curve: cationic starch; lower
curve: PAE-CMC.

18.7. This is much lower than the value of 40 km inferred from the single fiber data (which itself is probably too high to be representative of the average strength of all the fibers because of the selection process described above) and moderately lower than the average value of 25 from the thin wood section testing (which may be low, owing to stress concentration effects). It was therefore concluded that either the fibers were being weakened during fiberization, that falsely low zero-span data were being obtained, or both. Likely causes of low zero-span results are insufficient bonding (which results in sensitivity of the result to slippage under the jaws of the tester and minor deviations from true zero-span) and poor formation (which results in uneven clamping and stress concentration).

Figure 3 consists of two light micrographs of specimens which were broken in the zero-span test, showing the rupture line. They suggest that both problems referred to above were present. The failure line is not straight, indicating that some fibers were pulled out and not broken. In addition, formation was very poor, as shown by the existence of many large open areas and bundles of parallel fibers. In the vicinity of the failure line these bundles tended to be oriented parallel to it, suggesting that the more nearly perpendicular ones had been pulled out.

In an attempt to solve the formation problem, samples of accepted fiber were processed for various lengths of time in the British disintegrator. It was hoped that the mechanical action experienced by the fiber bundles in the mixer would be sufficiently vigorous to separate them and sufficiently mild to have little or no effect on the fiber strength. Tables 8 and 9 show the effect of this treatment on the fiber classification and properties of handsheets made from this material. Changes in both categories were slight; there was a decrease in

Figure 3. Fiber rupture during zero-span testing.

the 2 coarse fractions and an increase in the middle fraction; there was also a decrease in freeness and increases in formation index and scattering coefficient. A slight improvement in formation is observed after a sixty minute beating as shown by two light micrographs in Fig. 4.

Table 8. Bauer McNett Classification of Asplund pine fibers.

Disintegration Time	On 14 mesh, %	On 28 mesh, %	On 48 mesh, %	On 100 mesh, %	Through 100 mesh, %
0	14	43	25.3	11.7	6
30	13.9	44.7	26.6	11.7	3.1
60	13	40	24.4	10.5	12.1
120	10.7	42.7	27.7	12.1	6.8
180	--	--	--	--	--

Table 9. Handsheet properties of Asplund pine fibers.

Disintegration, Time, min	Freeness, CSF	Zero-span, km	Formation, Thwing	Scattering Coefficient, cm^2/g
0	770	6.8	18.4	169.9
30	770	6.46	21.4	176.0
60	750	6.98	21.9	181.2
120	730	7.03	19.1	164.4
180	625	6.63	23.3	187.6

Shive counts were also done on samples of fiber which had been agitated for various periods in the disintegrator. Figure 5 shows how they responded. The total number of shives decreased by about 40% during the first hour and changed little thereafter. On the other hand, the larger shives (consisting of 6 or more fibers) were not affected, as shown in Fig. 5.

The problem of improving formation and bonding in coarse pine fiber sheets without changing yield or fiber mechanical properties remains. It was set aside so that we could proceed to obtain some information on the behavior of spruce fibers, which are generally easier to deal with than the thicker-walled,

Figure 4. Effect of beating time on the formation of high-yield pine fibers.

more resinous pine fibers. Once again, the objective was to determine the

effect of fiber separation under various conditions on fiber properties, with

emphasis on fiber strength and, as far as possible to draw inferences concerning

the mechanism of fiber separation.

$\square$ <6 fibers (9 obs)   + >6 fibers (9 obs)
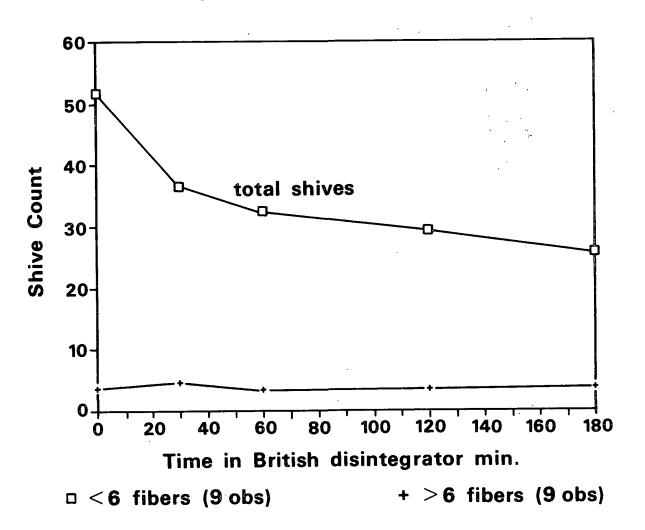
Figure 5. Effect of beating time in the British disintegrator on fiber bundles.

The experimental design adopted for this work was a full factorial

comprising three levels of fiberization temperature (80, 120 and 160°C), three

levels of fiberization time (1, 2 and 4 minutes), and two levels of sulfonation

prior to fiberization (none and 30 min. at 140°C with 120 g/L Na_2SO_3).

To date, the experiments at 120°C with no sulfonation have been completed. Table 10 summarizes classification data for the three pulps. Perhaps the most interesting feature of the data is their constancy with increasing fiberization time. This suggests that the size distribution of the comminuted material is determined at the time of its separation from the wood chips and is not changed thereafter.

Table 10. Bauer McNett classification of spruce wood chips.

Run No.	Fiberization Time, min	Accepts, %	On 14 mesh, %	On 28 mesh, %	On 48 mesh, %	On 100 mesh, %	Through 100 mesh, %
4	1	37.4	23.7	32.9	17.8	7.1	18.5
5	2	48.8	22.4	32.7	18.1	7.1	19.7
6	4	63.4	24.4	32.6	18.3	7.9	19.7

Handsheet properties after various disintegration times are shown in Table 11. Comparisons with the pine data of Table 9 show that the spruce fibers are more readily refined by the action of the disintegrator and exhibit higher zero-span strength. An interesting feature is that the maximum zero-span tensile strength increases with increasing fiberization time, presumably as a result of increased bonding. Nevertheless, this observation suggests that fibers, once separated, do not undergo strength reduction as a result of continued mechanical action.

The highest zero-span value of 9.5, when multiplied by 8/3 to correct for the random fiber orientation, gives 25.3. This value, although higher than the corresponding value of 18.7 for pine, is considerably lower than that to be expected on the basis of the thin wood section measurements (about 39). Further work is needed to determine the extent to which the difference can be attributed

to deficiencies in the zero-span test as an indicator of fiber strength and to find ways of removing those deficiencies.

Table 11. Handsheet properties of spruce refined pulp.

Run No.	Fiber-ization Time, min	Disinte-gration Time, min	C.S. Free-ness, mL	Zero-span, km	Tensile Index, Nm/g	Burst Index, kPa·m²/g	Tear Factor	Stiffness, lb/inch	Scatter-ing Coeff., cm²/g
4	1	0	760	6.81	1.92	0.00	16.9	112	219.39
		60	725	7.86	8.31	0.37	42.9	358	244.78
		120	670	8.47	12.37	0.62	46.9	398	258.08
		180	590	8.30	15.62	0.94	52.9	425	271.90
5	2	0	750	7.31	3.46	0.00	30.2	148	243.49
		60	680	8.52	10.78	0.57	44.4	349	268.08
		120	660	8.36	14.52	0.76	50.0	384	279.32
		180	550	8.75	19.72	1.18	63.7	449	295.64
6	4	0	730	7.56	4.77	0.00	33.3	221	255.43
		60	660	8.56	15.89	0.79	48.0	493	286.30
		120	620	8.31	18.63	1.08	59.3	571	295.34
		180	520	9.46	23.50	1.61	73.5	667	316.99

In the meantime, direct determination of fiber strength, a reliable but tedious method, will be used. The results of such a determination are contained in Table 12. Comparison with the pine data of Table 7 show that the load bearing ability of the spruce fibers is much lower, but so is their cross-sectional area. The result is that the breaking stresses of fibers of the two species are remarkably similar. This is a somewhat unexpected result in view of the decidedly superior strength of the spruce wood sections, and may indicate that spruce fiber strength is reduced in the process of separation and that this occurs to a greater extent than in the case of pine.

Table 12. Single fiber analysis of sample No. 6.

Pulp Type	No. of Fibers	Load, g	C.S.A., μm²	Stress, kg/mm²	El. Modulus, kg/mm²	Strain, %
Spruce	49	11.5 ± 0.8	231 ± 16	54 ± 4	1014 ± 97	7.5 ± 0.4
Pine RMP (Table 7)	43	32 ± 4	582 ± 73	59 ± 8	1111 ± 274	7.2 ± 0.9

CONCLUSIONS

1. Latewood sections of both spruce and pine have about 50% higher longitudinal
    tensile strength than the corresponding earlywood sections. Spruce sections
    are 30-50% stronger than pine sections. It may be inferred that the same
    conclusions hold true for the corresponding fibers.

2. Sulfonation of southern pine earlywood sections does not affect their load
    bearing ability. This implies that sulfonation does not affect fiber
    strength. Fiberization of sulfonated southern pine chips gives fibers
    having the same strength as fibers separated from unsulfonated chips.

3. In the high-yield pine pulps examined, fibers from the 48 mesh fraction were
    weaker than those from the 28 mesh fraction. This may indicate that reduc-
    tions in fiber length are accompanied by reductions in fiber strength, or
    that initially weaker fibers are more likely to be shortened, or both.

4. Sulfonated chemimechanical pulp from southern pine has low strength, showing
    little or no superiority over the corresponding refiner mechanical pulp.

5. Comparison of high-yield pine pulp single fiber properties with literature
    data for a pine kraft pulp leads to the tentative conclusion that high-yield
    fibers have twice the load bearing capacity of kraft fibers.

6. Single fibers from the 28 and 48 mesh fractions of high-yield pine pulps
    have a higher average breaking length than the wood from which the pulps
    were made. This is probably the combined result of stress concentrations
    during the zero-span testing of the wood and the likely superiority of the
    strengths of the long fibers to those of the remaining pulp elements.

7. Sheets of coarse fibrous material made from southern pine have a zero-span
    breaking length of about 7 km. This corresponds to a single fiber breaking
    length of about 19 km, which may be compared to the value of 25 expected on

the basis of wood section test results. The difference is due to a combination of fiber damage associated with fiberization and poor bonding and formation in the zero-span sheets.

8. Single fibers from a coarse spruce mechanical pulp have a breaking length which is about the same as that of the wood from which it was made. This differs from the pine result in a way that suggests that spruce fibers are more susceptible to strength loss during fiberization.

PLANS

1. Complete statistical analysis of existing data and write two membership reports and two publications.

2. Complete the study of effects of fiberization variables on spruce fiber properties.

3. Improve quality of zero-span sheets made from coarse fiber; concentrate on removal of fiber bundles. Attempt to establish an unequivocal relationship between zero-span strength and average single fiber strength.

4. Extend single fiber properties measurement to fiber fragments passing through 48 mesh screen.

5. Determine effect of fiberization conditions on southern pine fiber properties.

6. Determine maximum sheet strength currently achievable by using bonding agents with strong high-yield fibers of the types already produced.

7. Investigate feasibility of relating thin wood section zero-span tensile strength to average single fiber strength by mathematically modelling an assemblage of parallel fibers undergoing tensile failure.

8. Assess usefulness of mathematical models of mechanical behavior of single fibers as a means of setting goals for research on chemical modification of the fiber wall.

9. Conduct initial experiments to evaluate feasibility of improving fiber properties by selective wall component modification.

10. Plan and initiate activity in the areas of (a) correlation of wood properties and fiberization behavior, (b) alternative fiber separation methods, and (c) biological pretreatment of wood. Collaborate with Engineering Division to determine effects of impulse drying on properties of sheets made from coarse high-yield fiber.

ACKNOWLEDGMENTS

The skillful experimental assistance of Kristie Rankin, Cecilia Nordberg, Harry Grady and members of the Paper Testing and Fiber Science Groups is gratefully acknowledged.

REFERENCES

1. Status Report, Project 3566, February, 1984.

2. Status Report, Project 3566, October, 1984.

3. Nordberg, C. M., Independent Studies Report, May 31, 1985.

THE INSTITUTE OF PAPER CHEMISTRY

Thomas J. McDonough
Group Leader, Pulping/Bleaching
Pulping Sciences
Chemical Sciences Division

Salman Aziz
Supervisor, Pulp Laboratory
Pulping Sciences
Chemical Sciences Division

APPENDIX

LITERATURE SEARCH ON APPLICATIONS OF BIOTECHNOLOGY
TO HIGH YIELD PULPING PROCESSES

A Report Submitted To:

Dr. Earl Malcolm, Director
Dr. Tom McDonough, Group Leader
Chemical Sciences Division
The Institute of Paper Chemistry
P.O. Box 1039
Appleton, WI 54912

By:

J. V. Maxham, Ph.D., P.E.

Consultant
33 Tracy Court
Appleton, WI 54915
(414)734-2506

May 3, 1985

EXECUTIVE SUMMARY

Biological pulping (retting) and enzymatic pulping of nonwoody plant materials are practical means to produce papermaking fibers. The literature articles reviewed showed that retting times can be as little as 4 days and enzymatic pulping times as little as 4 hours. Enzymatic pulping times, therefore, were not much longer than chemical pulping times. In some instances, the biological/enzymatic pulps produced had a higher yield than a chemical pulp and possessed similar, sometimes superior, mechanical and physical properties.

Experimental results reported in the literature where microorganisms (principally white-rot fungi) were grown on wood chips or on coarse mechanical pulp were not encouraging. Pulping times were at least two weeks and therefore excessive. Microbial attack was sometimes beneficial in substantially increasing the water retention value of the pulp or reducing the refining energy input to achieve a given freeness level or strength index. Microbial pulping also resulted in little wood weight loss, typically less than 2%.

Several different microbial species (both bacteria and fungi) have been isolated that possess wood delignifying capabilities. The technology now exists to splice the DNA segments responsible for delignifying enzyme replication from these organisms into the fast growing E. coli. A genetically engineered E. coli could, in theory, produce the enzyme in substantial quantities at a reasonable price. One researcher has in fact successfully cloned a delignifying enzyme gene into an E. coli.

This biotechnological breakthrough suggests that concentrated delignifying enzyme solutions may soon be available for experimental purposes. Pulp and Paper Industry interest in enzymatic pulping will encourage the high tech biotechnology firms to produce experimental pulping enzyme solutions. IPC would be

an ideal place to evaluate such enzyme products. IPC, therefore, should consider initiation of a modest biopulping research project in conjunction with the High Yield Pulping project. The goal of the biopulping project would be to produce a high yield and high strength pulp with minimal energy input by digesting wood chips or coarse mechanical pulp with delignifying enzyme solutions.

The areas of enzymatic wood pulping and enzymatic modification of wood pulp appear to be very promising. If the experience with enzymatic pulping of nonwood plant materials can be extrapolated to wood, it is expected that the enzymatic pulping rate will be comparable to chemical pulping rates. Enzymatic pulping yields are expected to be higher than chemical pulping yields with no deterioration of mechanical and strength properties. This is because enzymatic reactions are usually very specific: only certain bonds in the lignin molecule would be cleaved with little or no attack on the cellulose and hemicellulose. This would be done with very little enzymatic pulping energy input since the pulping would probably be carried out at a temperature below 40°C.

Because enzymatic pulping promises to result in substantial energy savings, a logical source of outside funding for a biopulping project would be the Department of Energy.

INTRODUCTION

The principal objective of the High Yield Pulping project at IPC is to research methods that produce pulps with high yield, strength, conformability, and brightness, while minimizing the pulping energy input. The current emphasis of the High Yield Pulping project are pulping techniques that result in a high yield and high strength pulp. Producing a pulp with both high yield and strength is a difficult proposition. Conventional pulping processes that produce pulp

with high yield (e.g., groundwood pulping) invariably result in a low strength
pulp. The converse of this is true since a low yield pulping process (e.g.,
Kraft and sulfite chemical pulping) normally results in a high strength pulp.
Chemimechanical processes produce pulps of intermediate yield and strength. It
appears that the more lignin contained in the pulp, the lower the pulp strength.

A pulping process that produces a pulp with both high yield and
strength requires that the middle lamella lignin be degraded only slightly;
enough to allow easy separation of the fibers in a mechanical defiberizing pro-
cess. Once separated, the lignin containing fibers must be modified to allow
the fibers to collapse to create high fiber contact area.

It is of interest to conduct a literature search of biotechnological
wood pulping techniques. Microorganisms produce enzymes that catalyze specific
biochemical reactions. By isolating microbial delignifying enzymes that break
specific lignin bonds, it might be possible to first digest wood chips with a
delignifying enzyme solution then separate the fibers essentially intact in a
mechanical process with little lignin removal and low energy input. Other enzy-
mes could be used to treat the defiberized pulp to modify fiber surface proper-
ties. The possibilities of biological/enzymatic pulping are intriguing and
should be investigated.

This report begins by first reviewing current applications of bio-
technology to the Pulp and Paper Industry. These applications include the
retting and enzymatic pulping of non-woody plant materials, starch enzymatic
conversion in papermaking, and biological wastewater treatment. Research into
the biological pulping of wood is then reviewed. Though the biological/
enzymatic pulping of wood is in the R&D stage with little promise to become com-
mercially viable in the near future, recent biotechnological breakthroughs

ensure the eventual introduction of biotechnological pulping and bleaching pro-

cesses to the Pulp and Paper Industry.

CURRENT APPLICATIONS OF BIOTECHNOLOGY
TO THE PULP AND PAPER INDUSTRY

Retting and Enzymatic Pulping of Nonwoody Plant Tissue

Retting has been used for several thousand years to free cellulose

fibers from nonwoody plant tissue. Stanier et al.[1] gives a brief description of

this ancient process first used to free the bast fibers from flax and hemp.

Plant stems are first immersed in vats of water. As they become waterlogged,

anaerobic butyric acid bacteria develop which rapidly attack the plant pectin

material that cements the bast fibers together. Once the stem structure is suf-

ficiently loosened, the retting process is halted. Unduly prolonging the

retting process results in the formation of the cellulose fermenting bacteria

which will destroy the bast fibers.

Retting and enzymatic processes are used today in Japan to pulp non-

woody plant tissue. Several recent articles by Kobayashi and Matsuo[2-7] of the

Government Industrial Research Institute, Shikoku, Japan were reviewed that

relate to this subject. One of the articles[2] looked at the enzymatic pulping of

decorticated pineapple leaf fiber. Four commercially available enzyme solutions

were evaluated. Two of the enzyme solutions mainly attacked pectin (pectinases);

the other two enzyme solutions mainly attacked cellulose (cellulases). The

enzymatic pulping temperature was 37°C, enzyme concentration was 0.1%, leaf con-

sistency was 3.0%, and the pH was in the range of 2.0-5.0. Pulping times of 3,

5, and 24 hours were investigated. A chemical pulp was also prepared to serve

as a comparison. The chemical pulp was made by cooking the pineapple leaf fiber

in a autoclave containing NaOH solution at 150°C for 1 hour at a liquor to fiber

ratio of 7 and alkali ratio of 0.15. The pulping yields of the pectinase pulps were in the range of 72.8-87.8% and compared favorably with the chemical pulp yield of 74.3%. The cellulase pulp yields were much lower (46.0-78.0%). In general, the physical properties of handsheets of the enzymatic pulps were inferior to that of the chemical pulp. At a given freeness level, the bulk density of the pectinase pulps were about the same as the chemical pulp though the breaking length was about one-half that of the chemical pulp. The cellulase pulps had lower bulk densities and breaking lengths than either the chemical or pectinase pulps. The enzymatic pulps had lower tear and burst factors than the chemical pulp.

In another article,[3] Kobayashi and Matsuo looked at the enzymatic pulping of mitsumata bast fiber by two commercially available pectinase solutions. Mitsumata contained considerably more pectic substance (8.6-14.8%) than pineapple leaf fiber (1.2%) and therefore it was expected that the two pectinase solutions would be more successful in pulping mitsumata than pineapple leaf fiber. Pulping conditions were similar to that mentioned above. The pectinase pulp yields were in the range of 66-82% and compared favorably with the chemical pulp yield of 53%. The highest yields were obtained when the enzyme concentration was low (0.025%) and pulping time was low (4 hours). Both the average fiber length and single fiber strength of one of the pectinase pulps was slightly higher than the chemical pulp. The zero-span tensile strength, however, of the pectinase pulps were somewhat lower than the chemical pulp. The physical properties of handsheets were measured. The bulk density of the enzymatic pulps was about the same as the chemical pulp but the breaking length was 18-30% less. The tear factor of the enzymatic pulps were superior to the chemical pulp. The burst factor of the enzymatic pulps were inferior to the chemical pulp when

enzyme concentration was low (0.025-.10%) but about the same at high enzyme con-
centrations (1.0%). The folding endurance of the chemical pulp was superior to
the enzymatic pulp which was attributed to the higher lignin content of the
enzymatic pulps. A key point of this article is the fact that the mitsumata was
sufficiently pulped enzymatically in 24 hours at a low enzyme concentration
(0.025%). Increasing the enzyme concentration up to 1.0% reduced the pulping
time to as low as 4 hours.

Two articles[4,5] by Kobayashi and Matsuo gave results in the enzymatic
pulping of mitsumata under alkaline conditions. Alkaline conditions cause
swelling of the bast thereby increasing the enzyme penetration rate. Alkaline
tolerant pectolytic enzyme solutions were obtained by growing bacterial cultures
of Erwinia and Streptomyces. Enzymatic pulps with nearly the same quality of
chemical pulp were made in only 5-7 hours with the enzyme solutions of two
species of Erwinia. The pulping temperature for the Erwinia species was only
30°C. The yields were not given. Though mitsumata was successfully pulped with
Erwinia enzyme solutions, Cuban and Thai kenaf were not effectively pulped.
This was attributed to the much higher lignin content of kenaf compared to mit-
sumata.

Kobayashi et al.[6] gave results in the alkaline enzymatic pulping of
kozo (paper mulberry) using an enzyme solution of Erwinia. Pulping was carried
out at 30°C for up to 24 hours. The enzymatic pulp papers proved to be superior
to the chemical pulp papers in many respects. The enzymatic pulp paper had
greater homogeniety in basis weight, better dynamic printing smoothness and
superior brightness. The zero-span tensile strength, breaking length, tear fac-
tor, and folding endurance of enzymatic pulp fibers were about the same as the
chemical pulp.

Yoshihara and Kobayashi[7] examined the retting of mitsumata under alkaline conditions using a Bacillus. The optimum concentration of sodium carbonate was 1.0-1.5% yielding an initial pH of 10.1-10.3. The retting temperature was 30°C. Under optimum conditions, the retting was completed in about 4 days with an overall pulp yield of approximately 70%. This yield was about 10% higher than the chemical pulp yield. The physical strength properties of the paper sheets made from the retted pulp were comparable, and in some cases superior to those of the paper made from chemical pulp. The retted sheets exhibited good formation and the surface of the sheets was milder and softer than the chemical pulp sheets.

Retting and enzymatic pulping are similar in the respect that enzymes secreted by microorganisms are used to attack the plant material (e.g., pectin) that cements the cellulose fibers together. In retting, the microorganisms are allowed to grow directly on the plant material. Retting times are quite long due to the fact that substantial time is necessary to grow the biomass from the initial inoculum. Increasing the inoculum amount should substantially decrease retting time. Probably 1-2 days would be sufficient. In enzymatic pulping, only enzyme solutions are allowed to contact the plant materials. The results contained in the literature articles reviewed, show that pulping times are generally less than a day and as low as a few hours. This makes enzymatic pulping times for nonwoody plant materials about the same as for chemical pulping.

Enzymatic pulping has a distinct energy advantage compared to chemical pulping since the pulping is carried out at moderate temperatures. Enzymatic pulp yields tend to be higher than chemical pulp yields and the physical properties of enzymatic pulp handsheets are sometimes superior to those of chemical pulp. It is critical, however, to select the proper enzyme(s) to pulp the raw

material. A particular enzyme or enzyme solution that works well for one par-
ticular raw material will not work well on another.

It is worthy to notice that enzyme solutions were prepared in some
cases by growing wild type bacterial strains in pure culture then separating the
cell suspension from the culture fluid. The culture fluid was then used as the
enzymatic pulping solution. The first task in this process is to isolate pro-
mising bacterial cultures from the environment. Yoshihara and Kobayashi[7] iso-
lated about 800 bacterial strains from soil, sewage, and decomposed manure
before selecting the few strains used in their retting experiments. In this
case, the strains had to be alkaline tolerant since alkaline conditions were
favorable to speeding up the retting process. The next task in enzymatic
pulping is to grow the bacterial stain in pure culture under conditions that
optimize the production of enzyme. The process can either be batch or con-
tinuous. Separating the cells from the culture fluid may not be necessary. The
enzyme solution could be concentrated if neccessary by employing membrane
separation technology.

The tasks associated with producing enzyme solutions are well established
and are known to the microbiologist and biochemical engineer. The key question
is whether the economics of enzymatic pulping compare favorably with chemical
pulping. The answer is probably yes if the enzymatic pulping yield is higher
than the chemical pulping yield and the properties of the two pulps are similar.
However, the cost of producing the enzyme will be high. This cost is ameliorated
by the fact that little enzyme is required for pulping and that the enzyme can
be reused. The low energy requirement of enzymatic pulping will also help keep
total pulping costs down.

Enzyme Conversion of Starch in the Paper Mill

Starch has been used for many years in papermaking as a surface sizing or a coating binder. However, in order to use starch for this purpose its viscosity must be reduced. Either a thermochemical or enzymatic process can be used to reduce starch viscosity. Mayatt[8] reviewed the enzymatic processes used to convert starch as currently practiced. Enzymatic conversion of starch was first introduced into the Paper Industry in the early 1960's. It is estimated that 30% of all starch used is now enzyme converted.

Amylases are the enzymes responsible for starch conversion and are produced by both bacteria and fungi. Amylase solutions are available commercially and can be obtained to fit a specific application. A paper mill, in general, does not culture its own bacteria or fungi to produce amylase but purchases it from a supplier. Mayatt claims that the payback period in converting from a thermochemical to enzymatic starch conversion system can be as short as a few months.

Typically very little enzyme solution is required to convert starch. Mayatt gives a typical enzyme conversion program where 50 mL of a fungal enzyme solution is added to 1000 kg of potato starch and 4000 liters of water. This shows that an enzyme solution can have a very high activity.

The enzymatic conversion of starch is an example showing that enzymatic processes are competitive with thermochemical processes once enzymes with the right properties are available. It can be speculated that once enzymatic pulping processes become developed, the Pulp Mill would probably purchase the enzyme solutions from an outside supplier rather than make its own enzyme solutions from scratch by culturing microorganisms.

Biological Wastewater Treatment

The most prevalent application of biotechnology in the Pulp and Paper industry is the treatment of wastewaters for environmental protection. Biological treatment processes such as lagoons and activated sludge processes are used to remove soluble organic materials from wastewaters after settleable solids are first removed by sedimentation. It is significant that physical-chemical processes are not economical in comparison to biological processes in wastewater treatment. This is in spite of the fact that the physical size of a biological process is often much larger than a physical-chemical process that can accomplish the same task. The advantage of the biological process lies in its simplicity of design and operation, low maintenance requirements, and tolerance (within limits) of variations of wastewater flow and composition. It can be speculated that a biological pulping process may enjoy many of these same advantages but would have a rather large physical volume.

Other Potential Applications

A potential biotechnology application is the pulping of wood, the major raw material by far to produce paper products. The remainder of this report will be devoted to this subject. Other potential applications include the biological/enzymatic bleaching of pulp and treatment of effluents containing lignin-derived wastes. The lignin wastes would either be destroyed by a biological/enzymatic process or converted to useful chemicals.

BIOLOGICAL AND ENZYMATIC PULPING OF WOOD

Introduction

It is conceivable that a biological or enzymatic pulping process could be developed for wood that would be similiar in principle to the retting and enzymatic pulping processes described previously for nonwoody plant materials.

Zaborsky[9] summarized the incentives to develop a biological/enzymatic delignification process and the drawbacks associated with present chemical/physical delignificaton processes. These are presented in Table 1.

Table 1.

Drawbacks of Present Delignification Processes (Chemical, Physical)

      Energy intensive

      Environmental incompatibility

      Moderate resource utilization (conversion yield)

      High consumption of chemicals

      Sulfur-containing lignin products

Incentives of a Biological/Enzymatic Delignification Process

      High selectivity and activity of enzymes

      Low conventional energy requirement

      Environmental compatibility

      Renewable catalysts

      Nonsulfur-containing lignin products

Presumedly, a definate advantage that a chemical delignification process would have over a biological/enzymatic process would be a high reaction rate. The high temperature and harsh chemical environment of a Kraft or sulfite process serves to delignify wood at a relatively rapid rate. A biological/enzymatic pulping process would probably be conducted at a temperature in the range of 25-40°C though thermophilic microorganisms exist that can grow at temperatures up to around 70°C. The enzymes produced by these organisms are also tolerant of high temperatures. It is likely, however, that the biological/enzymatic pulping would proceed at a much lower rate than a chemical

pulping process due mainly to the lower temperature. This means that a biological/enzymatic pulping reactor would be very large in comparison to a chemical pulping reactor. Nevertheless, the biological/enzymatic reactor may be less expensive than the chemical pulping reactor because the low temperature and pressure pulping would result in a simple reactor design and relatively inexpensive materials of construction.

The fact that enzymatic pulping of nonwoody plant materials proceeds at a rate similar to chemical pulping may be evidence that a enzymatic pulping process for wood will not be much slower than a chemical pulping process. The key to the successful enzymatic pulping of wood is the production of delignifying enzyme solutions that have a high activity toward the wood pulped. These enzyme solutions need not be produced at the mill but could be purchased from a supplier.

In the biological/enzymatic pulping of wood, it would be essential to first debark and chip the roundwood as done conventionally. At this point several different biological/enzymatic pulping schemes can be imagined. For example the biological/enzymatic pulping could proceed in an existing chip pile by sprinkling the top of the chip pile with a biological/enzyme solution. The solution would trickle through the pile and be collected at the bottom. A portion of the solution would be wasted with the remainder recycled and supplemented with fresh solution. Unfortunately, it would be difficult in this approach to ensure uniform contact of the chips with the solution and to prevent undesirable microbial growth from occuring. It would be better to have a chip tower dedicated to the purpose of contacting the microbial/enzyme solution with the chips. Steaming the chips prior to introducing them to the tower would sterilize the chips preventing undesirable microbial growth from occurring and allowing better penetration of the biological/enzyme solution.

It is also possible to carry out the biological/enzymatic pulping in vessels that allow the chips to be completely submerged in the biological/enzyme solution. Hopefully, the reaction would proceed quickly enough to allow the use of existing chemical pulping vessels. In biological pulping, the vessel would need to be aerated since the delignification reaction is oxidative.

Whether a chip tower or submerged vessel is used, the options available in biological/enzymatic pulping are: 1. Grow the microorganisms directly on the chips from an initial innoculum. 2. Grow the microorganisms in a separate process and contact the chips with the culture fluid that contains the appropriate enzymes. 3. Purchase concentrated enzyme solutions and make-up the pulping solution. Later on when the literature on biological wood pulping is reviewed, it will be seen that the main approach has been to grow the organisms directly on the wood chips. This is probably the least desirable of the three approaches. One reason is that the wood pulp will be contaminated with biomass that probably will not enhance the pulp quality. The pulping process rate will probably be slower as evidenced by the difference in rates between retting and enzymatic pulping of nonwoody plant materials. However, the enzymatic delignification of wood is a complex process requiring several different enzymes. Developing the appropriate enzyme solutions will be a difficult task. Comparing approaches 2 and 3, a mill would probably opt for purchasing the enzyme solution if the price is right. However, waste streams exist in an integated mill (e.g., excess whitewater) that contains nutrients needed to grow a microbial culture. These waste streams could conceiveably be utilized as a "free" raw material to grow the microbial suspensions. Pure culture conditions though need to be maintained making utilization of the waste materials difficult. Probably the glucose and other nutrients needed to grow the microorganisms would be purchased or made from wood fiber by hydrolysis.

Biological/enzymatic pulping would require a mill to hire a substantial staff competent in microbiology and biochemical engineering unless the enzyme solutions could be purchased from a supplier. It is therefore likely that the biological/enzymatic pulping development work will be left to the high tech biotechnology firms who would later profit by selling the appropriate enzyme solutions. In this regard there has been many significant advances in the biotechnology area. Now enzymes and other complex biomolecules can be produced cheaply and in quantity by using gene splicing techniques. In this technique, the DNA segment in a gene that replicates the biomolecule, is spliced out and inserted in the DNA of a fast growing bacteria (e.g., Escherichia coli, a human intestial organism). The DNA segment can come from any organism, even a human being. Genentech successfully markets a genetically engineered product.[40] It is human insulin derived by splicing a human insulin gene into E. coli and then culturing the microorganism. There was a report in Chemical and Engineering News[10] about a microbiologist at Louisiana State University, V. R. Srinivasan, that spliced a lignin degrading enzyme into E. coli. The enzyme cleaves both alkyl and aryl-aryl ether linkages in lignin. The enzyme can supposedly degrade lignin in two hours. This appears to be a significant breakthrough that may lead to the commercialization of biochemical pulping.

The biological/enzymatic pulping could be conducted to achieve nearly complete delignification or only partial delignification. For high yield pulping only partial delignification would be required. Steaming and presoaking the chips in alkaline solution may be beneficial in speeding up the biological/ enzymatic degradation. The hoped for advantage of an enzymatic degradation compared to a chemical degradation would be that only specific lignin bonds would be broken allowing the fibers to be easily separated without substantial loss of

the hemicellulose and cellulose and with little defiberization energy input. An

enzymatic pulping process would be very similar to conventional chemimechanical

pulping processes.

After defiberizing and washing the pulp, enzyme solutions could be used

to alter the fiber surface properties before refining. Bleaching with enzymes

is also a possibility.

Currently biological/enzymatic wood pulping technology is in a nascent

stage. Many investigators, however, have performed research in this area and

the results of their studies will now be reviewed.

Biological Wood Pulping Literature

Karl-Erik Eriksson of the Swedish Forest Products Research Laboratory

in Stockholm, Sweden is one of the world's leading researchers in the area of

biological delignification of wood. Eriksson and co-workers have published a

number of articles[11-15] relating to the subject of biological pulping of wood.

In a paper presented at the 1976 Weyerhaeuser Biological Delignification

Symposium,[11] Eriksson reported results obtained in treatment of pine chips for

one month with a cellulase-less mutant of Sporotrichum pulverulentum, a white-

rot fungus. About two percent of the lignin was removed in this time period.

The breaking length, burst index, and tear index of a mechanical pulp made from

fungal treated pine chips was 20 to 30% higher than a mechanical pulp made from

untreated pine chips. In this paper, Eriksson describes his patented biological

delignification process which has yet to be commercially exploited. The chips

enter a very large tower that allows an average residence time of 7 days. The

chips in the tower are continuously sprayed with a mutant microbial solution.

The microbial solution is produced in a separate fermentor where presumedly pure

culture conditions are maintained. The fermentor is fed a solution of sugars from a substrate tank. The sugar solution could be excess whitewater from the paper mill. For a 500 ton/day mill, Eriksson estimates that the tower volume would be 15,000 m^3, the fermentor volume would be 25 m^3, and the substrate tank volume would be 150 m^3. After treatment with the mutant fungus for one week, the chips would be mechanically refined. Eriksson claimed that biological pretreatment of the chips results in substantial energy savings in mechanical pulping that justifies the capital investment.

In another article,[12] Eriksson describes results obtained in a 20 liter composting apparatus where birch and pine chips were rotted with the cellulase-less mutant of S. pulverulentum for a two week period. The chips were then steamed and mechanically refined. A maximum weight loss of 2.5% occurred with pine chips. At that weight loss, the refining energy was 30% less than the control when refining was carried down to a freeness level of 435 CSF. However, when refining was carried down to a freeness level of 125 CSF, the energy saving was only 10%. The energy savings where less significant for pine chips rotted at weight losses of 0.7 and 1.5%. In studies of fungal rotting of birch chips, about a 30% energy saving was estimated when refining to a freeness level of 650 CSF. The mechanical pulp produced from birch wood had very low strength. No difference in strength value was observed between rotted and nonrotted chips. The paper sheets form the rotted chips had a 3 to 4% lower brightness value. For pine chips, the strength properties, tear and tensile indices were the same for pulp from rotted and nonrotted pine chips. The brightness of the pulp from the rotted chips was, however, 7 to 8% lower.

Eriksson et al.[13] described results obtained in rotting pine wood chips and fiberized pulp with wild-type and cellulase-less mutants of Phlebia radiata,

a white-rot fungus. Treating pine wood chips with wild-type fungus for a two
week period, resulted in the same tensile index at a given refiner energy input
as untreated wood chips. Fungal treatment of fiberized pulp resulted in lower
tensile index at a given refiner energy input. Therefore, fungal treatment was
not beneficial in improving pulp strength properties at a given refiner energy
input. When pine chips and fiberized pulp was treated with a cellulase-less
mutant, the tensile index at a given refiner energy input for both treated pine
chips and fiberized pulp was the same as untreated pulp. Carrying out the defi-
berization at 170°C instead of at 127°C, caused the tensile index to increase
for both mutant fungi treated pine chips and fiberized pulp in comparison to the
untreated pulp. Fungal treatment also affected pulp beatability. Less energy
was required to beat the fungal treated pulp to a given freeness level. How-
ever, fungal treated pulp had a lower strength than an untreated pulp at a given
freeness level. Also, the fungal treated pulps had a lower brightness than the
untreated pulp. By and large, these results did not give much justification for
fungal treatment of chips or fiberized pulp.

Somewhat more encouraging results were obtained by Eriksson[14] in a
later study with the cellulase-less mutant of S. pulverulentum. Eriksson first
impregnated the pine wood chips with glucose to a 1.7 wt% level. This prevented
substantial hemicellulose degradation during delignification. The chips were
rotted for 2 weeks before defibration and refining. Wood weight loss was less
than 1% after rotting. In order to obtain a given tensile index on refining,
the rotted chips required about 23% less energy than the untreated chips. Fungal
treatment of nonimprenated wood, however, did not result in any energy savings.
In all cases, the fungus treated pulp suffered loss of brightness compared to
the reference pulp.

T. Kent Kirk of the USDA Forest Products Laboratory has a very active research group in the biological delignification area and has published extensively. Five articles[16-20] by Kirk were found where the subject of biological pulping was mentioned. Though these articles mainly reviewed the work done by other researchers, one article[18] presented the results of experiments performed in Kirk's laboratory. Coarse thermomechanical pulp was treated with a white-rot fungus (Phanerochaete chrysosporium) for a 2 week period. Glucose was added to pulp to suppress degradation of the cellulose and hemicellulose. Energy requirements for refining the fungus-treated pulp to develop a given freeness were decreased by 25-30% compared to those of the control. Energy requirements for refining the fungus-treated pulp to develop a given freeness were decreased by 50% compared to those of the control after swelling in alkali. These results were obtained without any loss in pulp strength properties. The fungus treatment reduced the lignin content of the TMP by 19% with no loss in total carbohydrates. If glucose was not added, no energy advantages were gained. Pulp brightness was not affected by the fungal treatment. These results were much more encouraging than the results obtained by Eriksson and coworkers.

In another article,[20] Kirk mentions the fact that several researchers have isolated crude delignifying enzyme solutions from microbial cultures. This may pave the way to development of enzymatic pulping techniques for wood.

Fukuzumi[21] made pulps from rotted chips of the fungus Quercus serrata. In the abstract of this article, it is claimed that the strength and brightness of the fungal pulp was somewhat superior to a control chemical pulp.

Pilon et al.[22,23] grew several species of fungi on refiner mechanical pulp. It was observed that the water retention value (an indirect measurement of pulp mechanical properties) of the pulp increased by the fungal treatments.

The best result was obtained with the white-rot fungus, Schizophyllum commune.
The water retention value increased by 88% after 14 days incubation with this
organism.

These results show that direct fungal growth on wood chips and wood
pulp can result in refining energy savings without deterioration in pulp quality
in some cases. However, treatment times appear to be excessive. It is not
known to what extent the treatment time can be reduced. Erikkson[11] believes
that a treatment time of one-week is possible. If this is the best that can be
done, the future of biological pulping would not appear to be very bright.
However, the results of biological pulping are encouraging enough to suggest
that an enzymatic treatment of wood chips or wood pulp might be very successful
if the right enzymes could be isolated, produced in substantial quantities, and
concentrated.

Basic Research in Lignin Biodegradation

Studying the basic mechanisms of microbial degradation of lignin occupies
the time of many talented researchers throughout the world. The most notable
among them are Eriksson of the Swedish Forest Products Laboratory, Kirk of the
USDA Forest Products Laboratory, R. Crawford of the Gray Freshwater Biological
Institute, D. Crawford of the University of Idaho, Chang of North Carolina State
University, Higuchi of Kyoto University, and Fukuzumi of the University of
Tokyo. It is easy to justify the importance of research in this area. Lignin
is one of the most abundant biopolymers produced in the world. It is also one
of the most difficult to biologically degrade. It is of interest to determine
how the complex lignin molecule is broken down to carbon dioxide and water and
thereby recycled in nature. Lignin is also believed to be the principal precur-
sor of coal and oil. It is of interest to study how lignin is converted

(probably with the help of microorganisms) to these fossil fuels. Possible

applications of knowledge accumulated about microbial lignin biodegradation

include biological/enzymatic pulping and bleaching, conversion of lignin into

industrially important chemicals, improving the food value of lignocellulosic

materials used as animal feed, and new wastewater treatment processes to handle

lignin containing wastewater.

The proceedings of a symposium on biological delignification sponsored

by Weyerhaeuser in 1976[24] has papers given by Eriksson, Kirk, R. Crawford, and

Pulp and Paper Industry researchers (e.g., Abson, Guthrie, Eudy, Procter, and

Wollwage). Industrial research in biological delignification was minimal with

the focus on removing color from Kraft pulp mill effluents using lignin

degrading microorganisms. An international seminar on lignin biodegradation was

held at the USDA Forest Products Laboratory in Madison, Wisconsin on May 9 to

11, 1978. The proceedings of that seminar were published in 1980.[25] The

Weyerhaeuser and USDA proceedings provided an excellent introduction to the

technical literature on lignin biodegradation which is quite extensive. The

author also reviewed other articles[27-39] in the technical literature on lignin

biodegradation that were recently published and were thought to contain signifi-

cant information. Several of these articles[32-39] were presented at the 1983

International Symposium of Wood and Pulping Chemistry in Japan. An article by

Crawford and Crawford[26] provided a good review of current knowledge concerning

the microbial degradation of lignin. Most of the information that follows was

based on the information presented in that article.

Lignin biodegradation is predominantly an aerobic process (i.e.,

requires oxygen). A microbial culture that can degrade lignin anaerobically has

yet to be isolated though many low molecular weight aromatic compounds are

readily degraded by anaerobic microorganisms. Perhaps in nature, anaerobic microorganisms assist in lignin biodegradation by metabolizing low molecular weight lignin fragments that have been produced by aerobic microorganisms in depolymerizing the lignin macromolecules.

The range of aerobic microorganisms now known to degrade lignin includes a wide variety of both fungi and bacteria. However, only a few kinds of microorganisms (e.g., the white-rot fungi) have the enzymatic capability to attack all the varied structural components of the complex lignin molecule and therefore degrade lignin completely. Other microorganisms only partially attack lignin producing fragments that cannot be further metabolized. The microorganisms that only partially attack lignin would need to form symbiotic relationships with other microorganisms to achieve complete lignin degradation. Formation of humic materials is probably the result of partial attack of lignin by micro-organisms.

Of the lignin degrading microorganisms, the fungi have been the most extensively studied. The three main groups capable of degrading lignin are the soft-rot, the brown-rot, and the white-rot fungi. As a rule, both the soft-rot and brown-rot fungi will preferentially attack the cellulose or hemicellulose in wood before the lignin and then will only incompletely attack lignin. The white-rot fungi are the only microorganisms proven capable of totally degrading all the major components of wood to carbon dioxide and water. In white-rot attack on lignin, initially the number of aliphatic and phenol hydroxyl groups are reduced while carboxyl and carbonyl groups increase. Extensive demethylation also occurs and aromatic rings are opened. Both oxygenases and dioxygenases are implicated in these lignin degrading reactions.

It appears necessary for carbohydrate (e.g., cellulose, glucose, etc.) to be present in order for a white-rot organism to degrade lignin. The carbohydrate serves as a growth substrate. Lignin by itself will not support microbial growth. This is certainly a serious drawback as concerns development of a biological wood pulping process. In order to degrade lignin, the organism must be allowed to degrade a portion of the cellulose or hemicelulose in the wood or carbohydrate must be added to satisfy growth needs. It has also been shown that the nitrogen concentration in the growth media is important in lignin degradation. Depletion of the nitrogen source in an actively growing culture causes the organism to produce lignin degrading enzymes at the maximum rate.

Other fungi (e.g., species of Aspergillus and Fusarium) and many bacteria (e.g., species of Norcardia, Bacillus, Streptomyces, Pseudomonas, Flavobacterium, Aeromonas, and Xanthomonas) have been conclusively shown to at least partially degrade lignin. Xanthomonas was shown to attack lignin as the sole source of carbon and energy.

Determining the structure of native lignins and microbial attack mechanisms on lignin are the subjects of current research. Getting to the middle lamella lignin in wood chips would seem to be a significant problem for microorganisms. Electron microscopy[29-31] has shown that the white-rot fungi spreads hyphae through the wood fibers by utilizing the naturally existing connections (e.g., pits). Growth begins in the lumen and spreads outwards. Sometimes the fungus will form its own bore holes. The wild-type white-rot fungus will cause a progressive thinning of the cell wall starting from the lumen and continuing outwards. The cellulase-less mutants, however, do not cause such thinning. A separation between cells within or adjacent to the compound middle lamella has been observed after fungal treatment.

Basic research in microbial lignin degradation has progressed to the point where numerous lignin degrading microorganisms have been isolated. It is only a matter of time before biotechnology researchers successfully clone lignin degrading enzyme DNA segments from these organisms into E. coli to produce a genetically engineered microorganism capable of producing the enzyme at a high rate. One such successful cloning of a lignin degrading enzyme into E. coli has already been reported.[10] Many other successful attempts will probably be reported in the future.

POSSIBLE ROLE OF IPC IN BIOPULPING DEVELOPMENT RESEARCH

IPC should consider the immediate initiation of a modest biopulping research effort in conjunction with its High Yield Pulping project. The research would focus on the pulping of wood chips and/or modification of high yield mechanical, thermomechanical, or chemimechanical pulps using enzyme solutions. The goal of the enzymatic treatments would be to produce a high yield and strength pulp with minimal energy input. Initially IPC would not produce the enzyme solutions in its own laboratories but would purchase or obtain the enzymes (when available) from other research laboratories and high tech bioengineering firms (e.g., Genentech, Genex, Cetus, Biogen, etc.). The enzymes probably would be available in sufficient quantity for research purposes. IPC would be well equipped to perform this type of research.

Once a biopulping research effort was on firm ground, it would be worthwhile to set up facilities where microorganisms are grown in pure culture to generate enzyme solutions that are then used to digest wood chips or treat high yield wood pulp. Microorganisms would be obtained from culture collections or isolated by IPC personnel from appropiate sources. This type of activity

would require the services of a microbiologist and biochemical engineer. IPC would have much of the equipment needed to perform this type of research.

Since biological/enzymatic pulping promises to reduce energy consumption, a possible source of funding of a biological/enzymatic pulping research effort would be the Department of Energy. Substantial funding would be needed to staff and equip a laboratory dedicated to gene splicing techniques. In the long term, however, IPC would be well advised to get into this promising research area.

REFERENCES

1. Stanier, R. Y.; Doudoroff, M.; Adelberg, E. A. The Microbial World, third edition, Prentice-Hall, Englewood Cliffs, N.J., 1970.

2. Kobayashi, Y.; Matsuo, R. Chemical and enzymatic pulping of the decorticated pineapple leaf fiber and some physical properties of its paper, Cellulose Chem. Technol. 11:487-99(1977).

3. Kobayashi, Y.; Matsuo, R. Enzymatic pulps prepared by Mould-producing enzyme preparations and their paper, Cellulose Chem. Technol. 12:177-97 (1978).

4. Kobayashi, Y.; Matsuo, R. Enzymatic pulping of bast fibers by alkaline pectolytic enzymes, Cellulose Chem. Technol. 15:639-47(1981).

5. Kobayashi, Y.; Matsuo, R. Enzymatic pulping of Mitsumata bast by alkaline pectolytic enzymes; effect of conditions on sheet properties, Cellulose Chem. Technol. 15:649-59(1981).

6. Kobayashi, Y.; Matsuo, R.; Komae, K.; Okawa, A.; Ebuchi, E. Alkaline enzymatic pulping of Kozo (Paper Mulberry) bast for Japanese fine papermaking - effects of alkaline presoaking on pulping and paper properties, 1983 International Symposium on Wood and Pulping Chemistry, Japan Paper Association (sponsor), 2:102-7(1983).

7. Yoshihara, K.; Kobayashi, Y. Retting of Mitsumata bast by alkalophilic bacillus in papermaking, Agric. Biol. Chem. 46(1):109-17(1982).

8. Mayatt, J. H. "Paper," in industrial enzymology: the applications of enzymes in industry, T. Godfrey and J. Reichelt, editors, The Nature Press, New York, New York (1983).

9. Zaborsky, O. R. Comments on biological delignification, in biological delignification: present status and future directions, Proceedings of a Symposium Sponsored by Weyerhaeuser Company, August 30, 1976:79-90.

10. Anon. Gene cloning speeds lignin degradation, C&EN, Oct. 1,1984:5-6.

11. Eriksson, K.-E. Delignification of wood chips by mutant white-rot fungi, in biological delignification: present status and future directions, Proceedings of a Symposium Sponsored by Weyerhaeuser Company, August 30, 1976:5-30.

12. Eriksson, K.-E.; Vallander, L. Biomechanical pulping, Chap. 14 in lignin biodegradation: microbiology, chemistry, and potential applications, T. Kirk, T. Higuchi, and H-m Chang, editors, Vol. II, CRC Press, Boca Raton, Florida, 1980:213-24.

13. Samuelsson, L.; Mjoberg, P. J.; Hartler, N.; Vallander, L.; Eriksson, K.-E. Influence of fungal treatment on the strength versus energy relationship in mechanical pulping, Svensk Papperstid. 83(8):221-25(1980).

14. Eriksson, K.-E.; Vallander, L. Properties of pulps from thermomechanical pulping of chips pretreated with fungi, Svensk Papperstid. 85(6):R33-8 (1982).

15. Eriksson, K.-E. Swedish developments in biotechnology based on lignocellulosic materials, Advances in Biochemical Engineering, 20:193-204(1981).

16. Kirk, T. K. Biodelignification research at the U.S. Forest Products laboratory, in biological delignification: present status and future directions, Proceedings of a Symposium Sponsored by Weyerhaeuser Company, August 30, 1976:31-54.

17. Kirk, T. K.; Chang, H.-M. Potential applications of bio-liginolytic systems, enzyme and microbial technology, 3(3):189-96(1981).

18. Bar-Lev, S. S.; Kirk, T. K.; Chang, H.-M. Fungal treatments can reduce energy requirements for secondary refining of TMP, Tappi J. 65(10):111-13 (Oct. 1982).

19. Kirk, T. K.; Jeffries, T. W.; Leatham, G. F. Biotechnology: applications and implications for the pulp and paper industry, Tappi J. 66(5):45-51 (May 1983).

20. Kirk, T. K. Pulping and bleaching with delignifying enzymes, Pima Mag., Dec. 1983:44-5.

21. Fukuzumi, T. Biological pulping: fundamental principles and technological problems, Japan Tappi 34(12):761-8(Dec. 1980).

22. Pilon, L.; Desrochers, M.; Jurasek, L.; Neumann, P. J. Increasing water retention of mechanical pulp by biological treatments, Proceedings of the 1981 Tappi Annual Meeting, March, 1981:293-7.

23. Pilon, L.; Desrochers, M.; Jurasek, L.; Neumann, P. J. Increasing water retention of mechanical pulp by biological treatments, Tappi J. 65(6):93-6 (June 1982).

24. Abson, D., editor, Biological delignification: p esent status and future
     directions, Proceedings of a Symposium Sponsored by Weyerhaeuser Company,
     (August 30, 1976).

25. Kirk, T.; Higuchi, T.; Chang, H.-M., editors, Lignin biodegradation:
     microbiology, chemistry, and potential applications, Vol. I and II, CRC
     Press, Boca Raton, Florida (1980).

26. Crawford, D. L.; Crawford, R. L. Microbial degradation of lignin, enzyme
     and microbial Tech., 2(1):11-22(1980).

27. Ander, P.; Eriksson, K.-E. Influence of carbohydrates on lignin degrada-
     tion by the white-rot fungus sporotrichum Pulverultum. Svensk Papperstid.
     78(18):643-52(1975).

28. Eriksson, K.-E.; Grunewald, A.; Vallander, L. Studies of growth conditions
     in wood for three white-rot fungi and their cellulaseless mutants, Biotech.
     and Bioeng. 22:363-76(1980).

29. Eriksson, K.-E.; Grunewald, A.; Nilsson, T.; Vallander, L. A scanning
     electron microscopy study of the growth and attack on wood by three
     white-rot fungi and their cellulase-less mutants, Holzforschung 34(6):
     207-13(1980).

30. Ruel, K.; Barnoud, F.; Eriksson, K.-E. Micromorphological and ultrastruc-
     tural aspects of spruce wood degradation by wild-type sporotrichum
     pulverulentum and its cellulase-less mutant cel 44, Holzforschung 35(4):
     157-71(1981).

31. Ruel, K.; Barnoud, F.; Eriksson, K.-E. Ultrastructural aspects of wood
     degradation by sporotrichum pulverulentum, Holzforschung 38(2):61-8(1984).

32. Kirk, T. K. What have studies of model compounds revealed about the fungal
     degradation of lignin, 1983 International Symposium on Wood and Pulping
     Chemistry, Japan Paper Association (sponsor), 3:7-12(1983).

33. Chen, C.-L.; Tai, D.; Terazawa, M.; Chang, H.-M.; and Kirk, T. K.
     Chemistry of birch lignin biodegradation by Phanerochaete chrysosporium,
     1983 International Symposium on Wood and Pulping Chemistry, Japan Paper
     Association (sponsor), 3:13-18(1983).

34. Palmer, J. M.; Evans, C. S. Extracellular enzymes produced by Coriolus
     versicolor in relationship to the degradation of lignin, 1983 International
     Symposium on Wood and Pulping Chemistry, Japan Paper Association (sponsor),
     3:19-24(1983).

35. Fukuzumi, T. Enzymatic hydrolysis products from lignin or lignin-
     carbohydrate in wood, 1983 International Symposium on Wood and Pulping
     Chemistry, Japan Paper Association (sponsor), 4:140-3(1983).

36. Tai, D.; Terazawa, M.; Chen, C.-L.; Chang, H.-M.; Kirk, T. K. Character-
     ization of biodegraded lignins isolated from birch wood decayed by
     Phanerochaete chrysosporium by ^{13}C NMR spectroscopy, 1983 International
     Symposium on Wood and Pulping Chemistry, Japan Paper Association (sponsor),
     4:144-9(1983).

37. Terazawa, M.; Tai, D.; Chen, C.-L.; Chang, H.-M.; Kirk, T. K. Identifica-
     tion of the constituents of low molecular weight fraction obtained from
     birch wood degraded by Phanerochaete chrysosporium, 1983 International
     Symposium on Wood and Pulping Chemistry, Japan Paper Association (sponsor),
     4:150-5(1983).

38. Hiroi, T.; Tamai, A. Degradation of wood components by white-rot fungi,
     1983 International Symposium on Wood and Pulping Chemistry, Japan Paper
     Association (sponsor), 4:156-60(1983).

39. Onderka-Leclair, E.; Cyr, N. Degradation of wood components in aspen
     poplar by fomes igniarius, white-rot fungi, 1983 International Symposium on
     Wood and Pulping Chemistry, Japan Paper Association (sponsor), 4:161-4
     (1983).

40. Bass, A. B. Managing for success: the genentech story, Technology Review,
     88(4):28-9(May/June 1985).